Lublin University of Technology
Electrical Engineering and Computer Science Faculty

Institute of Electrical Engineering & Electrotechnologies
Polish Society of Theoretical and Applied Electrical Engineering
PSTAEE (PTETiS)

POLSKA AKADEMIA NAUK
ODDZIAŁ W LUBLINIE

Polish Academy of Sciences Branch in Lublin

Proceedings
of

the 8th International Conference

ELMECO-8

ELECTROMAGNETIC DEVICES AND PROCESSES
IN ENVIRONMENT PROTECTION

joint with

11th Seminar

AoS-11

APPLICATIONS OF SUPERCONDUCTORS

September 28 – October 01, 2014
Nałęczów, Poland

Institute of Electrical Engineering and Electrotechnologies
Lublin University of Technology
38a Nadbystrzycka St. 20-618 Lublin

Tel./fax: +48 81 53 84 289, +48 81 53 84 643
E-mail: we.ipee@pollub.pl
http://ipee.pollub.pl/elmeco_aos

8th International Conference
ELMECO-8
"ELECTROMAGNETIC DEVICES AND PROCESSES
IN ENVIRONMENT PROTECTION"

joint with

11th Seminar
AoS-11
"APPLICATIONS OF SUPERCONDUCTORS"

September 28 – October 1, 2014
Nałęczów, Poland

Organized by:

Institute of Electrical Engineering and Electrotechnologies
Lublin University of Technology

Polish Academy of Sciences Branch in Lublin

Polish Society of Theoretical and Applied Electrical Engineering PSTAEE (PTETiS)

Conference venue:
Conference Centre ENERGETYK
10 Paderewskiego St., 24 - 140 Nałęczów
tel. +48 81 50 14 604

Scientific Committee

Tadeusz Janowski	(Lublin University of Technology, Poland) - honorary chair
Henryka D. Stryczewska	(Lublin University of Technology, Poland) – chair
Kazimierz Adamiak	(University of Western Ontario, Canada)
Shin-ichi Aoqui	(Sojo University, Japan)
Antoni Cieśla	(AGH University of Science and Technology, Cracow, Poland)
Marian Ciszek	(Inst. of Low Temp. & Struct. Res., PAS, Wrocław, Poland)
Vladimir Datskov	(Joint Institute for Nuclear Research, Dubna, Russia)
Kenji Ebihara	(Kumamoto University, Japan)
Bartek A. Głowacki	(University of Cambridge, UK)
Bogusław Grzesik	(Silesian University of Technology, Gliwice, Poland)
Zbigniew Kołaciński	(Technical University of Łódź, Poland)
Sławomir Kozak	(Electrotechnical Institute, Warsaw, Poland)
Jan Leszczyński	(University of Social Sciences, Łódź, Poland)
Bolesław Mazurek	(Electrotechnical Institute, Wrocław, Poland)
Jerzy Mizeraczyk	(Institute of Fluid Flow Machinery, PAS, Gdańsk, Poland)
Anthony J. Moses	(Cardiff University, UK)
Andrzej Nafalski	(University of South Australia, Adelaide)
Ryszard Pałka	(West Pomeranian University of Technology, Szczecin, Poland)
Krzysztof Schmidt-Szałowski	(Warsaw University of Technology, Poland)
Andrzej Siemko	(CERN, Geneva, Switzerland)
Jacek Sosnowski	(Electrotechnical Institute, Warsaw, Poland)
Petro G. Stakhiv	(Technical University of Lviv, Ukraine)
Paweł Surdacki	(Lublin University of Technology, Poland)
Bronisław Susła	(Poznań University of Technology, Poland)
Jan Sykulski	(University of Southampton, UK)
Andrzej Wac-Włodarczyk	(Lublin University of Technology, Poland)
Chobei Yamabe	(Saga University, Japan)
Sotoshi Yamada	(Kanazawa University, Japan)
Kazimierz Zakrzewski	(Technical University of Łódź, Poland)
Andrzej Zaleski	(Inst. of Low Temp. & Struct. Res., PAS, Wrocław, Poland)

Organising Committee

Dariusz Czerwiński
Jarosław Diatczyk
Renata Jaroszyńska
Leszek Jaroszyński
Joanna Kozieł
Michał Majka
Joanna Pawłat
Paweł Surdacki

ISBN: 978-83-7947-082-2

The proceedings have been published based on papers delivered by authors

Short programme
of the Conference
ELMECO-8 & AoS-11

Sunday, 28 Sept. 2014	
17:00 - 19:00	**Registration - Conference Centre "ENERGETYK" in Nałęczów**
19:00 -	**Welcome reception and dinner**
Monday, 29 Sept. 2014	
08:00 - 09:00	**Breakfast**
08:30 - 09:30	**Registration**
09:30 - 09:45	**Opening session**
09:45 - 11:00	**Oral session O1**
11:00 - 11:30	**Coffee break**
11:30 – 13:00	**Oral session O2**
13:15 - 14:15	**Lunch**
14:30 - 15:45	**Oral session O3**
15:45 - 16:15	**Coffee break**
16:15 - 17:15	**Poster session P1**
17:15 - 17:30	**Coffee break (posters change)**
17:30 - 18:30	**Poster session P2**
19:00 -	**Conference Dinner**
Tuesday, 30 Sept. 2014	
08:00 - 09:00	**Breakfast**
09:00 - 14:00	**Excursion to Janowiec and Kazimierz Dolny**
14:00 - 15:00	**Lunch**
15:30 - 16:30	**Oral session O4**
16:30 - 17:00	**Coffee break**
17:00 - 18:15	**Oral session O5**
19:00 -	**Barbecue**
Wednesday, 1 Oct. 2014	
08:00 - 09:00	**Breakfast**
09:00 - 10:00	**Panel discussion and closing session**
10:15 - 12:15	**Nałęczów sightseeing**
12:30 - 13:30	**Lunch**

Programme
of the Conference
ELMECO-8 & AoS-11

8th International Conference
ELECTROMAGNETIC DEVICES AND PROCESSES IN ENVIRONMENT PROTECTION
& 11th Seminar APPLICATIONS OF SUPERCONDUCTORS
28.09 – 01.10.2014, Nałęczów, Poland

Sunday, 28 Sept. 2014

17:00 - 19:00	**Registration - Conference Centre "ENERGETYK" in Nałęczów**
19:00 -	**Welcome reception and dinner**

Monday, 29 Sept. 2014

08:00 - 09:00	**Breakfast**
08:30 - 09:30	**Registration**
09:30 - 09:45	**Opening session** Chairs: Henryka D. Stryczewska, Tadeusz Janowski

09:45 - 11:00 Oral session O1

1. **Agnieszka Łękawa-Raus (invited speaker)**
   Electrical performance of carbon nanotube fibres
2. **Bogdan Ulejczyk**
   Gas composition influence on the halocarbons decomposition
   in the non-equilibrium plasma
3. **Michał Kwiatkowski**, Piotr Terebun, Piotr Krupski, Jarosław Diatczyk,
   Joanna Pawłat, Henryka D. Stryczewska
   Water contact angles on polymeric material exposed on plasma generated
   in dielectric barrier discharge plasma jet
4. **Piotr Terebun**, Piotr Krupski, Michał Kwiatkowski, Jarosław Diatczyk,
   Joanna Pawłat, Henryka D. Stryczewska
   Water contact angles on high impact polystyrene exposed to radio frequency
   atmospheric pressure plasma jet

11:00 - 11:30 **Coffee break**

11:30 – 13:00 <u>Oral session O2</u>

1. **Jerzy Mizeraczyk (invited speaker)**, Mariusz Jasiński, Mirosław Dors
   Hydrogen production from gaseous hydrogen compounds using plasma
2. **Grzegorz Raniszewski**
   Carbon nanotubes synthesis in low pressure arc discharge
3. **Łukasz Szymański**
   Plasma reactor for continuous process of CNTs synthesis

13:15 - 14:15 **Lunch**

14:30 - 15:45 <u>Oral session O3</u>

1. **Janusz Kozak (invited speaker)**, Michał Majka
   Medium voltage superconducting fault current limiter
2. **Bogusław Grzesik**
   HTS SQUID – a tool for learning
3. **Monika Lewandowska**, Kamil Sedlak
   Thermal-hydraulic analysis of the improved LTS conductor design concepts for the DEMO TF coil
4. **Mariusz Stępień**, Bogusław Grzesik
   Efficient coupled numerical FEM model of coated conductor in self magnetic field

15:45 - 16:15 **Coffee break**

16:15 - 17:15 <u>Poster session P1</u>

1. **Robert Miotk**, Helena Nowakowska, Mariusz Jasiński, Mirosław Dors, Jerzy Mizeraczyk
   Tuning characteristics of microwave plasma source for hydrogen production from liquid fuels
2. **Fumiaki Mitsugi**, Tomoaki Ikegami, Toshiyuki Nakamiya, Yoshito Sonoda
   Measurement of ultrasonic wave for atmospheric discharge with multi-channel optical wave microphones

3. **Michał Młotek**, Ewelina Reda, Krzysztof Krawczyk
Toluene conversion in a new type of gliding discharge reactor supplied by a ferro-resonance system

4. **Takuya Nagatomo**, Keisuke Takigawa, Yuki Yamasaki, Takamasa Sakai, Fumiaki Mitsugi, Tomoaki Ikegami, Kenji Ebihara, Kazuhiro Nagahama
Effect of ozone treatment on soil acidity and nutrient

5. **Adam Piotrowicz**, Krzysztof Jahołkowski, Janusz Ozonek
Application of low-temperature plasma for treatment of off-gases from bitumen production

6. **Ewelina Reda**, Michał Młotek, Krzysztof Krawczyk
Plasma – catalytic conversion of cyclohexane

7. **Yoshitaka Yamashita**, Toshifumi Yamashita, Yukio Hashimoto, Kenji Ebihara, Fumiaki Mitsugi, Tomoaki Ikegami, Henryka D. Stryczewska, Joanna Pawlat, Shinriki Teii, Ta-Lun Sung
Backpack-type ozone-mist sterilization system developed for non-chemical agriculture processes

8. **Shin-ichi Aoqui**, , Noriko Horibe, Fumiaki Mitsugi, Takuya Nagatomo, Kazuhiro Nagahama
Investigation of microbe's sterilization effect on depth directions in a soil by ozone treatment

9. **Joanna Pawłat**, Jarosław Diatczyk, Radosław Samoń, Małgorzata Płonka, Jakub Czapiński, Henryka Stryczewska, Jarosław Grządziel
Atmospheric pressure plasma jet for sterilization of heat sensitive surfaces

10. **Justyna Jaroszyńska-Wolińska**
Advanced technological plasmas

11. Robert Ranecki, **Maciej Kamiński**, Mirosław Szybowicz, Anna Dychalska, Małgorzata Błaszyk, Tadeusz Luciński, Bronisław Susła
Magnetic properties of multilayers $[Ni\text{-}Fe/Au/Co/Au]_6$

12. Leszek Woźny, Jan Ziaja, **Anna Kisiel**
The ceramic superconductors doped by ZrO_2-CeO_3 in sol-gel method

13. **Anna Kisiel**, Małgorzata Żabska, Radosław Chowaniec
Space charge distribution in PVDF nanocomposites with organoclay fillers

14. Andrzej Wac-Włodarczyk, **Andrzej Kaczor**
Conducted electromagnetic disturbances caused in the ignition electrode of the GlidArc plasma reactor

15. Jan Ziaja, Anna Kisiel, **Marcin Lewandowski**
Piezoelectric properties of ZnO doped with Y

16. **Eligiusz Pawłowski**
    Galvanic separation circuit for measuring systems in strong electromagnetic disturbances environment

17. **Piotr Filipek**, Żaklin Grądz
    System klimatyzacji oraz podgrzewu wody użytkowej zasilany z modułów fotowoltaicznych i sieci elektroenergetycznej

17:15 - 17:30 **Coffee break (posters change)**

17:30 - 18:30 Poster session P2

1. Grzegorz Wojtasiewicz, **Tadeusz Janowski**, Sławomir Kozak, Janusz Kozak, Michał Majka, Beata Kondratowicz-Kucewicz
   Transpozycjonery nadprzewodnikowych taśm równoległych jako alternatywa dla kabla Roebela

2. **Grzegorz Wojtasiewicz**, Tadeusz Janowski, Sławomir Kozak, Janusz Kozak, Michał Majka, Beata Kondratowicz-Kucewicz
   HTS 2G superconducting transformer as a fault current limiter - experimental investigation

3. **Leszek Jaroszyński**, Dariusz Czerwiński
   Overcurrent characteristics of SF4050 2G superconducting tape

4. **Rafał Kwoka**, Paweł Surdacki
   Model of superconducting racetrack winding using YBCO tape

5. **Łukasz Woźniak**, Grzegorz Wojtasiewicz, Paweł Surdacki, Grzegorz Komarzyniec
   Influence of superconducting transformer's parameters on transient current limiting

6. **Michał Majka,** , Janusz Kozak, Sławomir Kozak, Grzegorz Wojtasiewicz
   Numerical analysis of medium voltage class inductive superconducting fault current limiter

7. **Michał Łanczont**
   Numerical model of superconducting tape in Xcos/Coselica

8. **Grzegorz Komarzyniec**
   Analytical analysis of HTS transformer inrush current

9. **Marek Horyński**
   Przeciwdziałanie skutkom syndromu chorego budynku w inteligentnych systemach automatyki budynkowej

10. **Andrzej Sumorek**
The influence of construction of bifilar winding on efficiency of electrostatic precipitator

11. **Marcin Buczaj**
Supporting of power sources of decision-making devices and security system elements in building by photovoltaic cells

12. **Paweł Mazurek**
The interaction of the plasma reactor system with power system

13. **Ryszard Goleman**
Forces acting on particles and their trajectories in the surrounding of the collector in matrix separator

14. Andrzej Wac-Włodarczyk, **Piotr Ziń**, Tomasz Giżewski
Effect of insertion changes in a ferromagnet at the differential hysteresis loop for various frequencies of magnetic flux

15. **Paweł Powroźnik**, Dariusz Czerwiński
Emotional speech recognition based on artificial neural network

16. **Dariusz Czerwiński**, Ryszard Goleman
Lumped parameter thermal model for rectangular bar in an induction motor

17. **Joanna Kozieł**, Tadeusz Janowski
Analysis of the impact of secondary winding impedance on the parameters of transformer type superconducting current limiters

19:00 - **Conference Dinner**

Tuesday, 30 Sept. 2014

08:00 - 09:00 **Breakfast**

09:00 - 14:00 **Excursion to Janowiec and Kazimierz Dolny**

14:00 - 15:00 **Lunch**

15:30 - 16:30 Oral session O4

1. **Kenji Ebihara (invited speaker)**, Fumiaki Mitsugi, Tomoaki Ikegami, Yoshitaka Yamashita, Toshifumi Yamashita, Yukio Hashimoto ,Henryka D. Stryczewska, Joanna Pawlat, Shinriki Teii, Ta-Lun Sung, Masayuki Tamura
Biological evaluation of gaseous ozone spray system for non-chemical sterilization

2. **Marcin Hołub**
   Plasma – supported removal of formaldehyde, ammonia and methanol from exhaust gas mixtures

3. **Piotr Krupski,** Piotr Terebun, Michał Kwiatkowski, Jarosław Diatczyk, Joanna Pawłat, Henryka D. Stryczewska
   Applications of ,,Mini GlidArc" plasma reactor in the surface treatment and decontamination bacteria from the TEFLON

16:30 - 17:00 **Coffee break**

17:00 - 18:15 <u>Oral session O5</u>

1. **Andrzej Nafalski (invited speaker)**, Ranjeeta Kaur Singh, Özdemir Göl
   Geographical considerations in the design of an off-grid power system in remote South Australia

2. **Jacek Sosnowski**
   Selected issues of transport current flow in multilayered HTc superconductors

3. **Andrzej Morawski**, T. Cetner, A. Zaleski, D. Gajda, M. Rindfleish, M. Tomsic, R. Diduszko, T. Czujko, E. Żuchowska , S. Hossain, and S. X. Dou, A. Yamamoto
   Low costs MgB_2 superconducting wires for high J_c applications - e.g. ITER

4. **Daniel Gajda**, Andrzej Morawski, Andrzej Zaleski, Małgorzata Małecka, Emilia Żuchowska, Tomasz Cetner, Konstantin Nenkov, Wolfagang Haßler, Michael Tomsic, Matt Rindfleisch, Paweł Surdacki
   Influence of hot isostatic pressure (HIP) on J_c, F_p, T_c, B_{irr}, B_{c2} and microstructure of MgB_2 wires

19:00 - **Barbecue**

<u>Wednesday, 1 Oct. 2014</u>

08:00 - 09:00 **Breakfast**

09:00 - 10:00 **<u>Panel discussion and closing session</u>**
Chair: Henryka D. Stryczewska

10:15 - 12:15 **Nałęczów sightseeing**

12:30 - 13:30 **Lunch**

CONTENTS

INVESTIGATION OF MICROBE'S STERILIZATION EFFECT ON DEPTH DIRECTION IN A SOIL BY OZONE TREATMENT

Shinichi AOQUI[1], Noriko HORIBE[1], Fumiaki MITSUGI[2], Takuya NAGATOMO[2], Kazuhiro NAGAHAMA[1]

Sojo University (1), Kumamoto University (2)

***Abstract**. In recent years organic farming with limited use of pesticides has been studied. We confirmed that ozone treatment in the field of agriculture was an effective for soil sterylization. In this study, it was investigated how a is chemically changed by ozone treatment and in addition, it was confirmed that a sterilization effect was provided by penetration of ozone and oxygen to the depth direction of a soil. In ozone treatment of topsoil, it was able to sanitize 99% of bacteria of 5cm in depth of the surface.*

Keywords: ozone treatment, agriculture, sterilization, sanitization
Słowa kluczowe: ozonowanie, rolnictwo, sterylizacja, sanitacja.

Introduction

Detailed plan has been required for agriculture in countries small of level ground area like Japan. New generation agriculture aimed at a stable high yield of crops from small ground area. Effort that damage to crops due to insects became minimal has been accomplished at the same time. It was sure that this was an important element, but resulted in the side effect that a having many types and a large quantity of chemical materials to the crops were given to at the same time. In other words it is chemical fertilizer and pesticides, and more, genetically modified food. In addition, the problem of Postharvest should attract attention, too [1]. In recent years, as reflection to fight about these, reduced amount of agricultural chemicals agriculture, no pesticide agriculture draw attention. However, it is very difficult to cultivate crops without using chemical fertilizer and a pesticide. As an approach to realize it, we proposed that agriculture with ozone (O_3) and oxygen (O_2) treatment. Oxygen is stable and oxidation power is strong. On the other hand, ozone is an unstable substance and higher oxidation power than oxygen, and there is a property to return to oxygen when period of time passes. Ozone is expected by a field such as food, fisheries, animal husbandry, the agriculture and quality of water improvement to have a strong oxidation power. In addition, ozone generation equipment is commercialized as application to air purifier not only medical equipment in hospital but also family use to prevent viral infection. In recent years it is used as a deodorization system of a refrigerator and air condition. The strong oxidation power that ozone has is used for these. At the same time, that it is unstable molecules which do not remain behind as a dangerous chemical is used. About this ozonation technology, it should be classified in two that is to say a part which has been put to practical use enough and a part that a future study is expected. About the function that ozone decomposes a virus into strongly in the field of air purity, there is already little room for argument. On the other hand, an application to the field of agriculture using ozone generation equipment of high density is the field where a future study is expected. There are in particular few reported cases about a large area and the large-scale processing by ozone. Furthermore, a study to atomize ozone gas directly in a soil is carried out just a little [2-6].

In this study, it was measured how a characteristic of a soil changed by ozone injection to the soil. When a person who consider whether use in the field of agriculture, it is necessary to always take the general cost-effectiveness ratio into consideration because introduction cost of equipment and its operative cost are great factors. In the ozone generation equipment of low power and low density, the atmosphere often is just used for a source gas, but it is commonly used in the equipment of a high yield in high density that pure oxygen is used. As for this reason, because when atmosphere is used, a generation of a nitrogen oxide is not avoided. When a nitrogen oxide is dissolved in atmospheric vapour, it become a strong acid and deteriorates a discharge electrode in the long term. In addition, the released strong acid may affect pH value of a soil. Therefore, we used oxygen for a source gas in this study. Ozone is generated from ozone generation equipment, but oxygen of the source gas is released by high density at the same time.

In this paper, ozone treatment was carried out in a state that bacteria were put in a soil, and it was investigated how bacteria behaved. Because oxygen was released, as for ozone generation equipment, an oxygen reaction of bacteria was investigated.

Experiment

It was confirmed that a chemical reaction was caused by Ozone treatment of andosol. We got a temporary conclusion to remark that ozone decomposed organic matter and contributed to the activity of bacteria to. However, because oxidation ability of ozone is extremely strong, ozone influences bacteria itself and has a sterilization effect. Therefore in order to check this, Pseudomonas (official name: Pseudomonas syringae pv. phaseolicola PK2) which was a natural indigenous bacterium was planted by andosol, and ozone treatment was carried out. Figure 1 shows an experimental setup. Introductions of bacteria in test tubes are shown in Figure 2.

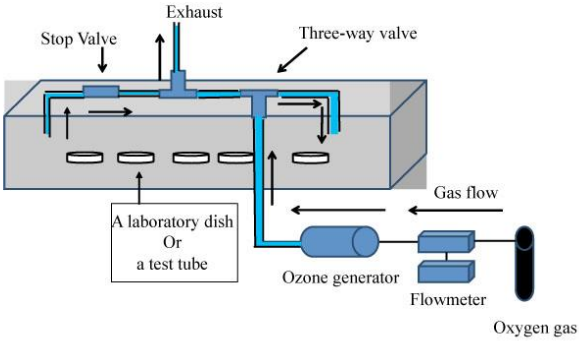

Fig.1. Experimental setup for ozone treatment for bacteria

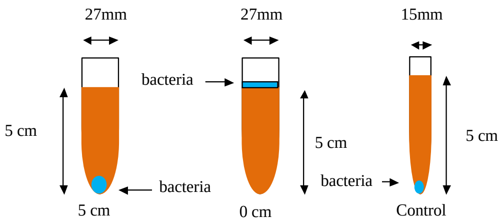

Fig.2. Introduction of bacteria in test tubes

Pure O_2 gas was introduced into ozone generator (Guangzhou Chuanghuan Ozone Electric Appliance Co., Ltd.: CH-PTF 2G) after it was measured flow rate by flowmeter. And then generated ozone gas was introduced into a processing box.

The experiment was carried out under two conditions as followings. One was that in a case it was planted bacteria by topsoil and on the other hand, andosol was put in test tubes (diameter ϕ = 27 mm and 15 mm), and bacteria were implanted in surface and 5cm in depth. We use soil as for andosol for this experiments, complete sterilization processing was carried out by an autoclave to confirm sterilization effect of bacteria by ozone treatment. In the case of a test tube, andosol which was finished with autoclave handling of 5 g was prepared for equally, and bacteria were planted by a bottom and a surface. Soil surface and the distance of the bottom were 5cm apart. A bacteria detection processing after ozone treatment was carried out in following procedures. Suspension of Pseudomonas of OD 610 = 1.5 (0.5 mL) was added to 10 mL isotonic sodium chloride solution 90 minutes after Ozone treatment. 100 μL was applied to NB+BTB nutrient medium after it was stirred in a laboratory dish. A quantity of liquid with quantity of addition 10 mL of an isotonic sodium chloride solution in total is 10.5 mL, because this was 21 times dilution, a bacteria density that we added in andosol became 0.07, and a bacteria suspension 0.1 mL of bacteria density OD 610 = 0.07 was applied to NB+BTB agar nutrient medium. Bacteria dilution solution of 1,000 times and 100,000 times was prepared for elsewhere, and it was compared with the control without the Ozone treatment.

Result and Discussion

Bacteria (a number of bacteria = $2*10^3$) put on a surface of a 27mm tube (soil weight= 20 g) were able to sterilize almost 100 %. Bacteria (a number of bacteria = $3.5*10^3$) put at bottom of 27mm tube (soil weight= 20 g) were able to sterilize approximately 90-80 %. Bacteria (a number of bacteria = 10^6) put at bottom of a 15mm tube (soil weight= 5 g) were able to sterilize approximately 99.9 %. Although it was controlled particle size of andosol beforehand, a particle size is not small enough. Therefore, invasions of ozone gas through a tube wall of a test tube may have been different by a diameter. Furthermore, invasion of ozone gas may have been different in a difference of tube aspect ratio by a diameter, too. However, as a result, the big difference was not found at 15mm and 27mm. as the result we considered that ozone gas penetrated from the whole plane of soil. The result showed a high sterilization rate either case, but at 27mm diameter, it was a value that was 10 to 15 % lower than 15mm. As having been shown from a chemical characteristic experiment result of 2.2, because a quantity of ozone used for a soil depends on a weight of a soil. Therefore in treatment time 90 minutes ozone did not reach saturated density of soil weight of 20 g.

To confirm sterilizing property of oxygen, stopped operation of the ozone equipment, and the same experiment was carried out of pure oxygen atmosphere. The treatment time of 3 hours was used. To compare with ozone treatment, approximately around 80% of sterilization rate was obtained by oxygen treatment.

Conclusion

An experiment of ozone treatment of andosol was carried out. In a sterilization experiment of bacteria in andosol, a sterilization rate of 80 to 99 % was high enough in an agriculture use practically or its application. It is a rather too high value for agriculture. In a soil, many chemical substances and a large number of living things live together. In this study, we confirmed that we could realize a chemical effect and a sterilization effect at the same time by adjusting time of the Ozone treatment. The pure O_2 atmosphere was different from natural atmosphere environment, and it was confirmed that the sterilization of oxygen to some extent was effective.

REFERENCES

[1] J. H. Guo, X. J. Liu, Y. Zhang, J. L. Shen, W. X. Han, W. F. Zhang, P.Christie, K. W. T., Goulding, P. M. Vitousek, and F. S. Zhang: SCIENCE 327 (2010) 1008.

[2] H. D. Stryczewska, K. Ebihara, M. Takayama, Y. Gyoutoku, M.Tachibana: Plasma Processes and Polymers 2(3) (2005) 238-245.

[3] K. Ebihara, M. Takayama, T. Ikegami, K. Ogata, H. D. Stryczewska, Y.Gyoutoku, and T. Sakai: Journal of Advanced Oxidation Technologies 9(2) (2006) 170-173.

[4] K. Ebihara, H. D. Stryczewska, T. Ikegami, F. Mitsugi, and J. Pawlat: PRZEGLAD ELEKTROTECHNICZNY 87(7) (2011) 148-152.

[5] T. Nagatomo, K. Takigawa, T. Sakai, F. Mitsugi, T. Ikegami, K. Ebihara: Proceedings of IIAI International conference on advanced applied informatics (2013) 121-124.

[6] M. Ito, T. Ohta, M. Hori: Journal of Korean Physical Society 60 (2012) 937-943.

***Authors**: prof. Shin-ichi Aoqui and prof. Noriko Horibe, Department of Computer & Information Sciences, Sojo University, Ikeda 4-22-1, Nishi-ku, Kumamoto, 860-0082 JAPAN, e-mail: {aoqui or horibe}@cis.sojo-u.ac.jp: prof. Kazuhiro Nagahama, Department of Applied Microbial Technology, Sojo University, Ikeda 4-22-1, Nishi-ku, Kumamoto, 860-0082 JAPAN,: prof. Fumiaki Mitsugi, Graduate school of science and technology, Kumamoto University, 2-39-1 Kurokami, Chuo-ku, Kumamoto, 860-8555 Japan e-mail:mitsugi@cs.kumamoto-u.ac.jp*

8th International Conference
Electromagnetic Devices and Processes in Environment Protection ELMECO-8
joint with 11th Seminar Applications of Superconductors AoS-11
September 28 - October 1, 2014, Nałęczów, Poland

SUPPORTING OF POWER SOURCES OF DECISION-MAKING DEVICES AND SECURITY SYSTEM ELEMENTS IN BUILDING BY PHOTOVOLTAIC CELLS

Marcin BUCZAJ

Lublin University of Technology, Department of Computer and Electrical Engineering

Abstract. *The article draws attention to the use of photovoltaic cells not only as a sources of cheap electricity, but as a reliable and predictable ways of energy supply final consumer. Reliable power supply is particularly important for systems that require continuous and uninterruptible operation. Such systems are decision-making devices and security and safety systems in object.*

Streszczenie. *W artykule zwrócono uwagę na wykorzystanie ogniw fotowoltaicznych nie tylko jako źródeł taniej energii elektrycznej, ale jako niezawodnych i przewidywalnych pod względem energetycznym sposoby zasilania odbiorcy finalnego. Niezawodne źródło zasilania jest szczególnie ważne w przypadku układów wymagających stałego i nieprzerwalnego działania. Takimi układami są układy decyzyjne i systemy bezpieczeństwa. Tytuł artykułu: Wspieranie źródeł zasilania urządzeń decyzyjnych i elementów systemu bezpieczeństwa w budynku przez ogniwa fotowoltaiczne.*

Keywords: photovoltaic cells, security systems, control and management systems.
Słowa kluczowe: ogniwa fotowoltaiczne, systemy bezpieczeństwa, układy sterowania i nadzoru.

Introduction

The correct execution of scheduled tasks and the proper functioning of control and supervision systems is possible when it is ensured a sufficient level of supply of these systems. Available power supply system is designed to meet the energy needs of the entire decision-making system and selected element security system. The power supplies of the safety system must continuously power all the essential elements in the system due to the protection objectives pursued. This condition must be satisfied in the event of an interruption in the power supply by mains supply [1, 2, 3].

Batteries are the most common method of power supply in devices of decision-making and security systems in times of main power failure (usually AC power adapter). The disadvantages of the use of batteries are additional costs associated with the purchase of batteries and the need for periodic replacement of batteries. The use of batteries as an additional source of energy also determines a limited work time without recharging (standby time). The limited work time of battery is associated with a specific capacity of batteries used to power the system. However, the use of the battery is the only way to offer electricity storage and use of the battery allows subsequent use this energy to power target [1, 2, 4, 5].

The use of photovoltaic cells is now seen as a cheap alternative source of electricity and allowing satisfy user energy needs. The paper presents the possibility of using solar panels as an additional independent power source for the decision-making system and safety system at the facility. Photovoltaic cells cooperation with the additional power supply in system in the form of batteries. Photovoltaic cells allow cyclic recharge the battery and allow extend the work time of additional power supply system [6, 7, 8]. In paper are presented possibility of the use of photovoltaic cells as a reliable and dependable source of electricity. Presents issues related to the availability of solar energy in real-world conditions and their variability in time cycles.

Photovoltaic cells as an alternative energy source

The greatest renewable source of energy is an energy stored in the solar radiation. Solar power concluded in the solar radiation is almost 10,000 times greater than the total electrical energy used in the world. Theoretical solar energy potential is about 1000 kWh/m2/year for Poland. Value of theoretical solar energy potential is slightly different for various Polish regions. The greatest strengths of the possibilities of using solar energy and the highest level of theoretical solar energy potential in Poland are in the Lublin region [7, 9].

Rating solar energy resources available in a given area requires the determination of the intensity of solar radiation and value of insolation. Researches requires a longer period of observation due to the variable nature of these parameters in time. Year of follow-up allows you to draw the conclusions enable the correct selection solar panels and parameters of exploitation of photovoltaic solar energy converters [9]. The distribution of solar radiation on an annual basis for each month are different (fig.1). In the winter the amount of solar energy available in Poland is up to 4 times less than the energy reaching the summer months. The variability of solar energy potential, the intensity of solar radiation and value of insolation in each month must therefore be reflected in the design of solar installations [7, 8, 9].

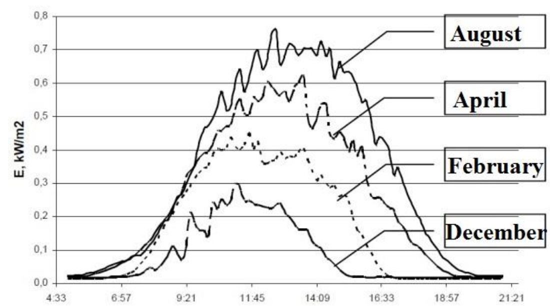

Fig. 1. The average intensity of solar radiation in the vicinity of Lublin in the months February, April, August and December in 2003

Only one is known in the technique method for the direct conversion of solar energy into electricity. It's the helioelectrical process. To convert solar energy into electrical energy are used photovoltaic cells (photovoltaic panels, solar cells, solar panels). The process of converting solar energy into electricity is called the photovoltaic conversion [10, 11].

A typical photovoltaic installation consists of the following elements:
- photovoltaic cell (solar panel) - this element converts solar energy into electrical energy (fig. 2);
- battery pack - this equipment allows storage of electricity produced in a photovoltaic cell;
- charge controller - this devices controls and manages the process of charging and discharging of the battery;
- inverter - converts DC energy stored in the batteries into AC parameters current parameters (usually network) for parameters required by the receiver.

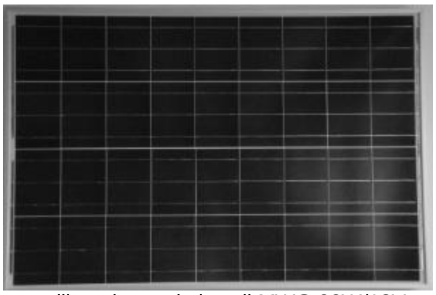

Fig.2. Polycrystalline photovoltaic cell MWG 90W/12V

Support of power supply system of devices of decision-making and security systems by photovoltaic cells system

Alternative power source is designed to supply electricity to the decision-making systems and safety system components in the case of prime power source failure. Support alternative power source of the security system is related to the supply by photovoltaic system additional electricity and allow the proper operation of alarm systems in times of power failure (AC power adapter) and in longer time cycles. This cooperation can rely on and be based on:
- batteries of security system are powered by a separation and an autonomous energy circuit of photovoltaic cells. The batteries are a basic system of alternative power source of the security system. The photovoltaic cells work for the security system only;
- batteries of security system are powered by a dedicated element of photovoltaic system and they work on the energy needs of the alarm system only in times of main power failure;
- use to the power supply of decision-making devices and security system elements the entire photovoltaic cells installation. The batteries use of solar installation energy depending on the needs of the power supply of the security system.

Determination of the energy needs for the photovoltaic cells system which support the work of the alarm system is connected with:
- determination of the minimum battery capacity which allows the assembly of electricity needed to meet the energy needs of the security system in within one circadian cycle;
- determination of minimum power of photovoltaic cell which enabling energy needs of the security system within one circadian cycle. Minimum power of the photovoltaic cell should be determined for the worst period of the year (the period with the lowest average intensity of radiation and the period with the least value of insolation in year);
- determination of minimum area photovoltaic cell capable to meet the energy needs of the security system within one circadian cycle. The area of the photovoltaic cell is dependent on the lowest monthly (daily) average solar radiation. The surface area of the photovoltaic cell is also associated with the parameter of efficiency photovoltaic conversion of solar panels used in the photovoltaic installation.

Summary

Photovoltaic cells can cooperate with existing power supply systems of decision-making systems and security systems. Such cooperation allows increase work time security system when mains power failure (AC power adapter).

Appropriate choice of power and the size of the photovoltaic cells system cooperating with the security system enables reliable and continuous operation of the alarm system, even for long periods or work of such systems in buildings without power supply.

When selecting the size of the photovoltaic cells system to support the power supply of decision-making devices and security system elements, be sure to determining the power and energy parameters obtained for the winter periods. The photovoltaic cells system is the least effective In the winter period. Selection of parameters of the photovoltaic cells system based on the energy parameters in winter periods allows proper operation of system throughout the year.

Battery capacity cooperating with a photovoltaic cells system should be sized to allow operation of the system for at least one daily cycle.

REFERENCES

[1] PN-EN 50131-6:2009, *Systemy alarmowe. Systemy sygnalizacji włamania i napadu. Część 6: Zasilanie*, Wydawnictwo PKN, Warszawa 2009
[2] Buczaj M., *Wpływ konfiguracji i sposobu integracji systemów alarmowych z systemami sterowania i zarządzania pracą urządzeń w budynkach na dobór wielkości zasilania rezerwowego*, Przegląd Elektrotechniczny 2013, nr 5, s. 278-280
[3] Szulc W., Rosiński A., *Zasady zasilania systemów sygnalizacji włamania i napadu*, Zabezpieczenia 2007, nr 5, s. 72-74
[4] Buczaj M., *Integracja systemów sterowania i nadzoru w budynkach w aspekcie realizacji przez nie zadań systemów alarmowych*, Logistyka 2011, nr 6, s. 335-342
[5] Brzęcki M., *Elektroniczne systemy ochrony osób i mienia. Poradnik praktyczny*, Wydawnictwo KaBe, Krosno 2013
[6] Horyński M., Styła S., Boguta A., Buczaj M., Sumorek A., *Model energooszczędnej instalacji domowej w warunkach budownictwa wiejskiego*, Motrol. Motoryzacja i energetyka rolnictwa 2013, nr 1, s. 47-52
[7] Malicki, W., Miedziński, B., Rutecki, K., Habrych, M., *Ogniwa fotowoltaiczne w elektrycznych instalacjach zasilających,* Mechanizacja i Automatyzacja Górnictwa 2010, nr 7, s. 121-125
[8] Tytko R., *Odnawialne źródła energii*, Wydawnictwo OWG, Warszawa 2009
[9] Ścibisz M., *Możliwości wykorzystania energii słonecznej w gospodarstwach województwa lubelskiego*, Inżynieria Rolnicza 2006, nr 13, s. 437-442
[10] Jastrzębska G., *Ogniwa słoneczne. Budowa, technologia i zastosowanie,* WKIŁ, Warszawa 2013
[11] Klugmann-Radziemska E., *Fotowoltaika w teorii i praktyce*, Wydawnictwo BTC, Legionowo 2010

***Authors**: dr inż. Marcin Buczaj, Politechnika Lubelska, Katedra Inżynierii Komputerowej i Elektrycznej, ul. Nadbystrzycka 38A, 20-618 Lublin, e-mail: m.buczaj@pollub.pl*

8th International Conference
Electromagnetic Devices and Processes in Environment Protection ELMECO-8
joint with 11th Seminar Applications of Superconductors AoS-11
September 28 - October 1, 2014, Nałęczów, Poland

LUMPED PARAMETER THERMAL MODEL FOR RECTANGULAR BAR IN AN INDUCTION MOTOR

Dariusz CZERWIŃSKI, Ryszard GOLEMAN

Lublin University of Technology, Institute of Electrical Engineering and Electrotechnologies

Abstract*. The paper proposes a temperature model with lumped parameters for rectangular bar of the winding cage induction motor using Coselica toolbox in Scilab software. The analysis of heating the cage's bar in a short circuit of the motor was carried out. It takes into consideration the heat transfer through the package of teeth for different thicknesses of air gap between the bar and the sheet package.*

Streszczenie. *W pracy zaproponowano model temperaturowy o parametrach skupionych dla prostokątnego pręta uzwojenia klatkowego silnika indukcyjnego z wykorzystaniem biblioteki Coselica w aplikacji Scilab. Przeprowadzono analizę nagrzewania się pręta klatki w stanie zwarcia silnika. Uwzględniono przejmowania ciepła przez pakiet zębów dla różnych grubości szczeliny powietrznej pomiędzy prętem a pakietem blach.*

Keywords: deep bar, induction motor, thermal circuit, modelling, Coselica, Scilab
Słowa kluczowe: silnik głębokożłobkowy, cieplny model obwodowy, Coselica, Scilab

Introduction

The electrodynamic and thermal interactions in the windings of cage induction motors are due to current flow in the bars of the cage. Especially in the case of high-power electric motors, the analysis of these phenomena is important at the design stage to ensure the requirements of motors during long start-up and increase their durability.

The heating analysis of the bars in the motor's cage in a short circuit indicates a fast rise of temperature in the region of the bars, which leads to an increase in mechanical stress in the cage [3, 4]. The temperature distribution in the bar depends on the efficiency of heat transfer by the teeth of the rotor, which is conditioned by the width of the technological air gap existing between the bar and the sheet package.

Temperature field analysis can be done by mathematical analysis with partial differential equations or using numerical methods [2]. Analytical methods are difficult to solve due to the geometry and nonlinearity of physical properties of materials. In numerical methods the FEM, BEM and equivalent thermal circuit can be distinguished. However there is the need of using the dedicated software or writhing the own one. Commercial analysis packages, which can be used, are: FLUX, Comsol Multiphysics, ANSYS, OPERA, QuickField, Matlab. In Open Source or free packages the FEMM, LISA, Elmer, Scilab/Xcos can be listed. In the case when the temperature distribution in whole model is not required the equivalent circuit model of heat transfer can be used.

In lumped parameter thermal model the structure of the model is simplified as also as the results of transient analysis are obtained much faster [1].

Circuit model of deep slot

In the motor short-circuit condition the transient analysis of rectangle bar heating with heat transfer in air gap and rotor package teeth was made. The simplified geometry of the rotor slot is shown in Fig. 1.

Deep slot was modelled as the second order circuit thermal model. Copper cage and iron teeth were presented as heat capacitor elements. In the copper cage the short circuit current is flowing with value equal to 7955 A.

This current generates the heat, which is represented by the fixed heat flow element in the model named Cu_bar shown in Fig 2.

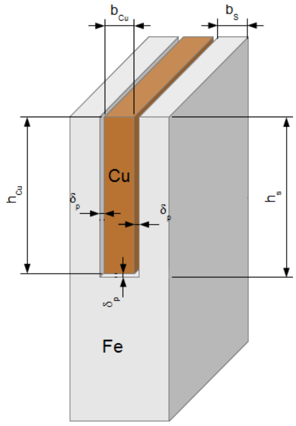

Fig.1. Simplified geometry of the rotor slot of electrical motor

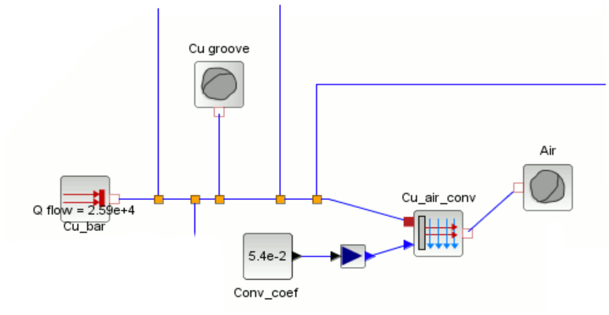

Fig. 2. Fragment of the model representing copper cage bar (Cu_groove) and heat source (Cu_bar)

The iron parts of rotor are connected through the thermal conductance Rp_right shown in Fig. 3, which represents the air gap. Uncovered parts of rotor are cooled with air, assuming the free convection condition. In the short circuit conditions there is no forced air flow around the rotor. The convection is represented by the Cu_air_conv and Fe_air_conv elements shown in Fig 2 and 3.

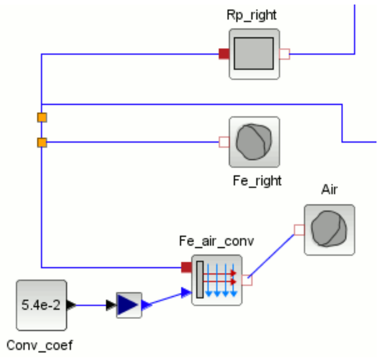

Fig. 3. Fragment of the model representing iron part of the rotor

The basic equation for heat convection between the solid and fluid is:

$$Q_{conv} = G_c \cdot (T_{\text{solid}} - T_{\text{fluid}}) \quad (1)$$

where:
T_{solid}, T_{fluid} – temperatures of solid and fluid respectively,
G_c – is an input signal to the components Cu_air_conv and Fe_air_conv, which depends on the cooling conditions.

Gc may be calculated according to:

$$G_c = A \cdot h \quad (2)$$

where:
A – convection area,
h - heat transfer coefficient

The heat transfer coefficient *h* is calculated from properties of the fluid flowing over the solid. In the case of the short circuit of an electrical motor the rotor is not moving and the free convection is assumed. In that case the heat transfer coefficient is constant and equal to:

$$h = 12 \frac{\text{W}}{\text{m}^2\text{K}} \quad (3)$$

Above assumptions allow to build thermal circuit model of the deep slot. Model was built in Scilab/Xcos environment, which is OpenSource clone of Matlab. Additionally in Xcos environment the Coselica toolbox, which implements the circuit thermal blocks, was installed.

Model consisting additional elements of the slot as also as temperature sensors was shown in Fig. 4.

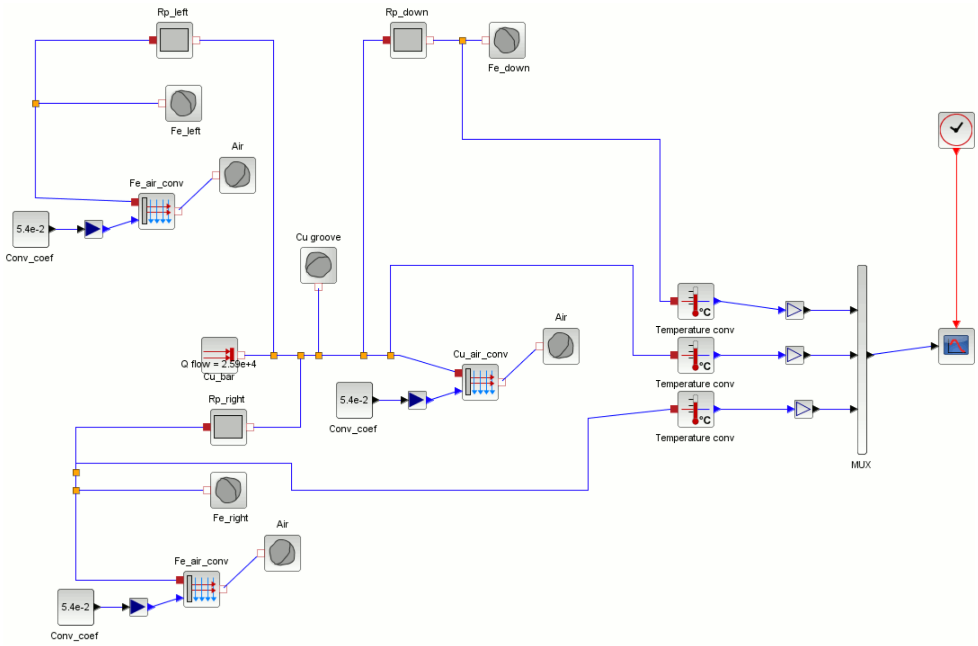

Fig. 4. Circuit thermal model of the deep groove

Conclusions

Circuit model allows to implement the heat calculations in the case of the deep slot of electrical motor in the short circuit conditions.

It is possible to calculate the changes of the temperature in time in individual parts of the groove.

REFERENCES

[1] Campo A., On the teaching of the lumped model for unsteady heat conduction; natural convection versus forced convection, Latian American and Caribbean Journal of Engineering Education, Vol 5(2), 2010, 1-5

[2] Lienhard IV J.,H., Lienhard V J.,H., A heat transfer textbook, Third Edition, Cambridge, Massachusetts, U.S.A., 2001

[3] Pliś D., Płoszyńska J., The effect of relative magnetic permeability of wedges closing stator slots in a cage induction motor on rotor cage heating during the starting phase, Przegląd Elektrotechniczny, 88 (2012), nr 12b, 89-92

[4] Rut R., Wpływ przejmowania ciepła przez rdzeń wirnika na szybkość narastania temperatury w głębokożłobkowych prostokątnych prętach uzwojenia klatkowego silnika indukcyjnego, Rozprawy Elektrotechniczne, 33 (1987), z.3-4, 787-797

***Authors**: dr hab. inż. Dariusz Czerwiński, e-mail: d.czerwinski@pollub.pl; dr inż. Ryszard Goleman, e-mail: r.goleman@pollub.p, Politechnika Lubelska, Instytut Podstaw Elektrotechniki i Elektrotechnologii, ul. Nadbystrzycka 38A, 20-618 Lublin*

8th International Conference
Electromagnetic Devices and Processes in Environment Protection ELMECO-8
joint with 11th Seminar Applications of Superconductors AoS-11
September 28 - October 1, 2014, Nałęczów, Poland

BIOLOGICAL EVALUATION OF GASEOUS OZONE SPRAY SYSTEM FOR NON-CHEMICAL STERILIZATION

Kenji EBIHARA[1], Fumiaki MITSUGI[2], Tomoaki IKEGAMI[2], Yoshitaka YAMAMASHITA[3], Toshifumi YAMASHITA[3], Yukio HASHIMOTO[3], Henryka D. STRYCZEWSKA[4], Joanna PAWLAT[4], Shinriki TEII[5], Ta-LUN SUNG[5], Masayuki TAMURA[6]

Environment and Energy Laboratory (1), Kumamoto University (2), Sanwa hi-tech Co.Ltd (3),
Lublin University of Technology (4), Lunghwa University of Science and Technology (5), Hiroshima University (6)

***Abstract**. Portable, backpack-type ozone sterilization system for agriculture has been developed. Biological aspects of sterilization processes for pest on plants and nematodes in soil are discussed. In a case of plant sterilization, the spray treatment time under selected conditions for the ozone-mist is limited to avoid plant damage. Concerning aphids, which transmit pathogenic viruses to plants, the sterilization rate of 80~95 % was achieved.*

***Streszczenie.** Zaprojektowano i wykonano przenośny, kompaktowy system sterylizacyjny do zastosowań agrarnych. Poddano analizie biologiczne aspekty procesu sterylizacji dla szkodników części naziemnych roślin oraz nicieni obecnych w glebie. Czas działania utleniaczy w przypadku roślin był odpowiednio ograniczony by zapobiec ich uszkodzeniu. W przypadku mszyc osiągnięto ograniczenie populacji w 80-95%.*

Keywords: ozone mist, sterilization, aphid, nematode, non-chemical agriculture.
Słowa kluczowe: mgła ozonowa, sterylizacja, mszyce, nicienie, eko-rolnictwo.

Introduction

Ozone has been used to sterilize pest (harmful insect) in agriculture because of the current phasing out methyl bromide. Ozone has life time of 15-30 min in air depending on the atmosphere conditions. When ozone reacts with water or water-mist, the ozone rapidly changes to many radical species in very short interval which have high strong oxidative and germicidal properties. On the other hand, the residual ozone after ozone-mist or ozone water treatment gives dangerous damage to farmers when they directly spray the pest on the plants.

Considering the situation, we have studied the ozone-mist sterilization method to secure health safety from farmers [1-3]. In practical use at agricultural farms, very short treatment time (about 10 sec) on each target object is required to increase the operation efficiency avoiding plant damages. We have also improved the ozone-mist sterilization system by introducing the ozone -mist generated from ozone and water with non-chemical foaming matter.

We report here the structure of the sterilization system and the characteristics on ozone –mist generated at various conditions. Sterilization effects on aphids on the plant and nematodes in agricultural soil are discussed.

Experimental

Our system of the ozone-mist sterilization is composed of an ozone generator, a water-mist supply system, an AC-DC inverter connected to Li-ion battery, a lightweight oxygen vessel (FRP) with a pressure regulator, a water tank and a movable spray rod with ozone-mist nozzle [1-3]. Fig.1 shows the outline of our sterilization system .

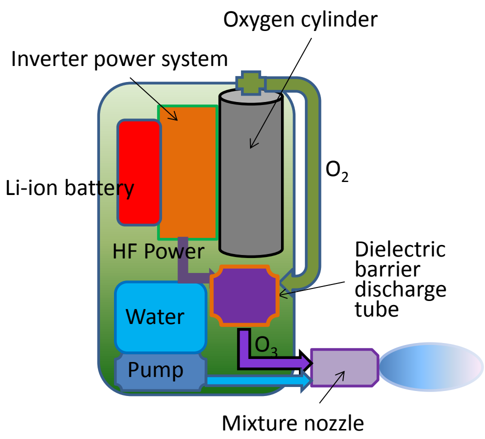

Fig.1 Structure of backpack type ozone-mist sterilization system

High dense ozone is generated by surface dielectric barrier discharge (SDBD). The dielectric barrier discharge was generated on the surface electrode placed on the dielectrics Al2O3 (146x146 mm). The AC electric power for the high frequency generator (15kHz, Vp-p=8kV) was supplied from the AC-DC inverter. The SDBD system was cooled by air. Although the concentration of the ozone generator changes with oxygen gas flow rate, a concentration of 70 g/m3 at an oxygen flow rate of 1 liter/min was used in this experiment.

In this pest sterilization, the target samples such as aphids were captured on the mesh sheet set at the bottom of a test PET cup (top diameter 90mm, bottom diameter 60mm).

In the cultivation of crops, soil deseases is infected with nomatodes in the soil. The nomotodes that live in the soil were separated by using the Bellmann method. The microscopic measurement was performed to detect nomatodes contained in a water drop of the water separated from the sample soil(30g).

Results and discussion

We counted the number of dead aphids (including apparent suspended death) every 30 min after the treatment. Fig.2 shows several insects after ozone-mist treatment for 10 sec . Our experiment showed that ozone-mist foam created with non-chemical addition can contribute to increasing sterilization rate. The survival rate defined as (alive number/ total number) is a dominant factor to evaluate the sterilization system.

Fig.2 Insects after ozone-mist treatment of 10 sec spray using foam addition.

Fig.3 shows normal distribution function F(x) of survival rate of aphids for 5sec and 10 sec treatments without non-chemical addition. These functions were obtained by analysing statistically many experimental data. These profiles indicate that most probable survival rates are 20% for 5 sec treatment and 12% for 10 sec treatment.

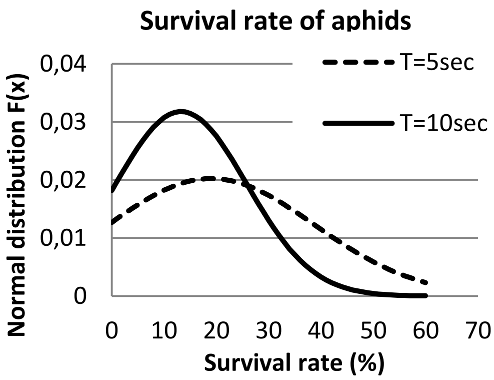

Fig.3 Normal distribution function F(x) of survival rate (x).

We studied the effect on ozone on nematodes dwelling in soil. Fig.4 shows nematodes detected in the water separated from non-ozone treated soil. When the soil was exposed to ozone gas of 70g/m^3 (1 liter/min) during 20min, few nematodes were observed. This result shows that the ozone gas treatment is a promising non-chemical method for agricultural soil.

Fig.4 Nomatodes in separated water of non-treated agricultural soil.

Conclusion

A portable ozone spray system was developed and applied to study the effect on aphids living on plants and nematodes dwelling in soil. The experiments show that probable survival rate for the aphids is 12% and that almost all nematodes in soil were killed by the 20min treatment of 70g/m3 ozone gas.

The non-chemical ozone sterilization method developed here will be a promising and practical technology in agriculture.

We would like to express sincere thanks to Professors Emeritus Chikahisa Honda and Masahisa Otsubo for their kind support and encouragement to promote this R&D project.

REFERENCES

[1] Ebihara K.,Stryczewska H.D., Ikegami T., Mitsugi F., Pawlat J., Electrical Review, R.87 NR7/2011, pp.148-152, 2011.
[2] Ebihara K.,Stryczewska H.D., Mitsugi F., Ikegami T., Sakai T., Pawlat J., Teii S., Electrical Review, R.88 NR6/2012, pp.92-94, 2012.
[3] Ebihara K., Mitsugi F., Ikegami T., Nakamura N., Hashimoto Y., Yamashita Y., Baba S., Stryczewska H.D., Pawlat J., Teii S., Sung T.L.,The European Physical Journal Applied Physics, Vol61, 24318, pp.1-5,201

Author: *Professor Emeritus Kenji EBIHARA, Environment and Energy Laboratory, Ohtemon 1-4-15-404, Chuouku, Fukuoka City, Fukuoka 810-0074 Japan, e-mail: kankyo@mild.ocn.ne.jp*

INFLUENCE OF HOT ISOSTATIC PRESSURE (HIP) ON J_c, F_p, T_c, B_{irr}, B_{c2} AND MICROSTRUCTURE OF MgB_2 WIRES

Daniel GAJDA[1] Andrzej MORAWSKI[2], Andrzej ZALESKI[3], Małgorzata MAŁECKA[3], Emilia ŻUCHOWSKA[4] Tomasz CETNER[2], Konstantin NENKOV[5], Wolfagang HAßLER[5], Michael TOMSIC[6], Matt RINDFLEISCH[6], Paweł SURDACKI[7]

International Laboratory of High Magnetic Fields and Low Temperature (1)
Institute of High Pressure Physics of PAS (2)
Institute of Low Temperature and Structure Research PAS (3)
Military Technical Academy (4)
Institute for Solid State and Materials Research Dresden (5)
Hyper Tech Research, Inc.(6)
Lublin University of Technology, Institute of Electrical Engineering and Electrotechnologies (7)

***Abstract**. We present results of critical current density (J_c), pinning force density (F_p) critical temperature (T_c), upper critical field (B_{c2}), irreversibility magnetic field (B_{irr}) investigations and analysis of dominant pinning mechanism which were made for multicore monel-sheathed type MgB_2 wires manufactured by continuous tube forming and filling (CTFF) method at Hypertech Inc. Ohio, USA. The in situ MgB_2 wires with Nb barrier and monel sheaths have been hot isostatic pressed (HIP) at Institute of High Pressure Physics (IHPP PAS).*

***Streszczenie**. Przedstawiono wyniki badań gęstości prądu krytycznego, gęstości siły zakotwiczenia, temperatury krytycznej, górnego pola krytycznego, indukcji nieodwracalnej i analizę mechanizmu zakotwiczenia dla przewodów MgB_2 wykonanych technologią CTFF przez Hypertech Inc. Ohio, USA. Przewody MgB_2 z Nb barierą i w monelowej osłonie były wygrzewane pod ciśnieniem izostatycznym w Instytucie Wysokich Ciśnień Polskiej Akademii Nauk.*

Keywords: MgB_2 wires, Hot Isostatic Pressure (HIP), critical current density (J_c).
Słowa kluczowe: przewody MgB_2, wygrzewanie pod ciśnieniem, gęstość prądu kryttcznego

Introduction

The MgB_2 superconducting material was discovered in 2001 [1]. Pure MgB_2 material has several advantages such as low price of components, low resistivity in the normal state, low specific weight, high J_c in zero magnetic field, low anisotropy, and long distance coherence of about 5 nm and high critical temperature 39 K [2]. These advantages cause that MgB_2 material has great potential in future applications.

Easy synthesis, low price, easy availability of components and allow to obtain MgB_2 tapes and wires are easier and cheaper than production of comparable HTS tapes and wires. High critical temperature of magnesium diboride allows to cool MgB_2 material not only by liquid helium, but also by liquid hydrogen, liquid neon or cryocooler. MgB_2 has low resistivity in the normal state from 0.0038 to 3 μΩm [3, 4]. Low resistivity is very important during the transition of superconducting material to normal state, because it reduces significantly the possibility of damage the superconducting wires.

However, MgB_2 material has several disadvantages such as inhomogeneous microstructure (pores and void) and low J_c in the middle and high magnetic fields, which limit its application. The results presented in articles [5, 6] suggest that high annealing pressure can improve microstructure of MgB_2 material, reduce pore size and introduce strain - dislocations. In papers [7, 8] the authors suggest that the dislocations create point pinning center, which increases J_c in high magnetic fields. The author in [9] suggests that the point pinning center can create not only intergranular precipitation, but also void similar in size to the coherence length. The effectiveness of the point pinning centers - voids are similar to the point pinning centers – precipitates.

The authors in the articles [10, 11] indicated that the doping of SiC and C can increase J_c and B_{irr} in high magnetic fields.

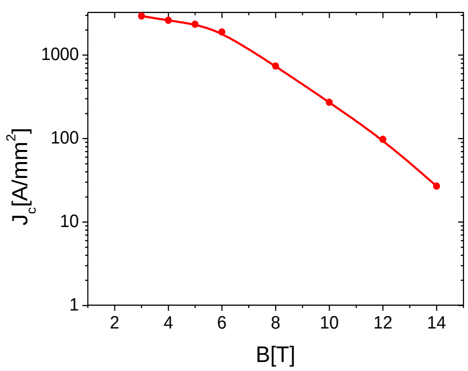

Fig.1. Transport J_c–B curves for undoped MgB_2 wires (OD = 0.83 mm) at 4.2 K.

Samples were annealed in Institute of High Pressure Physics PAS at argon gas pressure up to 1 GPa in the range of temperatures from 650 oC to 700 oC for various annealing times.

The I_c measurements at 4.2 K were performed in magnetic fields up to 14 T in Bitter type magnet installed in ILHMFLT and I_c measurements at 10 K, 20 K and 25 K in Institute for Solid State and Materials Research Dresden. The perpendicular field configuration was applied to the 20 mm length samples. Measurements of T_c, B_{irr} and B_{c2} were performed by the transport methods in ILHMFLT PAS. Microstructure investigations were performed with SEM in Institute of Low Temperature and Structure Research (Wrocław) and Military Technical Academy (Warsaw). The best results of J_c 1000 A/mm^2 in 8 T at 4.2 K (fig.1) and 100 A/mm^2 in 4,5 T at 20 K have been obtained during these investigations. The maximal F_p of 12 GN/m^3 in 5 T/4,2 K (fig.2).

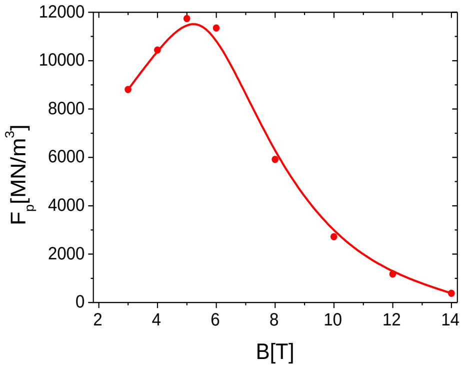

Fig.2. The reduced pinning force density F_p dependence on magnetic field for undoped MgB_2 wires (OD = 0.83 mm) at 4.2 K.

Studies indicate that the pressure of 1 GPa improved uniformity of microstructure and allows to obtain point pinning centers which increase J_c in the middle and high magnetic fields. These factors will increase the applicability of MgB_2 material in medicine, industry, mining and electrical engineering.

REFERENCES

[1] Nagamatsu N., Nakagawa, T., Muranaka, Y., Zentani and Akimitsu J, Superconductivity at 39 K in magnesium diboride, *Nature* 410, (2001) No 63

[2] Y. Takano, H. Takeya, H. Fujii, H. Kumakura, T. Hatano, K. Toganok, H. Kito, H. Ihara, Superconducting properties of MgB_2 bulk materials prepared by high-pressure sintering, *Applied Physics Letters.* 78 (2001) No 19, 2914-2916

[3] P.C. Canfield, D.K. Finnemore, S.L Bud'ko, J.E. Ostenson, G. Lapertot, C.E. Cunningham, C. Petrovic, Superconductivity in dense MgB_2 wires, *Physical Review Letters*, 86 (2001) No 11, 2423-2426

[4] P.A. Sharma, N. Hur, Y. Horibe, C.H. Chen, B.G. Kim, S. Guha, M.Z. Cieplak, W. Cheong, Percolative superconductivity in $Mg_{1-x}B_2$, *Physical Review Letters* 89 (2002) No 16, 167003/1-4

[5] J.H. Kim, A. Matsumoto, M. Maeda, Y. Yamada, K. Wada, K. Tachikawa , M. Rindfleisch, M. Tomsic, H. Kumakura, Influence of hot-pressing on MgB_2/Nb/Monel wires, *Physica C* 470 (2010) 1426 –1429

[6] A. Serquis, L. Civale, D. L. Hammon, X. Z. Liao, J. Y. Coulter, Y. T. Zhu, M. Jaime,D. E. Peterson, and F. M. Mueller, V. F. Nesterenko and Y. Gu, Hot isostatic pressing of powder in tube MgB_2 wires, *Applied Physics Letters.* 82 (2003) No 17, 2847-2849

[7] M. Panek, D. Pattanayak, R. Meier-Hirmer and H. Kűpfer, Influence of ternary additions and precipitation on the critical current density and other superconducting properties in Nb-65 wt.%Ti, *J.App.Phys.* 54 (1983) 7083 – 7088

[8] T. Matsushita and H. Kűpfer, Enhancement of the superconducting critical current from saturation in Nb-Ti wire. I. *J.App.Phys*. 63 (1988) 5048 – 5059

[9] J.D. Livingston, Structure and properties of high-field superconductors, *GE R&D Center Report* (ca. 1969-70)

[10] Neson Varghese, Krishnankutty Vinod, Sugathan Rahul, Pazhedath Anees, Kavazhikathu Mohandas Devadas, Syju Thomas, Athinarayanan Sundaresan, Sindhunil Barman Roy, Upendran Syamaprasad, Effect of Carbon Substitution on the Superconducting Properties of Nanocarbon-, Nanodiamond- and Nano-SiC-Doped MgB_2, *Journal of the American Ceramic Society*, 1137 (2011) 1133 – 1136

[11] Zongqing Ma, Hai Jiang and Yongchang Liu, The acceleration of low-temperature sintering of MgB_2 bulks with high critical density by minor Sn doping *Supercond. Sci. Technol*., 23 (2010) 025005

Authors:. *dr inż. Daniel Gajda,* International Laboratory of High Magnetic Fields and Low Temperature, *ul Gajowicka 95, 53 – 421 Wrocław, e-mail: dangajda@op.pl;*
dr Andrzej Morawski, Institute of High Pressure Physics, Polish Academy of Sciences, Sokołowska 29/37, 01-142 Warszawa, e-mail: amor@unipress.waw.pl
prof. Andrzej Zaleski Institute of Low Temperature and Structure Research Polish Academy of Sciences, Okólna 2, 50 -422 Wrocław, Poland, e-mail A.Zaleski@int.pan.wroc.pl
dr Małgorzata Małecka Institute of Low Temperature and Structure Research Polish Academy of Sciences, Okólna 2, 50 -422 Wrocław, Poland, e-mail m.malecka@int.pan.wroc.pl
mgr inż. Emilia Żuchowska Military Technical Academy, Gen. Sylwestra Kaliskiego 200-908 Warszawa, e-mail zuchowska.emila@wp.pl
mgr Tomasz Cetner, Institute of High Pressure Physics, Polish Academy of Sciences, Sokołowska 29/37, 01-142 Warszawa, e-mail tcetner@unipress.waw.pl
dr Konstantin Nenkov, Institute for Solid State and Materials Research Dresden, P.O. Box 270016, D-01171 Dresden
dr Wolfagang Haßler, Institute for Solid State and Materials Research Dresden, P.O. Box 270016, D-01171 Dresden e-mail w.haessler@ifw-dresden.de
dr Matt Rindfleisch Hyper Tech Research Inc., 539 Industrial Mile Road, Columbus, OH 43228-2412, USA e-mail mrindfleisch@hypertechresearch.com
dr Michael Tomsic Hyper Tech Research Inc., 539 Industrial Mile Road, Columbus, OH 43228-2412, USA
dr hab. inż. Paweł Surdacki, prof. of LUT, Lublin University of Technology, Institute of Electrical Engineering and Electrotechnologies, Nadbystrzycka 38 A, 20-618 Lublin, e-mail p.surdacki@pollub.pl

The correspondence address: e-mail: dangajda@op.pl

8th International Conference
Electromagnetic Devices and Processes in Environment Protection **ELMECO-8**
joint with 11th Seminar Applications of Superconductors **AoS-11**
September 28 - October 1, 2014, Nałęczów, Poland

FORCES ACTING ON PARTICLES AND THEIR TRAJECTORIES IN THE SURROUNDING OF THE COLLECTOR IN MATRIX SEPARATOR

Ryszard GOLEMAN

Lublin University of Technology, Institute of Electrical Engineering and Electrotechnologies

***Abstract**. In the paper, the forces and trajectories of paramagnetic and ferromagnetic particles moving in the surrounding of ferromagnetic capture element have been determined. The influence of flow speed of the medium, smooth section of the collector, the value of magnetic flux density and the properties of particles on the width zone of particle capture by the collector have been analysed*

***Streszczenie.** W pracy zostały wyznaczone siły i trajektorie paramagnetycznych oraz ferromagnetycznych cząstek poruszających się w otoczeniu ferromagnetycznego elementu wychwytującego matrycy. Analizowano wpływ prędkości przepływu medium, smukłości przekroju kolektora, wartość indukcji magnetycznej i właściwości cząstek na szerokości strefy wychwytywania cząstek.*

Keywords: magnetic separation, magnetic force, dynamic resistance force, simulation.
Słowa kluczowe: separacja magnetyczna, siła magnetyczna, siła oporu dynamicznego, symulacja.

Introduction

In matrix separators the inhomogeneous distribution of the magnetic field has been obtained through the application of the matrix in various forms depending on the separation process [1-6]. To reach relatively high value of magnetic force influencing the particle at constant value of magnetic flux density, the defined ratio of the collector radius and the particle can be preserved. In the case of an elliptic cylinder the value of magnetic force depends on the ratio of its semi-axis [2, 3]. The consideration is based on the analysis of three forces: magnetic, gravitational and hydrodynamic. The simplifying assumption is that a separated particle is spherical.

Magnetic force

Magnetic force due to inhomogeneity of the magnetic field acting on the particle should be the dominant one in the separation process. For the case that the particle and medium are homogeneous and isotropic, the magnetic force is the function of the intensity of outer magnetic field described by the following equation [5]

$$\mathbf{F}_\mathrm{m} = \frac{\mu_\mathrm{c} - \mu_1}{\mu_1 + \mathrm{D}(\mu_\mathrm{c} - \mu_1)} \cdot \mathrm{V}_\mathrm{c} \cdot (\mathbf{H} \cdot \nabla)\mathbf{B} \tag{1}$$

where: **B** - magnetic flux density, **H** - vector of the magnetic field intensity, V_c - volume of particle, μ_c , μ_1 - magnetic permeability of the particle and medium, D - particle's coefficient of demagnetization along the axis consistent with the direction of magnetic field intensity.

The considered ferromagnetic element (collector) is in the form of infinite long elliptic cylinder with its axis in perpendicular plane to the vector of homogeneous flux density. The issue has been considered as two-dimensional in the elliptic-cylindrical system of coordinates (Fig.1). Assuming that the axis of the collector covers the axis „z", the magnetic potential V_m is the function of coordinates η and φ, thus the Laplace's equation is given by the following relation.

$$\nabla^2 V_\mathrm{m} = \frac{1}{\mathrm{c}^2(\mathrm{ch}^2\eta - \cos^2\varphi)}\left(\frac{\partial^2 V_\mathrm{m}}{\partial\eta^2} + \frac{\partial^2 V_\mathrm{m}}{\partial\varphi^2}\right) = 0 \tag{2}$$

According to its solutions, calculating the magnetic field intensity as $\mathbf{H} = -\nabla V_m$, after some manipulation we obtain the expression for components of that field

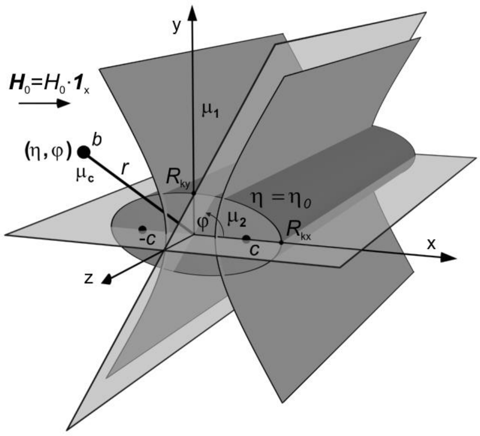

Fig.1. Elliptic cross-section collector and the particle placed in homogeneous magnetic field

Field of medium speed and dynamic resistance force

Because the matrix element is placed in a stream of liquid it affects the medium. Potential flows of the non-viscid and incompressible liquid can be described by the potential of speed Ψ which fulfils the Laplace's equation.

$$\nabla^2 \Psi = \frac{1}{\mathrm{c}^2(\mathrm{ch}^2\eta - \cos^2\varphi)}\left(\frac{\partial^2 \Psi}{\partial\eta^2} + \frac{\partial^2 \Psi}{\partial\varphi^2}\right) = 0 \tag{3}$$

In the considered case the potential of medium speed is the periodical and even function of φ. The vector of medium speed is described by gradient of the potential $\boldsymbol{\vartheta} = \nabla\Psi$. Since the particles of liquid flow around the matrix element, the vector component of speed which is perpendicular to the collector's surface is equal to zero. In some considerable distance from the matrix element the stream of liquid is homogeneous and its speed is $\boldsymbol{\vartheta} = \vartheta_o \mathbf{1}_x$. It can be shown that the components of the speed vector outside the matrix element converted to the rectangular coordinates have the form

$$
\begin{aligned}
\vartheta_x &= \frac{\vartheta_o \,\mathrm{sh}\eta \cos^2\varphi\left(\mathrm{ch}\,\eta_o \mathrm{sh}\eta - \mathrm{sh}\eta_o \mathrm{ch}\,\eta\right)}{\exp(-\eta_o)(\mathrm{ch}^2\eta - \cos^2\varphi)} + \\
&+ \frac{\vartheta_o \,\mathrm{ch}\,\eta \sin^2\varphi\left(\mathrm{ch}\,\eta_o \mathrm{ch}\,\eta - \mathrm{sh}\eta_o \mathrm{sh}\eta\right)}{\exp(-\eta_o)(\mathrm{ch}^2\eta - \cos^2\varphi)}, \\
\vartheta_y &= \frac{\vartheta_o \,\mathrm{ch}\eta \sin 2\varphi\left(\mathrm{ch}\,\eta_o \mathrm{sh}\eta - \mathrm{sh}\eta_o \mathrm{ch}\,\eta\right)}{2\exp(-\eta_o)(\mathrm{ch}^2\eta - \cos^2\varphi)} - \\
&- \frac{\vartheta_o \,\mathrm{sh}\eta \sin 2\varphi\left(\mathrm{ch}\,\eta_o \mathrm{ch}\,\eta - \mathrm{sh}\eta_o \mathrm{sh}\eta\right)}{2\exp(-\eta_o)(\mathrm{ch}^2\eta - \cos^2\varphi)}
\end{aligned} \tag{4}
$$

While considering the movement of small particles in the separation processes the force of dynamic resistance has been described by the Stoke's equation

$$\mathbf{F}_d = 6\,\pi\,\zeta\, b\left(\vartheta - \vartheta_c\right) \tag{5}$$

where: ζ – dynamic coefficient of medium viscosity, $\boldsymbol{\vartheta}$ – vector of medium speed, $\boldsymbol{\vartheta}_c$ – stands for the vector of particle speed.

Gravitational force is expressed by the following dependence:

$$\mathbf{F}_g = (\rho_c - \rho_o)\, V\, \mathbf{g} \tag{6}$$

where: ρ_c – particle density, ρ_o – medium's density, **g** – gravitational acceleration.

Equations for particle movement

To determine the trajectory of the particle the following system of equations should be solved

$$
\begin{aligned}
\frac{\mathrm{d}\vartheta_c}{\mathrm{d}t} &= \frac{\mathbf{F}_m + \mathbf{F}_g + \mathbf{F}_d}{m}, \\
\frac{\mathrm{d}\mathbf{s}}{\mathrm{d}t} &= \vartheta_c
\end{aligned} \tag{7}
$$

where: **s** – distance covered by a particle; m – particle mass.

The Runge-Kutty's method of the 4th rank with the automatic selection of the integration step has been used to solve the system of equations numerically. The following input data that characterize the separation process have been assumed: $\vartheta_o = 0.05$ m/s, $\rho_c = 5000$ kg/m^3, $\rho_o = 1000$ kg/m^3, radius of patrticle b = 7.5•10^{-6} m, magnetic susceptibility of paramagnetic particle $\chi_c = 0.007$ and the medium $\chi_o = 0$, $\zeta = 0.001$ N/m·s, g = 9.81 m/s^2. Magnetic properties of the collector and ferromagnetic particle are specified by the characteristics of the magnetization process *B*=f(*H*). Results of the calculations are shown in Fig. 2.

The width of the capture zone changes linearly along with the increase of the induction while the magnetic permeability of the collector and the particle are constant values. In case of the analyzed ferromagnetic particles and elliptic collector ($R_{kx}/R_{ky} = 2$) it is 5 times higher and for the circular collector almost four times higher at induction values ranging from 0.05 T to 0.4 T.

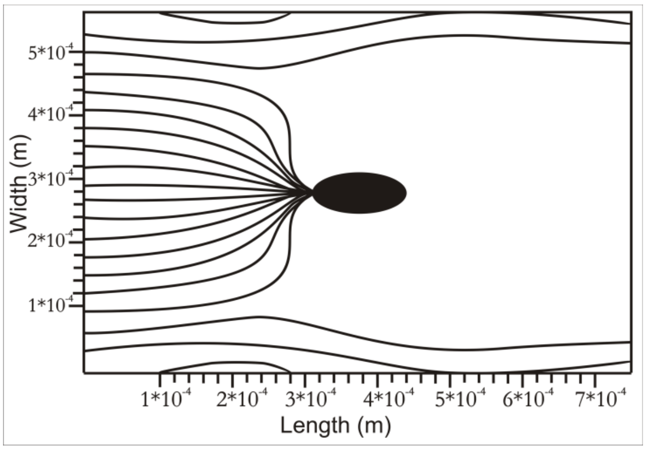

Fig.2. Trajectories of paramagnetic particles at magnetic induction *B* = 0,8 T, radii of collector's section R_{kx}=6x10^{-5} m, R_{ky}=3x10^{-5}m.ox

The growth of induction and the saturation of the collector clearly influences the width of the capture zone. At the assumed parameters of paramagnetic particles' separation the width rise of the capture zone is small in the field of induction value over 1.2 T.

Conclusion

Mathematical model presented in the paper enables us to analyse magnetic separation process more precisely and to assess its efficiency in relation to various parameters such as: magnetic flux density, velocity of medium flow, dimensions of semi-axis of matrix element, and properties of the particle and surrounding.

REFERENCES

[1] Aharoni A., Traction force on paramagnetic particles in magnetic separators, *IEEE Trans. Magn*., (1976), vol. MAG-12, 234-235

[2] Goleman R., Macroscopic model of particles' capture by the elliptic cross-section collector in magnetic separator, *Journal of Magnetism and Magnetic Materials*, 272-276 (2004), pp. 2348-2349,

[3] Goleman R., Złonkiewicz Z., Forces exerted on a particle and its trajectory in the vicinity of a separator matrix element, *Studies in Applied Electromagnetics and Mechanics*, vol.13, IOS Press,1998, 733-736

[4] Karmazin, V.V., Theoretical assessment of technological potential of magnetic and electrical separation, *Magnetic and Electrical Separation*," vol.8, (1997), 139-159

[5] Svoboda J, Extraction of ferromagnetic particles by a suspended magnet, *Magnetic and Electrical Separation*, vol.4, (1993),.223-239

[6] Svoboda J., Fujita T., Recent developments in magnetic methods of material separation, *Minerals Engineering*, Vol.16, Iss. 9 (2004), 2348-2349

***Author**: dr inż. Ryszard Goleman, e-mail: r.goleman@pollub.pl, Politechnika Lubelska, Instytut Podstaw Elektrotechniki i Elektrotechnologii, ul. Nadbystrzycka 38A, 20-618 Lublin*

8th International Conference
Electromagnetic Devices and Processes in Environment Protection ELMECO-8
joint with 11th Seminar Applications of Superconductors AoS-11
September 28 - October 1, 2014, Nałęczów, Poland

PLASMA – SUPPORTED REMOVAL OF FORMALDEHYDE, AMMONIA AND METHANOL FROM EXHAUST GAS MIXTURES

Marcin HOŁUB

West Pomeranian University of Technology, Szczecin

Abstract*. Experimental results are presented regarding plasma – supported formaldehyde, ammonia and methanol removal. A large –scale installation was investigated as a preparatory study for industrial application. Plasma – supported catalytic treatment proved removal rate of over 90%. Indirect plasma application was proved to have comparable efficiency to direct application but allows for polluted gas, electrode erosion minimization.*

Streszczenie. *Praca prezentuje przegląd wyników prac badawczych związanych z plazmowymi oraz plazmowo wspomaganymi metodami usuwania lotnych związków organicznych z przemysłowych gazów wylotowych. Przedstawione wyniki prezentują zalety wykorzystywania metod plazmowych przy ograniczonych stężeniach wlotowych substancji szkodliwych. Dodatkowo przedstawiono wyniki badań eksperymentalnych różnych konfiguracji systemu jednoczesnego unieszkodliwiana amoniaku, metanolu i formaldehydu. Wykorzystując efekt synergii plazmy niskotemperaturowej z katalizatorem zaprezentowano układ umożliwiający ponad 90% skuteczność usuwania zanieczyszczeń.*

Keywords: plasma – supported gas treatment, non - thermal plasma systems, industrial plasma applications.
Słowa kluczowe: plazmowo – wspomagane systemy oczyszczania gazów, systemy plazmy nietermicznej, technologie plazmowe.

Introduction

Many industrial processes contribute to gaseous pollutant emissions, in many cases volatile organic compounds (voc's) are emitted. Many of these substances are harmful for the environment and can present a threat for health and wellbeing of man. As a popular example ammonia (NH_3) emissions can be considered, a chemical compound not only poisonous for the environment but also irradiating the skin, eyes and the respiratory system [1]. A contact with gaseous ammonia with concentrations above 300 ppm can lead to permanent health damage or even death. Another example of popular exhaust air pollutants is formaldehyde (HCHO) suspected of cancerous influence on people [2]. Similar to formaldehyde methanol is not only irradiating the lungs but also suspected of negative influence on the nerve system [3].

Many methods of exhaust air treatment exist including filtration, scrubbing, absorption, catalytic treatment, thermal oxidation, bio filtration. Recent years have shown a rapid development of heterogeneous processes combining different technologies, including the non – thermal plasma processing [4, 5]. Plasma was documented to be efficient in reduction of voc's in case of limited concentrations (below $1gC_{org}/Nm^3$) [6]. Proposed paper concentrates on a hybrid, plasma – supported removal of above mentioned voc's. Experimental results and test – stand configuration is briefly described.

Experimental apparatus

All the measurement results presented were obtained in PlasmaTechnikum of Rafflenbeul Engineers in Germany. Test – stand configuration allowed to rapidly change the exhaust air treatment system configuration and operational parameters. Both direct and indirect methods were examined. Two exemplary configurations of the exhaust treatment systems are presented in Fig. 1. The practical construction of the test – stand is depicted in Fig. 2. Measurement equipment is listed in Table 1.

Typical exhaust gas flows of 200 Nm^3/h were used. However the overall flow, inlet concentration and pollutant type, plasma power and catalyst type and temperature were controllable and adjusted during experiments. A plate – to plate DBD reactor manufactured by Rafflenbeul Engineers was used. Power supply was a resonant – type, high efficiency converter [7].

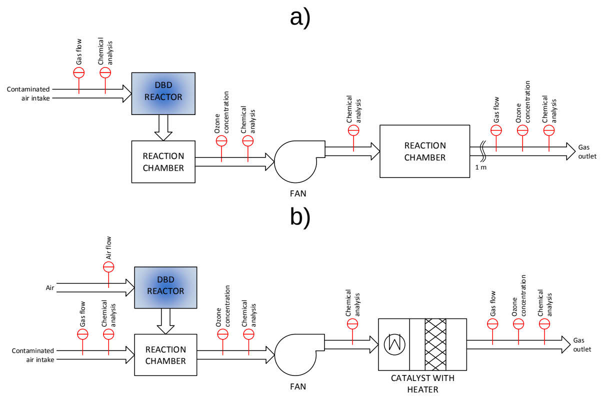

Fig.1. Exemplary configurations of the test – stand: a) direct plasma treatment; b) indirect, plasma – supported catalysis.

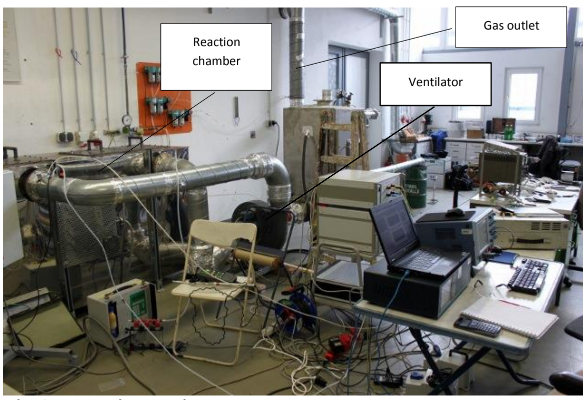

Fig.2. Experimental system setup.

Experimental results

Initially a direct plasma – based system was investigated for varying inlet concentrations, pollutant types and constant plasma power. Measurement results for ammonia, methanol and formaldehyde removal are presented in Fig. 3. As previously discussed a decreasing removal rate was noticed for increased input concentrations.

Table 1. Measurement equipment specification

Measured quantity	Device type	Device model
Ammonia concentration	Handheld ionizing detector	Tox-Meter PID Ex
	UV spectroscope	Probe preparation – Desaga Gasprobennehmer GS212, GS 312 Analysis – Hach – Lange DR 6000
Methanol concentration	Flame ionization detector	Bernath Atomic Modell 3005
	UV spectroscope	Probe preparation – Desaga Gasprobennehmer GS212, GS 312 Analysis – Hach – Lange DR 6000
Ozone concentration	Ozone monitor	MLU 450
Plasma reactor power	Digital oscilloscope	LeCroy 6100 A Wave Runner

a)

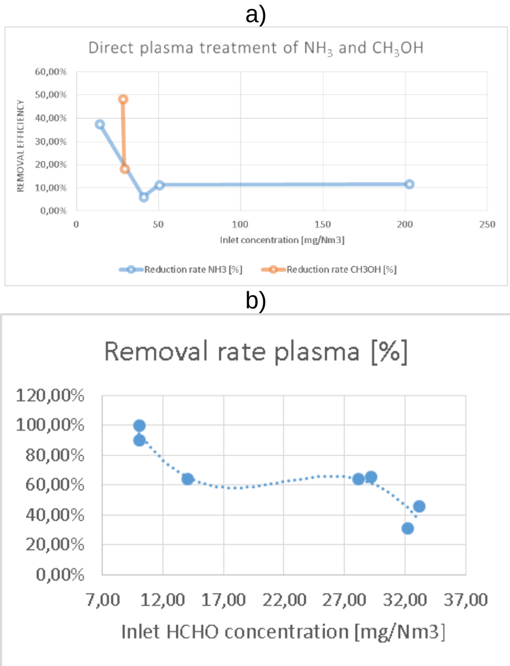

Fig.3. results of direct plasma treatment: a) removal of ammonia and methanol; b) removal of formaldehyde.

Indirect, plasma – assisted removal system, as presented in Fig. 1 b), was also examined under varying conditions. Exemplary results for ammonia removal are presented in Fig. 4. As can be noticed excellent removal rate of over 90% was achieved. A Cu-Mn-O catalyst was used with 230^{o}C bed temperature. Methanol removal rate is presented in Fig. 5.

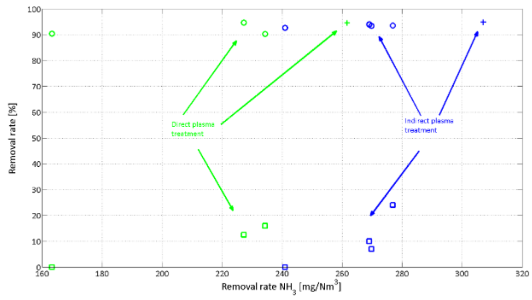

Fig.4. Ammonia removal rate for varying input concentrations. Squares represent plasma module removal efficiency.

Summary

A large – scale, plasma – assisted exhaust treatment facility was investigated for possible formaldehyde, methanol and ammonia removal operation. Plasma was proven to be effective but only for limited input concentrations, no significant differences between indirect and direct methods was noticed. Over 90% of removal efficiency was recorded for plasma – assisted catalytic treatment for a very broad range of input concentrations of all pollutants.

Acknowledgments: project supported using "Novel purification technique for the treatment of waste air in the manufacturing process of paraformaldehyde", project number LIFE11 ENV/DE/, task: ENV/DE/1073 (with financial contribution of the LIFE financial instrument of the European Union) and: "Industrial gas purification from VOC contaminants using non-thermal plasma units and hybrid plasma – catalytic systems", project number 14 0116-10/2010, financed by Narodowe Centrum Badań i Rozwoju, Polska.

REFERENCES

[1] Calvert S., Englund H.M., Handbook of Air Pollution Technology, Wiley, New York, 1984.
[2] National Research Council of the National Academies (US) 2011 Review of the Environmental Protection Agency's Draft IRIS Assessment of Formaldehyde (Washington: The National Academies Press) p. 134.
[3] US Environmental Protection Agency (US EPA), 2004. *Toxics Release Inventory* (TRI). <www.epa.gov/tri>.
[4] Holub, M, Borkowski, T. Jakubowski, T. Kalisiak, S. Myskow, J.: „Experimental Results of a Combined DBD Reactor-Catalyst Assembly for a Direct Marine Diesel-Engine Exhaust Treatment", *Ieee trans. on Plasma Science*, Volume: 41, Issue: 5, Pages: 1562-1569, Part: 2, DOI: 10.1109/TPS.2013.2254133
[5] Holub, M., Brandenburg, R. Grosch, H. Weinmann, S. Hansel, B.: „Plasma Supported Odour Removal from Waste Air in Water Treatment Plants: An Industrial Case Study", *Aerosol and Air Quality Research*, Volume: 14, Issue: 3, Pages: 697-707, DOI: 10.4209/aaqr.2013.05.0171.
[6] Rafflenbeul, R. (1998). Nicht-thermische Plasmaanlagen (NTP) zur Luftreinhaltung in der Abfallwirtschaft. *Müll und Abfall* 1/1998 (in german), pp. 38-44.
[7] Jakubowski T, Hołub M, Kalisiak S (2013) Resonant inverter with resonance frequency tracking for DBD plasma reactor supply. *Euro Phys J Appl Phys* 61 : 24304 - 24309. doi:10.1051/epjap/2012120430

***Author**: dr inż. Marcin Hołub, zachodniopomorski Uniwersytet Technologiczny w Szczecinie, Katedra Elektroenergetyki i Napędów Elektrycznych, ul. Sikorskiego 37, 70-313 Szczecin, e-mail: mholub@zut.edu.pl.*

PRZECIWDZIAŁANIE SKUTKOM SYNDROMU CHOREGO BUDYNKU W INTELIGENTNYCH SYSTEMACH AUTOMATYKI BUDYNKOWEJ

Marek B. HORYŃSKI

Lublin University of Technology

Abstract. *The building is said to be sick when its users complain about the onerous conditions of microclimate. This problem appeared upon the emergence of large office buildings fitted with a sealed bulkhead. It was assumed that the building is classified as sick as ca. 30% of people residing in it complains about bad indoor climate conditions.*

Streszczenie. *O chorym budynku mówi się wtedy, gdy jego użytkownicy skarżą się na uciążliwe warunki mikroklimatu. Problem ten pojawił z chwilą pojawienia się dużych budynków biurowych wyposażonych w szczelne przegrody. Przyjęto, że budynek jest klasyfikowany jako chory, gdy ok. 30 % osób przebywającym w nim uskarża się na złe warunki klimatu pomieszczeń.*

Keywords: sick building, intelligent building, sensors, concentration, automation.
Słowa kluczowe: chory budynek, inteligentna instalacja, czujniki, stężenie, automatyzacja.

Wstęp

W Polsce w okresie transformacji ustrojowej wiele budynków zmieniło przeznaczenie. Często łączyło się to z remontami w wyniku, których poprawiała się szczelność budynków oraz pogarszały warunki wymiany powietrza.
Zbyt oszczędnościowe projekty wentylacji powodowały pojawienie się wkrótce u mieszkańców przykrych dolegliwości, które są razem definiowane, jako czynniki powodujące syndrom chorego budynku (SBS). Jak wykazały badania Światowej Organizacji Zdrowia zaliczają się do nich:

- Niewłaściwa temperatura i wilgotność powietrza,
- Niewłaściwe oświetlenie,
- Zła jakość powietrza,
- Hałas.

SBS powoduje typowe reakcje alergiczne, takie jak zapalenie spojówek, problemy z układem oddechowym, np. zapalenia oskrzeli, astmy oskrzelowej i niealergiczne objawy takie jak - ból głowy, podrażnienie, zaburzenia koncentracji.

Źródłami zanieczyszczeń powietrza w pomieszczeniu mogą być organizmy żywe (np. produkty uboczne oddychania, pocenia się, grzyby, pleśnie), materiały budowlane i elementy wyposażenia wnętrz (np. rozpuszczalniki, impregnaty drewna, związki emitowane przez farby malarskie, azbest), systemy wentylacji i klimatyzacji (np. mikroorganizmy żyjące w nieczyszczonych przewodach wentylacyjnych), powietrze zewnętrzne (np. zanieczyszczenia chemiczne powietrza w dużych aglomeracjach miejskich) albo samo użytkowanie pomieszczeń (np. palenie tytoniu).

W 1984 Światowa Organizacja Zdrowia informowała, iż syndrom SBS występuje aż w 30% nowych i odnawianych budynków na świecie.
W Polsce przykładem chorego budynku był wybudowany na przełomie lat siedemdziesiątych i osiemdziesiątych budynek Intraco II w Warszawie. Zbyt mała ilość świeżego powietrza dostarczanego do pomieszczeń stała się przyczyną częstych omdleń pracowników.

Wybrane parametry klimatu wewnętrznego pomieszczeń

Człowiek jest gatunkiem stałocieplnym o temperaturze organizmu 36,60C.

Zmiana temperatury ciała może następować na skutek czynników wewnętrznych (I) lub zewnętrznych (II):
I: zaburzenia psychofizyczne, np. choroba, zmęczenie stres.
II: warunki środowiskowe, m.in.: temperatura otoczenia, wilgotność powietrza.
Optymalna temperatura dla człowieka zawiera się w zakresie 21-24^{0}C, właściwy jej dobór zależy od czynności aktualnie wykonywanej przez daną osobę, np. w czasie snu (18-19^{0}C).
Organizm został wyposażony w systemy uruchamiające procesy obronne pozwalające utrzymać stałą temperaturę ciała:

- pocenie się,
- skurcze mięśni (termogeneza drżeniowa).

W życiu codziennym bardzo ważne jest również, jaka jest temperatura odczuwalna, ponieważ wpływa to w znaczny sposób na zachowanie człowieka.

Na temperaturę odczuwalną mają wpływ inne warunki środowiskowe: wilgotność powietrza, prędkość wiatru i inne.
Wilgotność powietrza (%) informuje o zawartości pary wodnej w powietrzu.
Dla człowieka optymalna jej wartość zawiera się w przedziale 40-60%. Dla wyższych wartości zaczynają się pojawiać problemy z oddychaniem.
Jeżeli jednocześnie organizm poddany jest działaniu podwyższonych temperatur (25-29^{0}C) następuje zdecydowanie szybsze zmęczenie.

Kolejnym ważnym elementem klimatu wewnętrznego budynków jest skład chemiczny wdychanego powietrza, który ma wpływ na kondycję psychofizyczną człowieka. Powietrze powinno być zbliżone jak najbardziej do składu chemicznego powietrza atmosferycznego.
Niewłaściwy skład, np. nadmierne stężenie niektórych związków (CO^2), (CO - 100¸200 ppm – ból głowy) może być niebezpieczne dla człowieka i powodować dolegliwości: osłabienie, zaburzenia koncentracji, zawroty, depresje, arytmia serca.

Ważne jest również utrzymanie stałej cyrkulacji powietrza w pomieszczeniach użytkowanych przez człowieka. Każda osoba potrzebuje w ciągu godziny ok. 30 m^3 świeżego powietrza. Na samopoczucie człowieka ma również wpływ szybkość cyrkulacji powietrza.

Oprócz składu chemicznego powietrza, istotny jest także odpowiedni poziom jego zjonizowania. Nadmiar jonów dodatnich może powodować bóle głowy, zwiększone tętno, alergie i obniżoną odporność. Stwierdzono natomiast pozytywny wpływ jonów ujemnych. Stopień jonizacji powietrza w atmosferze waha się w zależności od pory roku oraz od lokalizacji, ale stosunek jonów dodatnich do ujemnych utrzymuje się na stałym poziomie i wynosi od 1 do 1,2. W skupiskach ludzkich z dużą ilością sprzętu elektronicznego i przemysłem występuje zwiększenie wytwarzania jonów dodatnich.

Kolejnym czynnikiem, który znacząco i długotrwale wpływa na człowieka jest stopień i jakość oświetlenia obiektów, w których on przebywa.

Promieniowanie słoneczne pozytywnie wpływa na układy kostne, sercowo-naczyniowe, immunologiczne. Dodatkowo zapobiega osteoporozie, atakom serca, udarom, sklerozie, cukrzycy.

Systemy zapewniające komfort w budynkach

Zmiana standardów, które pozwalają na zdefiniowanie poziomu luksusu, we współczesnych warunkach oprócz poprawy komfortu przyczyniła się do lepszego zabezpieczenia użytkowników przed syndromem chorego budynku SBS. Poprawiła się jednocześnie funkcjonalność budowli. Wprowadzone zmiany, często dzięki rozszerzeniu zakresu stosowania automatyzacji, pozwalają na zaoszczędzenie energii poprzez efektywne systemy obniżające zużycie energii elektrycznej. Dzięki nim mikroklimat kontrolowany przez inteligentne systemy o ściśle określonych parametrach komfortu stwarza bardzo dobre warunki do odpoczynku oraz do pracy zwiększając tym samym efektywność, jednocześnie minimalizując prawdopodobieństwo dotknięcia syndromem chorego budynku.

Do systemów zapewniających komfort zalicza się:

- Podsystem ogrzewania i chłodzenia
- Podsystem wentylacji i klimatyzacji
- Podsystem oświetlenia

W zależności od czynników wpływających na powstawanie tego syndromu oraz ze względu na choroby wywołane tymi czynnikami powinno dobrać się odpowiedni sposób przeciwdziałania. Wiąże się to oczywiście z ponoszonymi kosztami związanymi z wprowadzeniem poprawek oraz innowacji w pomieszczeniach. Do głównych sposobów przeciwdziałania możemy zaliczyć dwie grupy:

- Rozwiązania naturalne,
- Rozwiązania techniczne.

Rozwiązania naturalne opierają się głównie na zdroworozsądkowym użytkowaniu z danych pomieszczeń czy to mieszkalnych czy to biurowych przy zachowaniu czystości, wysokiej higieny, dobrego oświetlenia, natężenia dźwięku oraz dobrej jakości powietrza i innych czynnikach środowiskowych. Odpowiednie dbanie o środowisko wewnętrzne i korzystanie z urządzeń elektrycznych oraz optymalne wykorzystanie systemów będących na wyposażeniu w danym miejscu również stanowi pewną możliwość waliki i przeciwdziałaniem przeciwko danemu syndromowi.

Natomiast rozwiązania techniczne wykorzystują dostępną wiedzę i nowe technologie pozwalające zapobiegać syndromowi chorego budynku. Stanowią one, poprzez wprowadzenie odpowiednich rozwiązań technicznych, silny fundament pozwalający przeciwdziałać SBS. Dodatkowo umożliwiają monitorowanie parametrów środowiskowych wewnątrz pomieszczeń i sprawdzenie, czy wszystkie parametry znajdują się na określonym poziomie. Poza tymi zaletami wartością dodaną jest zwiększenie efektywności pracy dzięki poprawieniu samopoczucia, np. z pomocą systemów podnoszących komfort. Można tutaj wskazać na istotną rolę właściwego natężenia oświetlenia.

Ważnym elementem również jest zapewnienie odpowiedniej kolorystki ścian, stwierdzono bowiem istotny wpływ barwy na zachowanie człowieka. Ma on podłoże psychologiczne oraz fizjologiczne.

W Laboratorium Energooszczędnych Instalacji Budynkowych opracowano stanowisko badawcze, dzięki któremu możliwe jest badanie czynników wpływających na klimat pomieszczeń. Szczególną uwagę zwrócono w nim na implementację do tego celu systemów inteligentnego budynku. Na stanowisku laboratoryjnym zostały przeprowadzone pomiary, które wyjaśniają konieczność stosowania czujników parametrów otoczenia do stworzenia w pełni integralnej i funkcjonalnej sieci inteligentnej.

W celu zbadania warunków środowiskowych w danych pomieszczeniach tj.: sala konferencyjna, biuro, sale szkolne i przedszkolne oraz miejsce zamieszkania i miejsca, w których wentylacja jest ograniczona przydatny jest sensor jakości powietrza (air quality sensor). Konstrukcja stanowiska umożliwia prowadzenie symulacji odzwierciedlających rzeczywiste warunki panujące w budynku. Na podstawie obserwacji i manipulacji przyciskami czujniki odczytują stany logiczne na wejściach i odpowiednio reagują na zmianę temperatury, czy też ruch w pomieszczeniu.

Podsumowanie

Syndrom chorego budynku jest nadal trudny do identyfikacji ze względu na niską świadomość społeczeństwa oraz niski procent przebadanych pod tym kątem budynków. Brak jest rzetelnych badań i doświadczeń przedstawiających szkodliwość syndromu chorego budynku dla człowieka. Często bagatelizuje się SBS, który może okazać się dość poważnym problemem w wielu miejscach, które dotychczas nie były brane pod uwagę, np. przedszkola, czy domy opieki paliatywnej.

REFERENCES

[1] ABB. Materiały producenta na temat systemu KNX/EIB, 2014.

[2] Buczaj M., Sumorek A.: Wykorzystanie środowiska LabView do budowy systemu nadzoru kontrolującego parametry klimatyczne i techniczne w pomieszczeniach w gospodarstwie rolnym. Teka Komisji Motoryzacji i Energetyki Rolnictwa PAN, vol. 11, 2011.

[3] Gaziński B.: Zdrowy dom. Wydawnictwo Systherm, 2014.

[4] Horyński M., Styła S., Boguta A., Buczaj M., Sumorek A.: Model energooszczędnej instalacji domowej w warunkach budownictwa wiejskiego. Motrol. Motoryzacja i energetyka rolnictwa, nr 1, vol. 15, 2013.

[5] Kapica J., Ścibisz M.: Wykorzystanie środowiska LabView do tworzenia instrumentów wirtualnych wspomagających pomiary w inżynierii. Inżynieria Rolnicza, 2(90), 2007.

[6] Niezabitowska E.: Budynek inteligentny. Potrzeby użytkownika a standard budynku inteligentnego. Gliwice 2005.

[7] Trojanowska M., Szul T.: Determination of heat demand in rural communes. Teka Komisji Motoryzacji i Energetyki Rolnictwa PAN, 2008, 8a, s. 180–187.

***Autor**: dr inż. Marek B. Horyński, Politechnika Lubelska, Wydział Elektrotechniki i Informatyki, ul. Nadbystrzycka 38A, 20-618 Lublin, e-mail: m.horynski@pollub.pl*

8th International Conference
Electromagnetic Devices and Processes in Environment Protection ELMECO-8
joint with 11th Seminar Applications of Superconductors AoS-11
September 28 - October 1, 2014, Nałęczów, Poland

TRANSPOZYCJONERY NADPRZEWODNIKOWYCH TAŚM RÓWNOLEGŁYCH JAKO ALTERNATYWA DLA KABLA ROEBELA

Grzegorz WOJTASIEWICZ, Tadeusz JANOWSKI, Sławomir KOZAK, Janusz KOZAK, Michał MAJKA, Beata KONDRATOWICZ-KUCEWICZ

Electrotechnical Institute in Warsaw

Streszczenie. *W budowie transformatorów HTS koszt uzwojeń stanowi ponad połowę kosztów całkowitych, co przesądza o małym zainteresowaniu energetyki. Dotychczasowe doświadczenie autorów w zakresie projektowania i budowy modeli fizycznych elektrycznych urządzeń nadprzewodnikowych (elektromagnesy, transformatory, ograniczniki prądów zwarcia) wskazuje, że wyrównanie reaktancji w taśmach równoległych uzwojeń transformatora można wykonać dla całych cewek w odpowiednich „transpozycjonerach", uzyskując efekt jak w kablu Roebela CTC.*

Abstract. *The construction cost of the HTS transformer windings is more than half of the total transformer cost, which determines the low interest in the energy sector. Previous experience of the authors in the design and construction of physical models of superconducting electric devices (electromagnets, transformers, fault current limiter) indicates that the alignment of the transformer windings reactance, in parallel connected tapes, can be made for all coils in the appropriate "trans-positioners" to give effect similar as in the cable Roebel CTC (Continuously Transposed Cable).*

Słowa kluczowe: transformatory nadprzewodnikowe, taśmy nadprzewodnikowe HTS drugiej generacji, kabel Roebela, budowa uzwojeń
Keywords: superconducting transformer, 2G HTS tapes, Roebel Cable, windings construction

Wstęp

Obecnie wszystkie projekty energetycznych transformatorów nadprzewodnikowych zakładają wykonanie uzwojeń transformatorów z taśmy nadprzewodnikowej HTS 2-giej generacji (2G) [1]. Nadprzewodnikowe przewody HTS 2G mają strukturę warstwową, w której grubość warstwy nadprzewodnika wynosi około 1μm. O całkowitej grubości taśmy, (0,05 – 0,1) mm, decydują warstwy podłoża i stabilizatorów. Duża rezystywność warstw podłoża powoduje, że straty indukowane w warstwie nadprzewodnika przy prądzie przemiennym są bardzo małe.

W przypadku, gdy prądy robocze uzwojeń są większe od prądu krytycznego użytej taśmy nadprzewodnikowej, uzwojenia wykonuje się pakietem taśm równoległych. Poszczególne taśmy w pakiecie połączone są równolegle, a końce pakietu połączone są do zacisków zasilających [2]. Przy wielu taśmach w połączeniu równoległym, najbardziej oddalona od szczeliny powietrznej taśma jest skojarzona z najmniejszym strumieniem rozproszenia, zaś taśma położona najbliżej szczeliny – z największym (rys. 1).

Reaktancja poszczególnych taśm uzwojenia– ze względu na różne skojarzenie taśm ze strumieniem rozproszenia, nie są jednakowe. Jeżeli przyjmiemy że reaktancja $X_1 > X_2 > X_3 > X_n$ to popłyną prądy wyrównawcze $I_{w1} < I_{w2} < I_{w3} < I_{wn}$. Wyrównanie reaktancji poszczególnych warstw uzwojenia można uzyskać przez transpozycję taśm.

W przypadku uzwojeń transformatorów konwencjonalnych wykonanie transpozycji nie stwarza większych trudności [2]. Natomiast wykonanie „klasycznej„ transpozycji taśm nadprzewodnikowych jest w zasadzie niemożliwe ze względu na ich właściwości mechaniczne oraz proporcje w szerokości i grubości taśmy.

Obecnie największe nadzieje na ograniczenie prądów wyrównawczych w uzwojeniach nadprzewodnikowych transformatorów wiąże się ze stosowaniem przewodu CTC (Continuously Transposed Cable) –kabla Reobela, o ciągłej transpozycji przewodu nadprzewodnikowego [3]. Idea tego

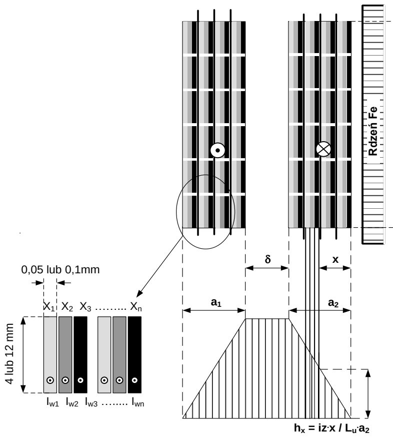

Rys. 1. Schemat uzwojenia nadprzewodnikowego nawiniętych czterema taśmami równoległymi: h_x – wartość chwilowa natężenia pola magnetycznego, a_1, a_2 – szerokość uzwojeń, L_u – wysokość uzwojeń, δ – szczelina powietrzna

kabla polega na odpowiednim ukształtowaniu i złożeniu (zapleceniu) pakietu równoległych taśm nadprzewodnikowych (wcześniej odpowiednio wyciętych), których liczba w pakiecie zależy od wymaganej wartości prądu krytycznego przewodu oraz spodziewanej wartości prądu krytycznego kabla [4].

„Bazowe" taśmy nadprzewodnikowe wykonane z nadprzewodnika HTS 2G o szerokości 12 mm lub 40 mm i grubości 0,1 mm – 0.2 mm tnie się na odpowiednio ukształtowane węższe „tasiemki" o szerokości 2 mm lub 5 mm. Prąd krytyczny taśmy o szerokości 5 mm wynosi około 100 A, a taśmy o szerokości 2 mm – około 50 A.

Aby uzyskać kabel Roebela o prądzie krytyczny 1000 A należy użyć 10 tasiemek o szerokości 5 mm (kabel 10/5) lub 20 tasiemek o szerokości 2 mm (kabel 20/2). Dla innych wartości prądu krytycznego liczba tasiemek w kablu będzie inna. Rysunek 2 przedstawia strukturę kabla Roebela 5/5, o prądzie krytycznym 500 A, a rys. 3 kabla 10/5, o prądzie krytycznym 1000 A. Rysunki te poza tym dobrze obrazują idee stałego przeplotu (transpozycji) taśm.

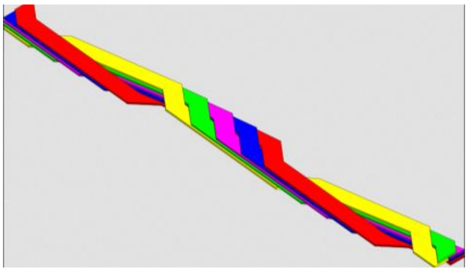

Rys. 2. Kabel Roebela 5/5 – 500 A. Kolorami oznaczono układ poszczególnych tasiemek w kablu

Rys. 3. Kabel Roebela 10/5 – 1000 A

Ze względu na wymagania technologiczne stawiane procesowi cięcia taśmy bazowej oraz procesowi ciągłej transpozycji, a także ze względu na duże straty w materiale taśmy bazowej podczas cięcia, cena kabla Roebela jest wysoka. Przykładowa cena 1 metra kabla Roebela 10/5 (10 taśm / 5 mm szerokich – łączna szerokość kabla – 12 mm) o prądzie krytycznym 1000 A wynosi około 3000 USD (dane producenta). Z tego względu kable te nie są powszechnie dostępne i produkowane są tylko na zamówienie. „Tradycyjne" nawinięcie uzwojenia transformatora pakietem taśm nadprzewodnikowych połączonych równolegle jest rozwiązaniem znacznie tańszym. Liczba taśm w pakiecie zależy od prądu krytycznego uzwojenia, a zatem od wartości prądu krytycznego zastosowanych taśm HTS. Za takim rozwiązaniem przemawia cena taśm nadprzewodnikowych 2G, która jest kilkakrotnie mniejsza od ceny kabla Roebela.

W tablicy 1 podano liczbę wybranych taśm HTS 2G, produkcji SuperPower Inc o szerokości 4 mm i 12 mm dedykowanych na uzwojenia transformatorów nadprzewodnikowych, połączonych równolegle w celu nawinięcia uzwojenia na prąd krytyczny 1000 A, grubość pakietu taśm oraz cenę jednostkową takiego pakietu .

Tablica 1. Liczba taśm w pakiecie, grubość i cena pakietu o prądzie krytycznym 1000 A

Taśma	Liczba taśm połączonych równolegle	Grubość pakietu taśm (z uwzględnieniem izolacji), mm	Cena pakietu taśm, USD/m
SCS 4050 @ 100 A	10	1,5	850
SF 4050 @ 100 A	10	1,1	650
SCS 12050 @ 300 A	4	0,6	520
SF 12050 @ 300 A	4	0,5	460
Grubość kabla Roebela 10/5, 1000 A – około 2 mm			

Aby całkowicie wyrównać rozpływ prądu w taśmach HTS 2G, połączonych równolegle, konieczne jest opracowanie technologii ich łączenia przy użyciu specjalnych łączników – transpozycjonerów, które pozwolą na swobodne łączenie taśm pomiędzy warstwami. Dotychczasowe analiza zjawisk, zachodzących w uzwojeniach nadprzewodnikowych transformatorów energetycznych, rozważania teoretyczne, a także doświadczenie autorów w łączeniu taśm nadprzewodnikowych oraz wykonywaniu uzwojeń urządzeń nadprzewodnikowych (elektromagnesy, transformatory, ograniczniki prądu zwarcia) prowadzi do hipotezy, że „przeplecenia taśm" można zrealizować poza zwojami uzwojeń przez transpozycjonujące łączniki. Idee transpozycjonowania taśm HTS połączonych równolegle przedstawia rys. 4

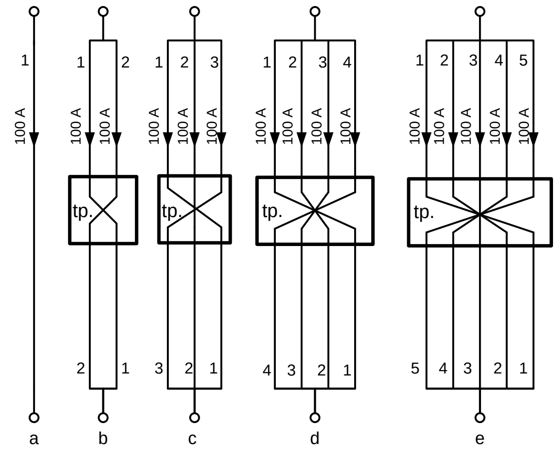

Rys. 4. Idea zastosowania transpozycjonerów (tp.) taśm HTS 2G połączonych równolegle (b – e): a – pojedyncza taśma HTS o prądzie krytycznym 100 A

Liczba i miejsce umieszczenia łączników zależy od parametrów, wymiarów i kształtu uzwojeń. Rozmiar i kształt łącznika oraz liczba „realizowanych" przepleceń zależy od miejsca jego umieszczenia oraz liczby taśm połączonych równolegle, a także ich szerokości (4 mm lub 12 mm) i wartości prądu krytycznego.

LITERATURA

[1] Wojtasiewicz G., Janowski T., Kozak S., Kozak J., Majka M., Kondratowicz-Kucewicz B., Tests and Performance Analysis of 2G HTS Transformer, *IEEE Trans. on Appl. Supercond.*, Vol. 23, Vo 3, Article No: 5500505, 2013

[2] Jezierski E., Transformatory: Budowa i projektowanie. WNT 1965

[3] Glasson N., Staines M., Buckley R., Pannu M., Kalsi S., Development of a 1 MVA 3-Phase Superconducting Transformer Using YBCO Roebel Cable, *IEEE Trans. on Appl. Supercond.*, Vol. 21, No 3, 2011, 1393-1396

[4] Long N. J., Badcock R. A., Hamilton K., Wright A, Jiang Z., Lakshmi L. S., Development of YBCO Roebel cables for high current transport and low AC loss applications, *Journal of Physics: Conference Series*, Vol. 234, Part 2, 2010 doi:10.1088/1742-6596/234/2/022021

***Autorzy**: dr inż. Grzegorz Wojtasiewicz, prof. dr hab. inż. Tadeusz Janowski, prof. dr hab. inż. Sławomir Kozak, dr inż. Janusz Kozak, dr inż. Michał Majka, mgr inż. Beata Kondratowicz-Kucewicz, Electrotechnical Institute in Warsaw, Laboratory of Superconducting Technologies in Lublin, Nadbystrzycka 36a, 20-618 Lublin, E-mail: g.wojtasiewicz@iel.waw.pl, t.janowski@pollub.pl, s.kozak@iel.waw.pl, j.kozak@iel.waw.pl, m.majka@iel.waw.pl, b.kondratowicz-kucewicz@iel.waw.pl*

8th International Conference
Electromagnetic Devices and Processes in Environment Protection ELMECO-8
joint with 11th Seminar Applications of Superconductors AoS-11
September 28 - October 1, 2014, Nałęczów, Poland

OVERCURRENT CHARACTERISTICS OF SF4050 2G SUPERCONDUCTING TAPE

Leszek JAROSZYŃSKI, Dariusz CZERWIŃSKI

Lublin University of Technology, Institute of Electrical Engineering and Electrotechnologies

***Abstract**. Authors made measurement for the SF4050 high-T_C superconductor coated tape produced by SuperPower Inc. The measurements were performed for the AC current amplitudes exceeding the critical value of this tape. The numerical model of the tape was build using PSpice environment. The model assumes the nonlinearities of tape parameters as the functions of temperature, as well as the variable cooling conditions during transient state. Simulation results were compared with measurement data.*

***Streszczenie.** Autorzy przeprowadzili pomiary dla taśmy nadprzewodnikowej SF4050 produkowanej przez SuperPower Inc. Badania wykonano dla prądu zmiennego o amplitudach przekraczających wartość krytyczną prądu taśmy. Przy wykorzystaniu środowiska PSpice zbudowano model numeryczny uwzględniający nieliniowość parametrów taśmy i warunków chłodzenia. Wyniki symulacji porównano z danymi pomiarowymi.*

Keywords: high temperature superconductor, HTS coated tape, superconducting fault current limiters, quench propagation.
Słowa kluczowe: nadprzewodnik wysokotemperaturowy, taśma nadprzewodnikowa drugiej generacji, nadprzewodnikowy ogranicznik prądów zwarciowych, propagacja strefy rezystywnej.

Introduction

Advancements in the manufacturing of the second generation (2G) high-T_C superconductor coated tapes, allows for the production of superconducting fault current limiters (SFCL) of unique characteristics. The analysis of the phenomena in YBCO coated conductors during transient state is very important for the reliable operation of superconducting device. A study of transient voltage responses in HTS materials has been performed in the past twenty years; transitions of thin YBCO films from superconducting to resistive state and back induced by a current pulse have been observed [1]-[3].

In our earlier research we developed efficient PSpice models for bulk HTS components and first generation (1G) tapes used for SFCLs [4-6]. Then, we modified the model for 2G HTS coated conductors [7]. Emphasis was put on the temperature dependent material parameters and the heat exchange in LN_2 bath for currents higher than the critical value. In this paper we continue the verification of this approach and we compare simulation results and laboratory data for SF4050 2G HTS tape produced by SuperPower Inc.

Measurements

The HTS layer thickness in the SF4050 tape is around 1 µm, what gives relatively high critical current value ranging from 110 A to 115 A at 77 K (self-field). Substrate is made of nonmagnetic metal alloy – Hastelloy C276. This tape has no copper stabilizers. Basic tape parameters are shown in Table 1.

Table 1. The parameters of the SF4050 tape

Parameter	Value
Tape width	4 mm
Tape thickness	55 µm
Critical current at 77 K (DC, self-field)	110-115 A
Critical temperature	93 K
HTS (Re)BCO layer thickness	1 µm
Silver overlayer thickness (upper/lower))	2.0/1.8 µm
Buffer stack thickness	0.2 µm
Substrate (Hastelloy C276) thickness	50 µm
Substrate resistivity	125 µΩcm

The experiment involved voltage measurements on the probes soldered to the HTS tape (7 probes spaced 2 cm, 6 tape segments) when it was supplied for a short period of time with AC current greater than the critical value. The tape was immersed in liquid nitrogen bath (LN_2) under atmospheric pressure. The voltages were measured differentially on each of tape segments (Fig.1).

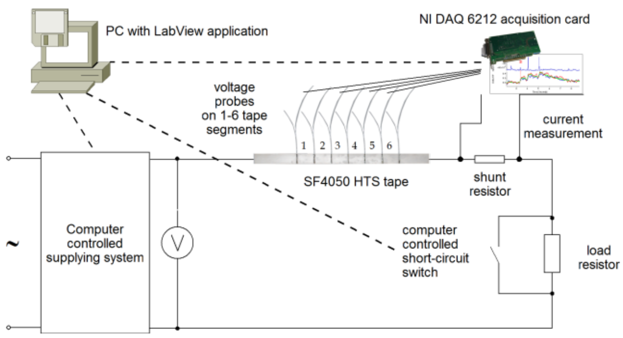

Fig.1. Measurement arrangement of HTS tapes

Test stand, shown in Fig.2, consists of three main elements: examined tape, data acquisition stand and supplying system. The SF4050 tape with soldered measuring probes is placed in the liquid nitrogen bath (1). Computer controlled supplying system (3) allows for automatic switching of the supply voltage and for the computer control of current amplitude. Data acquisition stand (2) contains: National Instrument DAQ Card, PC computer and data acquisition software written in LabView environment.

Before the overcurrent test, current of low value was passed through the tape for the observation of waveforms in steady state. After this, the overcurrent switch was turned on automatically by computer controlled supplying system. The amplitude of the quench current was also set in the supplying system. Current and corresponding voltage waveforms were recorded for supplying current higher than the critical value.

Fig.2. Test stand for measuring the overcurrent response of the tape: 1 – HTS 2G tape in LN_2 bath, 2 – data acquisition, 3 – computer controlled supplying system

For the tape batch the manufacturer reported the critical current value I_C=113 A. The exemplary measurement results are presented in Fig.3.

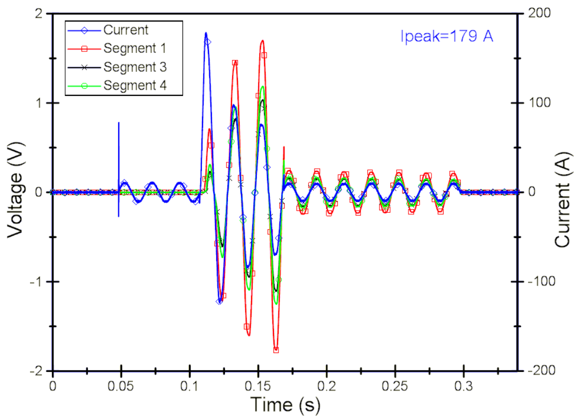

Fig.3. Voltage and current waveforms for tape segments that lost stability (I_m/I_C=1.584)

Numerical model

HTS coated tape simulations for SFCL devices can be performed with the use of FEM. The ratio of thickness of superconducting layer to HTS tape width can be high as 1:10000. These extremely thin subdomains are very difficult to mesh and to analyse using finite element method [8]. In this case, computer simulation of the SuperPower 2G HTS tape was completed using PSpice and its analogue behavioural modelling blocks. Non-linear components were built of voltage- and current-controlled sources [4-7].

Electric properties of the SF4050 tape may be described in a simplified form as shown in Fig. 4.

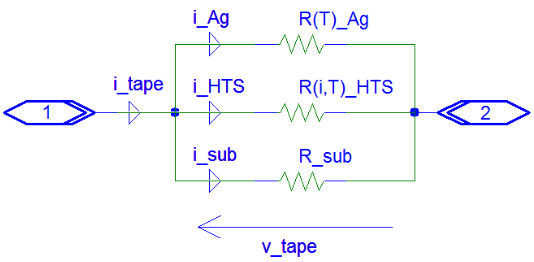

Fig.4. Equivalent circuit of the HTS tape

Equivalent circuit of a single tape section consists of two non-linear resistors representing high temperature superconductor and silver over-layer and the linear resistor of the substrate. YBCO buffer stack was not considered here.

Resistivity of the silver over-layer is considered as temperature-dependent. Hastelloy resistivity is stable in wide temperature range and its temperature dependence is ignored.

Neglecting magnetic field influence, HTS electric properties can be described by equation (1).

$$E(J) = E_C[J / J_C(T)]^{n(T)} \tag{1}$$

where: E – electric field strength, E_C – constant (transition criterion for HTS), J – current density, J_C – temperature dependent superconductor critical current density, n – temperature dependent power law n-exponent.

The tape cooling rate was determined by the different modes of liquid nitrogen boiling i.e.: nucleate, transition and film boiling.

Conclusion

The simplified approach makes the model fast and reliable as well. The numerical results show very good compatibility with the measurements made for SF4050 tape. The applied model is versatile and may represent, after simple parameter modifications, other types of YBCO coated conductors and superconducting coils built of 2G HTS in some cases.

REFERENCES

[1] Bluzer N., Temporal relaxation of nonequilibrium in YBaCuO measured from transient photoimpedance response", Phys. Rev., vol. B44 (1991), 10222-10333
[2] Hegmann F., Hughes R., Preston J., Picosecond photoresponse of epitaxial YBa2Cu3O7 thin films, Appl. Phys. Lett., vol. 64 (1994), 3172-3174
[3] Karasik B., Milostnaya I., Zorin M., Elantev A., Gol'tsman G., Gershenzon E., High Speed Current Switching of Homogeneous YBaCuO Film Between Superconducting and Resistive States, IEEE T. Appl. Supercon., vol. 5, no. 2 (1995), 3042-3045
[4] Czerwiński D., Jaroszyński L., Symulacja komputerowa materiałów HTS z użyciem PSPICE – Computer Simulation of HTS Components Using PSPICE, 7th Seminar & Workshop – Applications of Superconductors, Kazimierz Dolny June 1-3, 2006, Liber Duo, Lublin (2007), 139-146
[5] Jaroszyński L., Czerwiński D., Modelowanie numeryczne elementów nadprzewodnikowych – Numerical simulation of superconducting elements, 8th Seminar & Workshop – Applications of Superconductors, Nałęczów, June 17-21, 2007, Liber Duo, Lublin (2008), 112-121
[6] Czerwiński D., Jaroszyński L., Kozak J., Majka M., Equivalent Electromagnetic Model for Current Leads Made of HTS tapes, Prz. Elektrotechniczn., No. 9b (2012), 230-233
[7] Czerwiński D., Jaroszyński L., Janowski T., Majka M., Kozak J., Analysis of Alternating Overcurrent Response of 2G HTS Tape for SFCL, IEEE Trans. Appl. Supercon., vol. 24, issue 3 (2014), 5600104
[8] Jaroszyński L., Czerwiński D., Numerical Analysis of YBCO Coated Conductors, Prz. Elektrotechniczn., nr 10b (2012), 160-162

***Authors**: dr inż. Leszek Jaroszyński, e-mail: l.jaroszynski@pollub.pl, dr hab. inż. Dariusz Czerwiński, e-mail: d.czerwinski@pollub.pl; Politechnika Lubelska, Instytut Podstaw Elektrotechniki i Elektrotechnologii, ul. Nadbystrzycka 38A, 20-618 Lublin*

8th International Conference
Electromagnetic Devices and Processes in Environment Protection ELMECO-8
joint with 11th Seminar Applications of Superconductors AoS-11
September 28 - October 1, 2014, Nałęczów, Poland

CONDUCTED ELECTROMAGNETIC DISTURBANCES CAUSED BY THE IGNITION ELECTRODE OF THE GLIDARC PLASMA REACTOR

Andrzej WAC-WŁODARCZYK[1], Andrzej KACZOR[2]

Lublin University of Technology, Institute of Electrical Engineering and Electrotechnologies (1),
Office of Electronic Communications Lublin Branch (2)

Streszczenie. *Artykuł przedstawia zagadnienia związane z przewodzonymi zaburzeniami elektromagnetycznymi jakie emitują wyładowania elektrod zapłonowych reaktora plazmowego typu GlidArc. Na wartości emitowanych zaburzeń elektromagnetycznych mogą mieć wpływ różne parametry pracy reaktora oraz parametry zasilania reaktora w tym w szczególności zaburzenia pochodzące od elektrod zapłonowych. W pracy zaprezentowano różne pomiary napięć zaburzeń przewodzonych na liniach zasilających reaktor plazmowy.*

Summary. *The article presents issues connected with conducted electromagnetic disturbances, which emit ignition electrode discharges of a plasma reactor type GlidArc. Various parameters of the working reactor as well as power of the reactor including especially disturbances coming from ignition electrodes can have an influence on numbers of emitted electromagnetic disturbances. The paper presents different measurements of voltage disturbances conducted in the plasma reactor power lines.*

Keywords: Electromagnetic compatibility, conducted electromagnetic disturbances, plasma reactor, arc discharges.
Słowa kluczowe: Kompatybilność elektromagnetyczna, zaburzenia przewodzone, reaktor plazmowy, wyładowania łukowe.

Introduction

Plasma reactor with sliding arc discharge called also as GlidArc is a generator of non thermal plasma. Plasma is produced by discharges, which occur between working electrodes of the reactor [1].

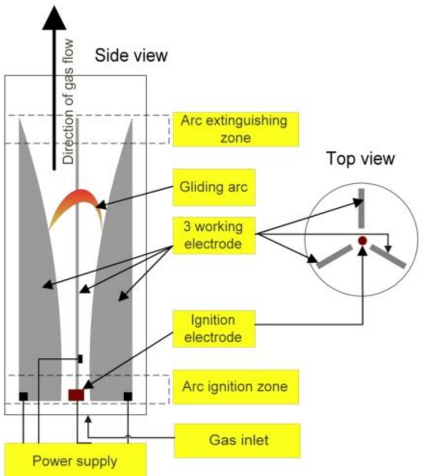

Fig.1. The diagram of plasma reactor type GlidArc

Discharges between electrodes are serial and their initiation frequency depends on many parameters of working reactor, such as the speed of working gas flow, voltage of working electrodes and the shape of electrodes.

In order to lower the voltage on working electrodes needed to initiate the arc we need to apply additional ignition electrode, which ionizes the working gas between working electrodes.

Discharges produced on ignition electrode are also the source of conducted disturbances. For this reason we need to take them into account during reactor measurement in the scope of electromagnetic compatibility.

Measurement of voltage conducted disturbances

Measurements of voltage conducted disturbances were carried out on the system presented on picture number 2. Two line impedance stabilization network were connected to the system, one triphase in the system of working electrodes and monophase in the ignition electrode system.

The system of working electrodes was supplied with three separate transformers, and ignition electrode was supplied with a single high voltage. In the power supply system of both working electrodes and ignition no additional electronic elements were used, which as a result could affect the values of measured voltage disturbances.

Fig.2. Measuring system of voltage conducted disturbances of plasma reactor type GlidArc

Line impedance stabilization networks fulfiled the role both filter, which made it impossible to flow the voltage disturbances from the external energy network to measuring system and measuring system to connect measuring device.

Measurings were done with out of order electrodes, and discharges inside the reactor came solely from ignition electrode system. Moreover, circuit diagram in power supply ignition electrodes system was changed. The same situation happened with the value voltage of their power supply and the value of air flow in column reactor.

Measurements were mostly carried out with the use of quasi peak and average detector worth with observation time of one second and 9 kHz filter. Due to long time of a single observation, measurements were carried out on selected frequencies from the full measuring scope from 150 kHz to 30 MHz.

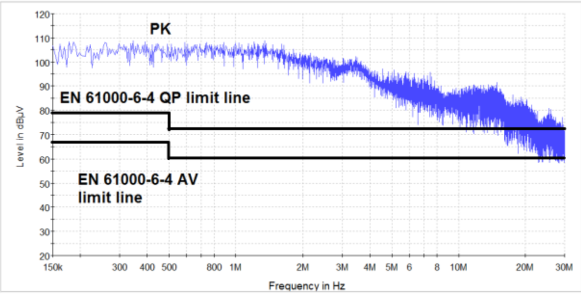

Fig.3. Values of voltage disturbances on the line powering working electrodes L1

For a better depiction of voltage disorders level, on picture number 3 we can see the values of measured voltage disorders with electrodes both working and ignition. Moreover, on this picture acceptable disturbances values for industrial environment specified by harmonized norm are marked [2].

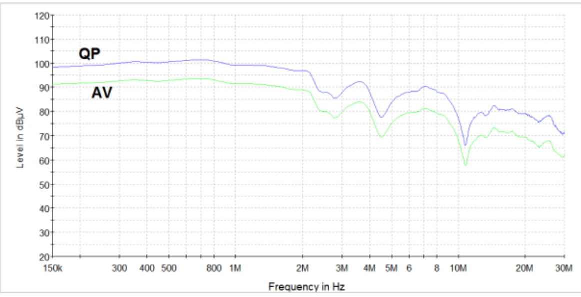

Fig.4. Values of voltage disturbances on the power supply line L1 (working electrodes) with working only ignition electrode (monoelectrode system)

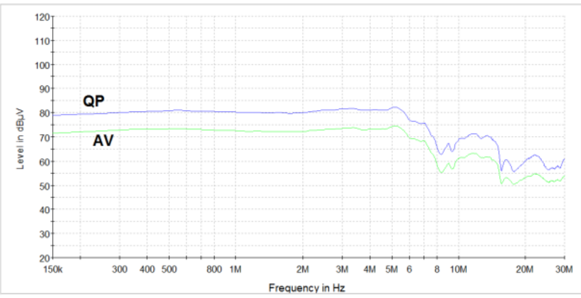

Fig.5. Values of voltage disturbances on the power supply line L (ignition electrode) with working only ignition electrode

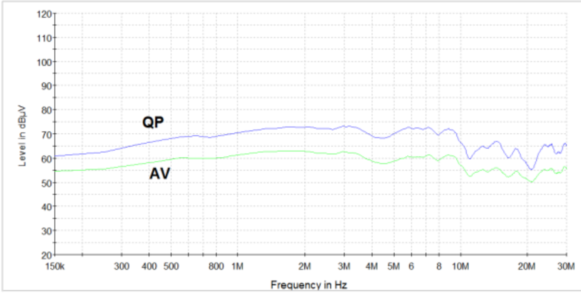

Fig.6. Values of voltage disturbances on the power supply line L1 (working electrodes) with working only ignition electrode (two electrode system)

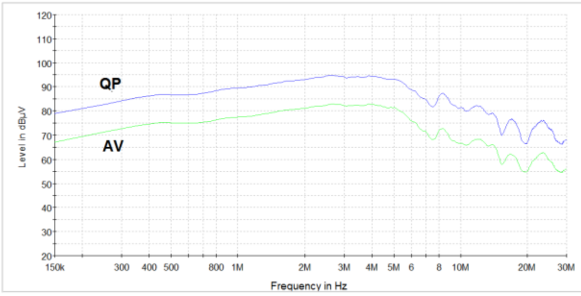

Fig.7. Values of voltage disturbances on the power supply line N (working electrodes) with working only ignition electrode (mono electrode system)

Conclusions

Measurements of voltage conducted disturbances on lines powering the plasma reactor type GlidArc both in working system and ignition indicates that acceptable levels specified by environmental norm are significantly exceeded [2]. These values are exceeded both with working reactor and with working only ignition electrodes. The level of voltage conducted disturbances depends on the place of measurement of disturbances on powering lines, ignition electrodes system and the value of ignition electrodes powering voltage and the flow of working gas.

Before putting the plasma reactor into operation, values of voltage conducted disturbances need to be measured in laboratory or at the place where it was installed – as a stationery installation [3]. As presented results show the measurements of voltage conducted disturbances coming from only discharges designed solely to ionize the working gas are slightly of a lower value than the levels of discharges coming from plasma reactor working. Such information needs to be taken into account both when designing the elements lowering values of voltage conducted disturbances and In the course of its further use.

REFERENCES

[1] Stryczewska H.D., "Technologie plazmowe w energetyce i inżynierii środowiska", Wydawnictwo Politechniki Lubelskiej, Lublin, (2009)

[2] PN-EN 61000-6-4:2004 "Kompatybilność elektromagnetyczna (EMC) Część 6-4: Normy Ogólne Norma emisji w środowiskach przemysłowych", Polski Komitet Normalizacyjny, Warszawa (2004)

[3] Kaczor A., Wac-Włodarczyk A. *"Ocena zgodności wyrobów z wymaganiami zasadniczymi w zakresie kompatybilności elektromagnetycznej"*, *Przegląd Elektrotechniczny*, 12 (2009), 61-64

Authors: prof. dr hab. inż. *Andrzej Wac-Włodarczyk, Politechnika Lubelska, Instytut Podstaw Elektrotechniki i Elektrotechnologii, ul. Nadbystrzycka 38a, 20-618 Lublin, Polska, e-mail: a.wac-wlodarczyk@pollub.pl; mgr inż. Andrzej Kaczor, Urząd Komunikacji Elektronicznej Delegatura w Lublinie, ul. Zana 38c, 20-601 Lublin, Polska, e-mail: a.kaczor@uke.gov.pl*

8th International Conference
Electromagnetic Devices and Processes in Environment Protection ELMECO-8
joint with 11th Seminar Applications of Superconductors AoS-11
September 28 - October 1, 2014, Nałęczów, Poland

MAGNETIC PROPERTIES OF MULTILAYERS [NI-FE/AU/CO/AU]$_6$.

Robert RANECKI[1,2], Maciej KAMIŃSKI[2], Mirosław SZYBOWICZ[2], Anna DYCHALSKA[2], Małgorzata BŁASZYK[1], Tadeusz LUCIŃSKI[1], Bronisław SUSŁA[2]

Institute of Molecular Physics Polish Academy of Sciences, Poznan (1), Poznan University of Technology (2)

Abstract*. We present the possibility to study magnetic properties of thin magnetic films using Raman spectrometer. The method is based on the observation of standing spin waves. Experimental data are presented for Si(111)[NiFe(2nm)/Au(2nm)/Co(0,8nm)/Au(2nm)]$_6$ multilayers which exhibit perpendicular anisotropy of cobalt film and giant magnetoresistance.*

Streszczenie. *Przedstawiamy możliwość badania właściwości magnetycznych cienkich warstw metali ferromagnetycznych za pomocą spektrometru ramanowskiego rozpraszania światła. Metoda opiera się na obserwacji stojących fal spinowych. Przedstawiono wyniki eksperymentu dla struktur Si(111)[NiFe(2nm)/Au(2nm)/Co(0.8nm)/Au(2nm)]$_6$* charakteryzujących się prostopadłą anizotropią warstwy kobaltu, oraz występowaniem gigantycznego magnetooporu.

Keywords: standing spin waves, magnetic multilayers, giant magnetoresistance.
Słowa kluczowe: stojące fale spinowe, wielowarstwy magnetyczne, gigantyczny magnetoopór.

Introduction

Magnetic multilayer structures exhibiting giant magnetoresistance (GMR) and perpendicular anisotropy attract much attention due to possibility to apply them commercially in high density data storage devices and magnetic field sensors. In particular, an increasing attention is devoted to [NiFe/Au/Co/Au]$_N$ multilayer systems, where the NiFe(2nm) layer exhibits parallel anisotropy, the Au(2nm) layer provides weak interlayer coupling and the Co(0.8nm) layer exhibits perpendicular anisotropy [1,2].

Magnetic properties of thin films were investigated in the past by Brillouin light scattering and spin wave resonance [3]. However, these methods are limited to small wave vector [3]. It was predicted theoretically, that measurements of large wave vector spin waves would allow determination of microscopic quantities [4]. So far, large wave vector spin waves were investigated by magnetic neutron scattering, however, interaction of neutrons with spin waves is to weak to measure thin magnetic films. The most recent publications on the topic present experimental data which shown that with the spin-polarized electron energy loss spectroscopy, by measuring scattering on standing spin waves, it was possible to determine exchange coupling constant of thin cobalt film [5,6].

Experimental details

[NiFe(2nm)/Au(2nm)/Co(0,8nm)/Au(2nm)]$_6$ multilayers were deposited onto Si(111) substrate using molecular beam epitaxy in an ultra-high vacuum chamber (base pressure 10^{-10} mbar range; from *PREVAC*). The deposition rates, calibrated using quartz microbalance (*Maxtec*), were 0.05 nm/s, 0.06 nm/s, and 0.05nm/s for NiFe, Au, and Co, respectively. Giant magnetoresistance was measured using four-point probe (*home made*) in a current-in-plane geometry. The magnetic field range was H=±2 T. Magnetic force microscopy (MFM) studies were performed in air using easyScan 2 AFM system (from *Nanosurf*) operating in MFM dynamic mode. The maximum scan area was 10×10μm^2. Raman light scattering spectra were recorded at room temperature using inVia Raman microscope (from *Renishaw*) operating in a 180° backscatter geometry. The excitation wavelength was 785 nm. Dielectric edge filter allowed to record Raman spectra from 100 to 3200 cm^{-1}.

Results and discussion

The GMR(H) data obtained for multilayers [NiFe(2nm)/Au(2nm)/Co(d_{Co})/Au(2nm)]$_6$ grown on Si(111) substrate are plotted in Figure 1. For perpendicular anisotropy of cobalt film (d_{Co}=0,8nm) in remanence, the demagnetization field, originating from each of the magnetic stripe-like domains of cobalt, causes a shift in the local magnetic torque of NiFe layer. This leads to a reduction in effective angle between the magnetic moments of the layers and reduces the magnetoresistance. At the value of magnetic field, in which the magnetic stripe domains of cobalt sublayers are nucleated or annihilated, characteristic growth of magnetoresistance, which value depend on direct changing of magnetic field, is observed. In the magnetic field range exceeding ±1T only the NiFe contribution is observed. The inset presents a 5×5 μm^2 MFM image of phase contrast in dynamic mode MFM (the tip sample distance was 65 nm). Stripe-like magnetic domain structure was observed.

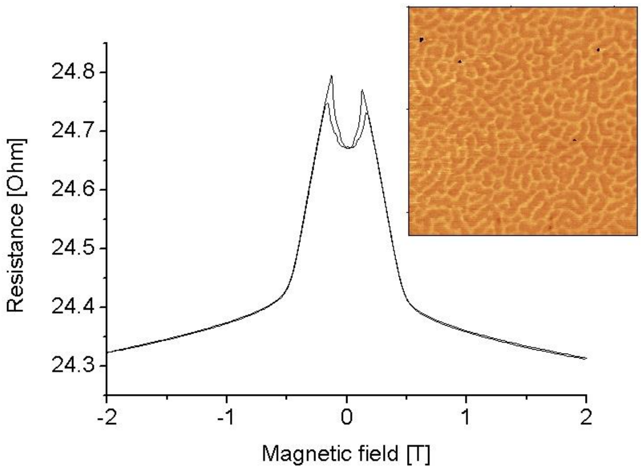

Fig.1 Room temperature giant magnetoresistance for perpendicularly applied magnetic field measured for [NiFe(2nm)/Au(2nm)/Co(d_{Co})/Au(2nm)]$_6$ on Si(111).

The Raman spectrum obtained for $[NiFe(2nm)/Au(2nm)/Co(d_{Co})/Au(2nm)]_6$ multilayer on Si(111) is presented in Figure 2. The first, second, and third order Raman optical modes of Si substrate yields energy 519 cm^{-1}, 950 cm^{-1}, 2500 cm^{-1} respectively. The peak observed around 301 cm^{-1} arises from second order Raman scattering by transverse acoustic phonons also of Si substrate. Based on the literature, other excitations could originate from standing spin waves [4-6].

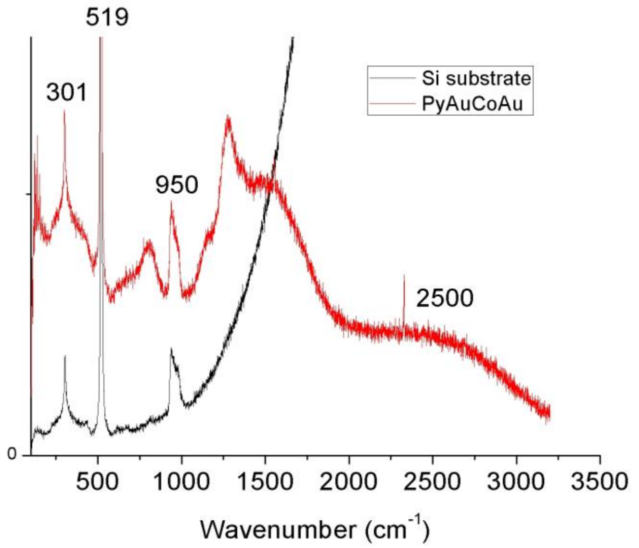

Fig.2. Raman spectra obtained at room temperature for $[NiFe(2nm)/Au(2nm)/Co(0,8nm)/Au(2nm)]_6$ on Si(111).

Conclusions

We present an accessible metod to determination of microscopic quantities in ultrathin magnetic films. This metod is based on observation of high energy and high wave vector standing spin wave modes using Raman spectrometer in comparison to theoretical studies [4], and the results of experiments [5,6].

Acknowledgments

This work was supported by the Poznań University of Technology Grant No 06/62/DSPB/0214.

REFERENCES

[1] F. Stobiecki, B. Szymański, T. Luciński, J. Dubowik, M. Urbaniak, K. Roell, J. Magn. Magn. Mater. 282, 32 (2004).
[2] B. Szymański, F. Stobiecki, M. Urbaniak, P. Siffalovic, E. Majkova, Acta Phys. Pol. 113, 205 (2008).
[3] Topics in Applied Physics, edited by B. Hillebrands and K. Ounadjela (Spinger-Verlag, Berlin, 2002), Vol. 83.
[4] R. Wieser, E. Y. Vedmedenko, and R. Wiesendanger, Phys. Rev. B 79, 144412 (2009).
[5] R. Vollmer, M. Etzkorn, P.S. Anil Kumar, H. Ibah, J. Kirchner, Phys. Rev. Lett. 91 147201 (2003).
[6] J. Rajeswari, H. Ibach, C. M. Schneider, Phys. Rev. Lett. 112, 127202 (2014).

***Authors**: mgr inż. Robert Ranecki e-mail: ranecki@ifmpan.poznan.pl*, dr Małgorzata Błaszyk e-mail: blaszyk@ifmpan.poznan.pl, *prof. IFMPAN dr hab. Tadeusz Luciński e-mail: lucinski@ifmpan.poznan.pl, Instytut Fizyki Molekularnej Polskiej Akademii Nauk, ul. Mariana Smoluchowskiego 17, 60-179 Poznań; dr* Maciej Kamiński e-mail: maciej.kaminski@put.poznan.pl, dr hab. Mirosław Szybowicz e-mail: miroslaw.szybowicz@put.poznan.pl, mgr inż. Anna Dychalska e-mail: anna.dychalska@put.poznan.pl, prof. dr hab. Bronisław Susła e-mail: bronisław.susla@put.poznan.pl, Politechnika Poznańska, Instytut Fizyki, ul. Nieszawska 13A, 60-985 Poznań, 85, 61-614 Poznań.

SPACE CHARGE DISTRIBUTION IN PVDF NANOCOMPOSITES WITH ORGANOCLAY FILLERS

Anna KISIEL[1], Małgorzata ŻABSKA[2], Radosław CHOWANIEC[1]

Institute of Electrical Engineering Fundamentals, Wroclaw University of Technology (1)
Polymers Engineering and Technology Division, Wroclaw University of Technology (2)

***Abstract**. The aim of the study was to determinate charge distribution in the PVDF nanocomposites with organically modified clay based on motmorillonite. Sample microstructure investigation revealed that the addition of organoclay can induce the piezoactive crystal phase – β-PVDF in all prepared composites.The results of space charge measurements made by the electrically stimulated acoustic wave method (ESAW) have shown the differences in space charge value and distribituion between the pure PVDF and its composites.*

***Streszczenie.** Celem prezentowanej pracy było określenie rozkładu ładunku przestrzennego w nanokompozytach PVDF z dodatkiem napełniaczy w postaci organicznie zmodyfikowanego montmorylonitu. Wyniki pomiaru ładunku przestrzennego, wykonane metodą elektrycznie stymulowanej fali akustycznej (ESAW), wskazują na różnice w wartości i rozkładzie ładunku w czystym polimerze PVDF i nanokompozytach na jego bazie.*

Keywords: ESAW method, electret, montmorillonite, nanocomposite.
Słowa kluczowe: metoda ESAW, elektret, montmorylonit, nanokompozyt.

Introduction

Analysing scientific publications in recent years can be seen that one of the most intensively studied groups of materials is now composite materials.

It has long been known ceramic, polymer and ceramic-polymer composites, but a new group of materials – nanocomposites has attracted a great interest of late. The addition of various kinds of nanoparticles significantly changes the physical and chemical properties of the composite. They differ from these using conventional fillers. Nanocomposites can exhibit an exceptionally high thermal conductivity, a very good electrical conductivity, high thermal and chemical stability or very good mechanical properties [1, 2]. One can also obtain materials having high non-flammability.

A particularly interesting group of nanocomposites are polymers with the addition of inorganic nano-fillers, organically modified. Properties of these compounds are closely related to the properties of the base polymer. They have been used, for example in the automotive industry for the production of extremely high mechanical strength car parts [3, 4].

One of the intensively investigated nanocomposites is polyvinylidene fluoride (PVDF) with organically modified clay - montmorillonite. The first data on the composites obtained on the basis of PVDF polymer with nanofillers were published by Priya and Jog [5]. According to previous experience and literature, the addition of organomontmorillonite (OMMT) into polymer matrix influences not only physical and mechanical properties of the material but also has significant effect on the crystallization. The presence of clay particles causes preferred orientation of polymer chains thus imparting anisotropy to the material. In the presence of nanofillers PVDF crystallized in desired β phase. The content of this phase is greater than in the unmodified polymer. The presence of this phase is responsible for the piezo-, pyro- and ferroelectric effect of polymer and thus has the greatest impact on the application of the material for the construction of various types of sensors and transducers [6].

The subject of the research presented in the paper are such composites manufactured on the basis of PVDF with organoclay fillers.

Sample preparation and characterization

Polymer composites with nanofillers were prepared in the Polymers Engineering and Technology Division at the Wroclaw University of Technology.

Composites based on poly(vinylidene fluoride) with 5 wt.% organoclay (OMMT) were prepared in extrusion process.

For the testing three types of samples were prepared (denoted as R1, R2, R3) and a reference sample (neat PVDF). All composites were prepared based on poly (vinylidene fluoride) but with different type of nanofillers.

Changes in supermolecular structure of the composites after the addition of nanoparticles were studied by Wide-Angle X-ray Scattering (WAXS). Results revealed that the addition of organoclay induced the piezoactive crystal phase – β-PVDF in all prepared samples.

For the preparation of electrets from polymer with nanofillers corona discharge method at an elevated temperature was used. For all tested composites the same polarization parameters were applied: t=15 min, U_p in the range of -9 kV to -6kV, T_p=60^{o}C). Application of electric field during polarization process allowed dipole alignment.

Experimental

In this work determination of the spatial charge distribution in all tested composites was carried out using electrically stimulated acoustic wave (ESAW) technique. This non-destructive method was originated by Takada, Maeno and co-workers [7,8]. The measurement procedure used during experiment is described in detail in works [9, 10].

Measurements were made on samples which were a two-layer system: polarized and unpolarized film is connected with a thin layer of silicone grease. The samples were placed in the measuring chamber. The pressure wave generated by step voltage propagated through the sample was detected by PVDF thin foil detector. Electrical signals generated in PVDF transducer were measured using digital oscilloscope. Then mathematical calculations necessary in the processing of the recorded voltage signals were applied.

Results

The example of space charge profiles obtained after the numerical analysis of electroacoustic signals recorded for a sample of pure PVDF and one of nanocomposites are depicted in in Fig. 1 and in Fig. 2, respectively.
The presented curves show space charge distribution (q_V) through the sample thickness (d) and dependence charge profiles on applied step voltage (u_S) and polarising voltage (u_O).

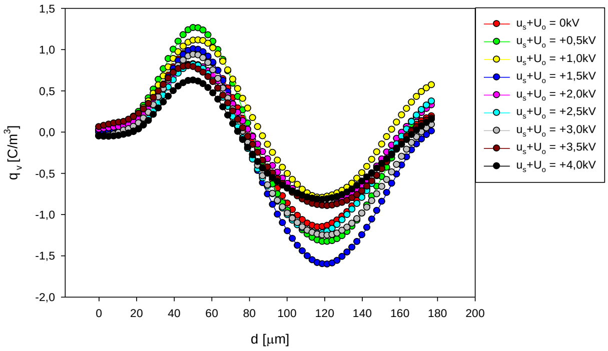

Fig.1. Space charge density profile for a neat PVDF

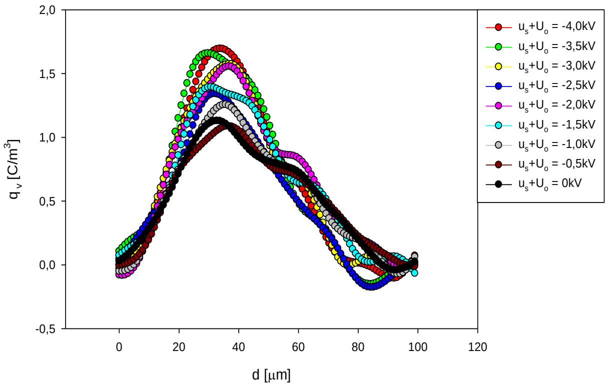

Fig.2. Space charge density profile for a PVDF sample with organoclay nanofiller (nanocomposite R2)

Conclusions

The results of research carried out lead to the following conclusions:

- It is possible to achieve an electret state in the composite structure of PVDF polymer with organoclay nanofillers.
- For the polarization of a new type of nanocomposites corona discharge at elevated temperature can be applied;
- The method of electrically stimulated acoustic wave (ESAW) allowed to investigate the spatial charge distribution in polymer composites with nanofillers in the form of organoclays;
- Space charge distribution is different for tested samples and depends on the type of filler used in nanocomposites;
- In the nanocomposites with a commercial filler (sample R2) the highest value of the accumulated electric charge was observed;
- The shape of curves (with many of irregularities) depicting the spatial charge distribution as a function of the sample thickness shows a large influence of interphases on charge accumulation and distribution inside the polymer nanocomposite material.

Studies on the distribution of electric charge in polymer with the montmorillonite nanofillers, as indicated by the literature, have not yet been performed. The results of work seem to be promising and may provide a basis for further research carried out in the future.

This work was supported by the statutory research of Institute of Electrical Engineering Fundamentals, Wrocław University of Technology.

REFERENCES

[1] Goel M.: Electret sensors, filters and MEMS devices: New challenges in material research, *Current Science*, 85(2003) No. 4.
[2] Wang M., Dong.:Enhanced electrochemical properties of nanocomposite polymer electrolyte based on co-polymer with exfoliated clays, *J Power Sources*, 170 (2007) 425-432.
[3] Spychaj T., Heneczkowski M., Pigłowski J., Oleksy M., Kowalczyk K., Kiersnowski A., Galina H.: *Inżynieria materiałowa*, 6(2006) 1296-1302.
[4] Zhang X., Mingyan, Gao J., Hu Ch.:Investigation on Microstructure and Dielectric Properties of Polyethylene/Montmorillonite Nano-composites, *Intenational Symposium on Electrical Insulating Materials*, June 5-9, 2005, Japan.
[5] Priya L., Jog J.:Intercalated poly(vinylidene fluoride)/clay nanocomposities: structure and properties, *J. Polym. Sci. Part B: Polym. Phys.,* 41(2003) 31-38.
[6] Ramasundaram S., Yoon S., Kim K.J., Park C.: Preferential formation of electroactive crystalline phases in poly(vinylidene fluoride)/organically modified silicate nanocomposites;, *Journal of Polymer Science: Part B: Polymer Physics* **46**, (2008) 2173-2187.
[7] Takada T., MaenoT., Kushibe H., IEEE Trans. Electr. Insul., 22(1087) 497-501.
[8] Maeno T., Futami T., Kushibe H., Takada T., Cooke C.M., IEEE Trans. Elecr. Insul. 23(1988) 433-439.
[9] Motyl E.: The Step-Electro-Acoustic Method for observation of the interfacial charges in insulators, *Dielectric Materials, Measurements and Applications Conference* Publication No. 473, IEEE 2000.
[10] Motyl E.: Ładunek przestrzenny w dielektrykach stałych. Analiza metod pomiarowych i badania, *Prace Naukowe Instytutu Podstaw Elektrotechniki i Elektrotechnologii Politechniki Wrocławskiej,* Wydawnictwo Politechniki Wrocławskiej, Wrocław 2000

***Authors**: : dr inż. Anna Kisiel, Wrocław University of Technology, Institute of Electrical Engineering Fundamentals, ul. Wybrzeże Wyspiańskiego 27, 50-370 Wrocław, Poland, e-mail: anna.kisiel@pwr.edu.pl; dr inż. Małgorzata Żabska, Wrocław University of Technology*, Polymers Engineering and Technology Division, *ul. Wybrzeże Wyspiańskiego 27, 50-370 Wrocław, Poland, e-mail: malgorzata.zabska@pwr.edu.pl; mgr inż. Radosław Chowaniec, Wrocław University of Technology, Institute of Electrical Engineering Fundamentals, ul. Wybrzeże Wyspiańskiego 27, 50-370 Wrocław, Poland, e-mail:*

8th International Conference
Electromagnetic Devices and Processes in Environment Protection **ELMECO-8**
joint with 11th Seminar Applications of Superconductors **AoS-11**
September 28 - October 1, 2014, Nałęczów, Poland

THE CERAMIC SUPERCONDUCTORS DOPED BY ZrO_2-CeO_3 IN SOL-GEL METHOD

Leszek WOŹNY, Jan ZIAJA, Anna KISIEL

Wroclaw University of Technology

Abstract. *The work presents the influence of the Zr and Ce oxides doping into BiSrCaCuO ceramic superconductors on their critical parameters. Metal oxides were added in sol-gel form. The basic physical low-temperature properties of obtained samples have been studied. The optimal concentration of Zr-Ce, for which the critical parameters reached the highest values, was determined. However, even the sample with optimum content of Zr-Ce dopant has shown worse superconducting properties compared to the pure superconductor.*

Streszczenie. *W pracy przedstawiono wpływ dodatków tlenków Zr i Ce na parametry krytyczne nadprzewodników ceramicznych typu BiSrCaCuO. Tlenki metali dodawano w postaci zol-żelu. Wskazano optymalne stężenie Zr i Ce, dla którego parametry krytyczne mają najwyższe wartości.*

Keywords: superconductor; critical current; BiSrCaCuO
Słowa kluczowe: nadprzewodnik; prąd krytyczny; BiSrCaCuO

Introduction

The common problem for high temperature ceramic superconductors is their relatively low value of critical current density [1-5]. This fact is related to the granular microstructure of these materials. They are built of weakly connected grains between which there are regions of low superconductive properties. This causes important problems for supercurrent flow and decreases the value of critical current density.

There are many methods that can be applied for improvement of transport superconducting properties of ceramic materials. One of them is silver addition in the appropriate amount. Silver atoms locate between crystallites of base superconducting phase improving connection between them and their crystal order.

In the previous works we pointed that the addition of silver or some metal oxides strongly affected the j_c value of $YBa_2Cu_3O_x$ superconductors. For technology and practical applications the materials with higher critical temperature than superconductors from Bi-Sr-Ca-Cu-O system are more interesting. In the presented study the Zr and Ce oxides were choosen as admixtures for Bi-based superconductors. In order to facilitate the penetration of the oxides into the superconducting BiSrCaCuO material and surrounding of its particular grains they were added in the sol-gel form.

Sample preparation

For the experiment the samples of $Bi_2Sr_2CaCu_2O_x$ with critical temperature T_c=80-90 K were prepared. The main reaction was carried out from precursors (Bi_2O_3, $SrCuO_3$, $CaCuO_3$ and CuO) at temperature of 800^oC for 8 h and at 860^oC for 48 h.

The additional metal Ce and Zr admixtures were prepared in sol-gel form. $Ce(NO_3)_3$•$6H_2O$ was solved in HNO_3 and ethyl glycol. Similar procedure was applied for Zr. Both components were mixed with powder of base BiSrCaCuO phase. The samples were sintered at 850^oC for various times in the range 198-396 h.

Measurements of superconducting properties

The obtained samples were tested by measurements of their voltage-temperature $U(T)$ and voltage-current $U(I)$ characteristics at fixed liquid nitrogen temperature (77 K). Measurements were carried out by four-point method. The results of critical temperature T_c, transition width ΔT_c and critical current density j_c for all samples are collected in tab. 1.

Table 1. Properties of samples: critical temperature T_c, transition width ΔT_c and critical current density j_c

Sample	P1	P2	P3	P4	P5	P6
T_c [K]	102.0	20.2	103.5	85.5	101.0	86.0
ΔT_c [K]	15.0	30.5	17.0	9.0	22.0	9.0
j_c [Acm^{-2}]	36.0	70.4	12.0	11.0	28.0	0.5

Conclusions

The addition of Zr-Ce oxides into BiSrCaCuO ceramics in a meaningful way affects their superconducting properties. With the increase in Zr-Ce concentration the basic critical parameters (T_c, ΔT_c, j_c) are subjected to noticeable changes.

For both T_c and j_c parameters there is the optimal concentration of Zr-Ce admixtures for which they reach maximum values. This maximum exists for 3.3% wt. ZrO_2-CeO_3 content. At this point critical temperature is T_c=103 K and critical current density is j_c=18 Acm^{-2}. The further enhancing of admixture concentration leads to decrease in both T_c and j_c values.

The characteristic feature of doped samples is the evident sensitivity of their T_c values on doping concentration. Critical temperature decreases with increasing of Zr-Ce concentration. The only exception is sample with 10% wt. Zr-Ce. Its T_c is relatively large. It can be caused by longer time of annealing. This fact is confirmed by increasing j_c value after additional annealing. It can be connected with further forming of chemical stable superconducting phase in Bi-Sr-Ca-Cu-O system.

Unfortunately, critical parameters of modified samples are worse than for superconductors without admixtures. Nevertheless, it seems that the properties of doped superconductors can be improved as a result of optimization of other preparation conditions such as annealing time and temperature.

This work was supported by the statutory research of Institute of Electrical Engineering Fundamentals, Wrocław University of Technology.

REFERENCES

[1] Lu X.Y., Nagata A., Sugawara K., Kamada S., Grain alignment and critical current densities of (Bi,Pb)-2223 phase in the partial-melting and sintering process, *Supercond. Sci. Technol.*, 12 (1999) 1098–1101

[2] Lelovic M., Krishnaraj P., Eror N.G., Iyer A.N., Balachandran U., Transport critical current density above 10^5 A cm^{-2} at 77 K in $Bi_{1.8}Pb_{0.4}Sr_{2.0}Ca_{2.2}Cu_{3.0}O_y$ superconducting tapes made by the Ag wire-in-tube method, *Supercond. Sci. Technol.*, 9 (1996) 201-204

[3] Lu Z., He Y., Yang S., Sun J., Huang X., Wang J., Duan Z., Zhang P., Yong F., Zhou L., Effect of axial tensile and bending strains on the critical current of Bi-2223 superconducting tapes, *Physica C: Superconductivity*, 337 (2000) 150–153

[4] Lim J.H., Jang S.H., Kim H.J., Joo J., Nah W., Kim C.W., Ryu K.-W., Ha H.-S., Oh S.-S., Effect of twisting on microstructure, critical current, and AC losses of Bi-2223 superconductor tape, *Physica C: Superconductivity*, 372–376 (2002) 988-991

[5] Fang Y., Danyluk S. and Lanagan M.T., Effects of cracks on critical current density in Ag-sheathed superconductor tape, C*ryogenics*, 36 (1996) 957–962

***Authors**: dr inż. Anna Kisiel, Wrocław University of Technology, Institute of Electrical Engineering Fundamentals, ul. Wybrzeże Wyspiańskiego 27, 50-370 Wrocław, Poland, e-mail: anna.kisiel@pwr.edu.pl; dr hab. inż. Jan Ziaja, Wrocław University of Technology, Institute of Electrical Engineering Fundamentals, ul. Wybrzeże Wyspiańskiego 27, 50-370 Wrocław, Poland, e-mail: jan.ziaja@pwr.edu.pl; dr inż. Leszek Woźny, Wrocław University of Technology, Institute of Electrical Engineering Fundamentals, ul. Wybrzeże Wyspiańskiego 27, 50-370 Wrocław, Poland, e-mail: leszek.wozny@pwr.edu.pl;*

8th International Conference
Electromagnetic Devices and Processes in Environment Protection ELMECO-8
joint with 11th Seminar Applications of Superconductors AoS-11
September 28 - October 1, 2014, Nałęczów, Poland

ANALYTICAL ANALYSIS OF HTS TRANSFORMER INRUSH CURRENT

Grzegorz KOMARZYNIEC

Lublin University of Technology

Abstract. *In this study we analyzed the inrush current of a one-phase superconducting transformer. We presented relations describing unidirectional current in two states of winding's functioning: superconductive state and resistive state. The relations were given for inrush current flow measured for HTS transformer of 8.5 kVA power.*

Streszczenie. *W pracy dokonano analizy prądu włączania jednofazowego transformatora nadprzewodnikowego. Podano zależności opisujące prąd jednokierunkowy dla dwóch stanów pracy uzwojenia: stanu nadprzewodzenia i stanu rezystywnego. Podane zależności odniesiono do przebiegu prądu włączania uzyskanego z pomiarów transformatora HTS o mocy 8,5 kVA.*

Keywords: inrush current, superconductivity, transformer
Słowa kluczowe: prąd włączania, nadprzewodnictwo, transformator.

Introduction

Value and decay time of inrush current in no-load transformer depend on transformer's electric and magnetic features, the power network impedance, and the initial conditions while switching the transformer on, that is instantaneous value of the voltage and core magnetization.

The flow of inrush current can be divided into two constituents: 1) fixed component representing transformer's no-load current and (2) transient component. The transient component appears with transformer's core saturation and it's the unidirectional current, described by the following formula [1]:

$$i = -\frac{\sqrt{2}EX}{Z^2}\left(\frac{R}{X}\sin\omega t - \cos\omega t + \left(\frac{R}{X}\sin\theta + \cos\theta\right)e^{-\frac{R}{X}(\omega t+\theta)}\right) \tag{1}$$

$$Z = \sqrt{R^2 + X^2} \tag{2}$$

$$\cos\theta = \frac{B_n - B_m - B_r}{B_m} \tag{3}$$

where: R – transformer's primary winding resistance, X – reactance coil without the iron core, E – voltage, B_n – core saturation induction, B_m – rated induction, B_r – residual magnetism induction, ω – pulsation.

Inrush current transient component. can be many times higher than the transformer's rated current and can cause a variety of disadvantageous phenomena both in the transformer and in the power network [2] [3]. The fixed component makes for only a small percentage of the inrush current and can be omitted.

HTS transformer inrush current

Formula (1) is correct, when transformer's primary winding resistance is greater than zero (R>0). The resistance causes reduction in the first inrush current impulse and damping of the following.

In the case of superconducting transformer (HTS) its primary winding resistance is greater than zero when the superconductor goes into normal state. This occurs only with significant transformer overloads. The transition is very quick, but not discrete and it depends on the superconductor's material type (Fig. 1) [4]. Loss in transformer's superconductive state occurs anytime a critical parameter of superconductor is crossed, i.e. critical temperature, critical field intensity or critical current density.

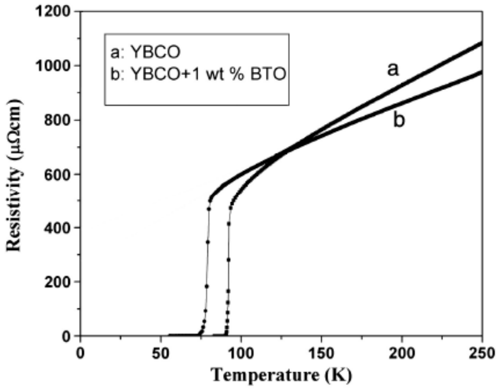

Fig. 1. Superconductor's material characteristics for resistivity and temperature

In HTS transformer's normal exploitation conditions the superconductor is in superconducting state, so the winding resistance equals zero (R=0). Formula (1) is reduced to the following relation:

$$i = \frac{\sqrt{2}E}{X}(\cos\omega t - \cos\theta) \tag{4}$$

It is concluded from relation (4), that in superconducting state there is no damping of the transient component. The unidirectional current has a set value, dependant on winding's reactance and momentary voltage value, as well as residual magnetism induction at switching transformer on.

In Figure 2 inrush current flow of a one-phase 8.5kVA HTS transformer was presented [5].

With great inrush current values, when transient component is greater than superconductor's critical current, transformer's windings lose superconductivity. It is concluded from Figure 1, that at switching 8.5 kVA transformer on, only the first impulse of inrush current exceeds the critical current (I_c=115A) of the superconductor of which the windings are made. The impulse analysis is presented in Figure 3. Points (a) and (b) marked on the curve of unidirectional current *i* designate moments in time, when loss in superconductive state and returning to it happen respectively.

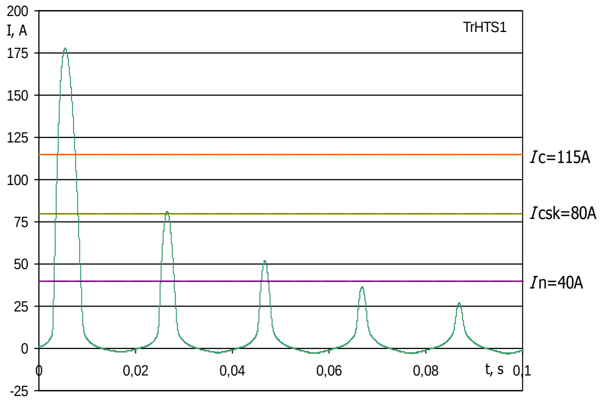

Fig. 2. HTS transformer inrush current [6] [7]; I_c - critical current of the superconductor, I_n - rated current of the transformer

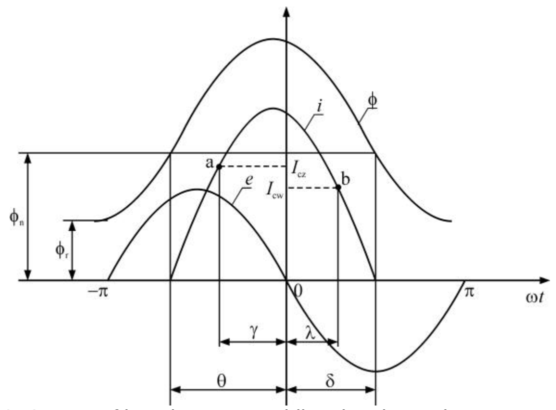

Fig. 3. Course of inrush current unidirectional constituent

In range between $-\theta$ and $-\gamma$ and between α and δ unidirectional current does not exceed superconductor's critical current and the winding's resistance equals zero (R=0). In this range of angles unidirectional current is described by formula (4). In range between $-\gamma$ to λ exceeding of critical current occurs and superconductor goes into normal state. At point (a) there's a discrete increase in winding's resistance (R>0) and unidirectional current is described by formula (1).

In superconductor's resistive state according to Joule's law amount of heat discharged by winding increases. Unidirectional current effective value can be derived from the relation:

(5) $$I = \left(\frac{\omega}{2\pi} \int_{-\gamma/\omega}^{\lambda/\omega} i^2 dt \right)^{\frac{1}{2}}$$

where current i is described by formula (1).

Increase in winding's temperature results in increase in its resistance, according to this known relation:

(6) $$R = R_0 (1 + \alpha \Delta T)$$

So the force of unidirectional current damping is a function of changes in winding's temperature. In Table 1 HTS 8.5 kVA transformer's winding resistance was given for chosen values of temperature [8].

Table 1. HTS 8.5 kVA transformer's winding resistance [8]

Superconductive state, 77K	Resistive state, 77K	Resistive state, 293K
$0.055 \cdot 10^{-18}\ \Omega$	$0.594\ \Omega$	$6.36\ \Omega$

Range of λ (Fig.3) depends on temperature reached by the winding, its thermal capacity and the capacity of cooling system. For great values of unidirectional current λ can equal the δ range. Winding's resistive state can persist. In extreme case the superconductor might not get back into superconducting state before another impulse of inrush current occurs.

Conclusions

The above analysis of superconducting transformer's inrush current allows describing the course of unidirectional current wave in superconductive and resistive state of primary winding. From the formulas given the effective current value in resistive state can be derived, and by the same token the amount of heat discharged in winding can be estimated.

The research was conducted in scope of the project "Analysis of inrush current phenomenon and the phenomena related in superconducting transformers". The project was financed with means of National Science Center given with the decision no. DEC-2012/05/D/ST8/02384

REFERENCES

[1] Z. Spoljaric, V. Jerkovic, M. Stojkov, Measurement system for transformer inrush current higher harmonics determination, *Annals & Proceedings of DAAAM International 2012, Vol. 23, No.1, 2012*

[2] M. Steurer, K. Fröhlich, The impact of inrush currents on the mechanical stress of high voltage power transformer coils, *IEEE Trans. Power Del., vol. 17, no. 1, pp. 155–160, Jan. 2002*

[3] R. A. Turner, K. S. Smith, Resonance Excited by Transformer Inrush Current in Inter-connected Offshore Power Systems, *IEEE Industry Applications Society Annual Meeting, Edmonton, Canada, October 2008*

[4] A. Kujur, D. Behera, DC electrical resistivity and magnetic studies in Yttrium Barium Copper oxide/barium titanate composite thin films, *Elsevier Thin Solid Films 520, pp. 2195–2199, 2012*

[5] G. Wojtasiewicz, T. Janowski, S. Kozak, J. Kozak, M. Majka, B. Kondratowicz-Kucewicz, Tests and Performance Analysis of 2G HTS Transformer, *IEEE Transactions on Applied Superconductivity, vol. 23 , issue 3, 2013*

[6] G. Wojtasiewicz, G. Komarzyniec, T. Janowski, S. Kozak, J. Kozak, M. Majka, B. Kondratowicz-Kucewicz, Inrush Current of Superconducting Transformer, *IEEE Transaction on Applied Superconductivity*, vol. 23, issue: 3, June 2013

[7] G. Komarzyniec, T. Janowski, G. Wojtasiewicz, M. Majka, J. Kozak, S. Kozak, B. Kondratowicz-Kucewicz, Prąd włączania transformatora nadprzewodnikowego, *Przegląd Elektrotechniczny*, no. 9, 2013

[8] G. Komarzyniec, T. Janowski, G. Wojtasiewicz, M. Majka, Thermal problems in HTS transfomer due to inrush current, *Przegląd Elektrotechniczny, no. 2, 2014*

***Authors**: dr inż. Grzegorz Komarzyniec,*
E-mail: g.komarzyniec@pollub.pl,
Lublin University of Technology,
Institute of Electrical Engineering and Electrotechnologies,
Nadbystrzycka 38a,
20-618 Lublin

8th International Conference
Electromagnetic Devices and Processes in Environment Protection ELMECO-8
joint with 11th Seminar Applications of Superconductors AoS-11
September 28 - October 1, 2014, Nałęczów, Poland

MEDIUM VOLTAGE SUPERCONDUCTING FAULT CURRENT LIMITER

Janusz KOZAK, Michał MAJKA

Electrotechnical Institute, Warsaw

***Abstract**. The superconducting fault current limiter (SFCL) is a device allowing for a more effective use of the existing power network infrastructure. The limitation of short-circuit currents by the SFCL to safe levels will result in the network elements being susceptible to smaller electrodynamic and thermal overloads. This paper presents the electrical scheme and design of the 15 kV class SFCL prototype.*

***Streszczenie.** Nadprzewodnikowy ogranicznik prądu zwarciowego (NOPZ) jest urządzeniem pozwalającego na lepsze wykorzystanie istniejącej infrastruktury sieciowej. Ograniczenie przez NOPZ prądów zwarciowych do bezpiecznego poziomu sprawi, że elementy sieci będą narażone na mniejsze przeciążenia cieplne i elektrodynamiczne. W artykule przedstawiono schemat elektryczny i projekt prototypu NOPZ na napięcie 15 kV.*

Keywords: Superconductivity, superconducting fault current limiter.
Słowa kluczowe: Nadprzewodnictwo, nadprzewodnikowy ogranicznik prądu zwarciowego.

Introduction

The fault current limiter (SFCL) introduces minimal impedance to the power system under normal conditions and high resistance during faults, limiting short circuit current. The SFCL responds before the first cycle peak and provides an effective means to limit excessive fault currents to safe levels without the disadvantages of conventional fault current mitigation methods. The SFCLs provide an economic solution for protecting transformers, switchgear and other components against excessive short circuit currents in case of faults [1]-[8]. The application of a SFCL leads to an increase of the allowable short-circuit power at the point of connection of new power generating sources, which is determined by the short-circuit parameters of the power network. This, in turn, will result in an increase of the capability of the power network for connecting distributed generation energy sources based on renewable energy sources. This will lead to the achievement of an environmental effect of reducing CO_2 emissions.

The design of the SFCL

A design of a 1-phase inductive type superconducting limiter is presented in Figures 1-4. The limiter was designed to work in a 15 kV power system. Its main parameters are presented in table 1. A three-winding superconducting fault current limiter has two primary windings and one secondary winding [1], [4], [5]. The primary winding, placed on the outer ring, is made of a copper wire. The second primary winding, placed in the inner ring, is made of a 2G superconducting tape. The third winding is a shorted secondary winding made of a 2G superconducting tape, placed in the inner ring. The primary winding made of 2G tape is connected in parallel with the copper primary winding. All three windings are magnetically coupled. The magnetic coupling between the 2G tape windings in the inner ring is greater than the magnetic coupling between the 2G tape winding and the copper winding in the outer ring. The limiter will be placed in a cryostat with an external vacuum insulation and cooled in a liquid nitrogen bath (Fig. 1). The cryostat of the limiter will be made of GFRP (Glass Fiber Reinforced Polymer). It will be fitted with four copper current leads (Fig. 1) to which the primary, both copper and HTS, windings terminals will be connected. This will allow to record the distribution of currents in these windings during short-circuit tests.

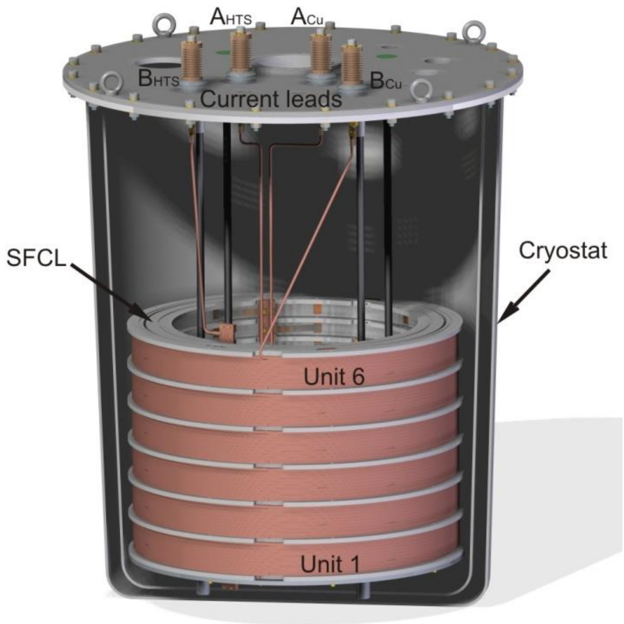

Fig. 1. Design of the SFCL (six identical units connected in series)

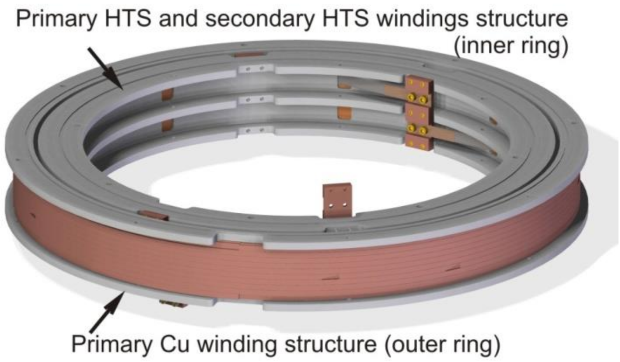

Fig. 2. View of one unit of the SFCL

The limiter consists of six identical modules connected in series (Fig. 1 - 4), which allows to lower the voltage of the individual windings.

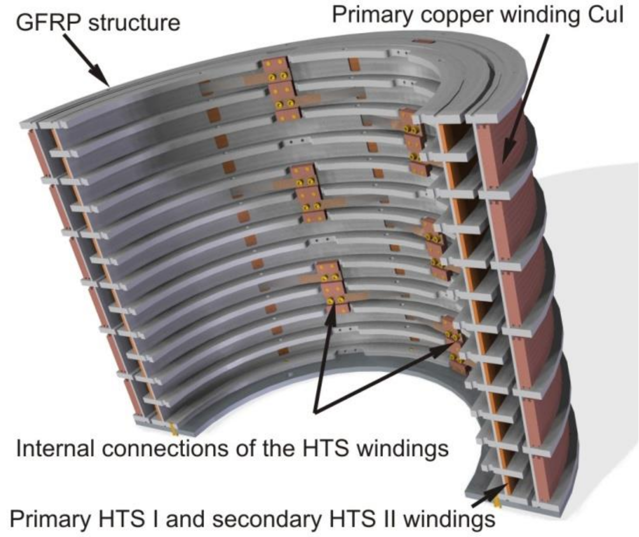

Fig. 3. Structure cross-section of SFCL

Each module consists of two carcasses of different diameters which are made of composite materials reinforced with fibreglass. The copper winding will be wound onto an external bobbin and the superconducting windings on an internal bobbin. In each of the six modules the primary copper winding has 36 turns and is connected in parallel with two primary superconducting windings. The primary superconducting windings have 12 turns each and are connected in series. The secondary superconducting windings consist of two shorted superconducting windings, each with 12 turns. Both the primary and the secondary superconducting windings are wound onto a single bobbin in such a way that their turns are positioned one on top of the other, which provides a very good magnetic coupling between the windings and this, in turn, reduces the voltage during the SFCL's performance in nominal conditions.

Table 1. Parameters of SFCL

Parameter		Value
Nominal voltage	U_N	15 kV
Nominal current	I_N	140 A
Voltage on the limiter @ I_N	U_{SCFL}	< 1 V
Prospective peak current	i_{peak}	40 kA
First peak limiting	i_p	4.7 kA
Limitation time	t_{lim}	160 ms
Operating temperature	T	77.4 K
Cryostat high	H	1 m
Cryostat diameter	O.D.	0.85 m
Copper winding diameter	I.D.	0.578 m
HTS windings diameter	I.D.	0.506 m
Number of copper turns	n_{Cu}	216
Number of primary HTS turns	$n_{HTS\,I}$	144
Number of secondary HTS turns	$n_{HTS\,II}$	144
Length of copper winding	l_{Cu}	393 m
Length of primary HTS winding	$l_{HTS\,I}$	229 m
Length of secondary HTS winding	$l_{HTS\,II}$	229 m

The primary copper winding will be wound using a 3 mm x 6 mm copper wire. The superconducting windings will be wound using the SF12050 superconducting tape with 2 μm silver layer and a resistance of HTS tape 0.311 Ω/m in resistive state at 77.4 K [3]. The primary and secondary superconducting windings are of the same length and have the same number of turns. A Kapton tape will be used to insulate the superconducting windings. Figure 4 represent the connections of the windings of each of the six modules.

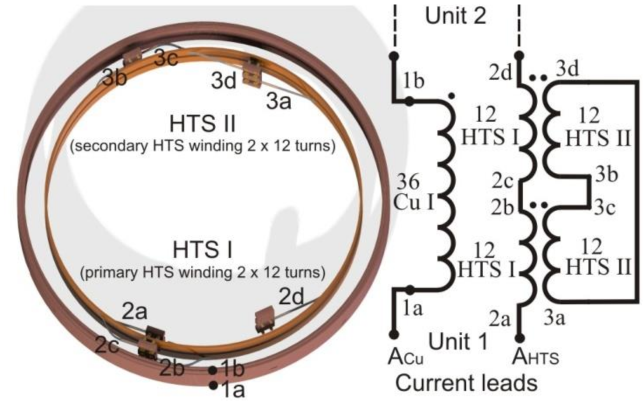

Fig. 4. One unit electrical connections of the SFCL

Conclusions

The developed design in which the superconducting windings are wound simultaneously onto a single bobbin allows to obtain a very high coupling factor between the windings and minimize the leakage reactance of the limiter, which minimizes the voltage in the limiter in the stand-by state. In case of a 2-winding design in which the primary copper winding is magnetically coupled with a secondary HTS winding, there always occurs leakage reactance, which causes losses in the stand-by state. The use of a connection in parallel of a copper coil and a superconducting coil in the primary winding protects the short circuit from opening in case when the superconducting tape is damaged. The fault current limiting capability of a 3-winding limiter is determined mostly by the impedance of the copper winding coupled in parallel with the primary superconducting winding.

This work was supported in part by the National Centre for Research and Development under Grant UMO-2012/05/B/ST8/01837.

REFERENCES

[1] Kozak J., Majka M., Janowski T., Kozak S., Wojtasiewicz G., Kondratowicz-Kucewicz B., "Tests and Performance Analysis of Coreless Inductive HTS Fault Current Limiters", *IEEE Trans. Appl. Supercond.*, 21 (2011), No. 3, 1303 – 1306,

[2] Naeckel O., Noe M., "Design and Test of an Air Coil Superconducting Fault Current Limiter Demonstrator ", *IEEE Trans. Appl. Supercond.*, 24 (2014), No. 3, 5601605

[3] Czerwinski D., Jaroszynski L., Majka M., Kozak J., "Analysis of Alternating Overcurrent Response of 2G HTS Tape for SFCL", *IEEE Trans. Appl. Supercond.*, 24 (2014), No. 3, 5600104

[4] Kozak J., Majka M., Kozak S., Janowski T., „Design and Tests of Coreless Inductive Superconducting Fault Current Limiter", *IEEE Trans. Appl. Supercond.*, 22 (2012), No. 3, 5601804

[5] Kozak J., Majka M., Kozak S., Janowski T., „Comparison of Inductive and Resistive SFCL", *IEEE Trans. Appl. Supercond.*, 23 (2013), No. 3, 5600604

[6] Heydari H., Sharifi R., "Three-Dimensional Pareto-Optimal Design of Inductive Superconducting Fault Current Limiters", *IEEE Trans. Appl. Supercond.*, 20 (2010), No. 5, 2301 - 2311

[7] Jingye Z., Shaotao D., Zikai W., Dong Z., Zhifeng Z., Fengyuan Z., Zhenling X., Zhiqin Z., Guomin Z., Xi X., Naihao S., Zhiyuan G., Liangzhen L., Liye X., "Design, Fabrication, and Tests of Three HTS Coils for a Model Fault Current Limiter", ", *IEEE Trans. Appl. Supercond.*, 20 (2010), No. 3, 1135 - 1138.

[8] Naeckel O., Noe M., "Conceptual Design Study of an Air Coil Fault Current Limiter ", *IEEE Trans. Appl. Supercond.*, 23 (2013), No. 3, 5602404.

***Authors**: dr inż. Janusz Kozak, Instytut Elektrotechniki, Zakład Wielkich Mocy, ul. Pożaryskiego 28, 04-703 Warszawa, e-mail: j.kozak@iel.waw.pl; dr inż. Michał Majka, e-mail: m.majka@iel.waw.pl.*

8th International Conference
Electromagnetic Devices and Processes in Environment Protection ELMECO-8
joint with 11th Seminar Applications of Superconductors AoS-11
September 28 - October 1, 2014, Nałęczów, Poland

ANALIZA WPŁYWU IMPEDANCJI UZWOJENIA WTÓRNEGO NA PARAMETRY NADPRZEWODNIKOWYCH OGRANICZNIKÓW PRĄDU TYPU TRANSFORMATOROWEGO

Joanna KOZIEŁ[1], Tadeusz JANOWSKI[2]

Politechnika Lubelska (1), Instytut Elektrotechniki w Warszawie (2)

Streszczenie *W artykule przedstawiono wyniki badań eksperymentalnych analizy wpływu uzwojenia wtórnego ogranicznika, zwartego elementem nadprzewodnikowym na parametry nadprzewodnikowych ograniczników prądu typu transformatorowego i przedstawiono wynikające z analizy wnioski. Przedstawiono zasadę budowy i działania nadprzewodnikowego ogranicznika prądu typu transformatorowego. Omówiono funkcjonalny model fizyczny takiego ogranicznika.*

Abstract*. The paper presents the results of experimental research of the analysis of the impact of the secondary winding limiter, shorted with a superconducting element, on the performance of superconducting current limiters of a transformer type and the conclusions from the analysis are introduced. The paper presents the principle of construction and operation of superconducting current limiter of transformer type is presented. Functional physical model of such a limiter is described.*

Keywords: transformer type superconducting fault-current limiter, secondary winding impedance.
Słowa kluczowe: nadprzewodnikowe ograniczniki prądu zwarcia typu transformatorowego, impedancja uzwojenia wtórnego.

Wprowadzenie

Nadprzewodnikowe ograniczniki prądu zwarcia (superconducting fault current limiter, SFCL) składają się z nieliniowych, nadprzewodnikowych elementów o zmiennej impedancji, włączanych szeregowo w obwód elektryczny [1]. Wykazują one małą impedancję podczas pracy w warunkach znamionowych chronionego obwodu elektrycznego oraz dużą impedancję w warunkach zwarcia w obwodzie chronionym. Szybki powrót zdolności do ograniczania prądu po ustąpieniu zwarcia oraz długi czas pracy przy niewielkich kosztach eksploatacyjnych to podstawowe zalety ograniczników nadprzewodnikowych.

Projekt i wykonanie modelu nadprzewodnikowego ogranicznika zwarcia prądu typu transformatorowego

W Pracowni Technologii Nadprzewodnikowych w Lublinie został zaprojektowany i wykonany funkcjonalny model jednofazowego nadprzewodnikowego ogranicznika prądu typu transformatorowego [1].

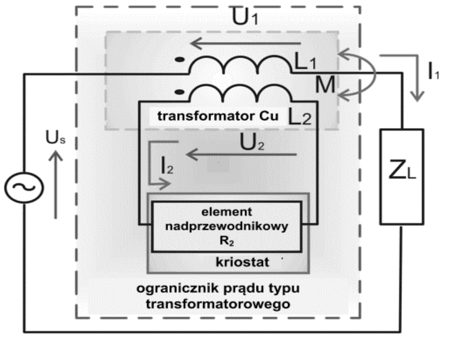

Rys.1. Budowa nadprzewodnikowego ogranicznika prądu zwarcia typu transformatorowego [1]:
I_1 – prąd strony pierwotnej transformatora, I_2 – prąd strony wtórnej transformatora, U_1 – napięcie strony pierwotnej transformatora,
U_2 – napięcie strony wtórnej transformatora,
L_1 – indukcyjność własna strony pierwotnej,
L_2 – indukcyjność własna strony wtórnej, U_S – napięcie sieci,
M – indukcyjność wzajemna uzwojeń, Z_L – obciążenie,
R_2 – rezystancja ograniczającego elementu nadprzewodnikowego.

Ogranicznik składa się z transformatora konwencjonalnego 10 kVA z wtórnym uzwojeniem miedzianym zwartym elementem nadprzewodnikowym. Na rys.1. przedstawiono ideę budowy i działania nadprzewodnikowego ogranicznika prądu zwarcia typu transformatorowego. Ogranicznik składa się z konwencjonalnego transformatora z uzwojeniami miedzianymi oraz elementu nadprzewodnikowego R_2, zwierającego wtórne uzwojenie transformatora konwencjonalnego. Element nadprzewodnikowym jest zwykle cewka, indukcyjna lub bifilarna, nawinięta taśmą nadprzewodnikową HTS.

W tabeli 1 przedstawiono parametry modelu transformatora konwencjonalnego Cu.

Tabela 1. Parametry modelu transformatora z uzwojeniami konwencjonalnymi Cu [1]

Parametry transformatora			
Rdzeń magnetyczny zwijany cięty o przekroju 70 x 70 mm^2 = 4900 mm^2 – RZC 70 / 230-70 B_{max} – 1,5 T			
Przewód nawojowy GN (pierwotne), mm			Cu 2 x 4
Przewód nawojowy DN (wtórne), mm			Cu 2 x 4
Napięcie zwojowe, V/ zw			1,74
Napięcie GN, V			230
Napięcie DN, V			115
Prąd znamionowy uzwojenia GN			44
Prąd znamionowy uzwojenia DN			88
Wymiary uzwojenia			
a_1, m	0,008	l_u, m	0,132
a_2, m	0,004	$l_{śrGN}$ / $l_{śrDN}$, m	0,513 / 0,424
b_1, m	0,0777	Zwoje z_{GN} / z_{DN}	132 / 66
b_2, m	0,0655	Warstwy m_{GN} / m_{DN}	4 / 2
r_1, m	0,0857	Zwojów / warstwę	33 / 33
r_2, m	0,0695	δ, m	0,01

Elementem nadprzewodnikowym jest cewka nadprzewodnikowa składająca się z dwóch niezależnych uzwojeń w_1, w_2 nawiniętych na wspólnym karkasie. Uzwojenia nadprzewodnikowe chłodzone są w kąpieli w ciekłym azocie. Parametry uzwojeń nadprzewodnikowych zamieszczono w tabeli 2.

Tabela 2. Parametry cewek nadprzewodnikowych w_1 i w_2 wykonanych z taśmy HTS 2G SCS4050 [1]

Parametr	Uzwojenie 1 (w_1)	Uzwojenie 2 (w_2)
Średnica zewnętrzna, m	0,068	0,066
Grubość, m	0,001	0,001
Wysokość, m	0,132	0,132
Liczba zwojów	132	66
Indukcyjność, mH	1,72	0,4

Oba uzwojenia wykonano z taśmy nadprzewodnikowej HTS 2G SCS4050 produkcji SuperPower. Jest to taśma o szerokości 4 mm i grubości 0,055 mm, dwustronnie laminowana miedzią, o prądzie krytycznym I_c = 115 A.

Maksymalny prąd znamionowy uzwojeń nadprzewodnikowych równy jest skutecznej wartości prądu krytycznego nadprzewodnika wynoszącej 82 A.

Badania laboratoryjne modelu nadprzewodnikowego ogranicznika prądu typu transformatorowego

Badania eksperymentalne przeprowadzono w celu sprawdzenia możliwości ograniczenia prądu zwarcia przez ogranicznik prądu typu transformatorowego oraz określenia poziomu ograniczenia prądu ze względu na parametry elementu nadprzewodnikowego (konfiguracja uzwojeń HTS) [1].

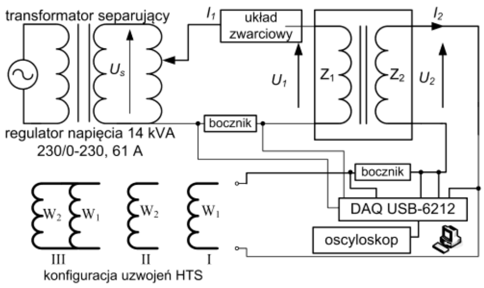

Rys.2. Zwarciowy układ pomiarowy nadprzewodnikowego ogranicznika prądu typu transformatorowego [1]

Badania zostały przeprowadzone w Pracowni Technologii Nadprzewodnikowych w układzie pomiarowym przedstawionym na rys. 2. Model nadprzewodnikowego ogranicznika prądu zasilany jest z regulatora napięcia połączonego z siecią poprzez transformator separujący. Boczniki użyte do przeprowadzenia pomiaru prądu mają wartość 1 mV/1 A. Pomiary wykonano za pomocą karty pomiarowej PC DAQ Card oraz oprogramowania LabView Software. Zwarcie było inicjowane przez układ zwarciowy. Czas trwania zwarcia 0,05s. Parametry elektryczne uzwojeń dla każdej konfiguracji cewek HTS przedstawiono w tabeli 3.

Tabela 3. Parametry uzwojeń nadprzewodnikowych dla trzech konfiguracji uzwojeń w_1 i w_2 [1].

Konfiguracja	I	II	III
Indukcyjność L_{HTS}, mH	1,72	0,40	0,30
Reaktancja X_{HTS}, Ω	0,55	0,12	0,09
Rezystancja R_{HTS}, Ω (w 77 K)	0,61	0,30	0,20
Impedancja Z_{HTS}, Ω	0,82	0,32	0,22

Analiza została przeprowadzona dla następujących konfiguracji uzwojeń nadprzewodnikowych w_1, i w_2: Konfiguracja I – wtórne uzwojenie transformatora Cu zwarte cewką w_1,konfiguracja II – wtórne uzwojenie transformatora Cu zwarte cewką w_2, konfiguracja III – wtórne uzwojenie transformatora Cu zwarte cewkami w_1 i w_2 połączonymi równolegle.

Rys.3 przedstawia przebiegi prądów po stronie pierwotnej i wtórnej ogranicznika dla wybranej konfiguracji uzwojeń.

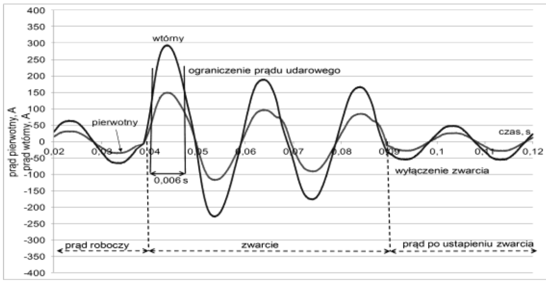

Rys.3. Przebiegi prądów pierwotnego i wtórnego dla II konfiguracji uzwojenia nadprzewodnikowego [1]

Impedancja zwarciowa ogranicznika Z_{zw}, jest sumą impedancji transformatora Cu – Z_{zwCu} oraz impedancji uzwojenia nadprzewodnikowego Z_{HTS}. Jeżeli założymy dla uproszczenia rozważań, że Z_{zwCu} ma wartość stałą, to wartość impedancji Z_{zw} zależy od wartości reaktancji X_{HTS} i rezystancji R_{HTS} uzwojenia nadprzewodnikowego HTS, a zatem od konfiguracji uzwojenia oraz rezystywności użytej taśmy nadprzewodnikowej w temperaturze 77 K. Czym większa wartość R_{HTS} i X_{HTS}, a zatem impedancja uzwojenia nadprzewodnikowego, tym większe jest ograniczenie prądu zwarcia. Czas, po którym ograniczony prąd udarowy osiągnie spodziewaną wartość ustalonego prądu zwarcia wynosi, dla II konfiguracji uzwojenia HTS, około 6 ms.

Wnioski

Przeprowadzone analizy i wyniki badań eksperymentalnych wskazują, że możliwa jest budowa nadprzewodnikowego ogranicznika prądu typu transformatorowego, wykorzystując istniejący transformator konwencjonalny z uzwojeniem wtórnym zawartym przez uzwojenie nadprzewodnikowe wykonane z taśmy HTS.

Poziom ograniczania prądu zwarcia, zwłaszcza pierwszego impulsu prądu udarowego, zależy od wartości impedancji zwarciowej ogranicznika, będącej sumą impedancji transformatora Cu i impedancji uzwojenia HTS. Impedancja uzwojenia HTS zależy od konfiguracji uzwojenia (cewki indukcyjne lub bifilarne, lub wiele cewek połączonych szeregowo bądź równoległe) oraz od rezystywności taśmy nadprzewodnikowej. Poprzez wybór odpowiedniej taśmy HTS oraz odpowiednią konfigurację uzwojenia nadprzewodnikowego, przy założeniu stałej wartości impedancji transformatora Cu, możemy zbudować nadprzewodnikowy ogranicznik prądu typu transformatorowego na dowolny poziom ograniczania prądu zwarcia.

LITERATURA

[1] Kozieł J., *„Analiza wpływu impedancji uzwojenia wtórnego na parametry nadprzewodnikowych ograniczników prądu typu transformatorowego"*, Rozprawa doktorska, Politechnika Lubelska, *Lublin 2014.*

***Autorzy**: prof. dr hab. inż. Tadeusz Janowski, Instytut Elektrotechniki w Warszawie, Pracownia Technologii Nadprzewodnikowych w Lublinie, ul. Nadbystrzycka 36a, 20-618 Lublin e-mail: t.janowski@pollub.pl,*
dr inż. Joanna Kozieł, Politechnika Lubelska, Instytut Podstaw Elektrotechniki i Elektrotechnologii, ul. Nadbystrzycka 38a, 20-618 Lublin, e-mail: j.koziel@pollub.pl

8th International Conference
Electromagnetic Devices and Processes in Environment Protection ELMECO-8
joint with 11th Seminar Applications of Superconductors AoS-11
September 28 - October 1, 2014, Nałęczów, Poland

ANGLES ON POLYMERIC MATERIAL EXPOSED ON PLASMA GENERATED IN DIELECTRIC BARRIER DISCHARGE PLASMA JET

Michał KWIATKOWSKI, Piotr TEREBUN, Piotr KRUPSKI, Jarosław DIATCZYK,

Joanna PAWŁAT, Henryka D. STRYCZEWSKA

Lublin University of Technology, Institute of Electrical Engineering and Electrotechnologies

Abstract. *For the polystyrene material surface properties a significant role is hydrophobicity of the surface of the material. The hydrophobicity is one of the main surface properties of polystyrene. This work shows the influence of non-thermal plasma on contact angle material treated using a reactor type barrier discharge jet.*

Streszczenie. *Dla właściwości powierzchni materiałów polistyrenu istotną rolę odgrywa hydrofobowość powierzchni materiału. Niniejsza praca przedstawia wpływ plazmy nietermicznej na kąt zwilżania materiału poddanego obróbce przy zastosowaniu reaktora typu dysza z wyładowaniem barierowym.*

Keywords: dielectric barrier discharge, atmospheric pressure plasma jet, contact angles.
Słowa kluczowe: wyładowanie dielektryczne, dysza plazmowa pracująca pod ciśnieniem atmosferycznym, kąty zwilżania.

Introduction

Materials made from plastics such as acrylonitrile-butadiene-styrene (ABS), homopolymer polypropylene (PP-H), and high impact polystyrene (HIPS) are characterized by different mechanical and thermal properties. Their common feature is the ease of heat and mechanical processing, as well as high resistance to chemical compounds. They are widely used in many fields, eg. buildings, advertising, food industry (packaging and pallets for food products), etc. [1, 2].

One feature of such materials is their hydrophobicity. It is the tendency of the chemical particles to repel water molecules apart (Fig. 1). As a measure for the hydrophobicity of the polymeric materials the surface contact angle can be defined [3, 4]. By the appropriate treatment (mechanical, thermal or chemical) hydrophobic properties may be changed depending on the current needs. One of the methods used to convert these properties is the use of non-thermal plasma [5-7]. This paper aims to examine the effectiveness of the plasma treatment on ABS, HIPS and PE-H materials by using a plasma jet reactor with dielectric barrier discharge.

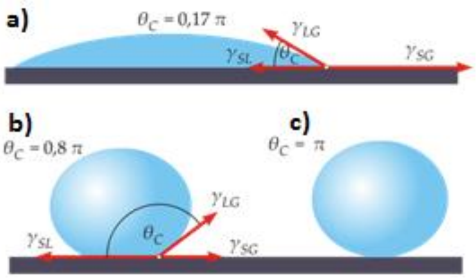

Fig.1. Good wetting (A) , poor (B), complete lack of wetting C) [8].

Experimental metod

Study the properties of materials treated with non-thermal plasma was carried out using a plasma jet type reactor, which construction is shown in Figure 2. The reactor was supplied by voltage of 4.43 kV with frequency of 17.3 kHz, distance between plasma jet and sample was 20 mm.

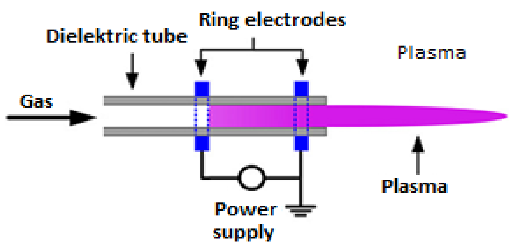

Fig.2. Diagram of DBD reactor in system of two ring electrodes on a ceramic tube.

All test samples had a size of 30 mm × 40 mm with a thickness of 2 mm. All measurements were made for gas temperature below the softening temperature of material with the smallest thermal resistance, which was 70 °C [9].

After applying plasma, all samples were placed in a specially prepared rack. Then the individual samples were wetted with 10 µl of distilled water using automatic pipette. After wetting, the picture of the sample was taken using a camera mounted in the same rack. Angle measurements were performed for each drop in the graphics processing.

Results

Figure 3 shows contact angles for PP-H, depending on the addition of air. Time of the plasma operation on the surface of the sample was 30 seconds. The contact angle of the control sample was approximately 79 degrees. The impact of the plasma on the surface decreased contact angle. The change in flow or increased air addition had no significant effect.

The contact angle for ABS (control angle of approximately 70 degrees) is shown in Figure 4. It can be seen that due the action of plasma, the contact angle decreased. Different results of plasma treatment for this material were observed with increased flow rate of helium (1.67 l/min).

The contact angle for the control sample of HIPS was about 85 degrees. During the plasma treatment, slightly increasing trend in contact angle value with increasing air flow can be observed in Fig. 5. Again, higher helium flow rate (1.66 l/min) caused different results.

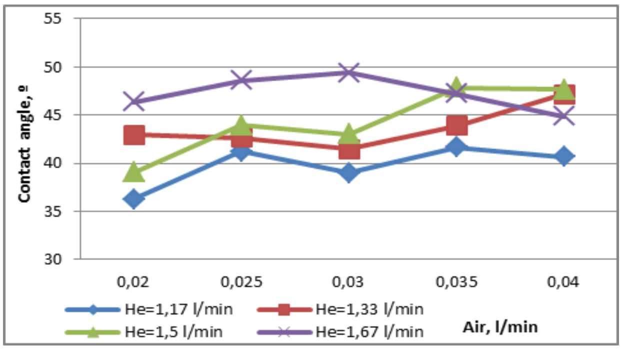

Fig.3. Contact angle of polypropylene homopolymer (PP-H) duration of plasma treatment: 30s.

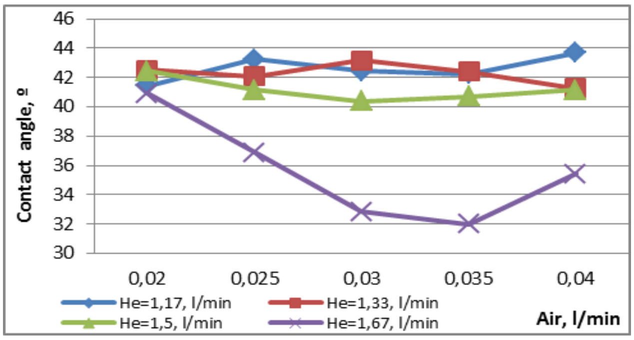

Fig.4. Contact angle of acrylonitrile-butadiene-styrene (ABS) duration of plasma treatment: 30s.

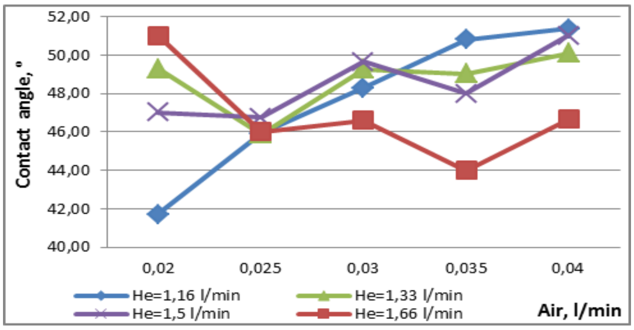

Fig.5. Contact angle of high impact polystyrene (HIPS) duration of plasma treatment: 30s.

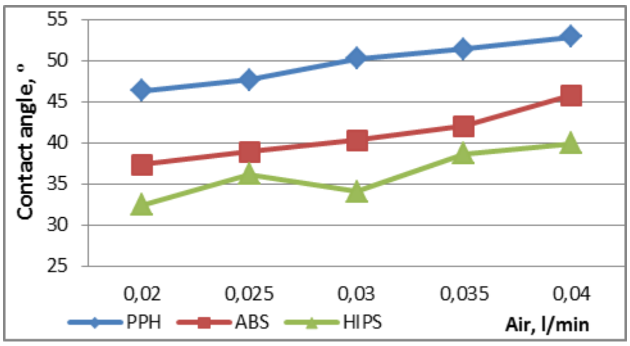

Fig.6. Comparison of contact angle for different materials in dependence on air flow. Plasma treatment time- 120s, helium flow rate-1.33 l/min.

Figure 6 shows the comparison of contact angles with three materials treated with plasma jet during 120 seconds. The smallest contact angles were achieved for HIPS material and the greatest for the PP-H material. For this case small angle increase with increasing addition of air was observed.

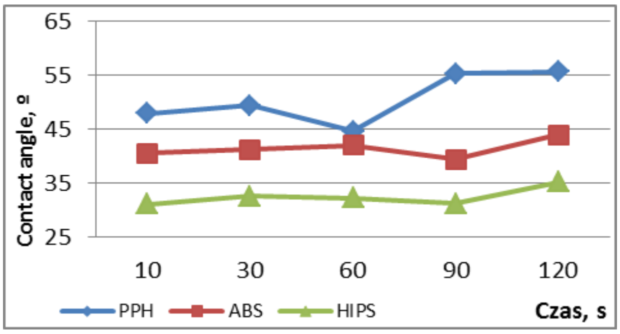

Fig.7. Contact angle depending on the duration of plasma. He = 1.33 l/min Air = 0.03 l/min

Figure 7 shows comparison of the contact angles according to the duration of plasma at a constant flow rate (helium-1.33 l/min, air- 0.03 l/min). The change of plasma exposure time had no significant effect on the result of the measurement of the contact angle.

Summary

The results show that the use of non-thermal plasma generated in the barrier discharge reactor significantly reduced the hydrophobicity of the polystyrene material. Increase in the gas flow rate or in air addition did not significantly affect these properties.

REFERENCES

[1] http://www.plastics.pl/
[2] http://www.audioplex.pl/
[3] http://chemwiki.ucdavis.edu/Physical_Chemistry/Physical_Properties_of_Matter/Bulk_Properties/Cohesive_And_Adhesive_Forces/Contact_Angles
[4] Maria Zielecka, Mehod of contact angle measurement as a tool for characterization of wettability of polymers
[5] Pawłat J., Atmospheric pressure plasma jet for sterilization of heat sensitive surfaces, *Przegląd Elektrotechniczny*, 10b, 139-140, 2012
[6] Singh, N.L.; Pelagade, S.M.; Rane, R.S.; Mukherjee, S.; Deshpande, U.P.; Ganeshan, V.; Shripathi, T., Influence of argon plasma treatment on polyethersulphone surface, *Pramana - Journal of Physics*, January 2013, 80(1):133-141
[7] Anzawa, E.; Kral, M.; Ogino, A.; Nagatsu, M., Improvement of hydrophilicity of polymer surface by surface-wave excited Ar plasma with acetic acid, *Electrical Engineering in Japan*, September 2011, 176(4):1-6
[8] http://www.face-kyowa.co.jp/english/en_science/en_theory/ en_what_contact_angle/
[9] http://www.plastics.pl/content/zdjecia/file/katalog_ tworzywa_ techniczne_32_34.pdf

Authors

Mgr inż. Michał Kwiatkowski[1]: m.kwiatkowski@pollub.pl
Mgr inż. Piotr Terebun[1]: piotr.terebun@gmail.com
Mgr inż. Piotr Krupski: piotr-jl@o2.pl
Dr inż. Jarosław Diatczyk: j.diatczyk@pollub.pl
Dr hab. inż. Joanna Pawłat: askmik@hotmail.com
Prof. dr hab. inż. Henryka Danuta Stryczewska: h.stryczewska@pollub.pl
Wydział Elektrotechniki i Informatyki, Politechnika Lubelska, ul. Nadbystrzycka 38d, 20-618 Lublin, Polska

[1]Participant of the project: "Qualifications for the labour market - employer friendly university", co-financed by European Union from European Social Fund.

8th International Conference
Electromagnetic Devices and Processes in Environment Protection ELMECO-8
joint with 11th Seminar Applications of Superconductors AoS-11
September 28 - October 1, 2014, Nałęczów, Poland

NUMERICAL MODELING OF SUPERCONDUCTING TAPE IN XCOS/COSELICA

Michał ŁANCZONT

Lublin University of Technology

***Abstract**. Usually numerical simulation of superconducting devices are made in FEM software, like FEMM or Comsol. It is possible to made an model in visual programming environment like Simulink or Xcos. The model made this way might take into account the multipath of the occurring phenomena. OpenSource software, as Xcos, gives possibility to create new modules tailored to individual needs.*

***Streszczenie.** Zazwyczaj symulacje numeryczne urządzeń nadprzewodnikowych wykonywane są w wyspecjalizowanych narzędziach obliczeniowych MES, takich jak Femm czy Comsol. Możliwe jest jednak budowanie modeli w środowiskach programowania wizualnego, takich jak Simulin czy Xcos. Możliwe jest budowanie modeli złożonych obwodowo-polowych. Oprogramowanie OpenSource umożliwia ponadto dostęp do kodu źródłowego i nierzadko daleko idące dostosowanie oprogramowania do indywidualnych potrzeb.*

Keywords: Scilab, Coselica, Visual Programming, Numerical simulation, Superconductor.
Słowa kluczowe: Scilab, Coselica, Programowanie wizualne, symulacje numeryczne, nadprzewodniki.

Introduction

Computer's simulations are impotent tools to modeling and analysis of electrical devices and phenomenon. There are two ways to build computer model, by using FEM software, or equivalent circuit model. Second of listed method, in spite of necessity of applying wider simplification then in FEM, it ensure that results will be in good compatibility with measurements, whereby the procedure of model build and modify is much easier[2, 3].

One of the computer adding tools for numerical simulations is Scilab/Xcos with Coselica toolbox. Coselica provide a wide set of tools for simulation of electrical circuits and thermal phenomena. Moreover, as an open software, it provide to modify and add user define calculation's blocks.

Paper presents numerical model of superconducting tape and description of authorial calculation blocks used in built computer model of superconducting tape.

Superconducting tape

The main application of superconducting materials are tapes, used to build complex superconducting devices, like fault current limiters, transformers, separators or SMES. There are two types of superconducting tapes, first and second type, as shown In Fig. 1. Currently the second type superconducting tape, call thin film tapes, are more popular. They are formed by sputtering of each layer to the substrate construction.

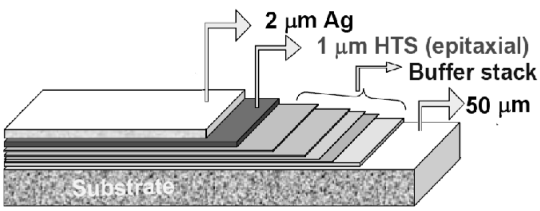

Fig.1. The structure of thin film HTS tape[1]

Electrical attribute of superconducting tape, like resistivity, strongly depends on three parameters: current density in superconductor, external magnetic field density and temperature of the superconductor. Exceeding of the critical value corresponding to each of listed parameters, causes a sharp increase in the value of superconductor resistance. This may result in overheating of the tape and consequently can lead to burnout it.

An important issue is therefore to analyze and study the spread of the resistive zone in the superconductor.

Coselica

Coselica is a free implementation of the Coselica for Scilab/Xcos environment. It provides tools to support mathematical calculations, modeling of electrical circuits, heat issues and problems of mechanics. It is possible to create conjugate models, eg thermo-electrical.

An important feature of Coselica is open source code, which allows to modify and add new blocks.

For the purposes of the test model was developed two new blocks. First applicable superconducting element, as shown in Fig. 2, take account effect of two critical parameters on the operating state of the superconductor.

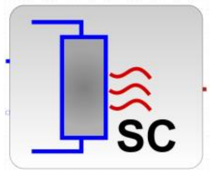

Fig.2. New calculating block of superconducting element

The second of created blocks simulate heat exchange between the metal and the liquid nitrogen, as shown in Fig. 3.

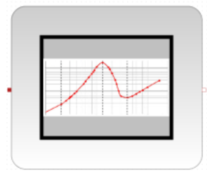

Fig.3. New calculating block of heat Exchange In LN

Model of the superconducting tape

Numerical model of superconducting tape was made base on second type of the tape, as show In Fig. 1. The simplifying assumption was made, during model preparation, to limit number of tape layer to two, superconducting and metallic, and that only the metal layer comes in contact with liquid nitrogen.

The analyzed tape was divided into ten parts, thus giving off ten sections of the model coupled with each, as shown in Fig. 4.

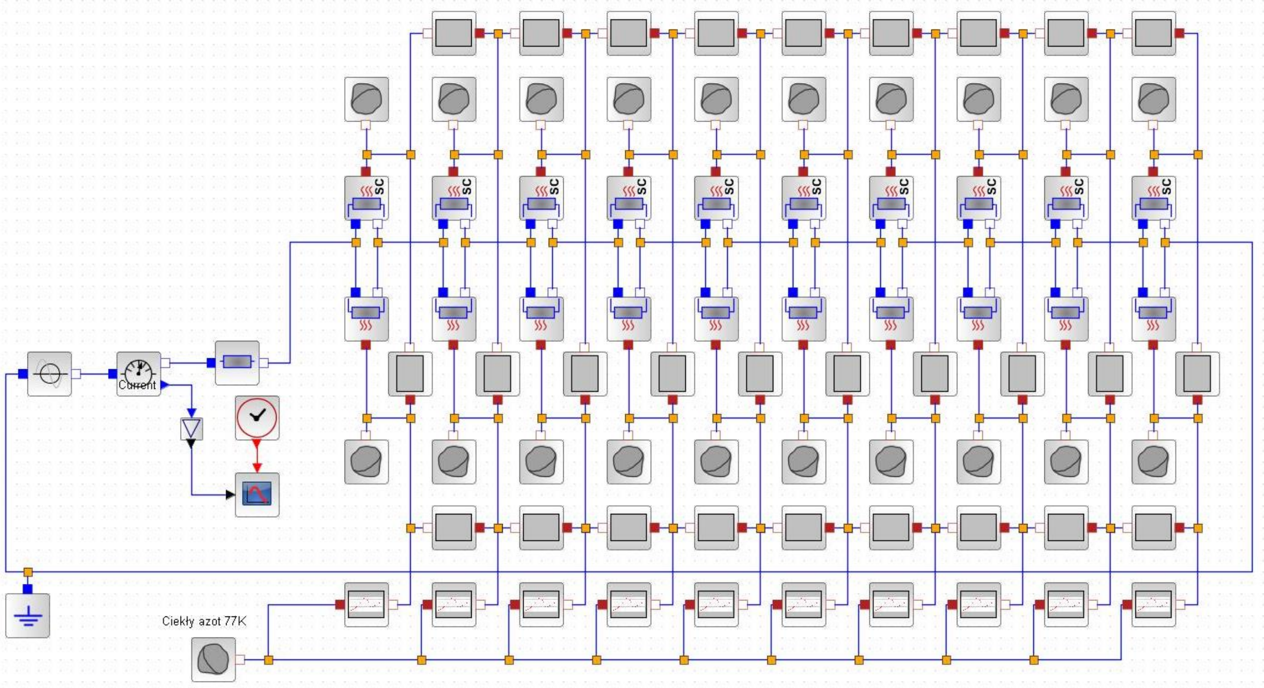

Rys.4. Numerical model of superconducting tape

The proposed model of superconducting tape include nonlinearity of superconducting material, current spreading between the parallel-to-serial connected section of superconductor-resistor, distribution and heat exchange between the tape and the cooling medium.

REFERENCES

[1] Czerwiński D., Dynamika zmian cieplnych w cienkowarstwowych taśmach HTS w stanach przejściowych, Przegląd Elektrotechniczny, R90 nr 2/2014,24-27

[2] Łanczont M., Rezystancyjny nadprzewodnikowy ogranicznik prądu – analiza numeryczna w środowisku SciLab, Przegląd Elektrotechniczny, 2013, nr 2b, vol. 89, s. 315-318

[3] Jaroszyński L, Czerwiński D., Symulacja komputerowa materiałów HTS z użyciem PSPICE, VII Seminarium i Warsztaty Zastosowania Nadprzewodników, 136-146, Kazimierz Dolny 2006

Author: *dr inż. Michał Łanczont, Politechnika Lubelska, Instytut Podstaw Elektrotechniki I Elektrotechnologii, ul. Nadbystrzycka 38A, 20-618 Lublin, e-mail: m.lanczont@pollub.pl.*

8th International Conference
Electromagnetic Devices and Processes in Environment Protection ELMECO-8
joint with 11th Seminar Applications of Superconductors AoS-11
September 28 - October 1, 2014, Nałęczów, Poland

ELECTRICAL PERFORMANCE OF CARBON NANOTUBE FIBRES

Agnieszka LEKAWA-RAUS

University of Cambridge, UK

Abstract*. Carbon nanotube fibres are new types of electrical conductors, which may find wide application in electrical and electronic engineering. However, their application is still limited by the insufficient control over their electrical performance. The following paper presents an overview of the recent results of the research on electrical conduction in carbon nanotube fibres. These studies are used to explore the mechanisms behind the electrical transport in nanotube fibres and their correlation with intrinsic structure of the fibres.*

Streszczenie. *Włókna z nanorurek węglowych stanowią nowy rodzaj przewodników elektrycznych, które mogą znaleźć szerokie zastosowanie elektrotechnice i elektronice. Zastosowanie tych przewodników jest jednak wciąż ograniczone przez niewystarczającą kontrolę nad ich właściwościami elektrycznymi. Poniższy artykuł przedstawia przegląd ostatnich wyników badań nad przewodzeniem włókien nanorurkowych. Wyniki tych badań posłużyły do analizy mechanizmów odpowiedzialnych za przewodzenie elektryczne we włóknach i ich korelacji ze strukturą włókien.*

Keywords: carbon nanotube fibres, electrical conductor, resistance-temperature dependence, magnetoresistance.
Słowa kluczowe: włókna z nanorurek węglowych, przewodniki elektryczne, zależność rezystancji od temperatury, magnetorezystancja

Introduction

It has been recently suggested carbon nanotubes (CNTs) could replace conventional conductive metals in the electrical wires [1]. Considering the unique physical properties of individual carbon nanotubes mainly ballistic electrical transport and very high current carrying capacity as well as low volumetric density and excellent mechanical strength it may be expected that wires made of carbon nanotubes should easily outperform traditional conductors. The only concern may be related to the feasibility of transfer of these unique properties into macroscale. The recently produced wire-like macroscopic assemblies made purely of carbon nanotubes – CNT fibres seem to be very promising in this respect. The recent theoretical calculations confirm that CNT fibres with very well controlled structure should be able to transport charge carriers practically like one long carbon nanotube [2]. However, up to now this goal has not been achieved in currently produced CNT fibres. Instead, due to their highly complex morphology as well as the nature of individual CNTs the fibres constitute very interesting material for the exploration of basic electrical transport in conductive materials. They are additionally interesting due to the severe differences between the fibres and traditional crystalline conductive metals, which entails that if CNT fibres are to replace copper or aluminium their electrical performance needs to be well explored and understood.

Morphology of CNT fibres

CNT fibres which would be ideal for electrical wires should comprise only very long armchair single-wall CNTs of one chirality [2-4]. The nanotubes should be of small diameters and defectless [5,6]. The fibre should be well condensed, free of impurities and the nanotubes well aligned in the axial direction of the fibre [1]. These conditions will ensure the ballistic electrical conduction within carbon nanotubes and practically resistanceless transfer of charge carriers between CNTs.

None of the currently employed fibre manufacture processes can produce fibres characterized by all these features. Some of the processes may give longer nanotubes, others less impurities etc. [1]. However, the overall morphology of all the fibres still remains very complex. Figure 1 presents an example of an internal structure of carbon nanotube fibre produced via floating catalyst chemical vapour deposition (CVD) process.

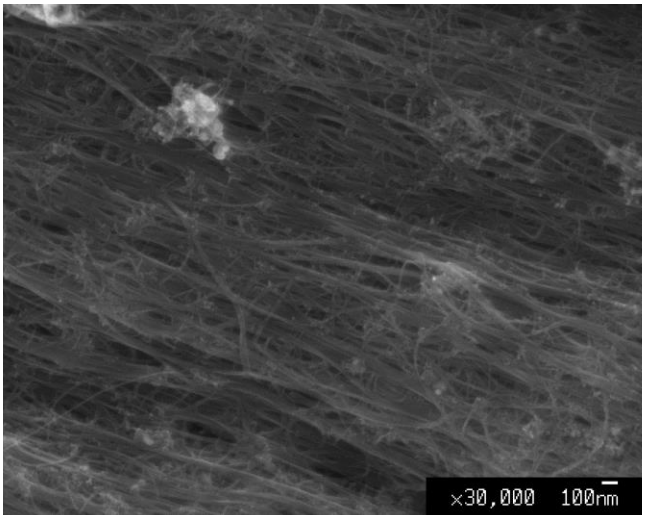

Fig.1. Scanning electron microscope image of carbon nanotube fibre.

In practice the electrical transport in these assemblies is the most similar to the disordered conductors such as conductive polymers, whose transport, depending on the type of disorder and doping levels, may be characterized by such phenomena as localization of charge carriers, hopping conduction or fluctuation induced tunnelling [7]. These mechanisms are recognised based on changes of electrical conductivity of the sample at low temperatures and in high magnetic fields.

However, the description of the electrical conduction in case of carbon nanotube fibres is not straightforward due to the large variety of morphologies of CNT fibres. Only the systematic studies of the resistance-temperature characteristics and magnetoresistance of CNT fibres provides some insight into the transport mechanisms and may provide some information on the bulk morphology of the CNT fibres. As an example Figure 2 presents the differences in the resistance changes with temperature of 17 samples produced via floating catalyst chemical vapour deposition process using four types of feedstock. It was recognised that structural changes in the CNT fibres due to change of feedstock produce systematic changes in the resistance-temperature plots [8].

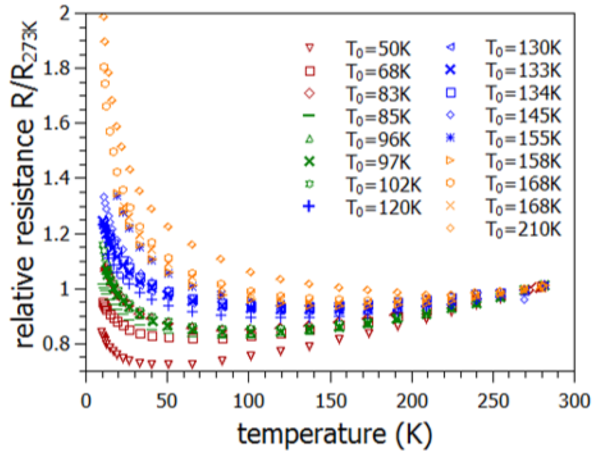

Fig.2. Resistance-temperature plots for 17 samples of various CNT fibers spun directly from the CVD reactor. Resistance values are referenced to the resistance of a given sample at 273 K

Similar changes may be observed in magnetoresistance of various fibres. Figure 3 presents examples for very good quality (Fig. 3 a)) and standard quality (Fig. 3 b)) fibres [9].

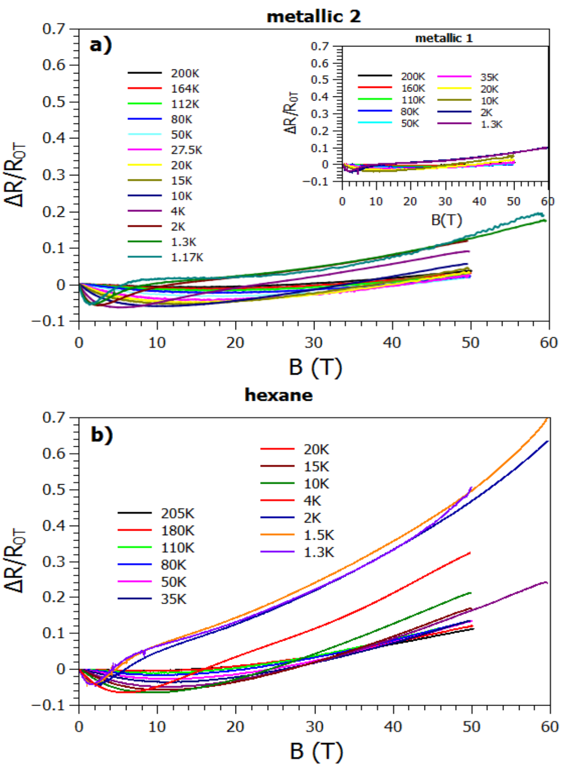

Fig.3. Magnetoresistance of a) good and b) standard quality samples produced via floating catalyst chemical vapour deposition process.

Finally, the differences in the electrical transport of fibre and any other standard conductive metal may be observed in the high currents transport as the fibres are very porous which facilitates the heat removal [10]. Also the changes in resistance upon tensile forces are strongly influenced by the nature of fibres constituents [11].
All these aspects of CNT fibres electrical performance need thorough exploration and understanding, before the fibres may be used in any large-scale applications.

Conclusions

Carbon nanotube fibres are very promising materials for the next generation of electrical conductors due to their unique building blocks – carbon nanotubes. However, before the CNT assemblies may be applied in real-life applications their structure needs to be optimized and their electrical transport well-understood. The current research concentrates on such aspects as electrical conductivity at low temperatures and at high magnetic field as well as under mechanical load and in the region of high currents. Although, a lot of research has already been performed in this area further studies are still necessary.

REFERENCES

[1] Lekawa-Raus A., Patmore J., Kurzepa L., Bulmer J., Koziol K., Electrical Properties of Carbon Nanotube Based Fibers and Their Future Use in Electrical Wiring, *Adv. Funct. Mat.*, 24 (2014), 3661-3682.
[2] Xu F., Sadrzadeh A., Xu Z., Yakobson B., Can carbon nanotube fibers achieve the ultimate conductivity?—Coupled-mode analysis for electron transport through the carbon nanotube contact, *J. Appl. Phys.* 114 (2013), 063714.
[3] Maarouf A., Kane C., Mele E., Electronic structure of carbon nanotube ropes, *Phys. Rev. B* 61, (2000), 11156.
[4] Tunney M., Cooper N., Effects of disorder and momentum relaxation on the intertube transport of incommensurate carbon nanotube ropes and multiwall nanotubes, *Phys. Rev. B* 74, (2006), 075406.
[5] Neophytou N., Ahmed S., Klimeck G., Influence of vacancies on metallic nanotube transport properties, *Appl. Phys. Lett.* 90, (2007), 182119.
[6] Giusca C., Tison Y., Ravi S., Silva P., Atomic and electronic structure in collapsed carbon nanotubes evidenced by scanning tunneling microscopy, *Phys. Rev. B* 76, (2007), 035429.
[7] Kaiser A., Electronic transport properties of conducting polymers and carbon nanotubes, *Rep. Prog. Phys.* 64, (2001) 1-49.
[8] Lekawa-Raus A., Walczak K., Kozlowski G., Wozniak M., Hopkins S., Koziol K., Resistance-temperature dependence in carbon nanotube fibers, *submitted to Carbon*.
[9] Lekawa-Raus A., Balakirev F., Bulmer J., Rickel D., Koziol K., Carbon nanotube fibres in ultrahigh magnetic fields, *manuscript in preparation*.
[10] Lekawa-Raus A., Lukawski D., Koziol K., Influence of condensation methods on electrical properties of carbon nanotube fibres, manuscript in preparation.
[11] Lekawa-Raus A., Koziol K., Windle A., Piezoresistivity in carbon nanotube fibers, *submitted to ACS Nano*.

***Author**: dr inż. Agnieszka Lekawa-Raus, Department of Materials Science and Metallurgy, University of Cambridge, 27 Charles Babbage Road, CB3 0FS, Cambridhe, UK*

8th International Conference
Electromagnetic Devices and Processes in Environment Protection ELMECO-8
joint with 11th Seminar Applications of Superconductors AoS-11
September 28 - October 1, 2014, Nałęczów, Poland

THERMAL-HYDRAULIC ANALYSIS OF THE IMPROVED LTS CONDUCTOR DESIGN CONCEPTS FOR THE DEMO TF COIL

Monika LEWANDOWSKA[1], Kamil SEDLAK[2]

West Pomeranian University of Technology, Szczecin (1), EPFL-CRPP, Villigen PSI (2)

***Abstract**. The improved design concepts for the LTS TF coil system of DEMO have been proposed in 2013 by EPFL-CRPP PSI Villigen and ENEA Frascati. The present study is focused on the thermal-hydraulic analysis of the conductor designs, which includes: hydraulic analysis, heat removal analysis and assessment of the hot spot temperature and the maximum pressure in each conductor during quench.*

***Streszczenie.** W 2013 r. zespoły z EPFL-CRPP i ENEA Frascati opracowały udoskonalone koncepcje projektowe kabli dla poszczególnych warstw cewki TF tokamaka DEMO. W pracy przedstawiono analizę cieplno – przepływową projektów kabli obejmującą: analizę hydrauliczną, oszacowanie zdolności usuwania ciepła oraz oszacowanie maksymalnej temperatury oraz maksymalnego ciśnienia podczas utraty stanu nadprzewodzenia.*

Keywords: thermal-hydraulic analysis, hot spot temperature, DEMO, TF coil.
Słowa kluczowe: analiza cieplno-przepływowa, temperatura gorącego punktu, DEMO, cewka TF.

Introduction

Long–term efforts of the European community towards the realization of fusion energy are currently focused on the design of DEMO - a demonstration fusion power plant producing net electricity for the grid at the level of a few hundred MW. It is foreseen that DEMO will start operation in the early 2040s [1]. The core of DEMO is an inductively driven tokamak with 16 toroidal field (TF) coils and the major radius of about 9 m [2]. Current design and assessment studies in the superconducting magnets for DEMO include activities both on low (LTS) and high (HTS) T_c superconductors, as well as engineering integration. LTS technology is fully mature, so the related activities are focused on the design and construction of coils which would fulfil the specific DEMO requirements. A parallel HTS R&D program includes studies, testing and development of different HTS cable concepts, such as e.g. twisted stack cable, Roebel assembled coated conductor (RACC) or conductor on round core (CORC), for possible future application to fusion [3]. Our work is a part of LTS activities.

Two preliminary design concepts for the LTS TF coil system of DEMO have been proposed in 2012 by EPFL-CRPP PSI Villigen and ENEA Frascati. The mechanical, electromagnetic and thermal-hydraulic analyses of the both preliminary design concepts revealed that they required some modifications. The improved design concepts have recently been proposed [2] and subjected to comprehensive analyses. The present work is focused on the thermal-hydraulic analysis of both candidate designs. The feedback from the analysis results will lead to further optimization of the conductor layouts.

Conductors' characteristics and model assumptions

The LTS TF coil designed for DEMO consists of 9 graded double layers (DLs) wound using:

a) CRPP design: "react & wind", flat multistage cables with two side cooling channels (Fig. 1a),
b) ENEA design: "wind & react", rectangular CICC with a central cooling channel separated from the bundle region with a thick steel perforated tube (Fig. 1b).

The six inner DLs (DL1-DL6) in a high magnetic field region, are made of Nb_3Sn superconductors, whereas the three outer DLs (DL7-DL9) are made of NbTi. The conductors' parameters relevant for the present analysis, are compiled in Table 1. In the 2nd column we show the lengths, L, of the inner (shortest) conductor in each DL. We calculated the effective bundle void fraction, φ, listed in the 3rd column, under the assumption that the outer copper layer is a part of the bundle. Symbol $D_{h,B}$ denotes the hydraulic diameter of the bundle, A is the cross section of different cable components and B_0 is the expected magnetic field at the nominal current I_0 = 82.4 kA. In both designs copper in superconducting strands (index Cu1) has RRR = 100, whereas copper in segregated strands and in the outer layer (index Cu2) is characterized by RRR = 400 and 300 in

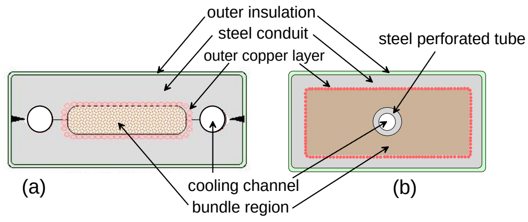

Fig.1. Schematic layout of (a) CRPP and (b) ENEA conductor.

Table 1. Conductors' characteristics used in the analysis

DL	L (m)	φ (-)	$D_{h,B}$ (mm)	$A_{He,B}$ (mm^2)	A_{sc} (mm^2)	A_{Cu1} (mm^2)	A_{Cu2} (mm^2)	A_{steel} (mm^2)	B_0 (T)
CRPP design									
1	438.3	0.19	0.91	227	276	276	413	3272	13.24
2	445.3	0.19	0.92	203	162	162	536	3290	11.86
3	452.1	0.19	0.92	195	126	126	559	3237	10.89
4	458.8	0.19	0.92	195	114	114	584	3127	10.07
5	543.0	0.19	0.92	183	94	94	575	2650	9.24
6	550.8	0.19	0.92	183	82	82	599	2650	8.12
7	558.6	0.28	0.92	437	265	397	487	2016	6.91
8	566.2	0.27	0.93	375	160	400	436	2161	5.68
9	491.9	0.27	0.93	375	160	400	436	2044	4.15
ENEA design									
1	512	0.25	0.54	486	353	353	696	1858	13.08
2	520	0.24	0.53	470	203	203	991	1853	11.43
3	528	0.24	0.53	419	151	151	941	1764	10.21
4	536	0.24	0.53	396	127	127	944	1748	9.33
5	544	0.24	0.53	396	101	101	980	1740	8.27
6	552	0.24	0.53	388	75	75	1017	1735	7.11
7	440	0.27	0.60	531	411	616	336	2044	5.80
8	446	0.27	0.59	492	91	137	1046	2021	4.80
9	410	0.27	0.59	437	46	68	1030	1907	3.57

the CRPP and ENEA design, respectively. The inner diameter of the cooling channel is D_{in} = 6 mm for all ENEA conductors, whereas in the CRPP design D_{in} = 10 mm for the conductors in DL1 and 6 mm in the rest of DLs.

Our thermal-hydraulic analysis of both candidate conductor designs includes: (i) hydraulic analysis – calculation of the mass flow rates in each conductor at the expected value of pressure drop in the coil at operating conditions, (ii) heat removal analysis – calculation of mass flow rates and the helium outlet temperatures in each conductor as functions of the heat deposition rate, (iii) assessment of the hot spot temperature and the maximum pressure in each conductor during quench. It is performed according to the methodology described in [4]. The quench simulations are done using two different tools, namely (i) a simple model representing the extreme scenario for maximum pressure: whole conductor is in normal state and all channels of flow are blocked and (ii) a more realistic scenario of quench development is obtained, using the CryoSoft code THEA [5], version 8.0 delta. In the THEA model we analyse two cases with different magnetic field profiles along the conductor: (a) $B(x)$ = B_0 = const, (b) constant field everywhere except a 10 m long region around x = 300 m, where the peak field follows the profile calculated for the DEMO TF coil.

Results

The results of the hydraulic analysis are presented in Fig. 2. The total mass flow rate in the TF coil, in case when there is no heat deposition, was assessed to be 224 g/s and 124 g/s for the CRPP and ENEA design, respectively.

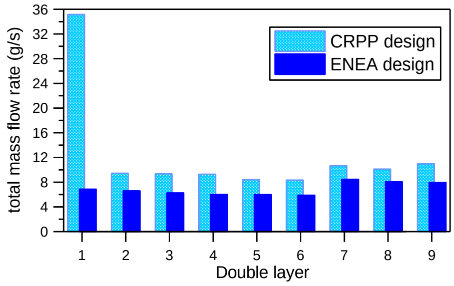

Fig. 2. Total mass flow rates in the shorter conductor in each DL of CRPP and ENEA coil (no heat deposition in the coil).

The expected nuclear heat deposition in the DL1 is of about 100 W. The safe operation of a cable is ensured if the temperature margin T_{cs} - T_{out} > 1.5 K. In Table 2 we show the values of the helium outlet temperature in the inner conductor of DL1 calculated for the heat deposition rate $\dot{Q} = 100$ W (the most pessimistic scenario – all power deposited in the inner conductor) and 50 W (heat deposited evenly in both conductors of DL1). It is seen that the temperature margin in the ENEA conductor is too small, even at the smallest expected heat deposition.

Table 2. The outlet helium temperature for the inner conductor in the first DL for the expected heat deposition rate

Design	T_{cs} (K)	$\dot{Q}$ = 50 W		$\dot{Q}$ = 100 W	
		T_{out} (K)	T_{cs} -T_{out} (K)	T_{out} (K)	T_{cs} -T_{out} (K)
CRPP	6.99	4.93	2.06	5.22	1.77
ENEA	6.31	**5.89**	**0.42**	**6.64**	**-0.67**

The maximum hot spot temperature and maximum pressure during quench, calculated using different approaches are presented in Table 3. It is seen that in the hot spot temperatures calculated with THEA in CRPP conductors are above the 250 K criterion specified in [6].

Table 3. Maximum temperature and pressure in the DEMO TF conductors calculated with the simplified model and with THEA.

DL	Simple model		THEA Case a		THEA Case b	
	T_{max} (K)	p_{max} (bar)	T_{max} (K)	p_{max} (bar)	T_{max} (K)	p_{max} (bar)
CRPP design						
1	68	166	214	58	220	53
2	65	161	220	115	244	93
3	65	160	237	118	273	92
4	63	156	227	104	266	76
5	70	172	266	123	322	93
6	66	163	250	101	309	66
7	53	130	62	96	67	94
8	54	131	73	94	85	89
9	46	110	63	73	76	67
ENEA design						
1	58	141	64	97	69	87
2	51	123	51	89	61	74
3	54	131	58	87	69	74
4	53	130	58	79	70	68
5	51	124	55	73	68	61
6	48	117	52	69	66	57
7	47	114	46	70	46	61
8	38	90	37	60	38	51
9	38	89	37	58	37	48

Conclusions

It results from our analysis that both CRPP and ENEA designs require some modifications in the next iteration of the design. To increase the heat removal capability and the related temperature margin we recommend to increase the diameter of the central cooling channel in the ENEA DL1 conductor. The copper cross section in CRPP DL2-DL6 conductors should be increased to reduce the hot spot temperature during quench.

Acknowledgement

This work was financed by the European Atomic Energy Community under the contract of Association between EURATOM and the IPPLM (No. FU07-CT-2007-00061) and is subject to the provisions of the EFDA. This work was supported within the framework of the scientific financial resources in 2013 allocated for the realization of the international co-financed project.

REFERENCES

[1] Romanelli F., Barabaschi P., Borba P., *et al.*, A roadmap to the realization of fusion energy, EFDA, Garching, Germany, 2012.

[2] Bruzzone P., Sedlak K., Stepanov B., Muzzi L., *et al.*, Design of large size, force flow superconductors for DEMO TF coils, *IEEE Trans Appl Supercon*, 24 (2014), No. 5, 4201504 (4 pp.)

[3] Fietz W.H., Barth Ch., Drotziger S., *et al.*, Prospects of High Temperature Superconductors for fusion magnets and power applications, Fus Eng Des, 88 (2013) 440– 445

[4] Lewandowska M., Sedlak K., Thermal-hydraulic analysis of LTS cables for the DEMO TF coil, *IEEE Trans Appl Supercon*, 24 (2014), No. 3, 4200305 (5 pp.)

[5] Bottura L., Rosso C., Breschi M., A general model for thermal, hydraulic and electric analysis of superconducting cables, Cryogenics, 40 (2000), No. 8–10, 617–626

[6] ITER design description document. Magnets. Section 1: Engineering description, ITER_D_22HV5L v2.2, 2006.

***Authors**: dr hab. inż. Monika Lewandowska, Zachodniopomorski Uniwersytet Technologiczny w Szczecinie, Wydział Inżynierii Mechanicznej i Mechatroniki, Instytut Fizyki, Al. Piastów 48, 70-311 Szczecin, e-mail: monika.lewandowska@zut.edu.pl ; dr Kamil Sedlak, Fusion Technology - Superconductivity Division, CH-5232 Villigen-PSI, Switzerland, e-mail: kamil.sedlak@psi.ch.*

8th International Conference
Electromagnetic Devices and Processes in Environment Protection ELMECO-8
joint with 11th Seminar Applications of Superconductors AoS-11
September 28 - October 1, 2014, Nałęczów, Poland

WŁAŚCIWOŚCI PIEZOELEKTRYCZNE MASYWNYCH PRÓBEK ZnO DOMIESZKOWANYCH Y_2O_3

Jan ZIAJA, Anna KISIEL, Marcin LEWANDOWSKI

Instytut Podstaw Elektrotechniki i Elektrotechnologii, Politechnika Wrocławska

***Abstract**. A process of the production of massive samples of ZnO is presented in this paper. The samples of ZnO were doped with Y_2O_3 in order to improve the piezoelectric properties The obtained results confirm the positive effect of doping ZnO on the piezoelectric properties.*

***Streszczenie.** W pracy przedstawiono proces wytwarzania masywnych próbek ZnO. W celu polepszenia właściwości piezoelektrycznych otrzymane próbki domieszkowano Y_2O_3. Uzyskane wyniki wskazują na pozytywny wpływ domieszkowania ZnO na jego właściwości piezoelektryczne.*

Keywords: piezoelectric properties, ZnO doped Y_2O_3, factor d_{33}
Słowa kluczowe: właściwości piezoelektryczne, ZnO domieszkowane Y_2O_3, współczynnik d_{33}

Wstęp

Rozwój przemysłu wymusza miniaturyzację urządzeń i przyrządów, które jednocześnie spełniają warunek energooszczędności. Dlatego też istnieje potrzeba poszukiwania nowych materiałów o ściśle określonych właściwościach elektrycznych. Do takich materiałów można zaliczyć tlenek cynku (ZnO), który znajduje szerokie zastosowanie w:

a) przemyśle elektrotechnicznym (zastosowanie w układach ochrony przepięciowej, ekrany chroniące ludzi i sprzęt przed szkodliwym działaniem pola elektromagnetycznego [1,2]),
b) przemyśle elektronicznym (zabezpieczeń czułych elementów i układów elektronicznych, takich jak: układy scalone, tranzystory, oscyloskopy czy mierniki o dużych dokładnościach[3]; elementy piezoelektryczne, warstwy izolacyjne w tranzystorach TFT [4], diody laserujące, technologie światłowodowe [5])
c) przemyśle chemicznym (pigment do farb i lakierów, wypełniacz, katalizator uwodorniania alkoholi, produkcja amoniaku (NH_3), metanolu (CH_3OH),
d) medycynie (wypełniacz stomatologiczny, składnik nadający właściwości antyseptyczne i ściągające),
e) kryminalistyce.

Zmieniając parametry technologiczne oraz stosując odpowiednie domieszki, można regulować przewodnictwo elektryczne warstw od typowo elektronowego do dziurowego. Otrzymywane warstwy mogą być przewodzące, półprzewodzące lub dielektryczne. Te właściwości powodują duże zainteresowanie przemysłu oraz ośrodków badawczych, o czy świadczy ciągle wzrastająca ilość publikacji.

Technologia wytwarzania masywnych próbek ZnO

W prezentowanej pracy przedstawiono wyniki badań wpływu czasu wygrzewania próbek czystego tlenku cynku (ZnO) oraz domieszkowanego tlenkiem itru (Y_2O_3) w ilości 10% wag. na wartość współczynnika d_{33}. Do badań wyselekcjonowano próbki wykonane z ZnO o wymiarach ziaren 32 i 72 μm. Po sprasowaniu próbki wygrzewano w temperaturze 1100°C w czasie od 2 do 10 godzin. Współczynnik d_{33} mierzono przyrządem piezometr PM3500 d_{33} Meter. Charakterystyki prądowo - napięciowe mierzono elektrometrem Keithley 617.

Wyniki

Na rysunku 1 oraz 2 przedstawiono charakterystyki prądowo - napięciowe otrzymanych próbek ZnO dla różnych wartości czasu spiekania i różnych wielkości ziaren (rysunek 1 – d = 32 μm, rysunek 2 – d = 72 μm.)

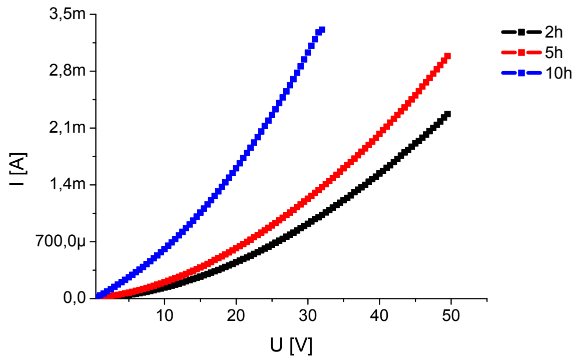

Rys.1. Charakterystyka I=f(U) dla próbek ZnO o średnicy ziaren *d* = 32 μm i czasie spiekania *t* = 2, 5 i 10 godzin

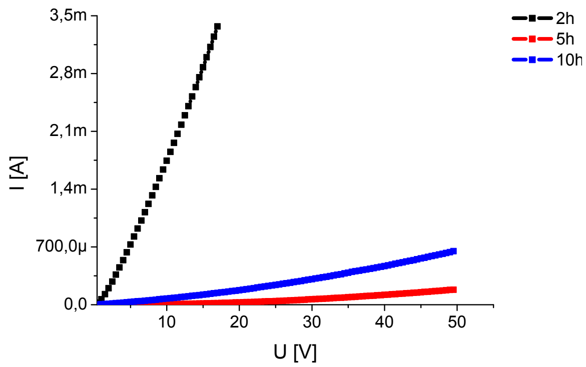

Rys.2. Charakterystyka I=f(U) dla próbek ZnO o średnicy ziaren *d* = 72 μm i czasie spiekania *t* = 2, 5 i 10 godzin

Na rysunku 3 przedstawiono charakterystyki prądowo - napięciowe próbek ZnO domieszkowanego w 10% Y_2O_3 dla różnych wartości czasu (wielkości ziaren *d* = 72 μm.).

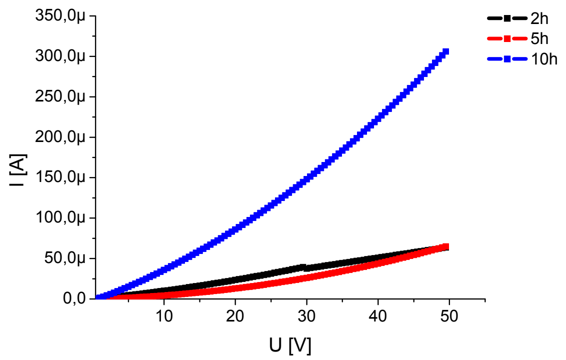

Rys.3. Charakterystyka I=f(U) dla próbek ZnO domieszkowanych w 10% Y_2O_3 o średnicy ziaren *d* = 72 μm i czasie spiekania *t* = 2, 5 i 10 godzin

Wartości współczynnika d_{33} dla otrzymanych próbek przedstawiono w tabeli 1

Table 1. Wartości współczynnika d_{33}.

numer próbki	średnica ziarna *d* [μm]	czas spiekania *t* [h]	domieszka	współczynnik d_{33} [pC/N]
1	32	2	-	3,3
2	32	5	-	3,2
3	32	10	-	3,6
4	72	2	-	3,6
5	72	5	-	3,0
6	72	10	-	3,2
7	72	2	10% Y_2O_3	6,3
8	72	5	10% Y_2O_3	6,7
9	72	10	10% Y_2O_3	6,5

Wnioski

- zastosowanie domieszki Y_2O_3 zwiększa dwukrotnie bazową wartość współczynnika d_{33},
- w prezentowanej technologii czas spiekania próbek nie ma większego wpływu na właściwości piezoelektryczne badanych próbek,
- współczynnik nieliniowości w charakterystykach prądowo – napięciowych wskazuje na słaby charakter warystorowy otrzymanych próbek.

REFERENCES

[1] Ziaja J., Jaroszewski M., *EMI shielding using composite materials with plasma layers, electromagnetic waves*, *Vitaliy Zhurbenko (ed)* 2011, 425–448

[2] Ziaja J., Koprowska J., Janukiewicz J., Using plasma metallization for manufacture of textile screens against electromagnetic fields, *Fibres & Textiles in Eastern Europe*, 2008, Vol. 16, nr 5, 64–66

[3] Faruque M., Hossaina, Nishiia J., Takagia S., Sugiharad T., Ohtomoa A., Fukumuraa T., Koinumaa H., Ohnoc H., Kawasakia M., Modeling of grain boundary barrier modulation in ZnO invisible thin film transistors, *Physica, 2004*, E 21, 911–915.

[4] Lee D. H., Park K. H., Sangsig K., Lee S.-Y., Effect of Ag doping on the performance of ZnO thin film transistor, *Thin Solid Films*, 2011,Vol. 520, 1160–1164.

[5] Kang H. S., Kang J. S., Kim J. W., Lee S. Y., Annealing effect on the property of ultraviolet and green emissions of ZnO thin films, *J. Appl. Phys*., 2004, 95, 1246–1250.

***Authors**: dr hab. inż. Jan Ziaja, dr inż. Anna Kisiel, dr inż. Marcin Lewandowski, Politechnika Wrocławska,* Instytut Podstaw Elektrotechniki i Elektrotechnologii, *wyb. Stanisława Wyspiańskiego 27, 50-370 Wrocław, E-mail: jan.ziaja@pwr.edu.pl, anna.kisiel@pwr.edu.pl, marcin.p.lewandowski@pwr.edu.pl.*

Praca finansowana w ramach badań statutowych Instytutu Podstaw Elektrotechniki i Elektrotechnologii Politechniki Wrocławskiej

8th International Conference
Electromagnetic Devices and Processes in Environment Protection ELMECO-8
joint with 11th Seminar Applications of Superconductors AoS-11
September 28 - October 1, 2014, Nałęczów, Poland

NUMERICAL ANALYSIS OF MEDIUM VOLTAGE CLASS INDUCTIVE SUPERCONDUCTING FAULT CURRENT LIMITER

Michal MAJKA, Janusz KOZAK, Slawomir KOZAK, Grzegorz WOJTASIEWICZ

Electrotechnical Institute, Warsaw

Abstract. *This paper presents the numerical model and the calculated electrical parameters of the new 15 kV class coreless superconducting fault current limiter (SFCL) prototype. The coreless SFCL consists of three windings: a primary and secondary windings made of SF12050 tape and a parallel connected primary copper winding. The FEM-circuit numerical model of SFCL was used to analyze the current, resistance and temperature of SFCL in the limitation state.*

Streszczenie. *W artykule zaprezentowano model numeryczny nowego prototypu nadprzewodnikowego ogranicznika prądu typu indukcyjnego dla sieci 15 kV. Bezrdzeniowy nadprzewodnikowy ogranicznika prądu składa się z trzech uzwojeń: pierwotnego i wtórnego wykonanego z taśmy SF12050 oraz równolegle podłączonego pierwotnego uzwojenia miedzianego. Polowo-obwodowy model numeryczny ogranicznika został użyty do wykonania analizy przepływu prądów oraz zmian rezystancji i temperatury uzwojeń ogranicznika w czasie ograniczania prądu.*

Keywords: superconducting inductive fault current limiter, SFCL, superconducting tape, numerical analysis.
Słowa kluczowe: nadprzewodnikowy ogranicznik prądu typu indukcyjnego, SFCL, taśma nadprzewodnikowa, analiza numeryczna.

Introduction

The electrodynamic forces occurring during the course of a fault current may damage the devices of the electric power system, such as transformers, generators or busbars in switching stations, within tens of milliseconds. Every such failure of an electric power network entails expensive and time-consuming repairs. A rapid increase of the resistance of a superconductor on crossing the current critical value I_c makes it possible to build reliable superconducting fault current limiters (SFCLs) [1, 2, 4, 5]. SFCLs react very rapidly by limiting the first, the most dangerous, surge current during a current fault condition, thus protecting the devices of the electric power network from the dynamic effects of current faults.

Design of the SFCL

A design of a 1-phase inductive type superconducting limiter is presented in fig. 1. The limiter was designed to work in a 15 kV power system [1, 3]. Its main parameters are presented in table I. A coreless three-winding superconducting fault current limiter has two primary windings and one secondary winding . The primary winding, placed on the outer ring, is made of a copper wire. The second primary winding, placed in the inner ring, is made of a 2G superconducting tape (SF12050). The third winding is a shorted secondary winding made of a 2G superconducting tape (SF12050), placed in the inner ring. The primary winding made of 2G tape is connected in parallel with the copper primary winding. All three windings are magnetically coupled. The limiter will be placed in a cryostat with an external vacuum insulation and cooled in a liquid nitrogen bath. The cryostat of the limiter will be made of GFRP (Glass Fiber Reinforced Polymer).

Numerical model of SFCL

The numerical model of the limiter was developed in the “Transient Magnetic” FEM-circuit Flux2D software. The geometry of the actual model of the limiter was substituted with a simplified axially symmetric geometry (Fig. 1c). Simulations were performed for models of limiter whose parameters are presented in table I. Thanks to the performed simulations, courses of a fault current in the circuit with and without the limiter were obtained (Fig. 2), as well as the changes of resistance and temperature of individual limiter windings during the limitation of the fault current (Fig. 3).

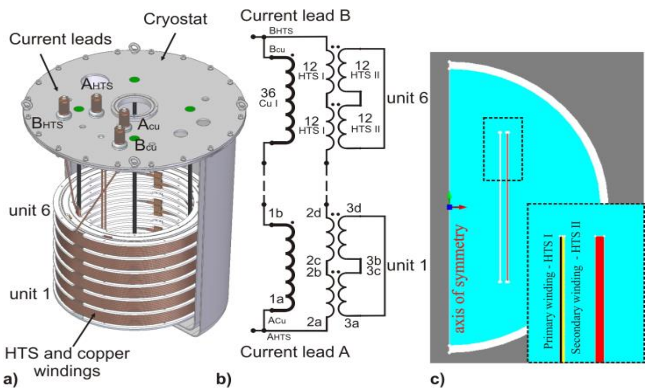

Fig.1. Design (a) and electrical circuit of the limiter consists of six identical units connected in series (b). Geometry of numerical model in Flux2D (c).

Table 1. Parameters of SFCL

Parameter		Value
Nominal voltage	U_N	15 kV
Nominal current	I_N	140 A
Voltage on the limiter @ I_N	U_{SCFL}	< 1 V
Prospective peak current	i_{peak}	40 kA
First peak limiting	i_p	4.7 kA
Limitation time	t_{lim}	160 ms
Operating temperature	T	77.4 K
Cryostat high	H	1 m
Cryostat diameter	O.D.	0.85 m
Copper winding diameter	I.D.	0.578 m
HTS windings diameter	I.O.	0.506 m
Total number of copper turns	n_{Cu}	216
Total number of prim. HTS turns	$n_{HTS\ I}$	144
Total number of sec. HTS turns	$n_{HTS\ II}$	144
Length of copper winding (3 mm x 6 mm)	l_{Cu}	393 m
Length of prim. HTS winding (SF12050)	$l_{HTS\ I}$	229 m

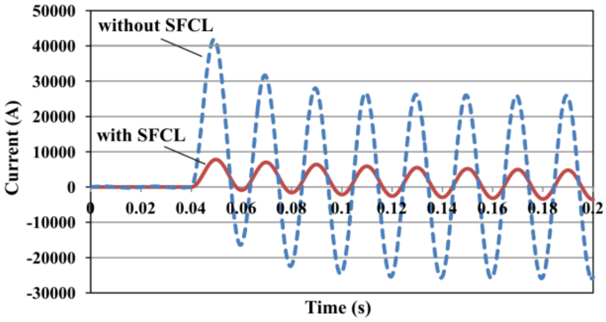

Fig. 2. Current waveforms in the circuit with and without SFCL

In the stand-by state, i.e. the first 40 ms of calculations, the superconducting windings of the limiter are in the superconducting state and a nominal current of 140 A flows through the limiter (Fig. 2). The voltage value in all models of the limiter is lower than 1 V, which results from a minor leakage reactance.

During a short-circuit lasting from 0.040 sec. to 0.200 sec., a fault current flows through the limiter. The peak value of the current in the shorted circuit i_p = 40 kA was limited to 4.7 kA (Fig. 2). The course of the fault current causes the HTS windings to heat up very rapidly. The temperature of the windings increases from an initial temperature of 77.4 K to a maximum temperature T_{max} which is reached at the moment of switching off of the short-circuit (Fig. 3c). The performed simulation shows that the temperature of the superconducting windings increases much faster than the temperature of the copper windings, and it reaches different values at the moment of switching off of the short-circuit. In designing the limiter, it was assumed that the maximum temperature of the limiter's superconducting windings at the moment of a short-circuit occurrence would not exceed 200 K and the fault current peak value would be below 5 kA.

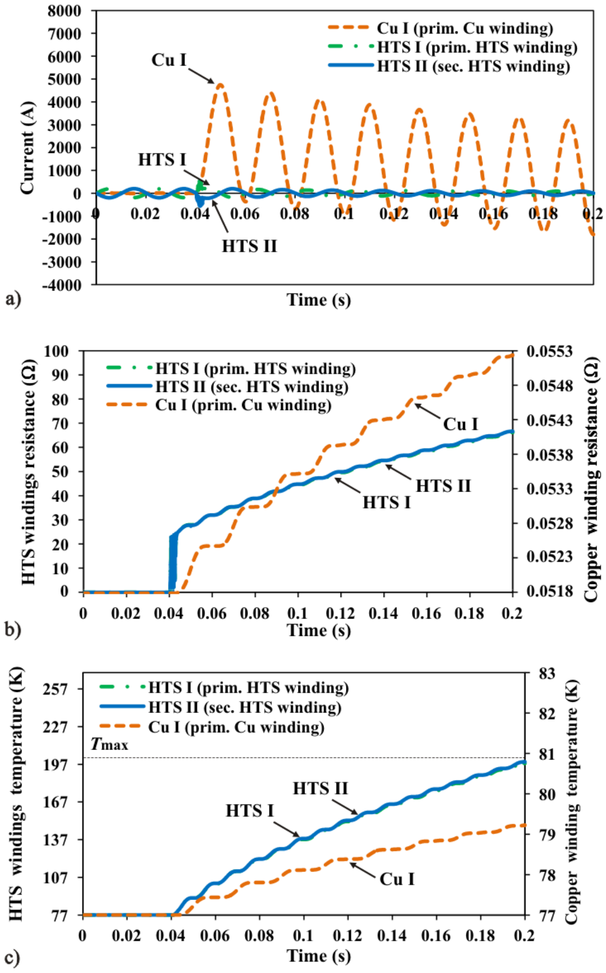

Fig. 3. Numerical model - current waveforms in the windings of the limiter (a), the changes of resistance (b) and temperatures of individual limiter windings (c) during the limitation of the fault current (graphs for HTS I and HTS II windings overlap)

Conclusion

An analysis of the results of the numerical simulations confirmed that it is possible to build an inductive type coreless superconducting fault current limiter that will effectively limit the peak value of the fault current from 40 kA to 5 kA within 160 ms. The developed design in which the superconducting windings are wound simultaneously onto a single bobbin allows to obtain a very high coupling factor between the windings and minimize the leakage reactance of the limiter, which minimizes the voltage in the limiter in the stand-by state. In case of a 2-winding design in which the primary copper winding is magnetically coupled with a secondary HTS winding, there always occurs leakage reactance, which causes losses in the stand-by state. The use of a connection in parallel of a copper coil and a superconducting coil in the primary winding protects the short circuit from opening in case when the superconducting tape is damaged. The fault current limiting capability of a 3-winding limiter is determined mostly by the impedance of the copper winding coupled in parallel with the primary superconducting winding. The number of turns in the primary copper winding and the superconducting tape length in the superconducting windings must be such that the temperature of the HTS windings does not exceed the maximum allowed temperature of the superconducting tape. Due to a substantial increase of the temperature of the limiter's HTS windings, the short circuit must be switched off by a conventional circuit breaker before the temperature of the HTS winding reaches the maximum value.

This work was supported in part by the National Centre for Research and Development under Grant UMO-2012/05/B/ST8/01837.

REFERENCES

[1] Kozak J., Majka M., Janowski T., Kozak S., Wojtasiewicz G., Kondratowicz-Kucewicz B., "Tests and Performance Analysis of Coreless Inductive HTS Fault Current Limiters", *IEEE Trans. Appl. Supercond.*, 21 (2011), No. 3, 1303 – 1306,

[2] Naeckel O., Noe M., "Design and Test of an Air Coil Superconducting Fault Current Limiter Demonstrator ", *IEEE Trans. Appl. Supercond.*, 24 (2014), No. 3, 5601605

[3] Kozak J., Majka M., Kozak S., Janowski T., „Design and Tests of Coreless Inductive Superconducting Fault Current Limiter", *IEEE Trans. Appl. Supercond.*, 22 (2012), No. 3, 5601804

[4] Kozak J., Majka M., Kozak S., Janowski T., „Comparison of Inductive and Resistive SFCL", *IEEE Trans. Appl. Supercond.*, 23 (2013), No. 3, 5600604

[5] Naeckel O., Noe M., "Conceptual Design Study of an Air Coil Fault Current Limiter ", *IEEE Trans. Appl. Supercond.*, 23 (2013), No. 3, 5602404.

***Authors**: dr inż. Michał Majka, Instytut Elektrotechniki, Zakład Wielkich Mocy, ul. Pożaryskiego 28, 04-703 Warszawa, e-mail: m.majka@iel.waw.pl; dr inż. Janusz Kozak, e-mail: j.kozak@iel.waw.pl; prof. dr hab. inż. Sławomir Kozak, e-mail: s.kozak@iel.waw.pl; dr inż. Grzegorz Wojtasiewicz, e-mail: g.wojtasiewicz@iel.waw.pl*

TUNING CHARACTERISTIC OF MICROWAVE PLASMA SOURCE FOR HYDROGEN PRODUCTION FROM LIQUID FUELS

Robert MIOTK[1, 2], Helena NOWAKOWSKA[1], Mariusz JASIŃSKI[1], Mirosław DORS[1], Jerzy MIZERACZYK[3]

The Szewalski Institute of Fluid-Flow Machinery, Polish Academy of Sciences (1),
Conjoint Doctoral School at the Faculty of Mechanical Engineering, Gdańsk University of Technology (2),
Department of Marine Electronics, Gdynia Maritime University (3)

***Abstract**. This paper presents investigations of the tuning characteristic of microwave plasma source designed for the hydrogen production from liquid fuels. The aim of the research was to estimate the electrons concentration n_e and electrons frequency collisions ν in the plasma generated in a mixture of nitrogen and ethanol vapor.*

***Streszczenie.** W niniejszej pracy przedstawiono badania charakterystyki strojenia mikrofalowego źródła plazmy przeznaczonego do produkcji wodoru z paliw płynnych. Celem prowadzonych badań było oszacowanie koncentracji n_e oraz częstotliwości zderzeń ν elektronów w plazmie generowanej w mieszaninie azotu i par etanolu*

Keywords: microwaves, microwave plasma source, tuning characteristics, electric field distributions.
Słowa kluczowe: mikrofale, mikrofalowe źródło plazmy, charakterystyka strojenia.

Introduction

Recently, the non-thermal microwave plasma has been used efficiently not only for the harmful gas [1] decomposition but also for the production of hydrogen by means of the plasma reforming of methane [2]. To meet industrial requirements for the production of hydrogen the MPS require optimization with the goal of improving the power coupling efficiency, i.e. the efficiency of power transfer from electric field to plasma, and stability of the MPS operation.

The efficiency of power transfer from electric field to plasma can be expressed as ratio P_R/P_I, where P_I, P_R are the power of the incident and reflected microwaves, respectively. Tuning characteristic of the MPS is a dependence of P_R/P_I on the position of the movable plunger l_s/λ_g (λ_g is the microwave wavelength in the WR 430 waveguide). The MPS is efficient when the value of ratio P_R/P_I is small; operates stable when the ratio does not depend on the movable plunger position.

In this paper, we analyze tuning characteristic of a waveguide-supplied metal-cylinder-based nozzleless MPS [3] designed for hydrogen production from liquid fuels. We anticipate that the use of liquid source of hydrogen can decrease the cost of hydrogen production due to much easier handling and greater availability than gaseous sources.

By comparing the calculated with the measured tuning characteristics of presented MPS the electron concentration n_e and electrons frequency collisions ν in the plasma generated in a mixture of nitrogen and ethanol vapor were estimated. The parameters n_e and ν are the basic properties that characterize plasma. Knowledge of these parameters is essential in the process of optimization of MPS construction (improving the power coupling efficiency).

Description of microwave plasma source

Sketch of the MPS is shown in fig. 1. This MPS was used by us for destruction of freon HFC-134a [4] and for producing hydrogen H_2 in the process of plasma reforming of methane CH_4 [5].

The MPS, operating at atmospheric pressure and frequency 2.45 GHz, is based on a standard rectangular waveguide WR 430 with a reduced-height section in the discharge region and two tapered sections on both sides. Microwave power is supplied to the MPS input plane (A-A') via a standard rectangular waveguide WR 430. A movable plunger on the other side of the MPS (output plane B-B') is a means of tuning, which allows for impedance matching and efficient transfer of the microwave power to the plasma. The plasma flame is generated inside a quartz tube which penetrated MPS through circular gaps on the axis of the waveguide wide wall and protruded below bottom waveguide wall. On the outside of the waveguide the quartz tube was surrounded by a metal cylinder with a slit for visualization. Working gas was introduced to the plasma by four gas ducts which formed a swirl flow inside the quartz tube.

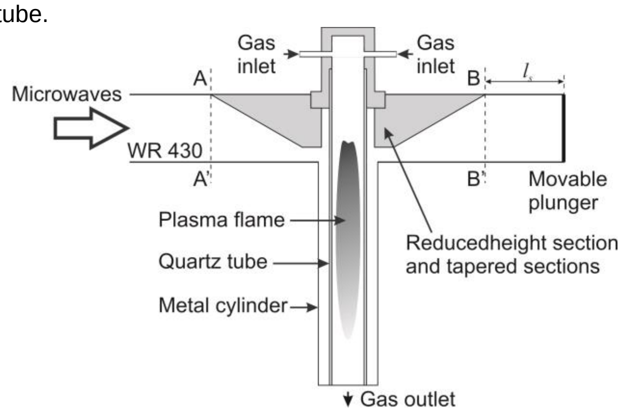

Fig. 1. Sketch of the microwave plasma source, A-A' – MPS input plane, B-B' – MPS output plane

Experiment and analysis of results

Nitrogen was used as a working gas. The nitrogen is one of the less expensive gases. The experiment test were performed with the working gas flow rate 2700 NL/h and incident microwave power P_I = 3 kW. Ethanol (C_2H_5OH) was introduced into the plasma using inductively heated vaporizer. The amount of C_2H_5OH was 0.8 kg/h. The purity of C_2H_5OH used in this investigations was 96%. For these working conditions tuning characteristics of presented MPS was measured (Fig. 2).

A method for calculating tuning characteristics of the MPS is presented in detail in ref. [6]. This method is treating the MPS as a two-port network, finding its scattering matrix coefficients and then calculating the reflection coefficient from analytical expressions. In this method, it is very important to properly assume volume of the plasma, spatial distribution of the electron concentration n_e and dielectric permittivity ε_p of the plasma.

In our investigations we assumed that plasma takes the form of a cylinder with the diameter of 1.6 cm and length of 12 cm (as observed experimentally). The axis of the plasma cylinder coincident with the axis of the quartz tube. Further, we assumed that the dielectric permittivity ε_p of plasma can be calculated from the Lorentz formula [6] and the concentration of electrons n_e at each point of the plasma cylinder is the same.

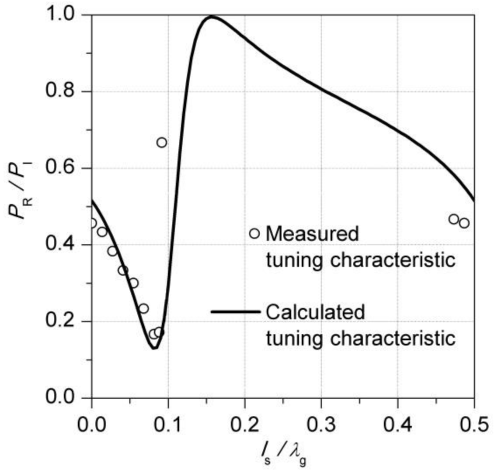

Fig. 2. Comparison of measured and calculated tuning characteristics

The calculated tuning characteristic is dependent on the values of parameters n_e and ν [6], which are unknown. These values can be estimated by comparing the calculated and measured tuning characteristics. A good agreement was found between the tuning characteristics obtained experimentally and numerically. For the present case of microwave discharge the best fit was obtained for the concentration n_e equal to 7.83×10^{11} cm^{-3} and collision frequency $\nu = 9.24\times10^{8}$ s^{-1} (Fig. 2).

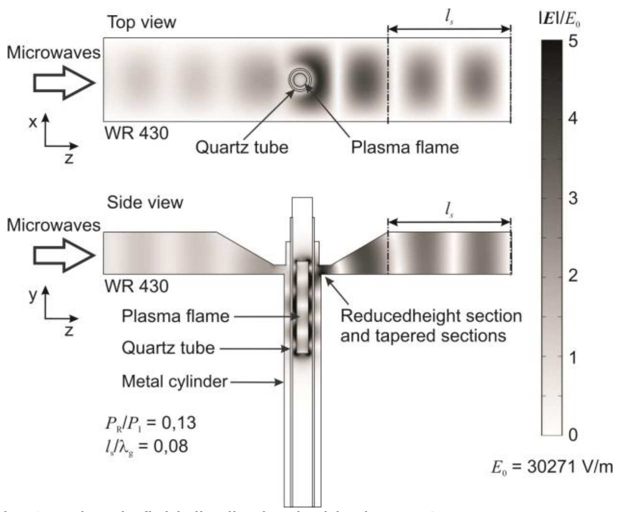

Fig. 3. Electric field distribution inside the MPS

Obtained tuning characteristics strongly depend on the position of the movable plunger. Fig. 2 show that the both characteristics measured and calculated has a minimum in $l_s/\lambda_g = 0.08$. This means that for this position of the movable plunger the efficiency of power transfer from electric field to plasma in MPS is highest. For this position the three-dimensional (3-D) distribution of electric field modules $|\boldsymbol{E}|$ in the MPS was determined by us numerically employing COMSOL software [7] (Fig. 3). In fig. 3 $|\boldsymbol{E}|$ were normalized to E_0 = 30271 V/m (E_0 - amplitude of the electric field in a lossless and perfectly matched waveguide WR 430 for P_I = 3 kW). The adoption scale $|\boldsymbol{E}|/E_0$ allowed to observe that in this position of the movable plunger the plasma cylinder is surrounded by electric field five times greater than the E_0.

Conclusions

The method by Nowakowska et al. [6] for calculating the tuning characteristic of MPS allows to estimate the concentration n_e and frequency collisions ν of electrons in the generated plasma. For the present case of microwave discharge (mixture of nitrogen and ethanol vapor) estimated parameters n_e and ν are equal to 7.83×10^{11} cm^{-3} and 9.24×10^{8} s^{-1}, respectively.

Results of present investigations allow us to optimize the construction of the tested MPS towards the improved power coupling efficiency. The aim of the optimization (modeling) of the MPS will be finding the optimal dimensions of the structural elements of the device which will ensure the minimum ratio P_R/P_I in the wide position range of movable plunger.

Acknowledgments

We are grateful to The National Science Centre (programme no. 2012/05/B/ST8/02789) for the financial support of this work.

REFERENCES

[1] Hong Y.C., Uhm H.S., Kim H.S., Kim M.J., Han H.S., Ko S.C., Park S.K., Decomposition of phosgene by microwave plasma-torch generated at atmospheric pressure, *IEEE Trans Plasma Sci*, 33 (2005), No. 2, 958–963

[2] Wang Y.F., Tsai Ch.H., Chang W.Y., Kuo Y.M., Methane steam reforming for producing hydrogen in an atmospheric-pressure microwave plasma reactor, *International Journal of Hydrogen Energy*, 35 (2010), 135–140

[3] Mizeraczyk J., Jasiński M., Nowakowska H., Dors M., Studies of atmospheric-pressure microwave plasmas used for gas processing, *Nukleonika*, 57 (2012), No. 2, 241−247

[4] Jasiński M., Dors M., Mizeraczyk J., Destruction of freon HFC-134a using a nozzleless microwave plasma source, *Plasma Chemistry and Plasma Processing*, 29 (2009), 363−372

[5] Jasiński M., Dors M., Nowakowska H., Nichipor G.V., Mizeraczyk J., Production of hydrogen via conversion of hydrocarbons using a microwave plasma, *Journal of Physics D: Applied Physics*, 44 (2011), 194002

[6] Nowakowska H., Jasiński M., Dębicki P., Mizeraczyk J., Numerical analysis and optimization of power coupling efficiency in waveguide-based microwave plasma source, *IEEE Trans Plasma Sci*, 39 (2011), No. 10, 1935–1942

[7] http://www.comsol.com

***Authors**: mgr Robert Miotk, dr inż. Helena Nowakowska, dr inż. Mariusz Jasiński, dr hab. inż. Mirosław Dors, The Szewalski Institute of Fluid-Flow Machinery, Polish Academy of Sciences, Fiszera 14, 80-231 Gdańsk, Poland, e-mail: rmiotk@imp.gda.pl, helena@imp.gda.pl, mj@imp.gda.pl, mdors@imp.gda.pl;*

prof. dr hab. inż. Jerzy Mizeraczyk, Department of Marine Electronics, Gdynia Maritime University, Morska 81-87, 81-225 Gdynia, Poland, e-mail: jmiz@imp.gda.pl.

8th International Conference
Electromagnetic Devices and Processes in Environment Protection ELMECO-8
joint with 11th Seminar Applications of Superconductors AoS-11
September 28 - October 1, 2014, Nałęczów, Poland

MEASUREMENT OF ULTRASONIC WAVE FOR ATMOSPHERIC DISCHARGE WITH MULTI-CHANNEL OPTICAL WAVE MICROPHONES

Fumiaki MITSUGI[1], Tomoaki IKEGAMI[1], Toshiyuki NAKAMIYA[2], Yoshito SONODA[2]

Kumamoto University (1), Tokai University (2)

***Abstract**. Fiber type multi-channel optical wave microphones system was developed for detection of changes in density of atmosphere such as sound waves. We applied the multi-channel optical wave microphones to detect ultrasonic waves emitted from atmospheric pressure plasma. Frequency analysis for measured ultrasonic waves in each channel was discussed.*

Keywords: optical wave microphones, atmospheric plasma, surface discharge
Słowa kluczowe: mikrofon optyczny, plazma atmosferyczna, wyładowanie powierzchniowe.

Introduction

Plasmas use the energy for generation of reactive species, optical emission, heat, and so on. We are focusing on discharge sound that ranges from audible to ultrasonic waves emitted from electric discharges because our concern is the energy transfer from a discharge to atmosphere in the form of pressure waves.

In the first line of research, we had used an optical wave microphone, which works based on Fraunhofer diffraction of a probe laser, for detecting discharge sound. Moreover, it was combined with a computer tomography scanning to cover the two dimensional visualization for ultrasonic waves emitted from a surface discharge. However, the method required longer scanning time and the assumption for stability of plasma in time.

Because state of plasma and atmosphere around the plasma changes in time especially in a closed space, we are developing a multi-channel optical wave microphones system to realize real-time observation for discharge sound. The use of optical fibber is necessary to increase spatial resolution, stability, sensitivity and signal to noise ratio of the system. The utilization of the system to a surface discharge is reported in this paper.

Experimental setup

Figure 1 shows an illustration for geometrical relationship between a surface barrier discharge device and four channels of a multi-channel optical wave microphones. Multi-channel optical wave microphones system was constructed using a fiber coupled semiconductor laser, a fiber divider, lenses and photo-detectors. The fiber coupled laser was divided into four outputs of fibers by the fiber divider. Optical power of each channel where sound is passed through was about 7.6 mW and its wavelength was 637 nm. Each laser beam was Fourier transformed with lens and conducted to the detector through a fiber. Distance between channels was 25 mm. The system (CH1) was set 5 mm over the top electrode of the surface discharge device. The four channels were arranged perpendicular to the direction of discharge sound propagation. The amplitude and frequency of the applied voltage to the electrode and the kinds of atmosphere around the surface discharge device were varied.

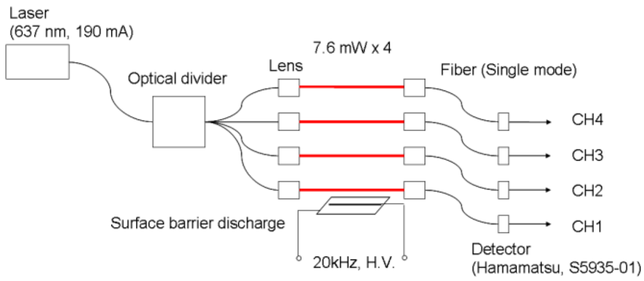

Fig.1. An experimental setup for multi-channel optical wave microphones.

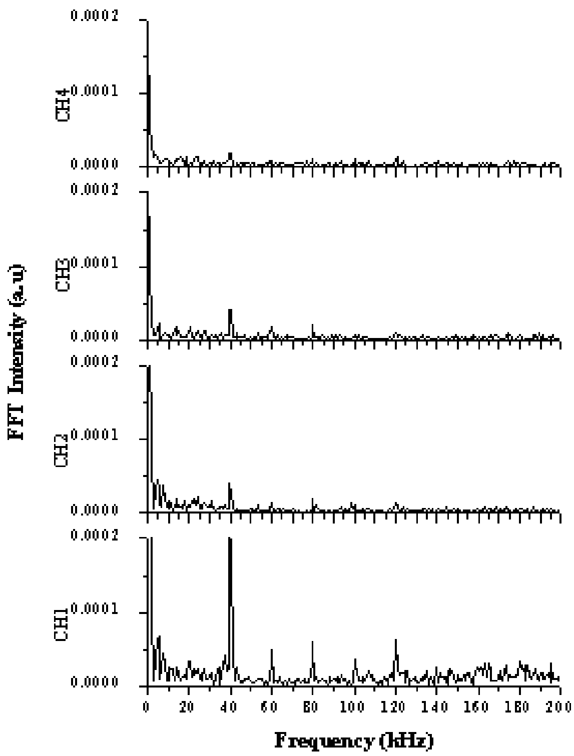

Fig.2. FFT analysis for ultrasonic waves emitted from surface barrier discharge.

Results and discussion

The multi-channel optical wave microphones improved its electromagnetic noise suppression drastically due to the use of optical fibers to detect discharge sound precisely. Therefore, slight ultrasonic sound could be identified even at position of CH4.

Attenuation and distribution of ultrasonic wave emitted from the surface discharge were analyzed using results measured by the four channel optical wave microphones system. Figure 2 shows Fast Fourier Transform analysis for ultrasonic waves, which were emitted from the surface discharge, detected by the four-channel optical wave microphones. The main frequency component was higher by a factor of two than that of power supply for the surface discharge because discharges occur mainly two times in one cycle of applied voltage and it was observable even at CH4. It can be considered that there is strong relation between applied electric field and ionic species for generation of ultrasonic wave.

Summary

In this work, we firstly employed the new system of multi-channel optical wave microphones system to detect and analysis ultrasonic wave propagation for surface discharge. The main frequency component of detected ultrasonic wave was higher by a factor of two than that of power supply for the surface discharge and it was observable even at CH4.

This research was supported by Grant-in-Aid for Young Scientists (B) 24760319.

REFERENCES

[1] Toshiyuki Nakamiya, Fumiaki Mitsugi, Shota Suyama, Tomoaki Ikegami, Kenji Ebihara, Yoshito Sonoda, Yoichiro Iwasaki, Shin-Ichi Aoqui, Henryka Stryczewska, Joanna Pawlat, Przeglad Elektrotechniczny (Electrical Review) 1/2011 (2011) 249-253

[2] Toshiyuki Nakamiya, Yoichiro Iwasaki, Fumiaki Mitsugi, Ryosuke Kozai, Tomoaki Ikegami, Yoshito Sonoda, and Ryoichi Tsuda, Journal of Advanced Oxidation Technologies 14(1) (2011) 63-70

[3] Fumiaki Mitsugi, Ryota Ide, Tomoaki Ikegami, Toshiyuki Nakamiya, Yoshito Sonoda, Thin Solid Films 521 (2012) 132-136

[4] Fumiaki Mitsugi, Tomoaki Ikegami, Toshiyuki Nakamiya, and Yoshito Sonoda, Japanese Journal of Applied Physics 51 (2012) 01AC10 1-5

[5] Toshiyuki Nakamiya, Fumiaki Mitsugi, Yoichiro Iwasaki, Tomoaki Ikegami, Ryoichi Tsuda, Yoshito Sonoda, Henryka Danuta Stryczewska, The European Physical Journal Applied Physics 61(2) (2013) 24310 1-8

***Authors**: Dr. Fumiaki Mitsugi, and Prof. Tomoaki Ikegami, Graduate School of Kumamoto University, Kurokami 2-39-1, Kumamoto city, Kumamoto 860-8555, Japan, E-mail: mitsugi@cs.kumamoto-u.ac.jp.; Prof. Toshiyuki Nakamiya and Prof. Yoshito Sonoda, Tokai University, Toroku 9-1-1, Kumamoto 862-8652, Japan, E-mail: nakamiya@tokai.ac.jp*

8th International Conference
Electromagnetic Devices and Processes in Environment Protection ELMECO-8
joint with 11th Seminar Applications of Superconductors AoS-11
September 28 - October 1, 2014, Nałęczów, Poland

HYDROGEN PRODUCTION FROM GASEOUS HYDROGEN COMPOUNDS USING PLASMA

Jerzy MIZERACZYK[1], Mariusz JASIŃSKI[2], Mirosław DORS[2]

Gdynia Maritime University (1), Szewalski Institute of Fluid-Flow Machinery, Gdańsk (2)

***Abstract**. Nowadays development of systems for hydrogen production are of high importance. Recently, several plasma methods have been proposed for the small-scale H_2 production. This paper is a short review of the plasma methods proposed for H_2 production mainly from gaseous fuels. The plasma methods for gaseous fuels processing to produce hydrogen are critically evaluated from the view point of H_2 production efficiency defined by the H_2 production rate (g(H_2)/h) and energy yield (g(H_2)/(kWh) and some other parameters.*

***Streszczenie.** W niniejszej pracy przedstawiono przegląd plazmowych metod produkcji wodoru z paliw gazowych. Metody porównano pod kątem efektywności produkcji wodoru wyrażonej przez wydajność masową i energetyczną procesu (g(H_2)/h i g(H_2)/(kWh), stopień przemiany surowca (%) oraz stężenie wodoru w gazie podprocesowym (%).*

Keywords: plasma, reforming, hydrogen.
Słowa kluczowe: plazma, reforming, wodór.

Introduction

Currently more than 80 % of the world energy supply comes from fossil fuels, resulting in strong ecological and environmental impacts. Such factors as the exhaustion of reserves and resources, air pollution and modification of the atmospheric composition, impacts on climate and on human health, are now of primary importance. It is a wide opinion that hydrogen has a great role to play as an energy carrier in the future energy sector.

Several processes have been developed for producing hydrogen mainly from fossil fuels and to some extent from water. Hydrogen can be produced from fossil fuels (or biomass and biomass-derived fuels) using such processes as steam reforming (mainly of natural gas), partial oxidation, auto-thermal reforming, and coal gasification. From any primary energy source (nuclear, wind, solar) converted into electricity hydrogen can be produced by the electrolysis of water. Hydrogen can also be produced using photochemical energy (photo-catalysis, bioconversion). At a large-scale in the chemical industry hydrogen has been produced as a by-product of sodium or potassium chloride electrolysis that gives chlorine and caustic soda or potash. Also hydrogen is a by-product of catalytic reforming of petroleum naphtha, made to improve the octane number, and of steam cracking of hydrocarbons for the production of ethylene. Smaller volumes of hydrogen are by-products in coke-ovens. In all the last cases hydrogen is mainly kept for internal use. More on various technologies related to hydrogen production by a so-called conventional methods can be found in a review of [1].

Recently another technology has been proposed for distributed hydrogen production [2]. This technology uses thermal and non-thermal plasmas for reforming gaseous and liquid compounds containing hydrogen. They can originate from fossil fuels and biomass.

This paper is a short review of the plasma methods proposed for hydrogen production mainly from gaseous fuels. In this review the plasma methods of gaseous fuels processing for hydrogen production are described and critically evaluated from the view point of hydrogen production efficiency defined by such parameters as the hydrogen production rate (g(H_2)/h), and energy yield (g(H_2)/(kWh)), precursor conversion degree (%) and volume hydrogen concentration in the outgas (%).

Plasma methods for hydrogen production

The majority of plasmas proposed for hydrogen production from gaseous fuels are generated by: electron beam, dielectric-barrier discharge, gliding arc, plasmatron arc and microwave discharge. Table 1 shows the energy yields of hydrogen production from CH_4 for different plasma methods. Methane is the most popular gaseous fuel used in the plasma production of H_2. For comparison, information on the energy yield of H_2 production by the conventional steam reforming of CH_4 (with a catalyst), water electrolysis, as well as dielectric barrier discharge and gliding arc, both employing alcohols as fuels, is given in Table 1.

Recently developed microwave plasma sources (MPSs) operated at atmospheric pressure exhibit a high potential for hydrogen production via pyrolysis, wet and dry reforming of various gaseous (natural gas, methane) and liquid fuels (gasoline, heavy oils and biofuels). They provide a plasma environment in which the heavy particles (atoms and molecules) have temperatures of 2000-6000 K while the electron temperature reaches 10000 K. Besides, the plasma contains ions and reactive radicals (H, OH, and O) which enhance conversion of hydrocarbon containing compounds into hydrogen. The wide range of the offered gas plasma temperatures enables choosing the temperature optimum for a given reforming path. This results in higher selectivity of hydrogen production. The other advantages of the use of plasma for hydrogen production are the compactness of the plasma system due to high energy density of the plasma and fast response time achieved by being powered by electricity.

We found that the most promising design of microwave plasma source for hydrogen production from gaseous fuels is the waveguide-supplied metal-cylinder-based system which at present exhibited a hydrogen production yield from methane above 40 g(H_2)/kWh ([9], Table 1).

When the waveguide-supplied metal-cylinder-based MPS is properly optimized and a swirling gas is injected into the operation region, the plasma is generated inside a metal cylinder or in the quartz cylinder inserted in it. The gas swirl stabilizes the plasma and also protects the cylinder wall (metal or quartz) from the discharge heat. The presented MPS showed stable operation at power levels from about 600 W up to 6000 W, provided that the total gas flow is sufficiently large (from 30 up to several hundred l/min).

Table 1. Conventional and plasma methods of H_2 production. Comparison of the energy yields of hydrogen production

Production method	Initial composition	Energy yield		Reference
		NL(H_2)/kWh	g(H_2)/kWh	
Conventional steam reforming of CH_4 (catalyst)	CH_4 +H_2O+ air	672	60 Established industrial process	K. Randolph, U.S. DoE, 2013, [3]
Water electrolysis	H_2O	224 - 448	20 - 40	K. Randolph, U.S. DoE, 2013, [3]
Electron beam radiolysis	CH_4+H_2O	40	3.6	T. Kappes et al., 2002, [4]
Dielectric barrier discharge	CH_4 +CO_2 / H_2O CH_3OH+CO_2 / H_2O CH_3CH_2OH+CO_2 / H_2O	5.6 37 75	0.5 3.3 6.7	B. Sarmiento et al., 2007, [5]
Gliding arc	CH_4+H_2O+air	448	40	J.M. Cormie, I. Rusu, 2001, [6]
Gliding arc (alcohol spray)	Alcohols+ Ar	2100	176	R. Burlica et al., 2011, [7]
Plasmatron with catalyst	CH_4+H_2O+air	2520	225	L. Bromberg et al., 2000, [8]
Metal-cylinder-based MPS	CH_4 +CO_2+H_2O	480	42.9	M. Jasiński et al., 2013, 4.5 kW, [9]
Waveguide supplied resonant-cavity-based MPS with catalyst	CH_4+H_2O	703	62.8	M. Jasiński et al., 2014, 2.5 kW,[10]

Table 2 Comparison of the efficiency of dry and combined steam reforming processing of methane in the waveguide-supplied metal-cylinder-based MPS. Absorbed microwave power - 3.5 kW.

MPS type	H_2 production method	Flow rate, NL/min	H_2 production rate NL(H_2)/h	Energy yield		Reference
				NL(H_2)/kWh	g(H_2)/kWh	
Metal-cylinder-based	Dry reforming	CH_4 – 50, Swirl CO_2 – 50, Swirl	790	230	20	M. Jasiński et al., 2013, [11]
		CH_4 – 100, Swirl CO_2 – 100, Swirl	1000	295	26	M. Jasiński et al., 2013, [11]
	Combined steam reforming	CH_4 – 50, Swirl CO_2 – 50,Swirl H_2Ogas – 62, Swirl	1520	466	42	M. Jasiński et al., 2014, [10]

The dry and combined steam processing of methane were studied using the waveguide-supplied metal-cylinder-based MPS. In our experiment, CH_4, CO_2 and H_2O_{gas} were mixed before entering the four inlets of MPS to form a gaseous mixture.

Table 2 summarizes results of the reforming of methane in these two processes. It is seen from Table 2 that the energy yield of hydrogen production is higher for the combined steam reforming and it equals 42 g(H_2)/kWh at 3.5 kW of absorbed microwave power. Although this value is lower than a target of 60 g(H_2)/kWh proposed by the U.S. Department of Energy, some improvements of the microwave source and technology to increase the energetic parameters are still possible.

Conclusions

Our investigation showed that the microwave plasma method (using either the metal-cylinder-based or resonant-cavity-based MPS) has a potential to become attractive in terms of the performance and hydrogen production rate and energy yield. At present the achieved energy yield of hydrogen production from methane is close to the DOE's 2020 target of 60 g(H_2)/kWh. Our preliminary experiment on hydrogen generation from a mixture of nitrogen and ethanol by the metal-cylinder-based MPS showed potential of the microwave discharges for hydrogen production from liquid fuels (the energy yield was several tens g(H_2)/kWh at a relatively low ethanol concentration).

Acknowledgments

This research was supported by the National Centre for Research and Development under the program NR14-0091-10/2010.

REFERENCES

[1] Holladay J.D., Hu J., King D.L., Wang Y., An overview of hydrogen production technologies, *Catalysis Today 139 (*2009), No. 4, 244–260

[2] Petitpas G., Rollier J.-D., Darmon A., Gonzalez-Aguilar J., Metkemeijer R., Fulcheri L., A comparative study of nonthermal plasma- assisted reforming technologies. *Int. J. Hydrogen Energy,* 32 (2007) No. 14, 2848–2867

[3] Randolph K., U.S. DOE, Hydrogen production – Session introduction, 2013 Annual Merit Review & Peer Evaluation Meeting, www.hydrogen.energy.gov/pdfs/review13/pd000_randolph_2013_o.pdf

[4] Kappes T., Schiene W., Hammer T., Energy balance of dielectric barrier discharge for hydrocarbon steam reforming, *8th Int. Symp. on High Pressure Low Temperature Plasma Chemistry*, pp. 196-200, 2002

[5] Sarmiento B., Brey J.J. Viera I.G., Gonzalez-Elipe, A.R., Cotrino J., Rico V.J., Hydrogen production by reforming of hydrocarbons and alcohols in a dielectric barrier discharge, *J. Power Sources* 169 (2007), No. 1, 140–143

[6] Cormier J.M., Rusu I., Syngas production via methane steam reforming with oxygen: plasma reactors versus chemical reactors, *J. Phys. D: Appl. Phys*. 34 (2001), No. 18, 2798

[7] R Burlica., Shih K.-Y., B Hnatiuc., Locke B.R., Hydrogen generation by pulsed gliding arc discharge plasma with sprays of alcohol solutions, *Ind. Eng. Chem. Res*. 50 (2011) 9466-9470

[8] Bromberg L., Cohn D.R., Rabinovich A., Alexeev N., Samokhin A., Ramprasad R., Tamhankar S., System optimization and cost analysis of plasma catalytic reforming of natural gas, *Int. J. Hydrogen Energy* 25 (2000) 1157-1161

[9] Jasiński M., Czylkowski D., Hrycak B., M Dors., Mizeraczyk J., Hydrogen production via methane conversion in an atmospheric pressure microwave (2.45 GHz) plasma, *5th World Hydrogen Technologies Convention, Shanghai, China, Proceedings of Abstracts*, pp. 206-207, 2013

[10] Jasiński M., Czylkowski D., Hrycak B., Dors M., Mizeraczyk J., unpublished, 2014.

[11] Jasiński M., Czylkowski D., Hrycak B., Dors M., Mizeraczyk J., Atmospheric pressure microwave plasma source for hydrogen production, *Int. J. Hydrogen Energy* 38, 11473-11483, 2013

***Authors**: prof. dr hab. inż. Jerzy Mizeraczyk, Akademia Morska w Gdyni, Katedra Elektroniki Morskiej, ul. Morska 81-87, 81-225 Gdynia, E-mail: jmiz@imp.gda.pl; dr inż. Mariusz Jasiński, dr hab. inż. Mirosław Dors, Instytut Maszyn Przepływowych im. R. Szewalskiego Polskiej Akadamii Nauk, ul. Fiszera 14, 80-231 Gdańsk, E-mail: mj@imp.gda.pl, mdors@imp.gda.pl*

TOLUENE CONVERSION IN A NEW TYPE OF GLIDING DISCHARGE REACTOR SUPPLIED BY A FERRO-RESONANCE SYSTEM

Michał MŁOTEK, Ewelina REDA, Krzysztof KRAWCZYK

Faculty of Chemistry, Warsaw University of Technology

Abstract. *A new type of gliding discharge reactor with a conical chamber with six high-voltage electrodes was investigated. The electrodes of the plasma reactor are supplied by a 6-phase ferro-resonance system formed of resonant capacitors and stray inductances of the high voltage transformers supplied from a digital inverter. Toluene decomposition was studied in this reactor.*

Streszczenie. *Przeprowadzono badanie rozkładu toluenu w nowym typie reaktora z wyładowaniem ślizgowym ze stożkową komorą wyładowczą , w której umieszczono sześć elektrod. Reaktor zasilany był za pomocą 6 fazowego ferro-rezonansowego układu utworzonego z transformatorów wysokiego napięcia o wysokiej indukcyjności i kondensatorów rezonansowych.*

Keywords: non-equilibrium plasma, gliding discharge, toluene conversion.
Słowa kluczowe: plazma nieównowagowa, wyładowanie ślizgowe, rozkład toluenu.

Introduction

The emission of hazardous substances, especially volatile organic compounds (VOCs), is a serious problem for a number of industrial processes. These are compounds which cause stratospheric ozone depletion, exhibit carcinogenic properties and give rise to the greenhouse effect. Another problem which significantly limits application of the gas after biomass pyrolysis for the production of electricity is a content of tar (higher hydrocarbons) in the gas, which is deposited on the surface of internal combustion engines or gas turbines.

Toluene, one of the aromatic volatile organic compounds (VOCs) is commonly used for industrial application in production of fiber, films or resin, including polymer fibers which are used for manufacturing household fabrics, carpets, and clothing. Toluene is also a model compound of the tars occurring in the biomass gasification process.

Over the last decade non-thermal plasma has been used as a new method of conversion of very stable chemical substances. The efficacy of the reaction in non-equilibrium plasma depends on the power supply, electron energy, gas flow rate and concentration of reagents. The shape of the discharge zone and the residence time have a serious influence on the process.

The non-thermal plasma of a gliding discharge has been tested in recent years for the decomposition of toxic and particularly stable chemical substances, conversion of methane and cleaning of water waste [1-3]. It is especially attractive due to the high quantity of radicals produced. Another advantage of this method is the possibility of using gas mixtures containing solid particles and of considerable humidity, and to perform the process at high flow rates.

In the commonly used gliding discharge reactors the fast gas stream is introduced between the electrodes. As a result, the reagents residence time in the plasma zone might not be long enough to achieve expected reaction rate or product yield. High voltage and large gas streams are used to expand the discharge chamber, which is created where the distance between the electrodes is the smallest. It causes problems with larger reactors and can result in gas passing by the reaction zone.

The purpose of this work was to study the effect of the initial concentration of toluene on the process of its decomposition in a new type of a reactor. The investigations were conducted in large-scale gliding-discharge reactor supplied by a ferro-resonance system.

Experimental

In this study a new construction of the reactor (Fig. 1) [4] and power supply was used [5]. The reactor consists of a cyclone gas chamber, and a conical chamber, where the six high voltage electrodes were placed. In the reactor rod electrodes were used. The gas inlet to the cyclone chamber is located tangentially to the inner wall. In the cyclone gas chamber the gas was introduced into a vortex flow by three nozzles and then it was introduced into the conical chamber through the Venturi orifice. The liquid reagent was introduced to the reactor by the nozzle placed in the upper part of cyclone chamber. The cyclone shape of gas inlet to reactor resulted in the very high vortex velocity of the gas introduced to the plasma zone. Due to that the reagents at the plasma zone inlet were very well mixed and the residence time of reagents in discharge zone became appreciably longer (Fig. 1).

The new power supply applied for the presented gliding discharge reactor was manufactured by Ertec-Poland. The new general idea of ferroresonant transformers supplied from transistor inverters allows for design of poly-phase multi-electrode reactor systems, where a high capacity utilization rate is reached with the user-set value of the total discharge current. The group of high-voltage transformers supplied from the three-phase inverter can deliver the output voltage of 1000-2000 V to each electrode. This feature has been attained by using a ferro-resonance system formed by resonant capacitors and stray inductances of the high-leakage-type transformers. In the presented power supply, the set of 6 transformers were used. The transformers have an increased level of the dispersion of the magnetic flux, achieved by branching the main flux with a magnetic shunt. The voltage ratio is 230/2100 V and the power range is 0.5 to 2 kW for every transformer. The power supplied to the reactor was measured by an energy meter in a low voltage circuit and by digital oscilloscope in a high-voltage circuit (Fig. 2). Voltage and current courses were measured by a Tektronix DPO 3034 oscilloscope with high voltage probe Tektronix P6015 and current probe TCP 0030 (Fig. 3).

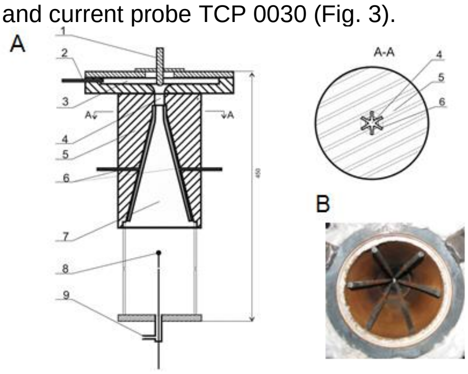

Fig. 1. Reactor with the rod electrodes for liquid substances decomposition. A - Cross section of the reactor with electrodes 1 – liquid nozzle, 2 – gas inlet, 3 – cyclone chamber, 4 - Venturi orifice, 5 – ceramic reactor body, 6 - electrodes, 7 - conical chamber, 8 – thermocouple, 9 – gas outlet; B - image of the reactor's body.

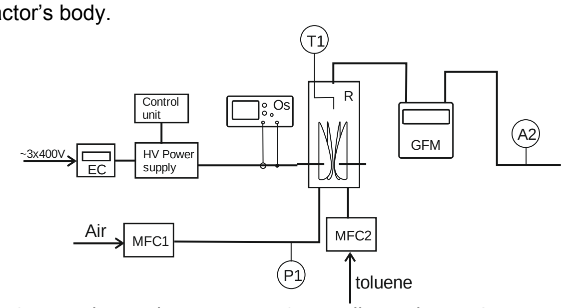

Fig. 2. Experimental setup. A1, A2 sampling points; EC energy meter; GFM gas flow meter; MFC 1, MFC 2 mass flow controllers; Os oscilloscope; P1 manometer; R reactor, T1 thermocouple.

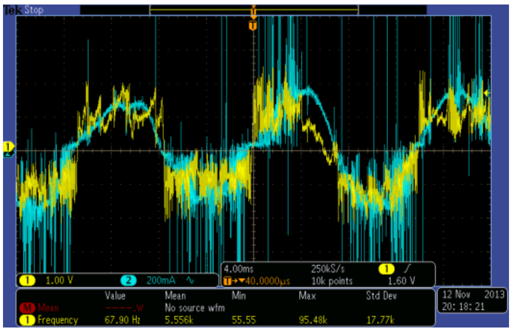

Fig 3. Current and voltage characteristics obtained in air from a single electrode. Overall discharge power ~ 1 kW.

The gases were analyzed by two chromatographs: Chrompack CP-9001 with HP 5 column and FID detector for hydrocarbons up to C7 and Chrompack CP-9002 with Carboplot P7 column and TCD detector for H_2, CO and CO_2.

The study was conducted for three gas flow rates: 4.2 Nm^3/h, 5 Nm^3/h and 6 Nm^3/h, and toluene concentration in range 0.9 – 2%. The discharge power was in the range 850-950 W, the frequency was 50 Hz. The overall toluene conversion strongly depended on the toluene initial concentration. It reached a value close to 1.0 for toluene initial concentration of about 1.1% and a gas flow rate of 4.2 Nm^3/h. A significant effect of gas flow rate on the overall toluene conversion was observed. With the increase of gas flow rate the overall toluene conversion decreased. However, for every used gas flow rate it is possible to reach an overall toluene conversion close to 1.0 (Fig. 4). The main products of the toluene decomposition were carbon dioxide and water. Carbon monoxide was observed when a low concentration of toluene was used. For a toluene initial concentration above 1.3 %, when the temperature reached 600°C, the overall toluene conversion exceeded 90%. Under these conditions the conversion of toluene into carbon monoxide decreased below 0.05 (Fig. 5).

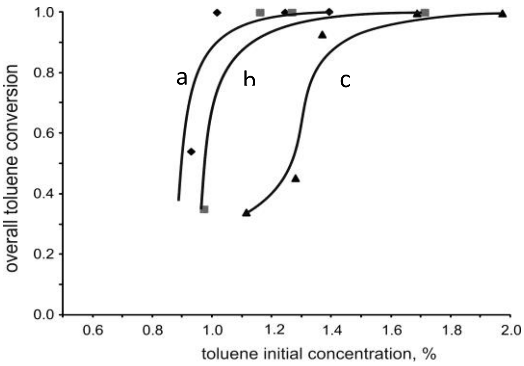

Fig. 4. Effect of gas flow rate on toluene conversion. Gas flow rate a –4.2 Nm^3/h, b - 5 Nm^3/h, c - 6 Nm^3/h. Discharge power ~ 900 W, frequency 50 Hz

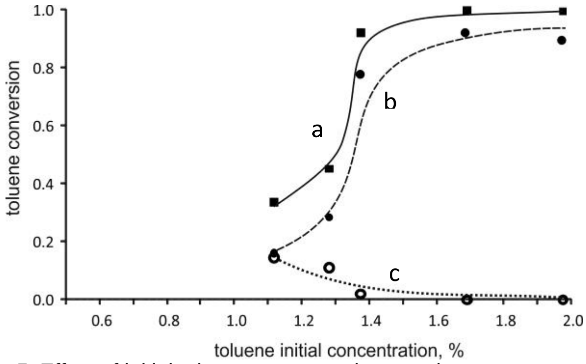

Fig. 5. Effect of initial toluene concentration on toluene conversions: a – overall, b – into CO_2, c – into CO. Gas flow rate 6 m^3/h. Discharge power ~ 900 W, frequency 50 Hz

Conclusion

The overall toluene decomposition mostly depends on the initial pollutant concentration and gas flow rate. The main products of the process were carbon dioxide and water. Small amounts of CO were observed when a low initial toluene concentration was used. In the toluene decomposition in a large-scale gliding discharge reactor soot or higher hydrocarbons were not detected. One can conclude that a use of the new construction of the reactor and power supply proved that in this system it is possible to achieve the toluene conversion of 100%. The effect of the initial concentration of toluene and gas flow rate on the conversion of toluene and selectivity of toluene conversion to CO and CO_2 was observed.

Aknowledgment

This work was supported by the National Center for Research and Development agreement no PBS2/A1/10/2013.

References

[1] J. Chapelle, A. Czernichowski, Industrie 4, 1992, 20
[2] J.-L. Brisset, D. Moussa, A. Doubla, E. Hnatiuc, B. Hnatiuc, G. K. Youbi, J.-M. Herry, M. Naitali, M.-N. Bellon-Fontaine, Ind. Eng. Chem. Res. 47, 2008, 5761.
[3] K. Schmidt-Szałowski, K. Krawczyk, J. Sentek, B. Ulejczyk, A. Górska, M. Młotek, Chem. Eng. Res. Design. 89, 2011, 2643-2651.
[4] Polish patent application P.403073.
[5] Polish patent application P.404973.

Author: *dr inż. Michał Motek, Warsaw University of Technology, Faculty of Chemistry, Noakowskiego 3, 00-664 Warsaw, Poland E-mail: mmlotek@ch.pw.edu.pl;*

8th International Conference
Electromagnetic Devices and Processes in Environment Protection ELMECO-8
joint with 11th Seminar Applications of Superconductors AoS-11
September 28 - October 1, 2014, Nałęczów, Poland

GEOGRAPHICAL CONSIDERATIONS IN THE DESIGN OF AN OFF-GRID POWER SYSTEM IN REMOTE SOUTH AUSTRALIA

Ranjeeta Kaur SINGH, Özdemir GÖL, Andrew NAFALSKI

University of South Australia, Adelaide

Abstract*. Remote communities suffer from geographical isolation in many regards which include logistics of supply of commodities and, especially, supply of electricity. This is particularly serious in countries with vast expanses between settlements such as Australia. This paper addresses the power supply needs of a remote community in South Australia and proposes a hybrid system integrating renewable energy with existing internal combustion engine driven generators, taking into account the geographical peculiarities of the site.*

Streszczenie. *Odlegle geograficznie miejscowosci doswiadczaja izolacji roznego rodzaju, m.in. zwiazanej z logistyka dostaw towarow i surowcow, szczegolnie zasilania w energie elektryczna. W artykule prezentowana jest propozycja hybrydowego ukladu integrujacego energie odnawialna z istniejacym generatorami elektrycznymi,, bioraca pod uwage szczegolne cechy geograficzne osiedla w Poludniowej Australii.*

Keywords: renewable energy, isolated power systems, hybrid energy systems, geographical conditions.
Słowa kluczowe: energia odnawialna, izolowane uklady energetyczne, energetyczne uklady hybrydowe,warunki geograficzne.

Introduction

In Australia, the federal government has made a commitment to ensuring that '20% of Australia's electricity supply comes from renewable sources by 2020' [1]. Renewable energy, despite being a sustainable and clean source of energy, is quite stochastic in nature and hence an unreliable source of power. Consequently, it is common practice to integrate renewable energy with conventional sources of energy such as diesel or Liquefied Petroleum Gas (LPG) generators [2] into so-called *hybrid energy system*.

Hybrid power systems in Australia

In July 2000, the Australian government introduced an initiative known as the Renewable Remote Power Generation Program (RRPGP) [3]. The various goals of the initiative are to:

- support the progress of the Australian renewable energy industry;
- provide cost effective electricity to remote off-grid communities;
- develop energy infrastructure in aboriginal communities;
- reduce greenhouse gas emissions.

As a result of the RRPGR, hybrid power systems have been established in many remote and rural parts of Australia to provide reliable, grid quality electricity to people residing in those areas.

The state of South Australia (SA) has thirteen remote off-grid communities, also known as Remote Area Energy Supply (RAES) sites (see Fig. 1) [4].

Oodnadatta: some background

The work presented in this paper focuses on Oodnadatta, which is a remote community in South Australia (SA). SA has a total surface area of 983,483km^2, which is more than three times that of Poland. Furthermore, the SA area is more than that of Germany and France combined.

The area of Oodnadatta covers approximately 7,680km^2 and is located 1,011km north of Adelaide, with a population of 277, of which 103 are indigenous Australians. The town has a number of facilities, namely, a petrol station, general store, post office, police station, medical centre, school and hotel. The power infrastructure in the area is owned and operated by the SA government [4].

The power supply in Oodnadatta is unreliable; for instance, the community experiences approximately five blackouts a year, which usually last more than 24 hours [5]. Te reference [6] states that the dependability of a standalone diesel generator can be enhanced through integration with renewable energy technologies. Thus, establishing a hybrid power system in Oodnadatta is bound to improve the reliability of the power supply for the residents.

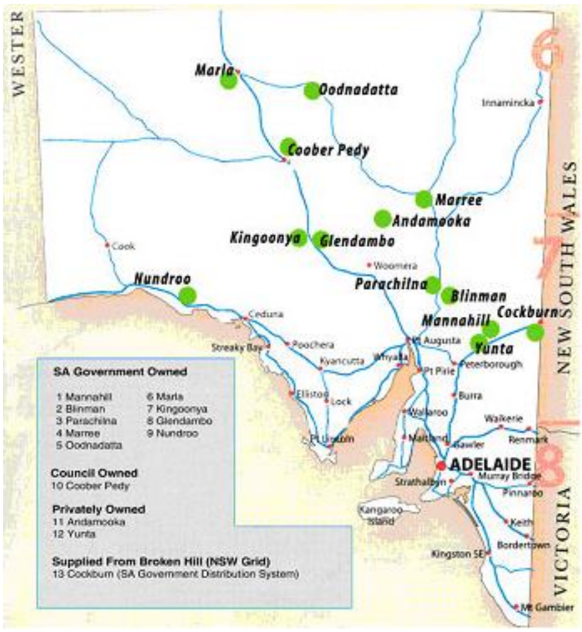

Fig.1. Remote Area Energy Supply (RAES) locations in SA

Oodnadatta: solar data

The mean daily global solar radiation per annum on a horizontal surface in Oodnadatta is approximately 6.29kWh/m^2, while on a solar module tilted at an angle of

37.6°, it amounts to 6.74kWh/m^2 [7]. While there is little variation between these values, the purpose of tilting the modules is to maximise power output during the winter months.

Another parameter used for assessing the solar potential of an area is the sunshine duration. hours per day.

The sunshine duration in Oodnadatta is comparable to that in Egypt and Saudi Arabia, the two countries with the greatest solar potential. The mean daily sunshine hours in these countries are 11 hours [8] and 8.9 hours [9], respectively.

Hybrid system design

HOMER software [10] performs three tasks: simulation, optimisation and sensitivity analysis. In the simulation process, HOMER investigates the performance of a particular power system configuration for each hour of the year to determine its technical feasibility and lifecycle cost.

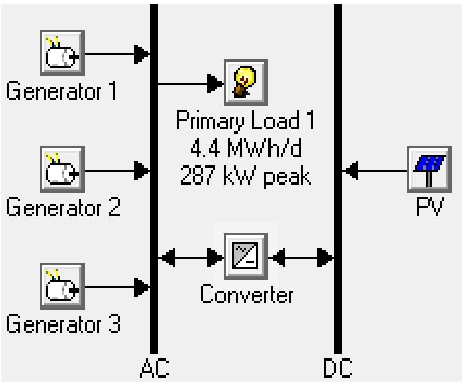

Fig.2. Proposed hybrid power system

Simulation of the hybrid power system (Fig.21) with the 95kW photovoltaic (PV) array and the 84kW inverter produced the following results. The PV array produces 225MWh of energy per year which is equivalent to 14% of the total energy produced by the hybrid power system. The energy contribution of Generator 1 (185kW) is 8%. This is a 5% reduction in energy produced by the generator when modelled in the conventional power system. Please note that Generator 2 (185kW) is a backup used only in emergency. The output of Generator 3 (254kW) has also decreased. When part of the conventional power system, its output comprised 87% of the total energy produced while in the hybrid power system it produces 80% of the total energy.

Integrating the PV array with the conventional power system in Oodnadatta has reduced the operating hours of Generator 1 from 3650 to 1644hours/yr. This is a 55% reduction compared with its operating hours in the conventional system.

Economic analysis

The capital cost of the PV array takes into account the cost of purchasing the 538 modules. In addition, the installation costs associated with the array and the inverter are included. The bulk of the overall capital cost of the hybrid system is due to the capital cost of the PV array (91%).

On average the Generator 1 operates for about four hours per day, between 5 pm and 9pm. Its fuel consumption has decreased by 55%, totalling to 20,628 litres of diesel per year.

On the other hand, the operating hours of Generator 3 have remained at 8760 hours per year. Nevertheless, its fuel consumption has also reduced, however, by only 7%.

Comparing the replacement as well as operation and maintenance (O&M) costs of the hybrid system and the conventional power systems it is evident that the costs have increased (5% and 13%, respectively).

A large proportion of the costs incurred are due to Generator 3. On the other hand, Generators 1 and 3 require less fuel to operate which has reduced the fuel cost by 16%. However, it still comprises a considerable share (78%) of the total net present cost (NPC), which decreased from $5 million (conventional power system) to $4.9 million (hybrid system).

Conclusions

The designed hybrid power system produces 1606MWh of energy per year. The solar contribution is 14% or 225MWh/yr. The two generators (240kW and 185kW) supply 86% of the energy. The 185kW generator operates for 1644hours/yr, which is a 55% reduction in its operating hours compared to its usage in the conventional system. On the other hand, the operating hours of the 240kW generator do not change. Due to the reduced operating hours of the hybrid system, it consumes less fuel thus emitting less carbon dioxide (633,113kg/yr). The conventional power system emits 745,337kg/yr. Thus the designed hybrid system offers economical and environmental benefits over the traditional system, in the particular geographical circumstances of a local remote South Australian community of Oodnadatta.

REFERENCES

[1] Department of the Environment, the Australian Government (2014), http://www.climatechange.gov.au/reducing-carbon/ renewable-energy/renewable-energy-target/ ret-scheme-updates/australian-government, viewed 31 August 2014,

[2] Shaahid, S.M.. & El-Amin, Techno-economic Evaluation of Off-grid Hybrid Photovoltaic-diesel-battery Power Systems for Rural Electrification in Saudi Arabia - A Way Forward for Sustainable Development, *Renewable and Sustainable Energy Reviews*, 13 (2009), 625-633.

[3] Office of Energy, Renewable Power, Western Australia, (2011) http://www.energy.wa.gov.au/ 2/3227/64/renewable_power.pm, viewed 31 August 2014.

[4] South Australian Government (2014), Remote Areas Energy Supplies Scheme, http://www.sa.gov.au/topics/water-energy-and-environment/energy/energy-supply-and-sources/remote-areas-energy-supplies-scheme, viewed 31 August 2014.

[5] ABC News (2009), 24hr Blackout Leaves Oodnadatta in the Dark (2009), http://www.abc.net.au/news/2009-09-18/24hr-blackout-leaves-oodnadatta-in-the-dark/1433300, viewed 31 August 2014,

[6] Muselli, M., Notton, G., Poggi, P & Louche, A., PV-hybrid Power Systems Sizing Incorporating Battery Storage: an Analysis via Simulation Calculations, *Renewable Energy*, 20 (2000), 1-7.

[7] Bureau of Meteorology (2014), Daily Solar Exposure for Australia, http://www.bom.gov.au/jsp/awap/solar, viewed 31 August 2014.

[8] Tadros, M.T.Y., Uses of Sunshine Duration to Estimate the Global Solar Radiation over Eight Meteorological Stations in Egypt, *Renewable Energy*, 21 (2000), 231- 246.

[9] Rehman, S. & Al-Hadhrami, L.M., Study of a Solar PV/diesel/battery Hybrid Power System for a Remotely Located Population near Rafha, Saudi Arabia, *Energy*, 35 (2010), No. 12, 4986 – 4995.

[10] HOMER Energy (2014), Homer Renewable Energy Software, http://www.homerenergy.com/software.html, viewed 31 August 2014.

***The corresponding author**: prof. dr hab. inż. Andrew Nafalski, University of South Australia, School of Engineering, 5095 Mawson Lakes, South Australia, email: nafalski@unisa.edu.au.*

8th International Conference
Electromagnetic Devices and Processes in Environment Protection ELMECO-8
joint with 11th Seminar Applications of Superconductors AoS-11
September 28 - October 1, 2014, Nałęczów, Poland

EFFECT OF OZONE TREATMENT ON SOIL ACIDITY AND NUTRIENT

Takuya NAGATOMO[1], Keisuke TAKIGAWA[1], Yuki YAMASAKI[1], Takamasa SAKAI[1], Fumiaki MITSUGI[1], Tomoaki IKEGAMI[1], Kenji EBIHARA[2], and Kazuhiro NAGAHAMA[3]

Graduate school of science and technology, Kumamoto University, Japan (1), Environment and energy laboratory, Japan (2), and Department of applied microbial tech., Sojo University, Japan (3)

Abstract*. In this study, influence of ozone treatment on physical properties of soil was investigated. We used a quartz container for ozone treatment of soil. The amount of soil used for treatment was 100 g. Treating time was changed. Flow rate of ozone gas was 1.5 L/min. We measured characteristics of soil such as inorganic nutrient (NO_3-N, NO_2-N, and NH_4-N), pH(H_2O), fungi, and DNA of soil before and after ozone treatment.*

Keywords: ozone sterilization, soil treatment, nitrate, and pH(H_2O).
Słowa kluczowe: sterylizacja ozonowa, obróbka gleby, azotan, i pH (H_2O)

Introduction

Recently, there are numerous studies about reactive oxygen species such as ozone and their effects on seeds, plants, residual toxic, virus, and pests. We have proposed the potential of ozone treatment for agricultural soil.

Ozone sterilization is one of the most important techniques to ensure the safety of food processing in agriculture. Sterilization of soil using pesticides is one of effective ways to resist the spread of diseases in the soil. However, contamination such as residual pesticides in the produce and NO_2 in groundwater caused by the overuse of chemicals has become a serious issue in agricultural fields. Therefore, we proposed the use of ozone in soil alternative to pesticide. Ozone has high oxidation energy compared to that of fluorine and does not produce residual toxins.

In this study, we developed an equipment for the sterilization of soil, which induced a quartz container rotated by a motor. The ozone generator, which uses the surface dielectric barrier discharge, provides a maximum ozone concentration of 78 g/m^3 at a flow rate of 1.5 L/min. We investigated the characteristics of soil such as inorganic nutrient content (NO_3-N, NO_2-N, and NH_4-N), pH(H_2O), fungi, and DNA of soil before and after ozone treatment.

Experimental setup

Fig. 1 shows the schematic illustration of the ozone treatment system for soil. An ozone generator that uses a surface dielectric barrier discharge provides the maximum ozone concentration of 78 g/m3 at a flow rate of 1.5 L/min. The generated ozone gas was injected into the soil directly in a quartz container that performed a rotation function. There was no leakage of gas in this equipment. The soil used for ozone treatment was andosol. The amount of andosol used for ozone treatment was 100 g. The treatment time was changed. The ozone dose rates, which are defined as ozone dose weight per unit weight of soil, were from 0.1 to 10.5 %. We measured the characteristics of soil such as inorganic nutrient content (NO_3-N, NO_2-N, and NH_4-N), pH(H_2O), fungi, and DNA of soil before and after ozone treatment.

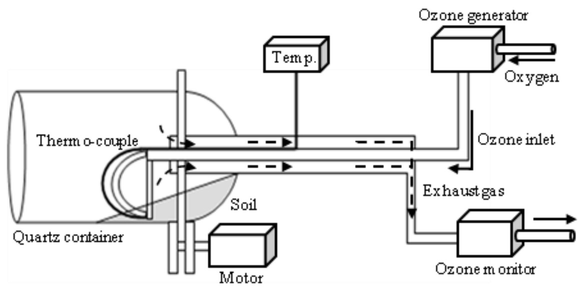

Fig.1. Schematic illustration of the ozone treatment system for soil.

Results and discussion

Contents of NO_3-N and NH_4-N increased after treatment and subsequently kept a constant quantity regardless of treating time, even though the number of nitrite and nitrate bacteria, 8×10^6 /mg and 2×10^7 /mg respectively, were not changed. However, these were maintained at a constant value with time as shown in Fig. 2. NO_3-N and NH_4-N with high ozone dose rate were higher than that with low. It was revealed that ozone treatment could induce the generation of nitrogen nutrients in the soil due to the strong decomposition power of ozone.

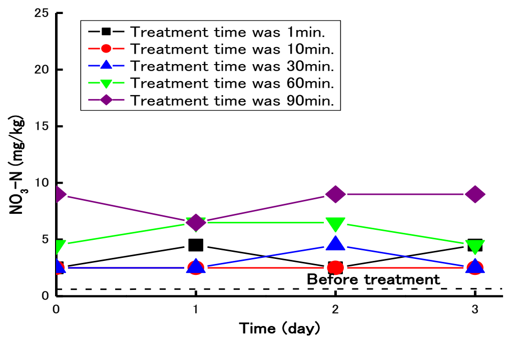

Fig.2. Inorganic nutrients change before and after ozone treatment.

The pH(H_2O) decreased just after ozone treatment regardless of treating time. However, the pH(H_2O) value recovered gradually with time as shown in Fig. 3. It considered that the buffering function for soil acidity performed after the ozone treatment. Exchangeable positive ions that adsorbed onto the surface of the soil colloid changed the positions with H^+ ions in the soil solution. Subsequently, the pH(H_2O) value recovered because of a decrease in H^+ ions in the soil solution.

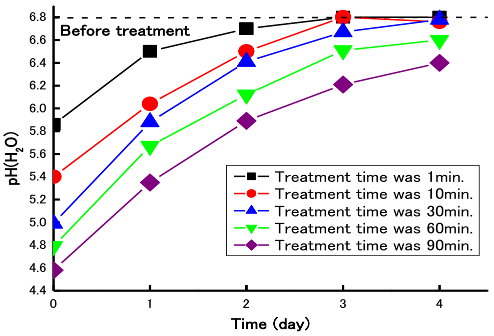

Fig.3. Recovery curve of pH(H_2O) after ozone treatment.

Conclusions

In this study, influence of ozone treatment on physical properties of soil was investigated. We used a quartz container for ozone treatment of soil. The contents of NO_3-N and NH_4-N increased after ozone treatment and subsequently kept a constant quantity. NO_3-N and NH_4-N with high ozone dose rate were higher than that with low. The pH(H_2O) decreased just after ozone treatment regardless of treating time. However, the pH(H_2O) value recovered gradually with time. It considered that the buffering function for soil acidity performed after the ozone treatment.

REFERENCES

[1] K. Ebihara, S. Sugimoto, T. Ikegami, F. Mitsugi, and H. D. Stryczewska, Przeglad Elektrotechniczny, 85(2009), 113-114

[2] K. Ebihara, H. D. Stryczewska, T. Ikegami, F. Mitsugi, and J. Pawlet, Przeglad Elektrotechniczny, 87(2011), 148-152

[3] K. Ebihara, H. D. Stryczewska, F. Mitsugi, T. Ikegami, T. Sakai, J. Pawlet, and S. Teii, Przeglad Elektrotechniczny, 88(2012), 92-94

[4] K. Ebihara, F. Mitsugi, T. Ikegami, N. Nakamura, Y. Hashimoto, Y. Yamashita, S. Baba, H. D. Stryczewska, J. Pawlet, S. Teii, and T. Sung, The European Physical Journal Applied Physics, 61(2013), 1-5

[5] T. Nagatomo, K. Takigawa, T. Sakai, F. Mtsugi, T. Ikegami, and K. Ebihara, Proceedings of IIAI International conference on advanced applied informatics, 2013, 121-124

***Authors**: mr. Takuya Nagatomo, Graduate of school of science and technology, Kumamoto University, 2-39-1, Kurokami, Kumamoto, 860-8555, Japan, e-mail: t-nagatomo@st.cs.kumamoto-u.ac.jp; mr. Keisuke Takigawa, Graduate of school of science and technology, Kumamoto University, 2-39-1, Kurokami, Kumamoto, 860-8555, Japan; mr. Yuki Yamasaki, Graduate of school of science and technology, Kumamoto University, 2-39-1, Kurokami, Kumamoto, 860-8555, Japan; mr. Takamasa Sakai, Graduate of school of science and technology, Kumamoto University, 2-39-1, Kurokami, Kumamoto, 860-8555, Japan; dr. Fumiaki Mitsugi, Graduate of school of science and technology, Kumamoto University, 2-39-1, Kurokami, Kumamoto, 860-8555, Japan,, e-mail: mitsugi@cs.kumamoto-u.ac.jp; prof. Tomoaki Ikegami, Graduate of school of science and technology, Kumamoto University, 2-39-1, Kurokami, Kumamoto, 860-8555, Japan; prof. Kenji Ebihara, Environment and energy laboratory, 1-4-15, Otemon, Fukuoka, 810-0074, Japan; prof. Kazuhiro Nagahama, Department of applied microbial tech., Sojo University, 4-22-1, Ikeda, Kumamoto,860-0082, Japan*

8th International Conference
Electromagnetic Devices and Processes in Environment Protection ELMECO-8
joint with 11th Seminar Applications of Superconductors AoS-11
September 28 - October 1, 2014, Nałęczów, Poland

APPLICATION OF LOW-TEMPERATURE PLASMA FOR TREATMENT OF OFF-GASES FROM BITUMEN PRODUCTION

Adam PIOTROWICZ, Krzysztof JAHOŁKOWSKI, Janusz OZONEK

Lublin University of Technology

Abstract. *In the experiment degradation of volatile organic compounds from asphalt industry, including odour causing compounds, was conducted. With this end in view a special plasmachemical reactor was developed. In analytical part solid phase microextraction and GC-MS was applied for identification and quantitative measurements. It was observed that compounds containing heteroatoms were easier degradable than compounds containing condensed rings and aliphatic substituted benzene rings.*

Streszczenie. *Przedstawiono wyniki badań półtechnicznych rozkładu związków organicznych powstających podczas produkcji asfaltów pod wpływem środowiska plazmy niskotemperaturowej. W badaniach zastosowano reaktor plazmochemiczny o specyficznej konstrukcji z elektrodami siatkowymi zasilany prądem o zmiennej częstotliwości.*

Keywords: low-temperature plasma, bitumen production, PAHs
Słowa kluczowe: plazma niskotemperaturowa, produkcja asfaltu, WWA

Introduction

Bitumen is one of the products derived from oil refining process and is mainly used in road construction and roofing. In paving operations bitumen is heated and mixed with mineral aggregates. Hot bitumen emits vapours and aerosols (fumes) that contain various compounds. These include polycyclic aromatic hydrocarbons (PAHs) and sulphur-containing organochemicals. Bitumen fumes contain 1–5 ring unsubstituted PAHs, alkylated PAHs, heterocyclic PAHs and terpenoids which may exhibit mutagenic and carcinogenic activity. Moreover some of these compounds are odour causing chemicals.

One of the effective ways of biochemical and chemical deactivation of carcinogenic and odour causing compounds can be the application of low temperature plasma environment [1, 2, 3, 4]. The main property of low-temperature plasma is the possibility of causing non-equilibrium reactions in ambient temperature. Highly energetic electrons generated in plasma environment are able to degrade pollutants present in off-gases. These electrons provide an energy sufficient to break the bonds of practically every gas molecule as a result of inelastic collisions with pollutant molecules. As a consequence of these reactions, under the influence of ionisation, excitation and dissociation, secondary electrons as well as highly reactive particles (radicals, ions and molecules such as ozone) are also formed [5]. These formed particles being in transition state also affect the conversion degree of pollutants found in effluent gases.

Materials and methods

The research on treatment of exhaust gases produced in bitumen mixing plant located in Lublin, south-eastern Poland, was conducted with the use of plasmachemical reactor of own construction [6]. Before proceeding with laboratory tests, an identification of the compounds arising in the course of technological process by means of chromatographic analysis was made [7]. The samples of gases were afterwards subject to degradation in the low-temperature plasma environment.

A scheme of laboratory stand used in the tests is depicted in Figure 1. The main element of the experimental set-up for the degradation of organic compounds arising during asphalt production constitutes a plasmachemical reactor with mesh electrodes. The reactor was powered from the system of inverter and high voltage transformer operating with the frequency of 1500 Hz and producing sinusoidally alternating voltage up to 10 kV. The measurement of the active power was carried out with the use of Kyoritsu power meter type KEW6310 with the EW8128 clamp sensor. The tests were carried out with different gas flow rates through the discharge zone.

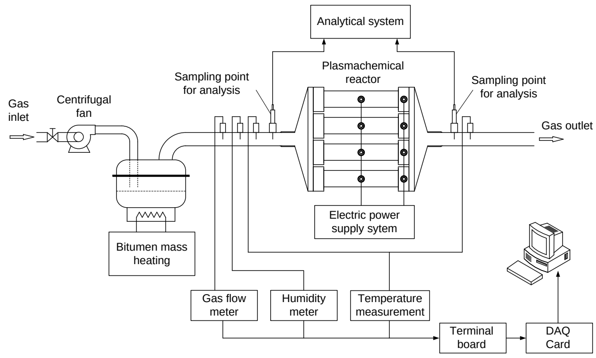

Fig.1. Scheme of laboratory test stand for treatment of compounds from asphalt production under non-thermal plasma conditions

In the experimental set-up several systems are included, namely the electric power supply, the measurement and the analytical system. Conditions prevailing in electric discharge zone can be changed through the modification of the voltage powering the reactor. The set-up was equipped with systems for the constant measurement of temperature, humidity, gas flow rate and ozone concentration. The whole experiment was monitored onboard and the measurement data were archived with the use of DAQ card and personal computer.

The structure of the plasmachemical reactor is of tubular shape. As a dielectric a sodium-silicon glass tube was used with the outer diameter of 37 mm and the thickness of 1.5 mm. The tube was covered on the inside and the outside with mesh electrodes made of acid-proof steel. Individual elements were joined in parallel and placed in a casing thus creating a modular plasmachemical reactor with four discharge elements (Figure 2).

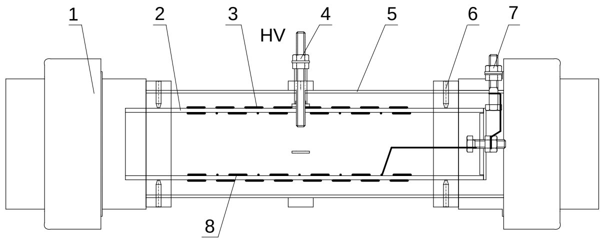

Fig.2. Plasma-chemical reactor with mesh electrodes, 1-insulating bracket, 2-dielectric, 3-high-voltage mesh electrode, 4-high-voltage cable, 5-reactor casing, 6-grounded mesh electrode, 7-power cable for grounded electrode

Identification of carcinogenic compounds present in off-gases from bitumen mixing plant was made with the use of gas chromatograph coupled to mass spectrometer Trace Ultra – POLARIS Q (by Thermo Electron) according to the method previously applied by Cai [7].

For air samples, the five litre Tedlar sampling bags were used. The bags are made of polyvinyl fluoride (PVF) with the thickness of 0.05 mm which is characterized by a very low permeability level as well as low surface-wall adsorption. Extraction of the gas samples was conducted with an SPME method (Solid Phase Microextraction) based on the partition between a mobile phase (gaseous) and a stationary phase coated on the fiber of SPME. In the analysis SUPELCO fibers coated with 100 μm of polidimethylosiloxane (PDMS) were utilised.

Results

During the experiments two kinds of asphalt were applied: the one modified with dicyclopentadiene and the 35/50 asphalt type.

In the analysed samples were detected alkylated monoaromatic hydrocarbons (styrene, xylenes, ethylbenzene, isopropylbenzene) as well as polycyclic aromatic hydrocarbons (ethylated naphthalenes, anthracene, phenanthrene and their methylated derivatives). Practically in every sample the traces of pyrene were also present.

An example of total ion current chromatograms before and after the degradation in low-temperature plasma environment as well as retention times of the compounds present in off-gases for the first type of asphalt are depicted in Figure 3.

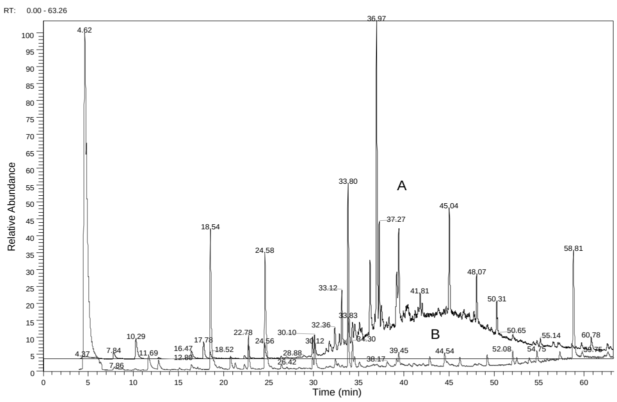

Fig.3. Total ion current chromatogram (TIC) before (A) and after (B) the low temperature plasma treatment of the vapors above the dicyclopentadiene modified asphalt (DCPD) heated to about 150 °C

The highest degradation levels were noticed for dicyclopentadiene (asphalt modifier) – 96.3% and styrene (SBS modified asphalts) – 89.2%. With respect to samples of non-modified asphalts the highest degradation degrees for bicyclic organic compounds were observed. Moreover, the decrease in aliphatic hydrocarbon chain length was noticed.

It was observed that compounds containing heteroatoms were easier degradable than compounds containing condensed rings and aliphatic substituted benzene rings.

Conclusions

Application of plasmachemical reactor containing a discharge element in the form of metal mesh attached to the surface of glass dielectric allowed to obtain technologically interesting results.

Preliminary research results have shown that the method of utilizing low-temperature plasma environment can be an effective way of treating effluent gases arising during the bitumen production process. However, these techniques can be applied only in specific conditions and after conducting precise tests determining parameters of the process and identifying the products formed during the reactions.

Application of low-temperature plasma environment exhibits many advantages, such as low running costs and no wastes.

Degradation degrees of trace pollutants contained in gas mixtures emitted during bitumen production process allow to state that the method could also prove effectiveness as far as full-scale off-gas treatment is concerned.

REFERENCES

[1] Kuwahara T., Okubo M., Kuroki T., Yamamoto T., Odor removal characteristics of laminated film-electrode packed-bed nonthermal plasma reactor, *Sensors*, 11 (2011), 5529-5542

[2] Monani F.A., Treatment of air containing volatile organic carbon: elimination and post treatment, *Environmental Engineering Science*, 24 (2007), 1038-1047

[3] Ogata A., Miyamae K., Mizuno K., Kushiyama S., Tezuka M., Decomposition of benzene in air in a plasma reactor, effect reactor type and operation conditions, *Plasma Chemistry and Plasma Processing*, 22 (2002), 537-552

[4] Shi Y., Ruan J-J., Wang X., Li W., Tan T., Evaluation of multiple corona reactor models and the application in odor removal, *Plasma Chemistry and Plasma Processing*, 26 (2006), 187-196.

[5] Kogelschatz U., Dielectric-barrier discharges: Their History, Discharge physics, and industrial applications, *Plasma Chemistry and Plasma Processing*, 23 (2003), 1-46

[6] Ozonek J., Fijalkowski S., Energetyczne i procesowe aspekty produkcji i zastosowań ozonu w technice, Monografie Komitetu Inżynierii Środowiska Polskiej Akademii Nauk, 47, Polska Akademia Nauk, Lublin, Poland, (2007) (in Polish)

[7] Cai L., Koziel J.A., Lo Y.C., Hoff S.J., Characterization of volatile organic compounds and odorants associated with swine barn particulate matter using solid-phase microextraction and gas chromatography-mass spectrometry-olfactometry, *J Chromatogr A.*, 1102 (2006), 60-72

***Authors**: prof. dr hab. inż. Janusz Ozonek, Politechnika Lubelska, Instytut Inżynierii Ochrony Środowiska, ul. Nadbystrzycka 38D, 20-618 Lublin, e-mail: j.ozonek@wis.pol.lublin.pl; dr inż. Adam Piotrowicz, Instytut Inżynierii Ochrony Środowiska, ul. Nadbystrzycka 38D, 20-618 Lublin, e-mail: a.piotrowicz@wis.pol.lublin.pl; mgr inż. Krzysztof Jahołkowski, Wydział Elektrotechniki i Informatyki, ul. Nadbystrzycka 38D, 20-618 Lublin, e-mail: k.jaholkowski@pollub.pl.*

8th International Conference
Electromagnetic Devices and Processes in Environment Protection **ELMECO-8**
joint with 11th Seminar Applications of Superconductors **AoS-11**
September 28 - October 1, 2014, Nałęczów, Poland

ATMOSPHERIC PRESSURE PLASMA JET FOR STERILIZATION OF HEAT SENSITIVE SURFACES

Joanna PAWŁAT[1], Jarosław DIATCZYK[1], Radosław SAMOŃ[1], Małgorzata PŁONKA[2], Jakub CZAPIŃSKI[2], Henryka D. STRYCZEWSKA[1], Jarosław GRZĄDZIEL[2]

Institute of Electrical Engineering and Electrotechnologies, Lublin University of Technology, Lublin, Poland (1)
Faculty of Biology and Biotechnology, UMCS, Lublin, Poland (2)

***Abstract**. The paper presents bactericidal results obtained using RF atmospheric pressure plasma jet. Decontamination effect for E. coli was clearly visible for 55 and 57°C of post discharge gas temperature after 5 min. treatment. This temperature is below pasteurization point what suggests that APPJ could be used for decontamination purposes without changing rigid properties of treated material.*

***Streszczenie.** W artykule omówiono możliwości usuwania bakterii E. coli przy użyciu niskotemperaturowej dyszy plazmowej zasilanej z generatora częstości fal radiowyc i pracującej po ciśnieniem atmosferycznym. Najlepsze rezultaty osiągnięto dla 5 min. cyklu dekontaminacyjnego przy użyciu gazu o temp. 55 i 57°C. Użycie gazu post-pazmowego o temperaturze nie przekraczającej temperatury pasteryzacji umożliwia zastosowanie dyszy do dekontaminacji materiałów nieodpornych na działanie wysokiej temperatury.*

Keywords: low temperature atmospheric pressure plasma jet, decontamination
Słowa kluczowe: niskotemperaturowa dysza plazmowa, dekontaminacja

Introduction

Many research groups concentrate on the efforts of designing plasma sterilizing device working in the ambient conditions [1-9] using variety of methods such as barrier discharge, pulsed corona reactors or plasma jets.

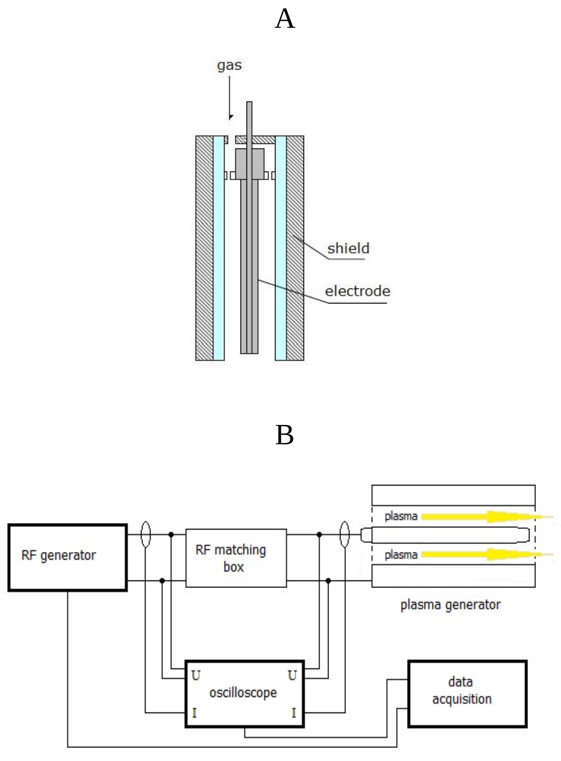

Fig 1. Atmospheric pressure plasma jet (A) and its electrical supply (B).

To maintain the uniform discharge under atmospheric pressure mainly quite expensive gases as helium and argon are used in high concentrations. Plasma disinfection time given in the literature varies from several minutes to even hours. Treatment can be considered as a surface one.

This work presents bactericidal results obtained with RF atmospheric pressure plasma jet [10-14], which is applicable toward broad range of materials and surfaces without damaging them irreversibly and is also operator- and environmental- friendly.

Experimental set-up

Proposed experimental set-up consisted of gas and liquid dosing sub-system, electrical discharge generating sub-system, control and data acquisition sub-system, and chemical and biological analyzing sub-system.

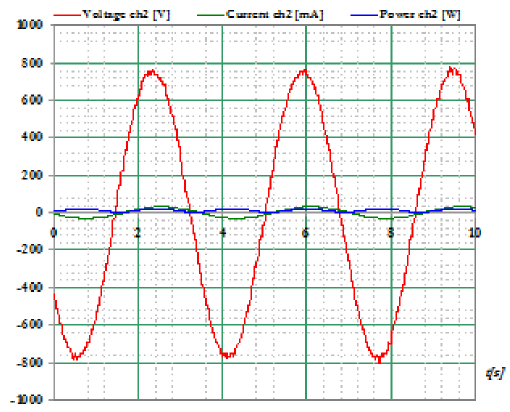

Fig 2. Current voltage characteristics for oxygen/helium gas mixture.

The main part of the device, which is presented in Fig. 1A, is RF-powered changeable rod electrode of tungsten or acid-proof stainless steel. 3 types of electrode shapes: flat surface, screw-type and turtle-type surface of 5mm diameter were tested. The electrode was powered by a regulated RF supply (AG 1021 RF generator, T&C Power Conversion) via impedance matching network (Fig. 1B).

It was possible to power plasma reactor with frequencies from 10 kHz to 20 MHz. Example of the current-voltage characteristic for oxygen/helium mixture is depicted in Fig. 2. Gas temperature was measured using K-type thermocouple with electronic temperature compensation multimeter. For this case, effects of charged particle irradiation on the thermocouple can be neglected. AFM (NT-MDT Ntegra Spectra) was used for observation of the surface structure of the samples.

. Experimental results and discussion

Ozone concentration was measured in dependence on the gas type, gas flow rate, power and the type of electrode via continuous gas sampling from sealed container (Fig. 3). Achieved ozone concentrations ranged 0.82 g/m3 (at 50 W and 40%O2/60%He feed gas mixture).

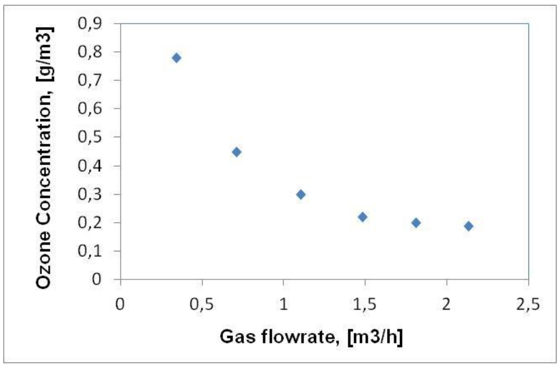

Fig 3. Gaseous ozone concentrations
(f = 14.23 MHz), P = 50 W, 40%O_2/60%He.

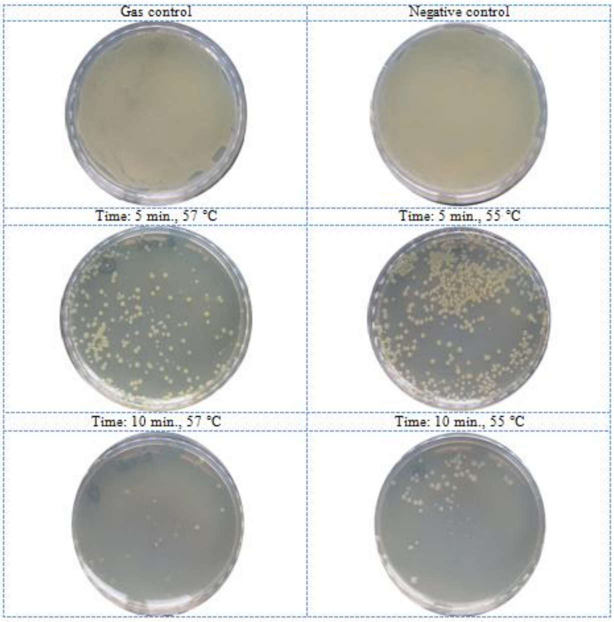

Fig 4. Plasma treatment influence on *E.coli.*

Decontamination properties of atmospheric pressure plasma for solid surfaces were tested for several selected pathogenic organisms. The best results were obtained for planctonic *E. coli* bacteria, placed overnight on polystyrene Petri dishes with 50 ml of LB-agar in liquid form to achieve OD600 ≈ 0,4 in following incubation conditions: temperature 37°C and 220 RPM. Petri dish with LB agar was homogenously inoculated with 50µl of post-incubation solution. Then samples were compared with the control to evaluate influence of plasma, gas flow and gas composition. Further step was observation of colonies growth in 37°C (optimum for *E.coli*) in 24 hours time. Experiment was done for variety of operation distances from the nozzle and gas flow regims effecting in change of surface temperature of the sample. Results presented in Fig. 4 concern 55 i 57°C temperature. Moreover gas control was performed without plasma ignition only with helium and oxygen gas.

Decontamination effect was clearly visible for 55 and 57°C after 5 min. treatment in comparison to negative and gas controls, where homogenous layer of microorganisms was observed. Treatment time extension resulted in further reduction of observable colonies, however increase of temperature and slight evaporation were also observed.

Acknowledgements:
Effort sponsored by Marie Curie Grant FP7-PEOPLE-PIRG05-GA-2009-249257, 1549/7 PRUE /2010/7 MENiS grant and KORANET.

REFERENCES

[1] M. Laroussi, F. Leipold, Int. J. Mass Spectrom. *233*, 2004, 81–86.
[2] M. Moisan, J. Barbeau, J. Pelletier, N. Philip, B. Saoudi, 13th CIP, 2001, 12–18.
[3] T. Montie, K. Kelly-Wintenberg, J.Roth, IEEE Trans Plasma Sci., *28 (1),* 2000, 41 – 50.
[4] M. Vleugels, G. Shama, X. Deng, E. Greenacre, T. Brocklehurst, M. Kong, IEEE Trans Plasma Sci., *33*, 2005, 824–828.
[5] J. Vrajová, L. Chalupová, F. Krčma, P. Sťahel, Chemické Listy, *102,* 2008, 1445-1449.
[6] Z. Kovaľová, K. Tarabová, K. Hensel, Z. Machala Eur. Phys. J. Appl. Phys. *61(2),* 2013, 24306.
[7] Z. Kovaľová, M. Zahoran, A. Zahoranová, Z. Machala J.Phys. D: Applied Physics *47(22)*, 2014, 224014.
[8] G. Raniszewski, Eur. Phys. J. Appl. Phys. , 61(2), 2013, 24311 - 24311
[9] J. Mizeraczyk, M. Dors, M. Jasiński, B. Hrycak, D. Czylkowski, Eur. Phys. J. Appl. Phys., 61, 2013, 24309.
[10] H. Stryczewska, T. Jakubowski, S. Kalisiak, T. Giżewski, J. Pawłat, JAOTs, *16(1),* 2013, 52-62,
[11] J. Pawłat, Eur. Phys. J. Appl. Phys., *61(2),* 2013, 24323.
[12] J. Pawłat, R. Samoń, H. Stryczewska, J. Diatczyk, T. Giżewski Eur. Phys. J. Appl. Phys., *61(2),* 2013, 324322.
[13] J. Pawłat, TMRSJ, *38(4),* 2013, 625-628.
[14] J. Pawłat, Przegląd Elektrotechniczny, *10b*, 2012, 139-140.

***Authors**:*
Joanna Pawłat, PhD., askmik@hotmail.com,
Jarosław Diatczyk, PhD. j.diatczyk@pollub.pl
Institute of Electrical Engineering and Electrotechnology Faculty of Electrical Engineering and Computer Science Lublin University of Technology, 38A Nadbystrzycka St.,20-618 Lublin, Poland.

8th International Conference
Electromagnetic Devices and Processes in Environment Protection ELMECO-8
joint with 11th Seminar Applications of Superconductors AoS-11
September 28 - October 1, 2014, Nałęczów, Poland

GALVANIC ISOLATION CIRCUIT FOR MEASURING SYSTEMS IN STRONG ELECTROMAGNETIC DISTURBANCES ENVIRONMENT

Eligiusz PAWŁOWSKI

Lublin University of Technology

***Abstract**. Measuring systems operating in environments with strong electromagnetic disturbances require proper technical solutions preventing excessive errors and measurement uncertainties. Commonly used solutions include shielding, earthing and galvanic isolation. This work presents a proposal for a new galvanic isolation circuit using a Light-to-Frequency Converter (LFC) working alongside a LED.*

***Streszczenie.** Systemy pomiarowe pracujące w środowisku silnych zakłóceń elektromagnetycznych wymagają stosowania odpowiednich rozwiązań zapobiegających pojawianiu się nadmiernych błędów pomiarowych. Stosuje się w tym celu ekranowanie, uziemianie oraz separację galwaniczną. W pracy przedstawia się propozycję nowego układu izolacji galwanicznej wykorzystującego przetwornik światło-częstotliwość sprzęgnięty z diodą LED.*

Keywords: galvanic isolation, Light-to-Frequency Converter, LFC, electromagnetic disturbances, linear optocoupler.
Słowa kluczowe: izolacja galwaniczna, przetwornik światło-częstotliwość, zaburzenia elektromagnetyczne, transoptor liniowy.

Introduction

Modern measuring systems often have to work in environments with strong electromagnetic disturbance. The result of this are additional measurement errors, increased risk of damage to devices and risk of equipment damage and danger of electric shock to human personnel. There are a few ways, in which interferences may occur in measuring systems: direct galvanic connection, capacitive coupling, magnetic coupling and electromagnetic radiation. In order to reduce such effects, proper shielding, earthing and galvanic isolation are used. Usage of galvanic isolation breaks the loop of common ground connecting each point of the measuring system with different potentials. Therefore, we have some beneficial effects: currents flowing in the common ground wires, which are the source of interference, are terminated; common mode voltage and the risk of electric shock are reduced. Galvanic isolation may be used in many points of the measuring system. Figure 1 represents a simplified block diagram of a measuring system containing: sensor S, signal conditioning systems C, acquisition systems ADC, digital processing DSP and display D. Galvanic isolation GI marked with a dotted line may be introduced in many points of a measuring system, between GND ground points with different potentials. Due to measuring errors, the most beneficial mode of conduct is using GI1 galvanic isolation near the sensor S, where the signal is the weakest and the interference is the strongest.

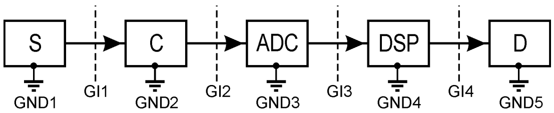

Fig.1. Simplified block diagram of a measuring system

Light-to-Frequency Converter

Modern galvanic isolation circuits use magnetic fields (transformers), electrical fields (capacitors) and light radiation (optocouplers) to transmit signals through the isolation barrier [1]. Galvanic isolation for analogue signal (GS1 and GS2 on fig. 1) requires a proper linear optocoupler. Commonly used optocouplers contain a LED, optically coupled with two photodiodes, which enable negative feedback, increasing the system's linearity. Many independent manufacturers offer such optocouplers.

Currently, there are also Light-to-Frequency Converters (LFC) [2], which enable a new type of galvanic isolation circuits. Using frequency as an information-carrying signal in the measuring system is very beneficial. Frequency, in comparison with the voltage signal, is much more resistant to interference and it can be sent over large distances without losing information and be precisely converted into a digital form using simple and cheap counters [3] or microcontrollers, without using expensive analogue-to-digital converters.

LFC is a monolithic integrated circuit containing a silicon photodiode connected to a current-to-frequency converter (CFC). A simplified electric diagram of such converter is presented on figure 2.

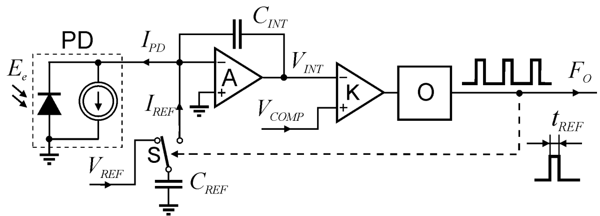

Fig.2. Simplified electric diagram of Light-to-Frequency Converter

Photodiode PD converts the incident irradiance E_e to photodiode current I_{PD} with the constant of proportionality equal to sensitivity of the photodiode S_{PD}. Integrator containing amplifier A and capacitor C_{INT}, comparator K, oscillator O and reference capacitor C_{REF} create a current-to-frequency converter. Reference capacitor C_{REF} is periodically charged to the reference voltage V_{REF} and connected via switch S to the integrator input. Negative feedback in this circuit causes the average current value I_{REF} supplied by the capacitor C_{REF} to the integrator to be equal to the photodiode's current value I_{PD}. Output frequency F_O is proportional to the incident irradiance E_e :

$$F_O = \frac{S_{PD}}{V_{REF} C_{REF}} E_e + F_D = R_e E_e + F_D \,, \tag{1}$$

where: R_e is the LFC responsivity given in kHz/(μW/cm^2), F_D is the output frequency for dark condition (E_e=0). According to the manufacturer's information, such converters have a dynamic range of even 160 dB, nonlinearity error of 0.1% of the measurement range and output frequency up to 1 MHz [2]. Since the frequency F_D is very small, so in most application it can be omitted.

Proposed new galvanic isolation circuit

Using a LFC together with a LED enables a galvanic separation circuit for analogue signals. An appropriate block diagram is shown on figure 3. The LED converts the current I_F to radiant flux Φ_e, which uses the transmission medium TM to fall on the photodiode PD placed in the LFC. Output frequency F_O is proportional to the current I_F flowing through the LED :

(2) $$F_O = \frac{CTR}{V_{REF}C_{REF}} I_F$$

where: CTR – current transfer ratio of the photodiode current I_{PD} to the LED current I_F.

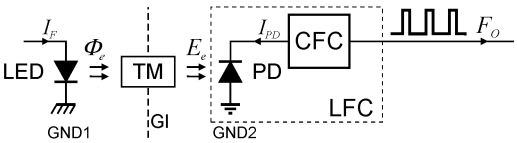

Fig.3. Galvanic isolation circuit

Static properties of the circuit

In order to assess metrological parameters of the proposed solution, a system was built in accordance with figure 3, using TSL235R TAOS Light-to-Frequency Converter [2] and IRL81A LED. Listed sensitivity of the LFC is 580 Hz·μW^{-1}cm^2 for 635 nm light wavelength, but maximum sensitivity occurs for 760 nm light wavelength. In order to obtain nominal output frequency F_O=500 kHz, a incident irradiance E_e of 0,7 mW·cm^{-2} is required. The IRL81A diode generates a flux Φ_e with a radiant intensity of I_e=1 mW·sr^{-1} for current I_F=20 mA, maximum radiation for 880 nm light wavelength. In order to obtain proper optical coupling (with medium value of CTR on fig. 4), both elements have been placed in the free air, 1 cm of each other, and enclosed in a lightproof case with black internal walls. Then, static processing characteristic of the system has been designated experimentally for three different CTR values, using a logarithmic scale on figure 4.

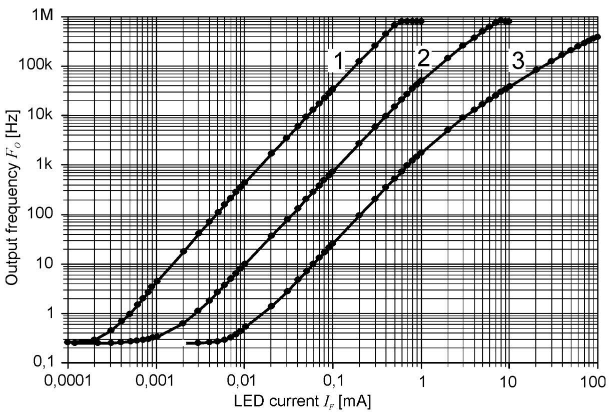

Fig.4. Static characteristic of the galvanic isolation circuit for different values of CTR: 1-high, 2-medium, 3-low

The circuit operates correctly within about 120 dB, which corresponds to frequency values F_O of the LFC from 0,5 Hz to 800 kHz. Nonlinearity depends on the CTR, it is better for higher values of the CTR.

Circuit operation in dynamic conditions

In dynamic conditions, the LED current value I_F is changing, therefore output frequency F_O is also changing. In order to determine instantaneous values of input signal (current I_F), it is necessary to measure instantaneous frequencies F_O. It requires usage of a proper system, which enables measuring all subsequent time intervals between subsequent output signal impulses of the converter [3]. The instantaneous frequency may be determined easily as the inverse of the time between subsequent impulses and should be assigned to the moment in time present midway in this time. Therefore, received results are placed irregularly in time, which makes their further processing more difficult. In order to obtain signal samples placed regularly in time, an approximation of the converter's output signal phase using polynomials may be used, and after calculating its derivative – new samples at regular time intervals may be specified [3].

In order to assess the operation of the system in dynamic conditions, a measuring system with a National Instruments NI 6602 measuring card connected to a PC has been used, along with appropriate LabVIEW software [3]. Figure 5 shows possible results for harmonic current with a constant of 0,5 mA and an amplitude of 0,3 mA, changing with the frequency of 200 Hz. The graph also shows that for lower current values, the signal samples are spread less frequently, and for higher values – more frequently, therefore sampling is nonuniform.

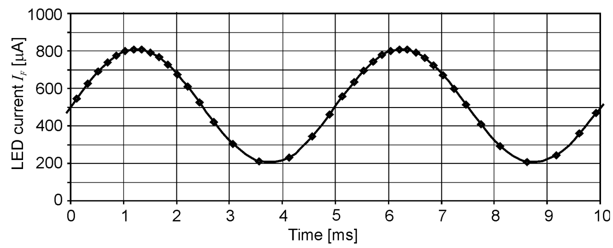

Fig.5. Sample measuring results in dynamic conditions

Summary

A new concept of a galvanic isolation system using a Light-to-Frequency Converter working alongside a LED is presented. Besides introducing the isolation barrier, using a frequency-measuring signal additionally increases resistance to strong electromagnetic interference. Results from a prepared system confirm proper linearity of static characteristic. After using an appropriate measuring system and an additional data processing algorithm, the circuit may also operate in dynamic conditions.

REFERENCES

[1] Texas Instruments Inc., AN-298 Isolation Techniques for Signal Conditioning, Application Report SNOA604B, May 2013.
[2] TAOS, TSL235R Light-to-Frequency Converter, Texas Advanced Optoelectronic Solutions, TAOS038E, 2007.
[3] Pawlowski E., Digital processing of pulse signal from light-to-frequency converter under dynamic condition, Proc. SPIE 9291, Aug. 2014, 929102, doi:10.1117/12.

***Author**: dr inż. Eligiusz Pawłowski, Politechnika Lubelska, Wydział Elektrotechniki i Informatyki, ul. Nadbystrzycka 38A, 20-618 Lublin, e-mail: e.pawlowski@pollub.pl*

8th International Conference
Electromagnetic Devices and Processes in Environment Protection ELMECO-8
joint with 11th Seminar Applications of Superconductors AoS-11
September 28 - October 1, 2014, Nałęczów, Poland

EMOTIONAL SPEECH RECOGNITION BASED ON ARTIFICAL NEURAL NETWORK

Paweł POWROŹNIK, Dariusz CZERWIŃSKI

Lublin University of Technology

Abstract*. These article presents the issue of emotion recognition based on Polish emotional speech. Researches were conducted with use of the Polish database of emotional speech prepared by Medical Electronics Division of the Lodz University of Technology. Four layer artificial neural network has bed used as emotion classifier. Conducted researches were focused on the following parameters extracted from normalised speech signal: speaker's sex, average value of speech signal, the minimum and maximum sample value for a given signal, energy of signal and standard deviation from samples. Six of the following emotional states were the object of research: joy, sadness, anger, fear, boredom and neutral state. Achieved results reached 57% of accuracy.*

Streszczenie. *Artykuł prezentuje możliwe zastosowanie sztucznych sieci neuronowych do identyfikacji stanów emocjonalnych mówcy w oparciu sygnału mowy. Do badań została wykorzystana polska baza mowy emocjonalnej opracowana przez Zakład Elektroniki Medycznej Politechniki Łódzkiej. Badania skupiają się wokół następujących stanów emocjonalnych: radości, smutku, złości, strachy, znudzeniu i stanu neutralnego.*

Keywords: emotional state recognition, artificial neural networks, speech signal processing.
Słowa kluczowe: identyfikacja stanu emocjonalnego, sztuczne sieci neuronowe, przetwarzanie sygnału mowy

Introduction

The recognition of the emotional state of a speaker, based on the analysis of speech signals, is a relatively new issue. However, Polish speech was in this researches omitted. During last few years only several polish academic centres begun to conduct researches involving this issue. One of the reasons of such a direction of changes is increase the importance of emotions in systems based on the human - computer type of communication and its dynamic development.

Support vector machine (SVM) and the k-Nearest Neighbours algorithm (or k-NN for short) are mostly common classifiers used in issues connecting with Polish emotional speech recognition [1, 2, 3].

Conducted researches were focused on well known, but omitted in publications about Polish emotional speech, artificial neural networks. The second aim of this research was to find the optimal input parameters for an artificial neural network allowing an effective recognition of the emotional states of a speaker. Carried out researches were based on databases contained samples matched with specific emotional tone of the voice.

Analysis of issue

One of prepared and commonly used emotionally touched voice samples set is Berlin Database of Emotional Speech [4]. This database contains recording prepared by 10 actors of both sexes, speaking sentences in seven emotional states: joy, sadness, anger, fear, boredom, disgust and neutral state [5]. Collections of files, contained records, prepared based on radio and television programs are also available. Polish emotional speech database was prepared and shared by The Lodz University of Technology [2].

The most important issue in researches in automatic emotion recognition is to find the proper feature vector, which comprehensively describes the speech signal. Descriptors, commonly use in this issue, do not significantly vary from the ones used the analysis and processing of speech signals. Signal energy or basic frequency are parameters which are wildly applied as that kind of descriptors [6]. Mel-frequency Cepstrum (MFCC) [7, 8], Perceptual Linear Predictive (PLC) and Linear Predictive Coding (LCP) factors are contemporary standards in detection of speech [9]. They also used in cases connected with emotional speech analysis.

The sets of attributes, determine based on speech signal parameters, are input vector for emotional speech classifiers. Support Vector Machine [10] and k - Nearest Neighbours algorithm [3] are used as Polish emotional speech classifier. However, global trends help draw the assumption of equally good performance of artificial neural networks in the analysis of the above issues [11].

Speech signals parameters and proposed classifier

Carried out research has not resulted in the determination of an universal set of features for speech analysing process so far. It results in a heuristic approach adoption [10]. This approach involves as many parameters, designated from signal, as possible. After this experimentally or by using algorithm, those parameters which best describe the case are selected. Among the parameters extracted from the signal the most useful ones are: the laryngeal tone, energy of the signal, formant values, and MFCC, LPC, PLP factors [1, 10].

Energy, average value and standard deviation of speech signal

The carried out researchers focused on both statistic and physics values of speech signal, that is average value, standard deviation from samples and energy. The average value of the whole signal is defined by equation (1) [12]:

$$\overline{x_N} = \lim_{n\to\infty} \frac{1}{2N+1} \sum_{n=-N}^{N} x(n) \tag{1}$$

where: x_N – average value of signal, N – total number of samples, $x(n)$ – value of n – sample.

In probability theory and statistics, the standard deviation measures the amount of variation from the average. A low standard deviation indicates that values tend to be very close to the mean a high standard deviation indicates that values are spread out over a large range of values. The standard deviation from samples is described by the following formula [12]:

$$SD=\sqrt{\frac{\sum_{n=1}^{N}(x-\overline{x_N})^2}{N-1}} \tag{2}$$

where: SD – standard deviation, N – total number of samples, x_N – average value of signal, x – n-sample value.

The energy of the signal is defined as the integral of the square of the signal, that is, energy emitted with unitary resistance. For digital signals it is described by the following formula [12]:

$$E_x=\sum_{n=0}^{N}x^2(n) \tag{3}$$

where: E_x – signal energy, n – sample number, $x^2(n)$ – square value of n – sample.

Before the determination of mentioned above parameters samples were undergone of normalisation process for the purpose of research. A standard algorithm of signal processing is based on three basic stages: preparation of the data set, the designation of the feature vector and classification. Thanks to the high quality of recordings the first stage has been limited to normalisation process.

The second step is to determine the feature vector describing the analysed matter as accurately as possible. In conducted researches this set of parameters was limited to six elements: the sex of the speaker (1 - woman, 0 - man), the energy of the signal, both the minimum and maximum sample value for a given signal, the standard deviation from samples and the average value of the whole signal. Mentioned above parameters become an input vector for used artificial neural network.

The last stage is classification. A four layer neuron network has been proposed as a classifier. The input layer was built by 6 neurons, two hidden layers contained 12 and 18 neurons, respectively, the output layer is composed of six neurons.

Neurons were activated by sigmoidal function. The research has been carried out in MatLab, where the neural network has been trained with the back-propagation algorithm with momentum and adaptation factor (traingdx). The learning process ended with either the achievement of the given number of epochs, that is, 1000 in the analysed cases, or the achievement of a normalised result different from the expected one by no more than 0.1. The achieved results have been depicted in figure 1. The confusion matrix has been shown in Table 1.

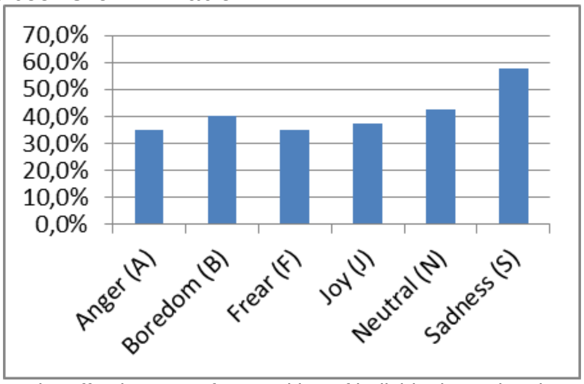

Fig.1. The effectiveness of recognition of individual emotional state

Table 1. Confusion matrix

		Actual emotional state					
Predicted emotional state		**A**	**B**	**F**	**J**	**N**	**S**
	A	**14**	4	10	10	1	1
	B	4	**16**	5	1	10	4
	F	10	9	**14**	3	2	2
	J	11	1	8	**15**	4	1
	N	3	8	2	1	**17**	9
	S	2	4	4	2	5	**23**

Conclusions

The explicit designation of emotional tone in the voice sample is not a trivial issue and the achieved results are far from ideal. Research conducted by Swiss scientists show, that the estimation of an emotional state is difficult even for a human being. They shown that average person can identify another, unknown person emotional state properly, only in 60% of all cases [13]. However it is possible to improve results achieved by used artificial neural network. One of the first step should be expansion of feature vector and extraction from speech signal more distinctive for emotion recognition features. As it was mentioned above MFCC and LPC factor are becoming a standard in analysis speech signals especial if we focused on English. It is absolutely necessary to include this parameter into feature vector. It is necessary to rearrange ANN, change activation function or transform it into another for of ANN, the Kohonen network for instance. The effectiveness of emotion recognition can be also increased by combining a voice analysis system with semantic analysis.

REFERENCES

[1] D. Kamińska, A. Pelikant, Zastosowanie multimedialnej klasyfikacji w rozpoznawaniu stanów emocjonalnych na podstawie mowy spontanicznej, *IAPGOŚ 03/2012.*

[2] Database of Polish Emotional Speech, available: http://www.eletel.p.lodz.pl/bronakowski/med_catalog/,) (Accessed 10.08.2014).

[3] K. Ślot, Rozpoznawanie biometryczne, WKiŁ, Warszawa, 2010.

[4] Berlin Database of Emotional Speech, available: http://www.expressive-speech.net/, (Accessed 10.08.2014).

[5] T. Polzehl, A. Schmitt, F. Metze, Approaching multi-lingual emotion recognition- from speech - on language dependency of acoustic/prosodic features for anger recognition, *Proc. of Speech Prosody*, Chicago 2010.

[6] Y. Yeqing, T. Tao, An new speech recognition method based on prosodic analysis and SVM in Zhuang language, *Proc. 2011 International Conference on Mechatronic Science, Electric Engineering and Computer*, 2011, p. 1209 – 1212.

[7] R. Plutchik, The nature of emotion, American Scientist, *Volume 89*, July-August 2001, p. 344-350.

[8] D. Niewiadomy, A. Pelikant, Implementation of isolated words boundaries recognition, Proc. XII International Conference System Modeling and Control SMC'2007, Zakopane 2006.

[9] A. Shauka, K. Chen, Emotional state recognition from speech via soft- competition on different acoustic representations, *Proc. Neural Networks (IJCNN)*, 2011, p. 1910 – 1917.

[10] A. Janicki, M. Turkot, Rozpoznawanie stanu emocjonalnego mówcy z wykorzystaniem maszyny wektorów wspierających (SVM), KSTiT 2008, Bydgoszcz, 2008.

[11] K. Soltani, R. Ainon, Speech emotion detection based on neural networks, *Proc. Signal Processing and Its Applications*, 2007, p.1-3.

[12] T. Zieliński, Cyfrowe przetwarzanie sygnałów. Od teorii do zastosowań, WKŁ 2009.

[13] K. Scherer, Vocal Communication of Emotions: A Review of Research Paradigms in Speech Communication, 40(2003), 227 – 256, Elsevier 2003.

***Authors**: mgr Paweł Powroźnik, Politechnika Lubelska, Instytut Podstaw Elektrotechniki I Elektrotechnologii, ul. Nadbystrzycka 38a, 20-618 Lublin, e-mail: pawel.powroznik@pollub.edu.pl; dr hab. Dariusz CZerwiński, Politechnika Lubelska, Instytut Podstaw Elektrotechniki I Elektrotechnologii, ul. Nadbystrzycka 38a, 20-618 Lublin, e-mail: d.czerwinski@pollub.pl*

8th International Conference
Electromagnetic Devices and Processes in Environment Protection ELMECO-8
joint with 11th Seminar Applications of Superconductors AoS-11
September 28 - October 1, 2014, Nałęczów, Poland

CARBON NANOTUBES SYNTHESIS IN LOW PRESSURE ARC DISCHARGE

Grzegorz RANISZEWSKI

Lodz University of Technology, Institute of Mechatronics and Information Systems, Lodz, Poland

***Abstract**. The paper describes an author's experience in electric arc discharge methods of carbon nanotubes synthesis under reduced pressure. Although in the arc discharge systems pressure does not exceed a half of atmospheric pressure it is assumed that the plasma is near local thermodynamic equilibrium state. The discussed problems are related to the anode jet parameters and its influence on containing carbon nanotubes cathode deposit.*

***Streszczenie.** Artykuł opisuje doświadczenia autora związane z zastosowaniem wyładowania łukowego do syntezy nanorurek węglowych pod obniżonym ciśnieniem. Chociaż ciśnienia w reaktorze łukowym nie przekraczają 0,5 atm, autor założył, że plazma tworząca depozyt katodowy jest w stanie bliskim równowagi termodynamicznej. Przedstawiona tematyka badań związana jest z parametrami strumienia anodowego tworzącego zawierający nanorurki węglowe depozyt katodowy.*

Keywords: carbon nanotubes, cathode deposit, arc discharge
Słowa kluczowe: nanorurki węglowe, depozyt katodowy, wyładowanie łukowe

Introduction

The most common methods for carbon nanotubes (CNTs) synthesis are various types of chemical vapour deposition (CVD) and arc discharge methods. In CVD methods usually as a source of carbon for CNTs formation gases containing carbon are used. In arc discharge methods carbon comes from graphite anode. In the arc reactors two types of carbon nanotubes can be collected: single-wall carbon nanotubes (SWNTs) and multiwall carbon nanotubes (MWNTs). MWNTs usually are located inside the cathode deposit. Synthesis of SWNTs usually needs application of catalysts and are deposited on the reactor walls, especially on the top of the reactor and in the anode area.

The system for carbon nanotubes synthesis

Generally the arc discharge method is the easiest way for carbon nanotubes production. In investigated reactor two graphite electrodes were used – anode with dia. 6 mm and cathode with dia. 50 mm. Graphite rods were placed inside the sealed chamber which was filled with inert gas (helium) at low pressure (between 100 and 700 mbar). The distance between electrodes was about 1 mm. Temperature of the arc discharge near the anode surface was higher than boiling point of carbon. This temperature caused vaporization of carbon elements and formation of plasma jet. The jet moved carbon elements toward relatively cold cathode surface and formed containing carbon nanotubes cathode deposit. Fig. 1 illustrates system for arc plasma CNTs synthesis.

Arc discharge methods enable synthesis of multiwall carbon nanotubes. In cases when single wall carbon nanotubes are needed it is necessary to application of catalysts. There are many catalysts in arc discharge systems such as Co [1], Gd [2], mixes with graphite Co:Y, Co:Fe, Ni:Y, Ni:Mg, Ni:Fe, Ni:Cu, Ni:Pt, Ni:Ti, Ru:Pt [3-5] but the most common are ferrous group metals [6-9]. Introduction of the catalyst influence on plasma parameters and geometry. Among several methods of catalysts introduction a method where a mixture catalyst-carbon is placed in a hole in the anode.

Fig. 1: View inside reactor where:1- diagnostic window, 2 – carbon elements on reactor walls, 3 – cathode deposit, 4 – cathode, 5 – cathode holder

Cathode deposit is composed of different forms of carbon, but up to 30% are carbon nanotubes. The final product is a mixture of components and requires separating nanotubes from the soot. Fig. 2 shows examples of deposits for different catalysts.

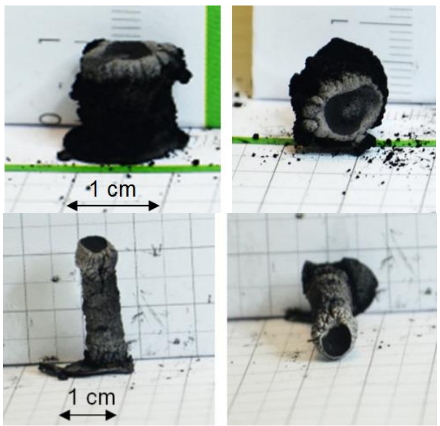

Fig. 2. Examples of cathode deposits where a) Ni as catalyst (5% wt.); b) Y as catalyst (5% wt.)

It was noticed that ferromagnetic nanotubes appear only on the walls of the reactor. In presented research set-up Co, Ni, Fe were used as catalysts.

The plasma jet

Although the applied systems use approximately half of the atmospheric pressure it is assumed that the plasma column is in the near local thermodynamic equilibrium state. Due to high evaporation ratio the local pressure between two electrodes is relatively high. Assumption that plasma is in the local thermodynamic equilibrium means that:

- temperatures (the average kinetic energy of particles) all of plasma components are equal,
- velocity distribution of all kinds of particles is described in Maxwell's law,
- distribution of particles with different energy levels is defined by the Boltzmann law,
- the plasma components concentration is defined by the Saha-Eggert equation,
- concentration of the individual components of chemical reactions is determined by the Guldberg-Waage law of mass action.

Due to the small distance between electrodes diameter of the radius of the plasma column r_n is relatively high

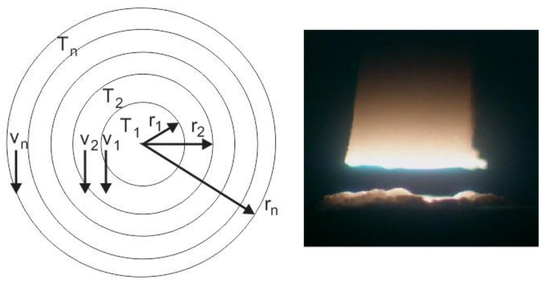

Fig. 3. Plasma column (right) and its crossection (left) where: T – temperature, r – distance from the axis, v - velocity

Due to the small distance between electrodes diameter of the radius of the plasma column r_n is relatively high. To measure plasma column temperature method of two spectral lines of the same element can be used [10]. The plasma column have different temperatures (T) with different distances (r) from the column axis. Moreover, plasma column is rotating what may be stabilized by additional external magnetic field [11].

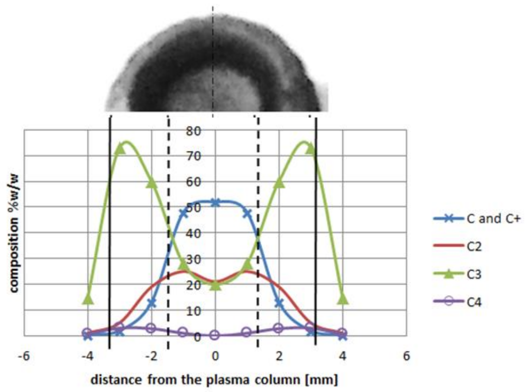

Fig. 4. Plasma column composition with carbon deposit composition (top).

Knowledge about temperature and knowledge about carbon elements decomposition in high temperatures enable determination of plasma jet composition.

Fig. 4 shows plasma column composition influence on deposit composition. The core containing carbon nanotubes grow in the zone of domination of small carbons and carbon ions. The hard shell is characteristic for the multiatom carbons flux.

Results

The results of experiments and calculations have a great practical potential in modeling of phenomena which occurs during the synthesis process. A new approach to the problem will improve the currently used technologies and increase the carbon nanotubes creation efficiency

- The average velocity of the plasma jet decreases with distance from the electrode (2,5-4,5 m/s)
- Metal vapor stream radius decreases with the distance from the electrode (1,6-2,4 mm)
- Metal vapor flux density decreases with distance from the electrode (0,08-0,14 kg/m3)
- The partial pressure of the catalyst decreases with distance from the electrode (0,5-3 Pa)
- Effective ionization potential increases with distance from the electrode

Acknowledgment:

Scientific work has been financed from the budget for science in the years 2013-2014 as a research project.

REFERENCES

[1] Iijima S., Ichihashi T., Single-shell carbon nanotubes of 1-nm diameter, *Nature* 363 (1993), pp. 603-605

[2] Subramoney S. et al., Radial single-layer nanotubes, *Nature* 366 (1993), p. 637

[3] Kiang C.H. et al., Subramoney S. et al., Catalytic effects of heavy metals on the growth of single-layer carbon nanotubes and nanoparticles, *Journal of Physical Chemistry*, Vol. 57 (1996), pp. 35-39

[4] Saito Y. et al., High yield of single-wall carbon nanotubes by arc discharge using Rh-Pt mixed catalysts, Chemical Physics Letters, Vol. 294, Issue 6 (1998), pp. 593-598

[5] Flahaut E. et al., Synthesis of single-walled carbon nanotubes using binary (Fe, Co, Ni) alloy nanoparticles prepared in situ by the reduction of oxide solid solutions, Chemical Physics Letters, Vol. 300, Issues 1-2 (1999), pp. 236-242

[6] Saito Y. et al., Cobalt particles wrapped in graphitic carbon prepared by an arc discharge method, *Journal of Applied Physics*, Vol. 75, Issue 1 (1994), pp. 134-137.

[7] Seraphin S., Zhou D., Single-walled carbon nanotubes produced at high yield by mixed catalysts, *Applied Physics Letters*, Vol. 64, Issue 16 (1994), p. 2087.

[8] Ebbesen T.W., Nanotubes, nanoparticles, and aspects of fullerene related materials, *Journal of Physics and Chemistry of Solids*, Vol.58, Issue 11 (1995), pp. 1979-1982.

[9] Lambert J.M., Ayajan, P.M., Bernier, P., Synthesis of single and multi-shell carbon nanotubes, *Synthetic Metals*, Vol. 70, Issues 1-3 (1995), pp. 1475-1476.

[10] Raniszewski G., Temperature measurements in arc-discharge synthesis of nanomaterials dedicated for medical applications, *Eur. Phys. J. Appl. Phys*. (2013) 61:24311

[11] Raniszewski G., Pyc M., Kolacinski Z., Optimization of magnetic field assisted synthesis of carbon nanotubes for sensing applications, *Sensors* (2014) (in printing)

***Authors**: Dr Grzegorz Raniszewski, Lodz University of Technology, Stefanowskiego Str. 18/22, 90-924 Lodz, Poland, grzegorz.raniszewski@p.lodz.pl*

8th International Conference
Electromagnetic Devices and Processes in Environment Protection ELMECO-8
joint with 11th Seminar Applications of Superconductors AoS-11
September 28 - October 1, 2014, Nałęczów, Poland

PLASMA – CATALYTIC CONVERSION OF CYCLOHEXANE

Ewelina REDA, Michał MŁOTEK, Krzysztof KRAWCZYK

Warsaw University of Technology

Abstract. *The conversion of cyclohexane in a 3-phase gliding discharge reactor has been tested. Two gas flow rates of an air+cyclohexane mixture were used (1000 and 1400 Nl/h). The studies were conducted in a homogeneous (without catalyst) and hybrid plasma-catalytic system (with NiO/cordierite and Ni_3Al catalysts). It was observed that the higher gas flow rate and higher initial cyclohaxane concentration have a positive impact on unit energy consumption.*

Streszczenie. *Przedmiotem badań była konwersja cykloheskanu w 3-fazowym reaktorze w którym generowano wyładowanie ślizgowe. Zastosowano dwa natężenia przepływu gazu (1000 i 1400 Nl/h). Badania prowadzono w układzie homogenicznym (bez katalizatora) a także w układzie plazmowo-katalitycznym. Zaobserwowano, że wyższe natężenie przepływu gazu, a także wyższe początkowe stężenie cykloheksanu korzystnie wpływa na jednostkowe zużycie energii.*

Keywords: VOCs removal, gliding discharge, non-equilibrium plasma.
Słowa kluczowe: usuwanie LZO, wyładowanie ślizgowe, plazma nierównowagowa.

Introduction

Cyclohexane is widely used as a non–polar organic solvent and is also the starting material for adipic acid and caprolactam production, which are precursors of nylon [1]. Unfortunately, due to a high vapour pressure, cyclohexane is classified as a volatile organic compound (VOC). VOCs have a harmful effect on human health and the environment. They cause photochemical smog and pollution of the biosphere. Moreover, some of them are carcinogenic. For these reasons emission of VOCs to the atmosphere is limited. There are many gas purification methods which can be applied in decomposition of volatile organic compounds (VOCs) including thermal and catalytic oxidation, biological methods, adsorption, absorption and condensation [2]. These methods often require the use of complex and expensive installations, whereas using conventional technologies such as catalytic or thermal oxidation, energy is wasted on gas heating [1]. Another method, adsorption on activated carbon is very effective. However, activated carbon is quite expensive and has to be regenerated thermally [3]. In recent years many studies were focused on the application of new technologies based on non–equilibrium plasma. Gliding discharge is especially attractive due to the high quantity of radicals produced and a possibility to perform the process at high gas flow rates. A disadvantage of plasma methods is often incomplete conversion, leading to even more toxic by-products. In order to solve this problem a plasma-catalyst system is used. Currently the main effort is directed to finding a catalyst which will improve the conversion and selectivity of VOC decomposition.

Experimental

The conversion of cyclohexane was tested in a 3–phase gliding discharge reactor (Fig. 1). The reactor, made of a quartz–glass tube with a 60 mm internal diameter, contained three converging duralumin electrodes [4]. The gas inlet was located at the bottom, between the electrodes. The power supply applied for this gliding discharge reactor was manufactured by Ertec, Poland. The new general idea of ferroresonant transformers energized from transistor inverters allows for the design of a poly–phase multi–electrode reactor systems, in which a high capacity utilization rate is reached with the user set value of the total discharge current. The group of high-voltage transformers supplied from the three–phase inverter with adjustable limits of both the amplitude and frequency can deliver the output voltage of 1000 – 2000 V to each electrode. The power supplied to the gliding reactor was in the range of 1 – 2 kW. The energy was measured by an energy meter.

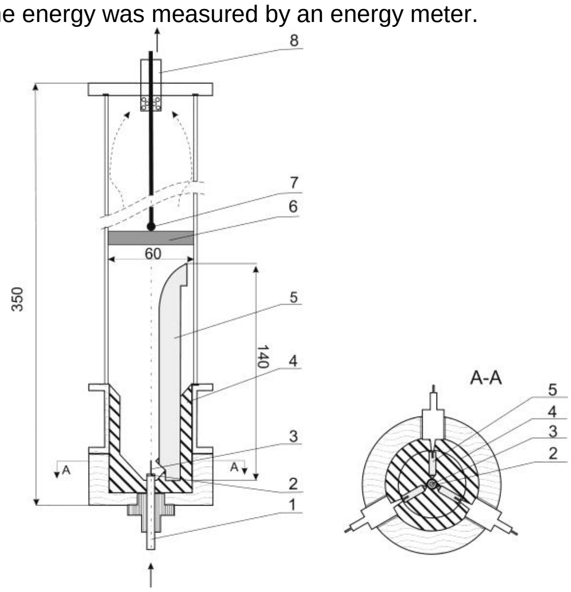

Fig.1. Three-phase gliding discharge reactor. 1 – gas inlet, 2 – gas nozzle, 3 – starting electrode, 4 – ceramic lining, 5 – electrode, 6 – catalyst bed, 7 – thermocouple, 8 – gas outlet.

Conversion of cyclohexane was tested in air at normal pressure. Two gas flow rates: 1000 Nl/h and 1400 Nl/h were used. Moreover, the effect of catalyst on conversion of cyclohexane was investigated. For that purpose, two different catalysts were selected: NiO on cordierite carrier and alloy Ni_3Al. To obtain the NiO/cordierite catalyst (containing about 3 wt. % of metal) commercial cordierite ceramic was impregnated with an aqueous solution of nickel nitrate, dried and calcined for 3 hours at 400ºC. The microcrystalline Ni_3Al foils with the nominal composition of Ni–22.1Al–0.26Zr–0.1 (at.%) were prepared in the shape of a “honey–comb” structure [5]. Tests in the homogeneous system were conducted in a wide range of initial cyclohexane concentrations (0.1 – 1% vol.) In tests with a catalyst bed two initial concentrations of cyclohexane (0.5 and 1% vol.) were used.

The gas temperature measured at the vessel axis over the upper ends of the electrodes reached 270 – 500°C, depending on the discharge power and presence of catalyst. The gaseous products were analyzed by gas chromatography using Agilent 6890N with HayesepQ column and the FID detector. Inorganic products (CO_2 and CO) were analyzed by Chrompack CP – 9002 with a Carboplot P7 column and a TCD detector.

The aim of this work was to investigate the effect of the gas flow rate, initial cyclohexane concentration and kind of catalyst on unit energy consumption.

$$Uec = \frac{P \times 3.6}{W[C_6H_{12}]} \quad (1)$$

where: Uec – unit energy consumption/MJ*mol^{-1}C_6H_{12}
P – power computed from energy meter/W
W[C_6H_{12}] – cyclohexane flow rate at the outlet/mol*h^{-1}

Results and discussion

The main products of C_6H_{12} decomposition were carbon oxides and water. Trace amounts of C2 – C3 hydrocarbons were also observed. With the increase of discharge power and gas flow rate, a decrease of unit energy consumption was observed (Fig. 2). It should be noted that this process is economically favourable for higher initial concentrations of cyclohexane (Figs. 2-4).

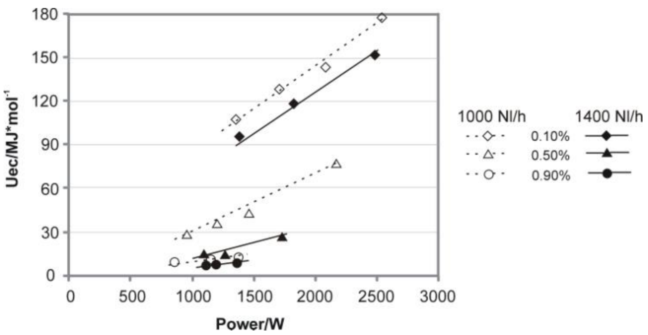

Fig.2. Effect of the initial cyclohexane concentration and gas flow rate on unit energy consumption in the homogeneous system.

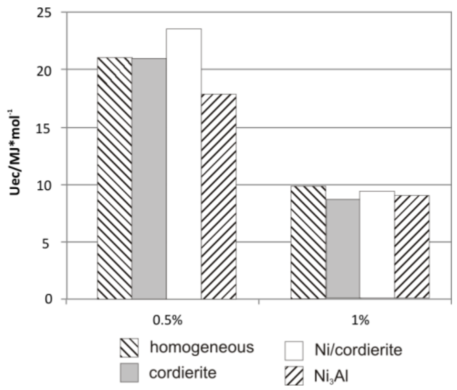

Fig.3. Effect of initial concentration of cyclohexane and catalyst on unit energy consumption. Gas flow rate – 1000 Nl/h. Discharge power – 1000 W.

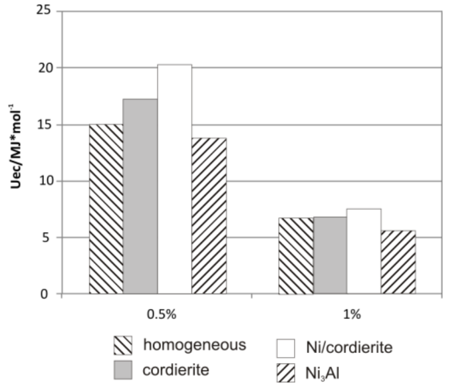

Fig.4. Effect of initial cyclohexane concentration and catalyst on unit energy consumption. Gas flow rate – 1400 Nl/h. Discharge power – 1000 W.

The effect of the catalyst on the energy consumption may be seen especially for the lower initial cyclohexane concentration. The highest unit energy consumption was obtained for NiO/cordierite and the lowest for Ni_3Al. It may suggest that Ni_3Al has better catalytic properties than NiO/cordierite.

Conclusions

It was shown that the unit energy consumption depends on the initial cyclohexane concentration, gas flow rate and kind of catalyst. A positive impact on unit energy consumption was noted for the higher initial concentration of cyclohexane and the higher gas flow rate. The greatest catalytic effect was obtained for Ni_3Al.

Acknowledgments

This work was supported by the National Center for Research and Development project No. PBS2/A1/10/2013.

References

[1] Harling A. M., Glover D. J., Whitehead J. C., Zhang K., The role of ozone in the plasma – catalytic destruction of environmental pollutants, *Applied Catalysis B: Environmental*, 90 (2009), 157-161

[2] Khan F. I., Ghoshal A. K., Removal of Volatile Organic Compounds from polluted air, *Journal of Loss Prevention in the Process Industries,* 13 (2000), 527-545

[3] Schmid S., Jecklin M. C., Zenobi R., Degradation of volatile organic compounds in a non-thermal plasma air purifier, *Chemosphere,* 79 (2010), 124-130

[4] Młotek M., Sentek J., Krawczyk K., Schmidt-Szałowski K., The hybrid plasma-catalytic process for non-oxidative methane coupling to ethylene and ethane, *Applied Catalysis A:General,* 366 (2009), 232-241

[5] Bojar Z., Jóźwik P., Bystrzycki J., Tensile properties and fracture behavior of nanocrystalline Ni_3Al intermetallic foil, *Scripta Materialia,* 55 (2006), 399-402

***Author**: mgr. inż. Ewelina Reda, Warsaw University of Technology, Faculty of Chemistry, 3 Noakowskiego Street, 00-664 Warsaw, e-mail: ereda@ch.pw.edu.pl;*

8th International Conference
Electromagnetic Devices and Processes in Environment Protection **ELMECO-8**
joint with 11th Seminar Applications of Superconductors **AoS-11**
September 28 - October 1, 2014, Nałęczów, Poland

SELECTED ISSUES OF THE TRANSPORT CURRENT FLOW IN MULTILAYERED HTc SUPERCONDUCTORS

Jacek SOSNOWSKI

Electrotechnical Institute, Warsaw

Abstract*. In the paper is analyzed influence of multilayered structure of HTc superconductors on the peculiarities of the transport current flow in these materials. The flow of the current in superconducting planes as well as in the direction perpendicular to the planes is regarded. The generation of the intrinsic Josephson's junctions is discussed, while for in-plane current flow description, mathematical model has been elaborated taking into account interlayers interaction, which well corresponds to experimental data, measured on BiPbSrCaCuO HTc superconductor.*

***Streszczenie.** W pracy zbadano wpływ wielowarstwowej struktury nadprzewodników wysokotemperaturowych na specyfikę transportu prądu przez te materiały. Rozpatrzono przepływ prądu wewnątrz płaszczyzn nadprzewodnikowych, jak też w kierunku prostopadłym. Zanalizowano powstanie wówczas samoistnych złącz Josephsonowskich oraz przedstawiono model przepływu prądu wewnątrz płaszczyzn nadprzewodnikowych.*

Keywords: multilayered HTc superconductors, applications, transport current flow.
Słowa kluczowe: wielowarstwowe nadprzewodniki wysokotemperaturowe, zastosowania, przepływ prądu transportu.

Introduction

HTc superconducting materials in the technical form of second generation tapes, as well as in microscopic scale of their crystal structure, are multilayered materials. Such peculiar structure influences the critical current and current-voltage characteristics in the respect to the current direction and interlayers interaction. These important technically topics are considered in the present paper.

Losses generated in multilayered tapes

In Fig. 1 is shown multilayered structure of the YBaCuO based second generation tape. HTc superconducting layer is epitaxially growing here on the hastelloy substrate, which is magnetic material containing more than 50 % of Ni.

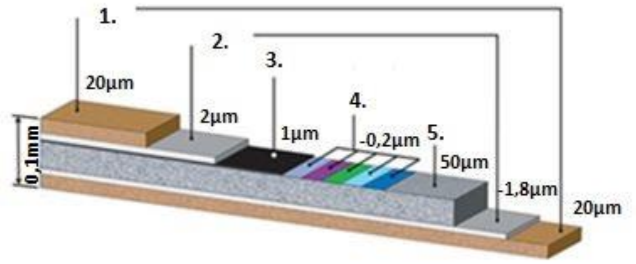

Fig. 1. Multilayered structure of the second generation HTc superconducting tape: 1- Cu stabilizer, 2- Ag layer, 3 – YBaCuO epitaxial film, 4 – Buffer layers, 5 – Hastelloy substrate

Multilayered structure leads therefore to enhancement of magnetic losses generated during the alternating current flow through the second generation superconducting tape. These losses are determined by the magnetic characteristics of the nickel substrate as it shows Fig. 2, in which is presented calculated influence of the magnetic characteristics of the magnetic substrate on the generated losses in units reduced to the current density.

Anisotropy of the current flow in multilayered HTc superconductors

Multilayered crystal structure of $HgBa_2CuO_{4+x}$ HTc superconductor, achieving largest known critical tempera-

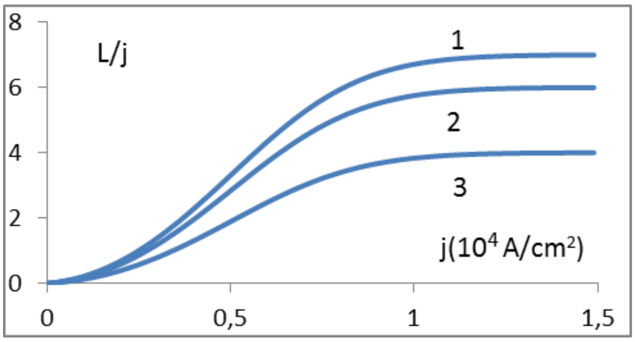

Fig. 2. Dependence of the losses L reduced to alternating current density j in multilayered structure of HTc superconducting tape as the function of the substrate magnetic characteristics: $B = \alpha$ th (0,6 H), where (1) α = 0,7, (2) 0,6, (3) 0,4

ture above 150 K, is presented in Fig. 3. Existence of CuO_2 layers and CuO chains is well seen here. Such structure leads to anisotropy of the transport current flow through this material. While in-plane current theoretically is described by the Ginzburg-Landau type relation:

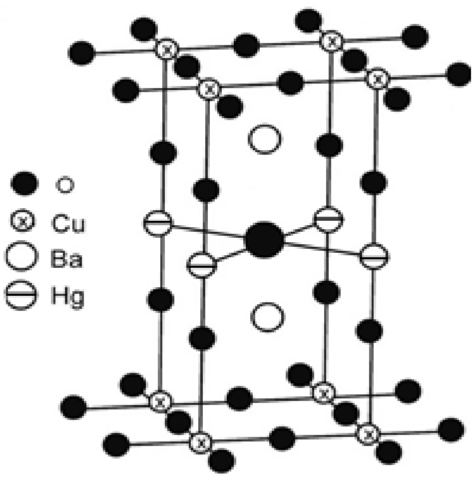

Fig. 3. Multilayered crystal structure of $HgBa_2CuO_{4+x}$ HTc superconductor

(1) $j_{\|} = \frac{-ie\hbar}{m_{\|}}(\Psi_n^+\nabla\Psi_n - \Psi_n\nabla\Psi_n^+) - \frac{4e^2}{m_{\|}c}|\Psi_n|^2 A_{\|}$

the interlayered currents are Josephson's like currents flowing through the intrinsically formed Josephson's junctions:

(2) $j_{\perp n+1,n} = \frac{-ie\hbar}{m_\perp w}\left[\begin{array}{c}\Psi_{n+1} exp\left(-\frac{2ie}{\hbar c}A_\perp w\right)\Psi_n^+ - \\ \Psi_{n+1}^+ exp\left(\frac{2ie}{\hbar c}A_\perp w\right)\Psi_n\end{array}\right]$

Ψ_n is electrons pair wavefunction in n-th plane, e, m – electron charge and mass, ħ reduced Planck's constant, c light velocity, A magnetic field vector potential, while indexes II and ⊥ denote parallel and perpendicular to the layers components, w is buffer layer thickness. In the present paper model has been proposed, for description intra-layers currents, based on Ginzburg-Landau theory, taking into account the capturing interaction of the pancake shape vortices with nanoscale defects, arising in the technological process of preparation superconducting tapes and then coils. Model leads to generation of the energy barrier ΔU, which should pass vortex during the flux creep process. This barrier is described by the relation:

(3) $\Delta U = \frac{\mu_0 H_c^2}{2} l\xi^2 \left[\frac{\pi}{2} - arcsin\left(\frac{j}{j_c}\right) - \frac{j}{j_c}\sqrt{1-\left(\frac{j}{j_c}\right)^2}\right]$

H_c is thermodynamic critical field, l superconducting layer thickness, j_c critical current density, ξ coherence length, μ_0 magnetic permeability. Decrease of the barrier with current amplitude leads to the pancake vortices initially creep and next flow leading to electric field generation. Model has been extended on the case of deformation of the elasticity energy of vortex lattice during capturing process and interlayers interaction has been taken into account in model too. In model has been assumed regular arrangement of the pinning centers. However its extension on other distribution of centers is under consideration Current-voltage characteristics are obtained in this way. The results of I-V curves calculations in individual plane are shown in Fig. 4 for various number of interacting planes.

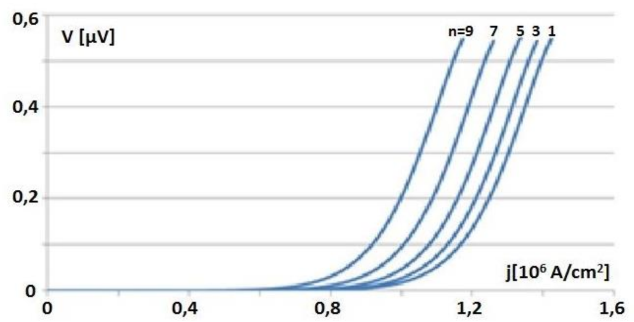

Fig. 4. Calculated current-voltage characteristics of individual plane in HTc multilayered superconductor in the function of the number of interacting planes, denoted by index n.

Observed here change of current-voltage characteristics in individual plane with number of interacting planes is connected with such effect that vortices of pancake form in surrounding planes induce shielding currents in given plane, influencing this way total current flowing through it. Total current-voltage characteristic of sample will be the sum of these individual characteristics. For better recognition and confirmation of theoretical model the comparison of it with experiment has been performed. The current-voltage characteristics of the superconducting $Bi_{1.6}Pb_{0.3}Sr_2Ca_2Cu_{3.06}O_8$ ceramic have been measured in liquid nitrogen temperature and static magnetic field. External magnetic field was generated by using copper solenoid coil immersed directly into liquid nitrogen bath. HTc superconducting sample mounted in sample holder was cooled to 77 K. Measured current-voltage characteristic were then the base of fitting procedure in theoretical calculations. One of the fitting parameters taken into account at calculation procedure was magnetic field. The comparison of measurements and results of theoretical calculations is shown in Fig. 5. The magnetic field values given at each curve are theoretical and correspond within the accuracy of few milliteslas to experimental data. Good agreement between theory and experiment has been observed, which indicates therefore on confirmation of validity of this model.

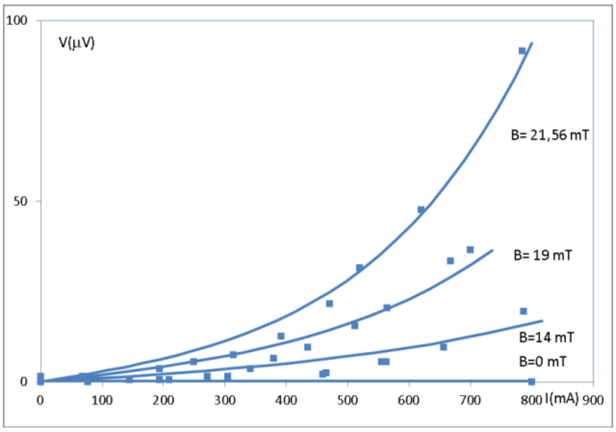

Fig. 5. Theoretical (—) and experimental (□) current-voltage characteristics of multilayered structure $Bi_{1.6}Pb_{0.3}Sr_2Ca_2Cu_{3.06}O_8$ superconductor in static magnetic field and T=77 K

Conclusions

Analysis of the transport current flow in multilayered HTc superconductors has been performed. It indicates on an importance of current direction against the layers orientation. From one side multi-layered structure limits the critical current value and causes strong anistropy, while from other side opens new possibility of an applications of HTc superconducting multilayered materials, especially in electronics. Between layers intrinsic Josephson's junctions are formed, which can be useful in superconducting electronic devices construction. Issue of transport current flow through such highly anisotropic, multilayered materials has meaning also for the work of large power devices, especially HTc cryocables [1], in which critical current is among other determined just by the capturing interaction of vortices with nano-sized defects.

REFERENCES

[1] Sosnowski J., Superconducting cryocables, Electr. Inst. Editor, (2012) 1-101, Warsaw, (in polish)

Author: *prof. dr hab. Jacek Sosnowski, Instytut Elektrotechniki, Zakład Wielkich Mocy, ul. Pożaryskiego 28, 04-703 Warszawa, e-mail: sosnowski.jacek@wp.pl.*

8th International Conference
Electromagnetic Devices and Processes in Environment Protection **ELMECO-8**
joint with 11th Seminar Applications of Superconductors **AoS-11**
September 28 - October 1, 2014, Nałęczów, Poland

EFFICIENT COUPLED NUMERICAL FEM MODEL OF COATED CONDUCTOR IN SELF MAGNETIC FIELD

Mariusz STĘPIEŃ, Bogusław GRZESIK

Silesian University of Technology, Gliwice, Poland

Abstract*. The paper is focused to develop efficient numerical model of coated conductor for modelling with full thermal electromagnetic coupling and critical parameters of superconductivity taken into account. The model is based on ANSYS APDL (ANSYS Parametric Design Language) procedures. In order to ensure efficient calculations 2D geometry has been selected. A time step for transient analysis under pulse load has been selected in a correspondence to E-J power law. As the results parameters of the transition from superconducting to normal state were derived.*

Streszczenie. *Artykuł poświęcony jest opracowaniu wydajnego w pełni sprzężonego modelu numerycznego taśmy nadprzewodnikowej 2G, uwzględniającego wpływ parametrów krytycznych. Model bazuje na procedurach ANSYS APDL. Geometria 2D zapewnia wydajność obliczeń. Krok analizy stanu nieustalonego przy wymuszeniu impulsowym dobrano uwzględniając zależność potęgową E-J. Jako wynik wyznaczone zostały parametry przejścia taśmy ze stanu nadprzewodzącego do stanu normalnego.*

Keywords: coated conductors, FEM modelling, ANSYS, quench propagation.
Słowa kluczowe: nadprzewodniki 2G, modelowanie MES, ANSYS, propagacja quenchu.

Introduction

Recent development of industrial superconducting applications influences on the development of manufacturing of superconducting wires and tapes. Development and optimisation of wires requires numerous tests of properties of different similar structures. Laboratory test are usually very expensive and time-consuming. A very efficient method for analysis and optimization is numerical modelling. In electrical engineering two types of modelling are commonly used, circuit modelling and FEM modelling.

In this paper a method for FEM modelling of HTS coated conductor is presented, based on commercial software ANSYS. A variety of models and modelling method is reported in literature [1], [2]. A model reported in this paper is a transient, fully coupled (electromagnetic and thermal) 2D model [3]. It allows to analyse the quench development and propagation is HTS tapes. Similar models reported in literature are usually simplified models with equivalent heat generation applied to the model [4]. The model, 2D with smooth mesh variation across the geometry allow to calculate results with very short time step, and high width to height tape ratio ensures minimisation of geometry simplification error. Presented in this paper results are an example of tape modelling under low frequency pulse load. This type of load has been selected because of some advantages. The most important is possibility to compare results of modelling to the results of non-destructive laboratory tests. Presented results were obtained for SuperPower® High Current wire (2G) with width of 4 mm and rated current 100 A.

Geometry of model

A geometry of the model has been transformed from 3D to 2D geometry assuming a width of the tape as infinitely long. An idea of such transformation is presented in Fig. 1. A final geometry is called as longitudinal geometry [5], and is different than the usual transverse geometry (based on wire/tape cross-section). Very important aspect of the model geometry is density of mesh. It results from big difference between thickness of layers in 2G tape. Smoothly varying mesh density in a part of model is shown in Fig. 2.

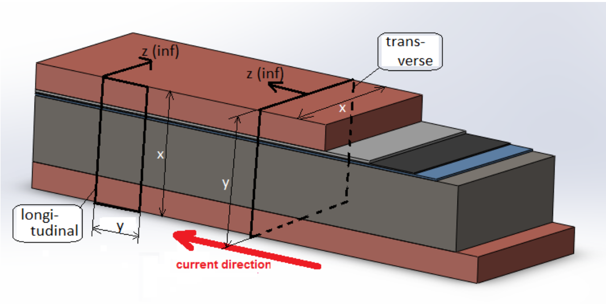

Fig.1. Definition of 2D longitudinal and transverse models

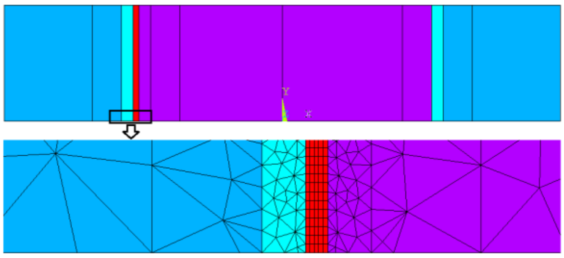

Fig.2. The geometry and mesh (part) in 2D longitudinal model

Material parameters and boundary conditions

The second important part of numerical model is a set of material parameters and boundary conditions. Properties of superconductors of respect of material parameters are very complicated. It results of surface of critical parameters – currents, temperature and magnetic fields and their mutual dependence. Additionally the transition from superconducting to normal (resistive) state is very rapid. In classical materials resistivity of conductor depends only on temperature. In superconductors this dependence is a function of three parameters. It is impossible to take directly into consideration using a commercial software. The dependence of critical parameters on the resistivity has been included into model using advanced programming based on APDL (ANSYS Parametric Design Language) and the procedure reported in literature as ARA (Adaptive Resistivity Algorithm) [6].

The boundary conditions were applied to the model in a classical way used for thermal – electrical modelling.

Influence of magnetic field

Resistivity of superconductors depends on surface of critical parameters. In 2D longitudinal model there is impossible to calculate distribution of magnetic field. In the model magnetic field was derived from 2D transverse model (magnetic field distribution is near the same in both superconductivity and resistive state). Because in 2D longitudinal model a tape width is infinitely long magnetic field was averaged to single value. It is shown in Fig. 3. The resistivity of superconductor was calculated using formula based on E-J power law [7]. Such material parameters of model are valid only for self-magnetic field influence.

a)

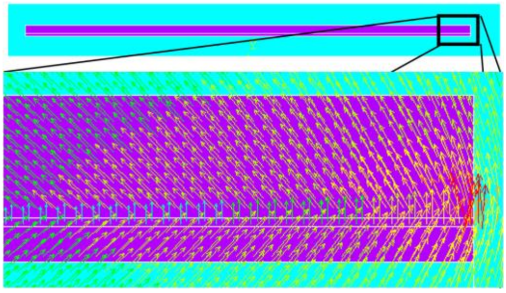

b)

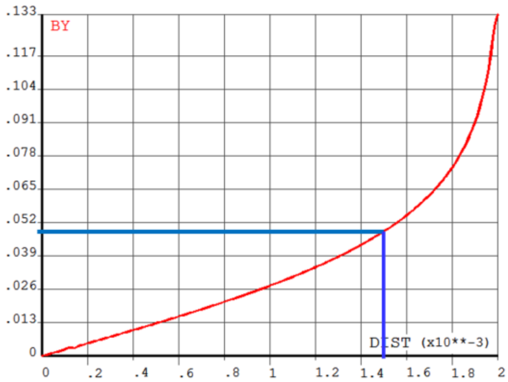

Fig.3. Magnetic flux distribution a) in and b) along tape width

Results of modelling under pulse load

Two types of results has been calculated. The first are waveforms of the voltage across the tape length and the temperature (at given location). The second are spatial distributions of current density, temperature and electrical potentials. In Fig. 4. waveforms of voltage and temperature calculated for one pulse of sinusoidal current (with amplitude of 110 A) is shown. One can observe oscillations resulting from ARA algorithm.

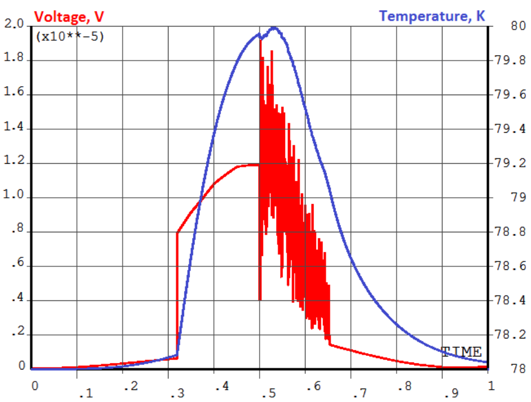

Fig.4. Voltage and temperature under sinusoidal 110 A pulse

Spatial distribution of current density at maximum value of load current (110 A) is shown in Fig. 5. One can observe hot spot of quench and current sharing in neighbour to superconductor layers (mainly in copper and silver).

Presented in this sections results are only an example of numerical modelling concerning 2G tapes. Such analysis can be carried out for variety of quantities (of circuit and field) important in respect of tape optimization

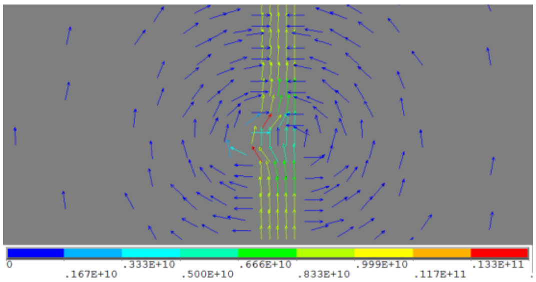

Fig.5. The current distribution during the quench at max. current

Conclusions

Described in the paper longitudinal 2D FEM model is an efficient tool for numerical characterization and optimization of 2G HTS tapes. It allows to take into account all parameters of critical surface. Advanced dependence of those parameters has been modelled by means of APDL.

Longitudinal 2D model is very important for modelling of quench propagation. It is more efficient than 3D one and more precise than 1D models.

Presented in the paper results shows that applications of ARA algorithm results with high amplitude oscillations. It can be reduced by applications of additional averaging procedure. It will be the goal of the future research.

REFERENCES

[1] Siahrang M. et al., A new numerical approach to find current distribution and AC losses in coaxial assembly of twisted HTS tapes in single layer, *J. Physics: Conf. Series*, 234, 2010, Art. No. 022034

[2] Morandi A., 2D electromagnetic modelling of superconduc-tors, , *Supercond. Sci. Technol.*, 25, 2012, 104003

[3] Stepien M. et al., Analysis of quench propagation using coupled electrical-thermal FEM model, *J. Physics: Conf. Series*, 234, 2010, Art. No. 022036

[4] Yamada R. et at., Preparation 2-D/3-D Quench Simu-lation Using ANSYS for Epoxy Impregnated Nb3Sn High Field Magnets, *IEEE Trans. Supercond.*, 13 (2003), 1696 - 1699

[5] Stepien M. et al., Analysis of transient state in HTS tapes under ripple DC load current, *J. Physics: Conf. Series*, 234, 2010, Art. No. 022036

[6] Farinon S. et al., Critical state and magnetization loss in multifilamentary superconducting wire solved through the commercial finite element code ANSYS, *Supercond. Sci. Technol.*, 23 2010 115004

[7] Wesche R. et al., HTS Conductors for Fusion. Thermal Stability and Quench, *HTS for Fusion Conductor Workshop*, 26-27.05.2011

***Authors**: dr inż. Mariusz Stępień, dr hab. inż. Bogusław Grzesik, prof. Pol. Śl., Politechnika Śląska, Katedra Energoelektroniki, Napędu Elektrycznego i Robotyki, ul. Krzywoustego 2, 44-100 Gliwice, E-mail: mariusz.stepien@polsl.pl.*

Acknowledgments

The work reported in the paper is supported by Polish National Center of Science on research project with contract No. UMO-2011/03/B/ST8/04908.

8th International Conference
Electromagnetic Devices and Processes in Environment Protection **ELMECO-8**
joint with 11th Seminar Applications of Superconductors **AoS-11**
September 28 - October 1, 2014, Nałęczów, Poland

THE INFLUENCE OF CONSTRUCTION OF BIFILAR WINDING ON EFFICIENCY OF ELECTROSTATIC PRECIPITATOR

Andrzej SUMOREK

Lublin University of Technology

***Abstract**. This paper presents a pilot scale version of the new construction of filter to remove pollution from the gas. The construction of the filter is based on the bifilar windings. The filter is designed for the removal dielectric dust particles from the air. A new chassis of bifilar winding is introduced recently. The most recent results of the filtering efficiency are presented in this paper.*

***Streszczenie.** W artykule zaprezentowano półprzemysłową wersję filtru nowej konstrukcji do usuwania zanieczyszczeń z gazu. Konstrukcja filtru oparta jest na uzwojeniach bifilarnych. Filtr zaprojektowano w celu usuwania cząstek zanieczyszczeń dielektrycznych z powietrza. W ostatnich testach wprowadzono nową ramę uzwojenia bifilarnego. W pracy zamieszczono najnowsze wyniki skuteczności odpylania zmodyfikowanego filtru.*

Keywords: electrostatic precipitator, electrofilter, bifilar filter.
Słowa kluczowe: odpylacz elektrostatyczny, elektrofiltr, filtr bifilarny.

Introduction

There are two methods of the removal dust from the gas – dry and wet. In the group of the dry dedusters we can find mechanical dedusters and electroseparators. There are discharge electrofilters and bifilar electrofilters in the group of electric precipitators. Discharge electrostatic precipitators have been widely applied for dust collection [5, 11].

The wires of windings are wounded alternately in bifilar separator. The neighbouring wires are connected to the opposite potential of a power source. The characteristic feature of the bifilar winding is the lack of inductance [7, 8].

The dust particles are dielectric particles typically. The most of organic dusts are classified as dielectric materials. The electric charges are distributed uniformly in this kind of particles. The powered wires of bifilar winding are source of electric field. Under the influence of the electric field the distribution of the electric charges changes in the particle. It is possible to notice an electric moment under the influence of the field. The result of electric field influence on dielectric charges in the dust particle is an electric force. Generated electric force acts on the particle (Fig. 1) [4].

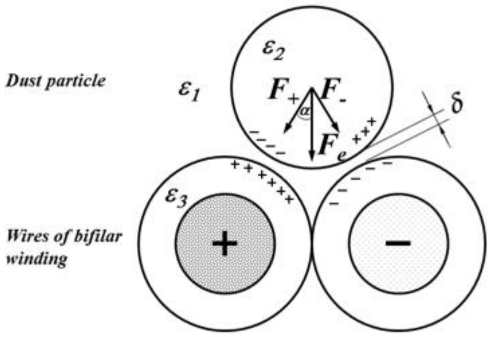

Fig. 1. Example of distribution of forces acting in a bifilar winding system [6]

It is possible to use DC and AC power source. In an alternating electric field the changes of the polarization of charges on the surfaces of dust and insulation follow the field changes. The direction of attracting force is constant. The precise calculation of the value of force is not easy [2, 10]. The attraction force depends on the intensity of the electric field and on free charge quantity that, in turn, depend on dust electric properties. The attraction force is influenced by the construction of the system of electrodes (diameter, distance between electrodes, dielectric permittivity and insulation conductivity) and dust particle parameters (dimensions, dielectric permittivity and conductivity) [4, 9].

Test stand

The main part of electrofilter is a filter chamber. The bifilar windings are situated inside a filter chamber. The area of bifilar winding covers the cross-sectional area of the filter chamber at 80 %. The dust particles are attracted to the windings from the air stream flowing over the windings (Fig. 2) [7]. There are three bifilar windings inside a filter chamber. The bifilar windings are connected together into a cassette. The mounting method of winding allows changing angle of windings in relation to the air flow.

A pilot scale version of filter chamber consists of standard ventilation profiles and it is made of steel. The complete length of filtration system is equal to about 1.0 m [6, 8]. The filtration cassette is placed inside a chamber (Fig. 2). The typical method of dusts removal consists in the use of impact mechanism through the striking the electrodes [3]. The „impact" cleaning method can be used in the bifilar electrofilters [1]. The frame of filtration cassette is so strong that it is possible to remove pollution using an "impact" method.

Fig. 2. Filter chamber equipped with cassette with bifilar windings

Two types of bifilar windings were utilized during filtration tests. First construction of winding was based on a bent copper pipe. The copper pipe was the backbone of the winding. The wires of winding were wound side by side (Fig. 3a). This construction is lightweight and even allows the flow of air between the wires of the winding. The disadvantage of the construction is moving relative to each other of the wires during exploitation of the filter (Fig. 3b). The resulting gap could lead to reduction of the dedusting efficiency.

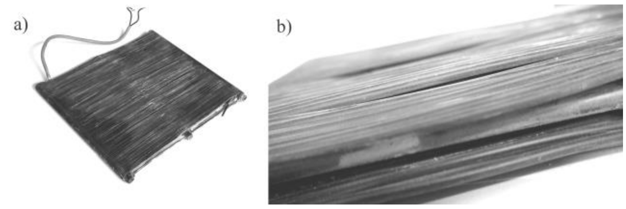

Fig. 3. Bifilar winding with a metal frame: a) general view, b) detail view

Because of windings deformation, a new construction of the winding is introduced. This construction of winding is based on an ebonite plate. The ebonite plate is the backbone. This heavy, ebonite construction is resistant to damage. Even after tests of dedusting of the gas and cleaning of the windings, bifilar windings wires are intact.

The windings of bifilar filter are made by using typical electric wire. The wire has a copper core and insulation made from PCV. The wires have cross-section surface area equal 0.5; 1.0; 1.5; 2.5 i 4 mm^2. This paper presents the results relating to the cross-section surface area equal 1 mm^2.

Results

The dust samples are real dust derived from "flour and pasta factory". The samples are picked from the following places in the factory line: a porridge line (sample A); a pasta line (sample B), a flour line (sample C). The fourth sample (sample D) is dust on the basis a wheat flour. The relative moisture content of dust material is 11.4 %÷19.3 % at relative humidity 31÷51 % [6, 8].

The temperature of air on the inlet of the chamber is 24.1÷27.1°C at air pressure 995-998 hPa. The air velocity is 0.18 $m \cdot s^{-1}$. The voltage of bifilar windings achieves value of 13 kV (maximal value for working without electric discharges in this configuration) [6, 8]. The following results are referred to the wire with cross sectional area of 1 mm^2 and gas velocity of 0.18 $m \cdot s^{-1}$.

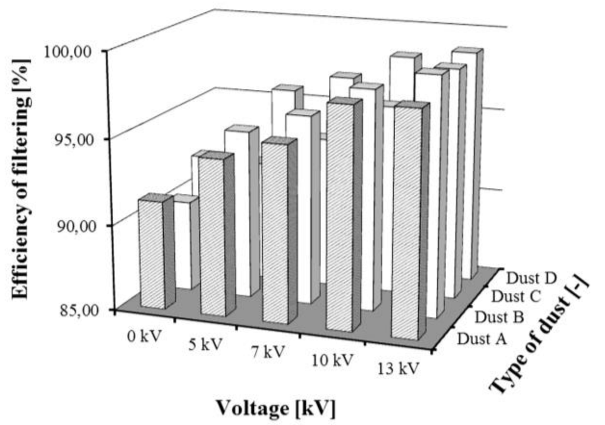

Fig. 4. Average dedusting efficiency for enhanced version of bifilar winding with chassis made of solid ebonite (wire cross-section 1.0 mm^2, gas velocity 0.18 $m \cdot s^{-1}$)

The filter chamber without voltage captures 90.0-91.8% of pollutants. The dust falls down on the bottom of the chamber under the influence of gravity forces. The application of voltage increases removal effectiveness to 95.8-96.9%.

New filer cassette is equipped with bifilar windings with a solid ebonite chassis. After changing the filter set, a similar set of tests were carried out. The filter chamber without voltage captures 90.2-92.3% of pollutants.

The application of voltage increases dust removal effectiveness to 97.9-98.9%. As before, the effectiveness increases together with the voltage increase. As before, the most effective removal has occurred for the particles of dust of type B (Fig. 4).

Conclusions

1. The filtration efficiency practically does not change when the filter chamber operates without electric power regardless of the type of the winding. The filtration efficiency increases slightly by 0.1-0.5%. It means that even in the winding with "empty" frame, air flows over the filter structure.

2. The filtration efficiency increases when enhanced version of bifilar winding with chassis made of solid ebonite is used. The filtration efficiency increases by 0.8-1.0 % at voltage of 5 kV. The filtration efficiency increases by 2.0-2.1 % at voltage of 13 kV.

3. Change the construction of bifilar winding introduces greater mechanical strength of filter cassette. There are no damages caused during bifilar winding cleaning. It has a positive influence on lifecycle of the device.

REFERENCES

[1] Boguta A., Oczyszczanie elektrofiltrów metodą udarową, *Electrotechnical Review*, 11 (2010), 163-165

[2] Cox J.B., Thamwattana N., Hill J.M., Electrostatic force between coated conducting spheres with applications to electrorheological nanofluids, *Journal of Electrostatics*, 65 (2007), 680-688

[3] Jonassen N., Electrostatics, Kluwer Academic Publishers, Massachusetts, USA (2002), ISBN 1-4020-7161-2

[4] Leonov V.S., Elektriceskije sily diejstvujuscije na siemena pri dielekticeskoj separaci, *M i E. S. Ch*., 5 (1980), 32-34

[5] Mizuno A., Electrostatic precipitation. *IEEE Transactions on Dielectrics and Electrical Insulation*, 7 (5) (2000), 615–624

[6] Pietrzyk W. (red.), Elektrofiltr bifilarny do usuwania pyłów pochodzenia roślinnego. Wydawnictwo Naukowe FRNA, Lublin (2008), ISBN-13: 978-83-60489-10-9

[7] Sumorek A., The comparison of potential use of electric filters with bifilar winding and discharge filters. *Electrotechnical Review*, 3b, vol. 89 (2013), 267-269.

[8] Sumorek A., The Influence of Granulation of Dust on Efficiency of Bifilar Winding, *Electrotechnical Review*, 7 (2010), 238-240

[9] Tarushkin W.I., Distribution of ponderomotive forces on grains during separation (in Russian*). M i E. S. Ch*., 12 (1983), 35-39

[10] Techaumnat B., Takuma T., Calculation of electric field in two-dimensional arrangements by the method of multipole images, *Journal of Electrostatics*, 64 (2006), 706-716

[11] Zhu J., Zhang X., Chen W., Shi Y., Yan K., Electrostatic precipitation of fine particles with a bipolar pre-charger. *Journal of Electrostatics*, 68 (2010), 174–178

Author: *Ph.D. Andrzej Sumorek, Lublin University of Technology, Faculty of Electrical Engineering and Computer Science, Department of Computer and Electrical Engineering, Nadbystrzycka 38A, 20-618 Lublin, e-mail: a.sumorek@pollub.pl.*

8th International Conference
Electromagnetic Devices and Processes in Environment Protection ELMECO-8
joint with 11th Seminar Applications of Superconductors AoS-11
September 28 - October 1, 2014, Nałęczów, Poland

PLASMA REACTOR FOR CONTINUOUS PROCESS OF CNTs SYNTHESIS

Lukasz SZYMANSKI, Zbigniew KOLACINSKI, Emilia GRYSKA

Lodz University of Technology

Abstract*. There is a lot of nanotubes production methods. The paper presents the research results of CNTs synthesis in a microwave plasma system in the atmospheric pressure.The magnetic properties of the synthesized CNTs are used for exploring possibilities of inducing hyperthermia and thermal ablation of cancer cells.*

Streszczenie. *Nanorurki węglowe są produkowane w wielu różnych procesach. W artykule zaprezentowano rezultaty syntezy nanorurek węglowych z użyciem reaktora mikrofalowego pracującego w ciśnieniu atmosferycznym. Właściwości magnetyczne wyprodukowanych nanorurek są wykorzystane do zbadania możliwości wywołania hipertermii i termicznej ablacji komórek rakowych.*

Keywords: carbon nanotubes, synthesis of carbon nanotubes, nanotubes in magnetic field.
Słowa kluczowe: nanorurki węglowe, synteza nanorurek węglowych, nanorurki węglowe w polu magnetycznym.

Introduction

Carbon-Nano-Tubes (CNTs) are required for many technological applications such as electron emitters, supercapacitors, rechargeable batteries, photovoltaic cells, etc [6]. One of the main challenges to obtain the optimal product properties is to work out a process of continuous synthesis and uniform dispersion of CNTs on a substrate.
The method widely used for this purpose is the CVD (Chemical Vapor Deposition).
It involves the pyrolysis of substances that contain carbon. In the next step the catalytic "formation of graphenes" in the structure of CNTs takes place. The carbon can be delivered with acetylene, benzene, ethylene, methane, propylene, CO and other gases containing carbon and also from evaporated solid material such as ferrocene. Catalysts are mainly iron, cobalt and nickel. Synthesis appears during a flow of carrier gas such as Ar or N_2 mixed with carbon containing gases at temperature range from 700 to 1100 K. In this method there are some difficulties with the activation of catalyst being in liquid or solid state. The use of the catalyst as a fluid injected to the furnace or as a solid/liquid evaporated from containers (boats) which mostly requires a horizontal furnace, do not guarantee the uniformity of the process.

Carbon nanotubes have gained interest of scientists as their properties offer multiple potential applications in various fields, including medicine and bioengineering. Catalytic synthesis using metal compounds as catalysts yields a production of metal-doped particles. Their ferromagnetic behavior as opposed to pure CNTs has been proved [7]. The magnetic functionalization stands a promising opportunity for inducing hyperthermia or thermal ablation in biological cells. Ferromagnetic particles can be efficiently heated when placed in an altering magnetic field. The particles exhibit a hysteretic behavior when placed in the field and the hysteresis losses due to changing particles' magnetization cause heating [8]. The magnetic field can be obtained in a radio frequency (RF) generator. RF is a non-ionizing radiation and the magnetic field presents good penetration in human tissue. Additionally no harmful effects on human body have been proved so far which justifies common use of the radiation in medicine.

Experimental Setup for CNTs synthesis

Synthesis of carbon nanotubes is followed in a steel chamber on a metal substrate, which is ideal for this purpose. Fig. 1 shows schematic diagram of the continuous microwave plasma system for CNTs synthesis (1 – reactor space, 2 - substrate – metal steel, 3 – microwave plasma head, 4 - microwave plasma torch, 5 – CNTs, 6 - cassettes to move metal substrate).

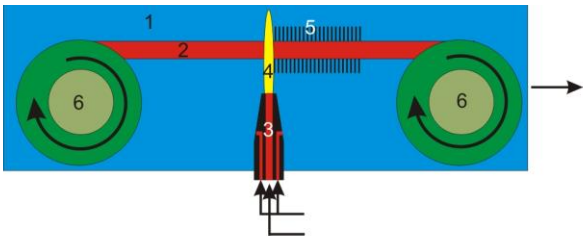

Fig.1. Schematic diagram of the continuous microwave plasma system for CNTs synthesis

In the system argon and nitrogen are used as the plasma gases whereas the hydrogen, ethylene provide carbon for CNTs formation. Carbon carrying gas is supplied through a microwave nozzle plasma where it is decomposing. Plasma heats the substrate with catalyst applied on the surface. The - ferrocene working as catalyst has been at first dissolved in xylene and before the plasma treatment the substrate surface has been covered with catalyst solution by a deep coating method. The temperature of substrate was controlled by IR thermometer. Fig.2. shows the photo of the reactor.

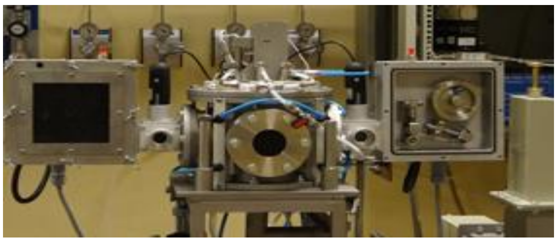

Fig.2. Photo of plasma system

Thermal decomposition of gaseous reagents

The synthesis process is composed of several stages such as venting, substrate annealing, and reduction with hydrogen. Every step has own parameters (gas flow, time and temperature). At the beginning of the work some computer simulations were made. In these simulations we used hydrogen, ethylene, acetylene, methane and other gaseous reagents. Fig. 3. shows the thermal decomposition of mixture: 1l of ethylene with 3l of hydrogen. This proportion has been used in our research. The temperature 800K it's the minimum temperature to obtain the carbon in solid stage that is suitable for synthesis of carbon nanotubes.

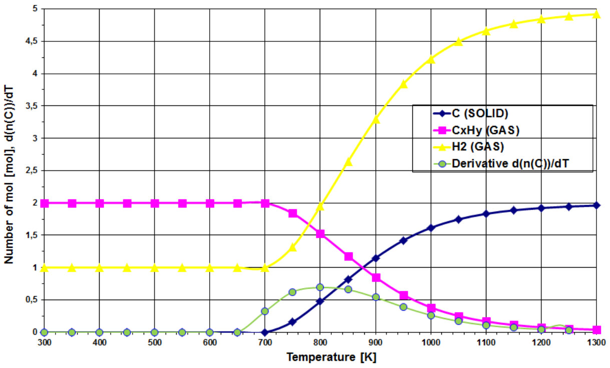

Fig.3. Thermal decomposition of mixture: 1l of ethylene with 3l of hydrogen

CNTs for hyperthermia and thermal ablation

CNTs produced in the continuous synthesis method (Fig. 4) were used to investigate the influence of magnetic field on the temperature rise of CNTs suspension consisting of CNTs, sodium dodecyl sulfate (SDS) as a dispersing agent and water.

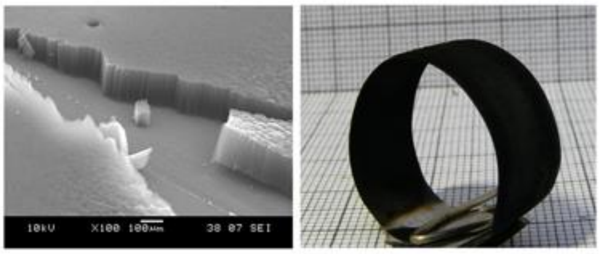

Fig.4. CNTs forest SEM photo (left) and CNTs carpet covering both sides on stainless steel # 0.01 mm

Prior to temperature measurement the suspension underwent sonic dispersion for total 4 hours 45 minutes with 250 Hz frequency, 750 W power and 40% amplitude to destroy nanotubes agglomerates. In our experiment the radio frequency generator of a frequency range 10-13MHz was used to investigate the temperature changes of CNTs suspended in the aqueous solution. These frequency ranges have been previously used for similar purposes and proved to be effective [9,10]. The experimental setup used for temperature measurement is presented in Fig 5. The 5 ml syringe was placed inside the generated field and the temperature was measured with a fibre optic thermometer probe Luxtron 812.

Fig 5. Experimental setup for temperature measurement

Results

The CNTs diameter obtained in experimental setup was in the range from 20 to 200 nm, CNTs length was up to 100μm on steel. In the reactor most synthesis was the MWNTs – up to 99% and some double and single-wall nanotubes. Efficiency of the conversion was up to 60%.
The temperature rise measurements in magnetic field showed satisfactory results which will be presented separately.

Acknowledgement

The research work is related to R&D Grants Nr N R01 0016 10 and Nr PBS2/A5/31/2013

REFERENCES

[1] Raniszewski G., Eur. Phys. J. Appl. Phys. , Vol. 61, Issue 02, (2013), pp. 24311-p1 - 24311-p6.

[2] Keidar M., Levchenko I., T. Arbel, M. Alexander, A. M. Waas, K. Ostrikov, Applied Physics Letters 92, 043129 (2008).

[3] Thess A., Lee R., Nikolaev P., Dai H., Petit P., Robert J., Xu C., Lee Y.H., Kim S.G., Rinzler A.G., Colbert D.T., Scuseria G.E., Tomanek D., Fischer J.E., Smalley R.E., Science, 273 (1996) 483.

[4] Laplaze D., Bernier P., Barbedette L., Lambert J.M.; Flamant, G.; Lebrun M.; Brunelle A.; Della-Negra S., Acad. Sci., Ser. II: Mec., Phys., Chim., Astron. 1994, 318 (6), 733–738.

[5] Hsu W.K., Hare J.P., Terrones M., Kroto H.W., Walton D.R.M., Harris P.J.F., Condensed-phase nanotubes. Nature (London) 1995, 377 (6551), 687.

[6] Jayalakshmi M., Balasubramanian K.: Simple Capacitors to Supercapacitors - An Overview, Int. J. Electrochem. Sci., 3, 1196 – 1217, (2008),

[7] K. Lipert and e. al, "Magnetic properties of carbon nanotubes with and without catalyst," Journal of Physics: Conference Series, vol. 200, 2010.

[8] A. A. M. M. E. Gendy, "Carbon-coated Nanomagnets: Synthesis, Characterization And Feasibility For Magnetic Hyperthermia," Naturwissenschaftlich - Mathematischen Gesamtfakultät der Ruprecht - Karls - Universität, Heidelberg, 2011.

[9] N. Levi-Polyachenko and J. Stewart IV, "Clinical Relevance of Nanoparticle Induced Hyperthermia for Drug," The Open Nanomedicine Journal, no. 3, pp. 24-37, 2011.

[10] M. Raoof and S. A. Curley, "Non-Invasive Radiofrequency-Induced Targeted Hyperthermia for the Treatment of Hepatocellular Carcinoma," International Journal of Hepatology, vol. 2011, 2011.

Authors: *dr inż. Łukasz Szymański, Prof. dr hab. inż. Zbigniew Kolacinski, Emilia Gryska: Instytut Mechatroniki i Systemów Informatycznych, Politechnika Łódzka, ul. Stefanowskiego 18/22, 90-924 Łódź, E-mail: lukasz.szymanski@p.lodz.pl*

8th International Conference
Electromagnetic Devices and Processes in Environment Protection **ELMECO-8**
joint with 11th Seminar Applications of Superconductors **AoS-11**
September 28 - October 1, 2014, Nałęczów, Poland

WATER CONTACT ANGLES ON HIGH IMPACT POLYSTYRENE EXPOSED TO RADIO FREQUENCY ATMOSPHERIC PRESSURE PLASMA JET

Piotr TEREBUN, Piotr KRUPSKI, Michał KWIATKOWSKI, Jarosław DIATCZYK,

Joanna PAWŁAT, Henryka D. STRYCZEWSKA

Lublin University of Technology, Institute of Electrical Engineering and Electrotechnologies

Abstract. *For some applications of polystyrene, important role is played by wettability of the material. In the present study, the radio frequency atmospheric pressure plasma jet source has been applied for the surface modification of the high impact polystyrene film. The measurements show that water contact angle change is dependent on the composition of working gas, the flow rate value and the distance from the plasma zone.*

Streszczenie. *Dla niektórych zastosowań polistyrenów istotną rolę odgrywa zwilżalność materiału. W niniejszej pracy do obróbki powierzchni polistyrenu wysokoudarowego (HIPS) użyto reaktora plazmowego typu plasma jet, pracującego z częstotliwością radiową przy ciśnieniu atmosferycznym. Otrzymane wyniki wskazują, że istotną rolę w zmianie kąta zwilżania materiału ma skład gazu roboczego, wartość jego przepływu oraz odległość od strefy plazmy.*

Keywords: atmospheric pressure plasma jet, high impact polystyrene, contact angles.
Słowa kluczowe: dysza plazmowa pracująca pod ciśnieniem atmosferycznym, polistyren wysokoudarowy, kąty zwilżania

Introduction

High impact polystyrene (HIPS) is a thermoplastic and antistatic polymer that is easy to machine and fabricate. It is characterised by good impact resistance, machinability, dimensional stability and low cost. HIPS boards are mainly used in advertising, industry sector and food processing applications [1-2]. For some applications, important role is played by contact angle which determine the hydrophobicity or hydrophilicity of the material. One of the method for modification material properties such as contact angle, is using non-thermal plasma [3-11]. In relation to the chemical, the use of plasma may allow not only to reduce costs but may also be more environmentally friendly [11]. Additional reduction in manufacturing cost can be achieved by the use of plasma reactors that do not require the use of vacuum, such as the atmospheric pressure plasma jet (APPJ). Due to the selectivity of energy, a non-equilibrium plasma jet reactors also allow to perform efficient physicochemical reaction at relatively low gas temperature which does not cause changes in deeper part of material [3-6]. The article presents results of research on water contact angles on HIPS exposed to non-equilibrium APPJ operating at radio frequency (14.355 MHz). The measurements were performed for the main factors that may affect the amount of generated active particles that reach the surface of the sample: composition of working gas, the flow rate value and the distance from the end of discharge.

Experimental method

In this study, a commercially available high impact polystyrene was used. Test samples had a size of 30 mm × 40 mm with a thickness of 2 mm. All measurements were made for gas temperature below the softening temperature of material, which was 90 °C [12].

The measurements were performed using radio frequency plasma jet with high voltage electrode inside the nozzle. The operating voltage, frequency and power are 500 V, 14.355 MHz and 40 W, respectively. Measurements were made for three mixtures of gases: helium with oxygen, argon with oxygen and helium with air. During the measurements, the reactor was directed perpendicularly to the surface of the sample.

Immediately after plasma treatment, 10 µl water drop was injected onto a treated surface for calculating the average contact angle from pictures made by CMOS camera.

Results

The results obtained for the different working gases are shown in figure 1.

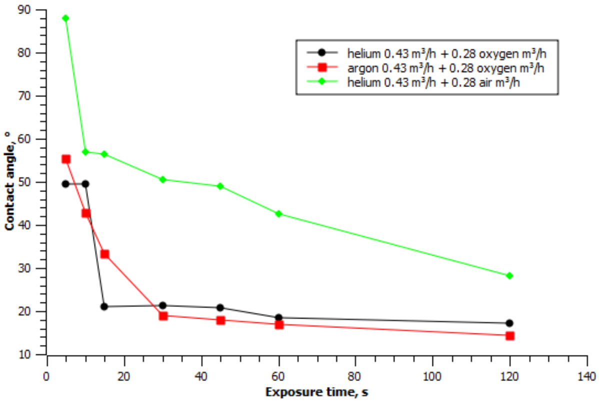

Fig. 1. The dependence between contact angle and treatment time for different gas mixtures

The smallest change was observed for a mixture of helium with air, but after two minutes of treatment angle decreased more than three times compared to control sample (90°). Better results obtained for mixtures containing oxygen can be explained by greater amount of oxygen radicals (like ozone) which can influence the behaviour of the sample surface. In these cases, 30 s plasma treatment enabled to reduce the contact angle of less than 22°.

Figure 2 shows results for two flow rates of mixtures of helium and oxygen for the same proportion of gases.

Increasing the flow rate by 50% resulted in less impact on the change of contact angle, which may be explained by a stronger gas spread over the surface of the sample and less concentration of active particles. Simultaneously it excludes the assumption of strong influence caused by the drying gas flow compared to the plasma treatment.

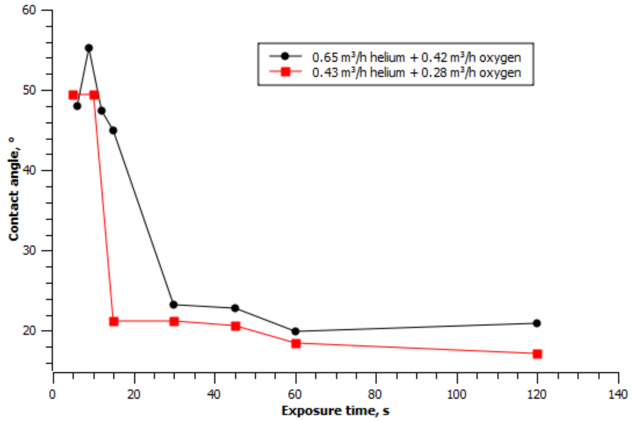

Fig. 2. The dependence between contact angle and treatment time for different flow rate

The results obtained at various distances from the end of reactor (figure 3) show significant influence of distance for treatment times less than one minute. For two minutes the angle was the same for all distances, which could allow to treat objects with more complex surfaces more freely.

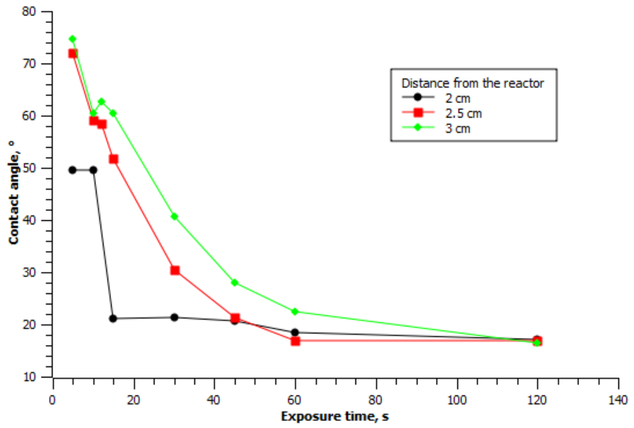

Fig. 3. The dependence between contact angle and treatment time for different distances from the end of reactor

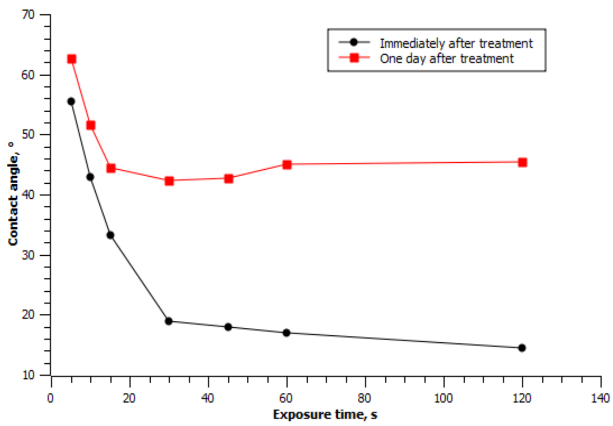

Fig. 4. The dependence between contact angle and treatment time immediately after the measurement and after one day (0.43 m^3/h argon + 0.28 m^3/h oxygen)

Figure 4 shows the comparison of the results obtained for a mixture of helium and argon immediately after the measurement, and after one day from the time of treatment. After one day, the contact angle started to return to its previous value, which is particularly evident at longer exposure times. This may indicate that the effect of plasma treatment in the material is not too deep, and the process is reversible.

Summary

The obtained results allow to conclude an effective change in contact angle through the use of the radio frequency APPJ source. Significant changes in the angle could be seen for treatment time of 15 seconds, which may be important in reducing the cost of modifying low cost materials such as HIPS. For the study, in the surface modification the most important role is played by the composition of working gas, which decides on the number of reactive species involved in changing the hydrophobicity of the material.

REFERENCES

[1] http://www.plastics.pl/produkty/reklama/plyty-hips

[2] https://www.plasticsintl.com/datasheets/Polystyrene.pdf

[3] Pawłat J., Atmospheric pressure plasma jet for sterilization of heat sensitive surfaces, *Przegląd Elektrotechniczny*, 10b, 139-140, 2012

[4] Stryczewska H., Technologie plazmowe w energetyce i inżynierii środowiska, *Wydawnictwo Politechniki Lubelskiej*, Lublin 2009

[5] Pawłat J.: Atmospheric pressure plasma jet for decontamination purposes, *European Physical Journal - Applied Physics* 61, 24323, 2013

[6] Pawłat J., Samoń R., Stryczewska H., Diatczyk J., Giżewski T., RF-powered atmospheric pressure plasma jet for surface treatment, *European Physical Journal - Applied Physics*, 61(2), (2013), 201324322

[7] Kolacinski Z., Szymanski L., Raniszewski G., LTE plasma reactors for materials conversion, *European Physical Journal - Applied Physics* 61(02): 24314 (2013)

[8] Gotoh K., Yasukawa A., Taniguchi K., Water contact angles on poly(ethylene terephthalate) film exposed to atmospheric pressure plasma, *Journal of Adhesion Science and Technology*, 1 January 2011, 25(1-3):307-322

[9] Jacobs T., Morent R., De Geyter N., Desmet T., Vlierberghe S., Dubruel P., Leys C., The Effect of Medium Pressure Plasma Treatment on Thin Poly-e-Caprolactone Layers, *Journal of Adhesion Science & Technology*. Sep/Oct2012, Vol. 26 Issue 18/19, p2239-2249

[10] Singh, N.L.; Pelagade, S.M.; Rane, R.S.; Mukherjee, S.; Deshpande, U.P.; Ganeshan, V.; Shripathi, T., Influence of argon plasma treatment on polyethersulphone surface, *Pramana - Journal of Physics*, January 2013, 80(1):133-141

[11] Anzawa, E.; Kral, M.; Ogino, A.; Nagatsu, M., Improvement of hydrophilicity of polymer surface by surface-wave excited Ar plasma with acetic acid, *Electrical Engineering in Japan*, September 2011, 176(4):1-6

[12] http://www.plastics.pl/content/zdjecia/file/katalog_tworzywa_techniczne_32_34.pdf

***Authors**:*
Mgr inż. Piotr Terebun[1]: piotr.terebun@gmail.com
Mgr inż. Piotr Krupski: piotr-jl@o2.pl
Mgr inż. Michał Kwiatkowski[1]: m.kwiatkowski@pollub.pl
Dr inż. Jarosław Diatczyk: j.diatczyk@pollub.pl
Dr hab. inż. Joanna Pawłat: askmik@hotmail.com
Prof. dr hab. inż. Henryka Danuta Stryczewska: h.stryczewska@pollub.pl
Wydział Elektrotechniki i Informatyki, Politechnika Lubelska, ul. Nadbystrzycka 38d, 20-618 Lublin, Polska

[1]Participant of the project: "Qualifications for the labour market - employer friendly university", co-financed by European Union from European Social Fund.

8th International Conference
Electromagnetic Devices and Processes in Environment Protection ELMECO-8
joint with 11th Seminar Applications of Superconductors AoS-11
September 28 - October 1, 2014, Nałęczów, Poland

GAS COMPOSITION INFLUENCE ON THE HALOCARBONS DECOMPOSITION IN THE NON-EQUILIBRIUM PLASMA

Bogdan ULEJCZYK

Warsaw University of Technology

Abstract. *The argon concentration influence on the process of trichlorethylene and chloroform decomposition is show in this paper. The chemical structure of halocarbons influences the process of theirs decomposition is also show. The study was performed in the barrier discharge powered by pulsed current. It was found that argon concentration in the gas, which was introduced into the reactor strongly influenced the halocarbons conversion. The halocarbons conversion increased with the increase of the argon concentration.*

Streszczenie. *W niniejszym artykule przedstawiono wpływ stężenia argonu na proces rozkładu trichloroetylenu i chloroformu. Przedstawiono także wpływ budowy halogenoweglowodorów na przebieg procesu ich rozkładu. Proces prowadzono w wyładowaniu barierowym zasilanym prądem impulsowym. Stwierdzono, że wzrost stężenia argonu w gazach wprowadzanych do reaktora powoduje wzrost stopnia przemiany halogenowęglowodorów.*

Keywords: plasma, trichloroethylene, chloroform, decomposition.
Słowa kluczowe: plazma, trichloroetylen, chloroform, rozkład.

Introduction

Plasma technology is one of the rapidly developing world science disciplines. New reactors and power supply systems are designed and tested extensively. New constructions are designed to improve efficiency of plasma processes [1-5].

The paper concerns the study of the decomposition of trichloroethylene (C_2HCl_3) and chloroform ($CHCl_3$) in the pulsed dielectric barrier discharge. These compounds are contained in set of the halocarbons. Halocarbons exhibit toxic properties and causes the greenhouse effect, but effective method of halocarbons utilization has not yet been developed.

Experimental set-up

Process of halocarbons decomposition was performed in the followed conditions:

- air and air-argon gas mixtures were used as carrier gases,
- argon concentrations in air-argon gas mixture were 25, 50 and 75%,
- the halocarbons concentration was 0.4% vol.,
- total gas flow rate was 10 Nl/h.

Process of halocarbons decomposition was performed in the reactor, which is shown in Fig. 1. The reactor consisted of a quartz tube, high-voltage and grounded electrodes. The high-voltage electrode was made of a stainless steel porous tube with an outer diameter of 10 mm and an open porosity of 19%. Gas was introduced by the porous electrode into the active zone of discharge (discharge gap). The grounded electrode was made by applying silver paste on the external part of the quartz tube. A wall thickness of the quartz tube was 1.3 mm. A discharge gap width was 3.3 mm.

The pulsed power supply system generated short (~1 μs) discharge pulses of high voltage (18 kV). Frequency of pulse repetition ranged from 130 to 850 Hz.

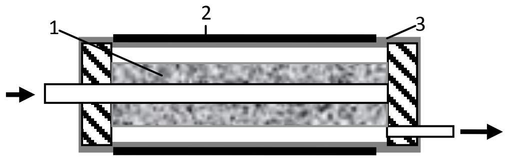

Fig. 1. Schema of the reactor. 1 – high-voltage electrode, 2 – grounded electrode, 3 – dielectric barrier.

Results

Argon concentration influenced the electric characteristics of the discharge. The energy of a single pulse increased with the increase of the Ar concentration in gas (Fig. 2). Consequently, the discharge power increased at the same frequency. The effects of discharge power and argon concentration on the overall conversion of C_2HCl_3 and $CHCl_3$ are show in Figs. 3 and 4 respectively. The overall conversion of C_2HCl_3 and $CHCl_3$ increased with the increase of the discharge power and the argon concentration.

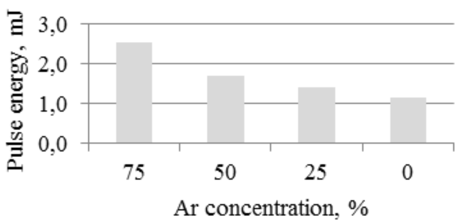

Fig. 2. Argon concentration influence on the energy of single pulse.

The effect halocarbons chemical structure on the overall halocarbons conversion is present in Figs. 3 and 4. The overall conversion of $CHCl_3$ was lower than overall conversion of C_2HCl_3. The difference between overall conversion of C_2HCl_3 and $CHCl_3$ decreased with the increase of the argon concentration. The overall conversion of C_2HCl_3 was ~3 times higher than the overall conversion of $CHCl_3$ for the process of halocarbons decomposition performed in air. For the process of halocarbons decomposition carried out in gas mixture of high Ar concentration (75%), the overall conversion of C_2HCl_3 was only ~10% higher than the overall conversion of $CHCl_3$.

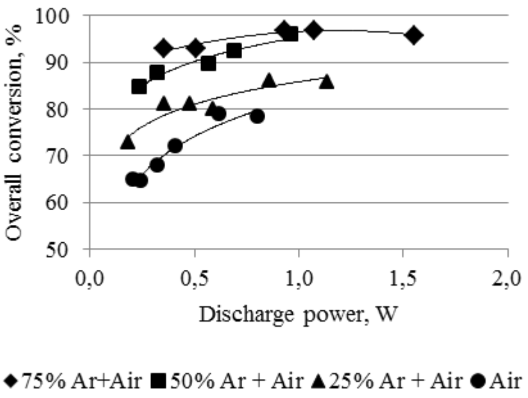

Fig. 3. The influence of discharge power and Ar concentration in gas mixture on C_2HCl_3 overall conversion.

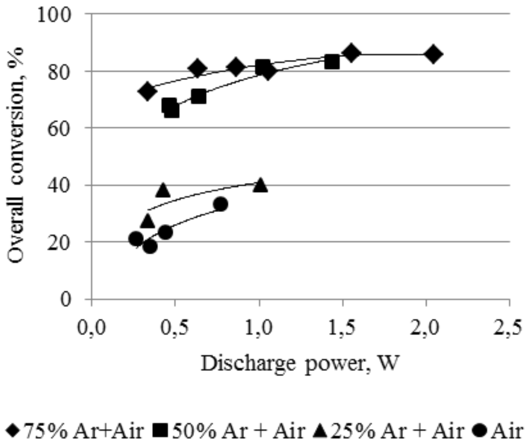

Fig. 4. The influence discharge power and Ar concentration in gas mixture on $CHCl_3$ overall conversion.

Discussion

The results (Figs. 3 and 4) indicate that Ar presence in gas mixture influences the mechanism of the halocarbons decomposition.

The process of the halocarbons decomposition in the dry air should be initiated by impact with the oxygen ($O^{\cdot}$) and nitrogen ($N^{\cdot}$) radicals or high-energy electrons (e). Due to the presence of unpaired electrons in radicals and negative charge of the electron, these molecules should be directed to the H atom in $CHCl_3$ and C_2HCl_3. On this atom there is located a partial positive charge (Figs. 5 and 6). The C-H bond dissociated as a result of the impact with $O^{\cdot}$, $N^{\cdot}$ or e. The main differences between C_2HCl_3 and $CHCl_3$ are the presence of a double bond C=C and positive partial charge on the C atom in C_2HCl_3. An independent rotation of CCl_2 and CHCl is disabled by a double bond C=C, therefore their relative spatial orientation is established. In C_2HCl_3, distances between H and Cl atoms are larger than in $CHCl_3$. As a result, the electron and radicals have easy access to the double bonds. The double bond consists of σ and π bonds. The π bond is a weak bond (2.5 eV) and it is very easy to dissociate. The σ bond is stronger (3.8 eV). Therefore, π bond dissociation does not cause decomposition of the C_2HCl_3 but unpaired electrons may migrate towards the Cl. As a result, a molecule may be decomposed in the detachment of chlorine anion (Cl^-) or free radicals ($Cl^{\cdot}$).

The process of halocarbons decomposition of Ar presence in the gas mixture may be initiated by the reaction of Ar^+. Ar^+ should be directed to Cl atoms, because on these atoms there is located the partial negative charge (Figs. 5 and 6). The C-Cl bond dissociated as a result of impact with Ar^+. The rate of reaction with Ar^+ should increase with the increase concentration of argon.

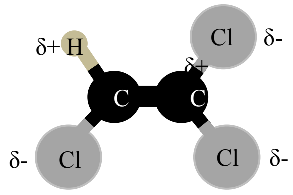

Fig. 5. Location of partial charges in C_2HCl_3.

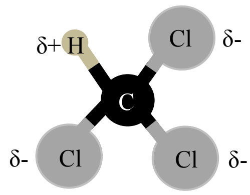

Fig. 6. Location of partial charges in $CHCl_3$.

Conclusions

The experiments show that the reactor can effectively decompose halocarbons in gas mixture with high argon concentration. For Ar concentration of 75% conversions of $CHCl_3$ and C_2HCl_3 reached 86 and 97% respectively. Decomposition of halocarbons in air was less effective. In air, overall conversions of $CHCl_3$ and C_2HCl_3 reached 33 and 79% respectively.

Discharge power influenced the overall halocarbons conversion. The overall halocarbons conversion increased with the increase of discharge power for each carrier gas.

This work was supported by The National Center for Research and Development (agreement No. PBS2/A1/10/2013).

REFERENCES

[1] Won Y.S., Thermal decomposition of trichloroethylene under a reducing atmosphere of hydrogen, *Korean Journal of Chemical Engineering,* 26: 36-41 (2009)

[2] Han S.B., Oda T., Improvement of the energy efficiency in the decomposition of dilute trichloroethylene by the barrier discharge, *IEEE Transactions on Industry Applications,* 41: 1343-1349 (2005)

[3] Magureanu M., Mandache N.B., Hu J., Richards R., Florea M., Parvulescu V.I., Plasma-assisted catalysis total oxidation of trichloroethylene over gold nano-particles embedded in SBA-15 catalysts, *Applied Catalysis B: Environmental*, 76: 275-281, (2007)

[4] Ulejczyk B., Decomposition of Halocarbons in the Pulsed Dielectric Barrier Discharge, In *14th International Conference on Optimization of Electrical and Electronic Equipment Proceedings*, 1053-1059. (2013)

[5] Ulejczyk B., Krawczyk K., Młotek M., Schmidt-Szałowski K., Nogal Ł., Kuca B., Decomposition of carbon tetrachloride in the reactor of dielectric barrier discharge with different power supplies, *European Physical Journal- Applied Physics*, 61: 24324p1-24324p7 (2013)

***Author**: dr. inż. Bogdan Ulejczyk, Politechnika Warszawska, Wydział Chemiczny, ul. Noakowskiego 3, 00-664 Warszawa, e-mail: bulejczyk@ch.pw.edu.pl.*

8th International Conference
Electromagnetic Devices and Processes in Environment Protection ELMECO-8
joint with 11th Seminar Applications of Superconductors AoS-11
September 28 - October 1, 2014, Nałęczów, Poland

HTS 2G SUPERCONDUCTING TRANSFORMER AS A FAULT CURRENT LIMITER - EXPERIMENTAL INVESTIGATION

Grzegorz WOJTASIEWICZ, Tadeusz JANOWSKI, Sławomir KOZAK, Janusz KOZAK,

Michał MAJKA, Beata KONDRATOWICZ-KUCEWICZ

Electrotechnical Institute in Warsaw

Abstract*. The new 2G superconducting tapes with high resistivity in the normal state allow to build transformers with high short-circuit strength. The short-circuit current limiting feature of the superconducting transformer, which is the most important benefit of replacing the conventional windings by the superconducting ones, provides protection and significantly reduces the wear and tear of circuit breakers and other substation power equipment. This paper describes the design and test results of a model of a 1-phase, 9 kVA superconducting transformer with windings made of 2G HTS tape. A special regard is given to the ability of the transformer's superconducting winding to limit of the short-circuit current.*

Streszczenie. *Dostępne obecnie taśmy nadprzewodnikowe 2G, o dużej rezystancji w stanie rezystywnym, stwarzają możliwość budowy transformatorów energetycznych odpornych na zwarcia. Możliwość ograniczania prądu zwarcia przez uzwojenia nadprzewodnikowe transformatora jest główną korzyścią płynącą z zastąpienia uzwojeń konwencjonalnych Cu uzwojeniami nadprzewodnikowymi.*

W artykule przedstawiono wyniki badań eksperymentalnych modelu 1-fazowego transformatora nadprzewodnikowego o mocy znamionowej 9 kVA, z uzwojeniami wykonanymi z taśmy HTS 2G, ze szczególnym uwzględnieniem zjawiska ograniczania prądu przez uzwojenia transformatora.

Keywords: 2G HTS tapes, HTS transformer, fault current limitation.
Słowa kluczowe: taśmy nadprzewodnikowe drugiej generacji, transformatory nadprzewodnikowe, ograniczanie prądu zwarcia.

Introduction

The resistance of superconducting transformers to short-circuit, which is the result of the fault current self-limitation effect of superconducting windings, is the most important benefit of replacing the conventional windings with the superconducting ones [1], [2]. The level to which the fault current is limited by the superconducting transformer depends on the operation characteristics of the transformer, construction of the windings and on the parameters of the HTS tapes used (i.e. their resistance at 77 K) [3], [4]. After transition of the superconducting transformer to the resistive state, the increase of the total winding resistance, which depends on the resistivity of the superconducting tape, causes, compared to its impedance in the superconducting state, a few to several hundred fold increase in the impedance of the transformer. A properly designed and built superconducting transformer reduces fault currents in a power network. A low short-circuit voltage causes the voltage fluctuation at changes of power network load to be smaller. Thus, generators can have a lighter excitation and as a result they will be cheaper. Also, the use of superconducting transformer allows us to reduce both the cost of fault protection system and the frequency of power network failures [1], [5].

This article presents the results of an experimental investigation of a 1-phase model of a 9 kVA superconducting transformer designed [5], built and tested in the Laboratory of Superconducting Technology. A special regard is given to the ability of the transformer's superconducting winding to limit of the short-circuit current.

Design of the HTS transformer

The single-phase model of a HTS transformer on which the tests were performed is presented in Fig. 1 [5]. This transformer consists of three windings: two HV windings and one LV winding (Fig 1 b.). One of the HV windings is wound directly on the LV winding while the other one is wound on a separate bobbin. Such construction

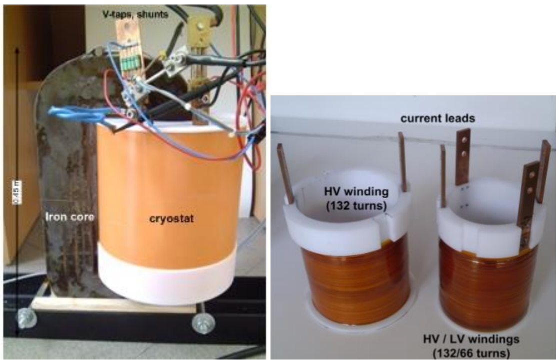

Fig. 1. Model of a single-phase 9 kVA HTS transformer and configuration of their windings

Table 1. Specification of the model of HTS transformer

Electrical parameters		
Frequency, Hz	50	
Voltage: primary (HV) / secondary (LV), V	220/110	
Rated current of primary / secondary winding, A	40 / 80	
turn ratio	2	
Magnetic core dimensions		
Iron core limb cross section, m^2	0.0049	
Iron core yoke cross section, m^2	0.0049	
Height/length of iron core window, m	0.23/0.07	
Windings dimensions		
	δ=0.01m	δ=0.001 m
a_1, m	0.001	0.001
a_2, m	0.001	0.001
b_1, m	0.0765	0.0685
b_2, m	0.0655	0.0655
r_1, m	0.0775	0.0695
r_2, m	0.0665	0.0665
L_w, m	0.132	0.132
D_{av}, m	0.900	0.840
layers $m_{prim} = m_{sec}$	4/2	4/2
length of HTS tapes, HV / LV, m	64/27	57/27

gives the possibility to configure the windings of the transformer to work with two values of air gap width: δ=0.01 m and δ=0.001 m. In this way, we can determine the impact of the air gap on the performance of the HTS transformer and its short-circuit current limiting features, as the values of short-circuit reactance X_f depend on the value of δ. All the windings are placed in a non-metallic cryostat with liquid nitrogen, while the iron core is situated at a room temperature. Table 1 presents the specifications of the HTS transformer with two air gap width values..

All the superconducting windings are made of SuperPower SCS4050 tape with critical current I_c=115 A. The rated currents of transformers windings are lower that I_{crms} = 82A.

Experimental investigation

The experimental studies included the determination of short-circuit tests in order to verify the ability of the superconducting winding to limit the short-circuit current [5], [6].

The primary winding is supplied with a voltage regulator coupled with the power source via a separating transformer. Loaded secondary winding is shorted by a short-circuit system. All the measurements are realized with a PC DAQ Card and the LabView Software. The short-circuit test results are represented by the waveforms in Fig. 2 and Fig. 3 for the windings with δ=0.01 m.

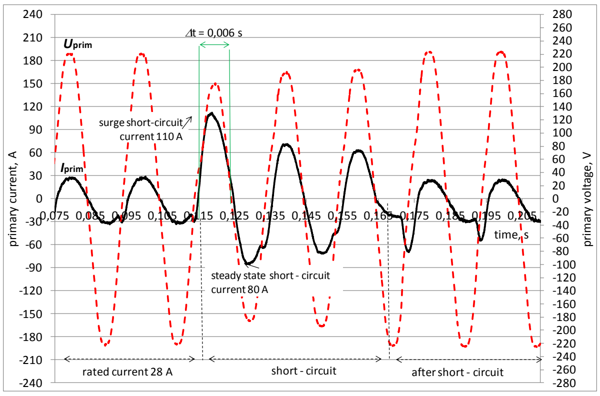

Fig. 2. Waveforms of primary voltage and current – δ = 0.01 m

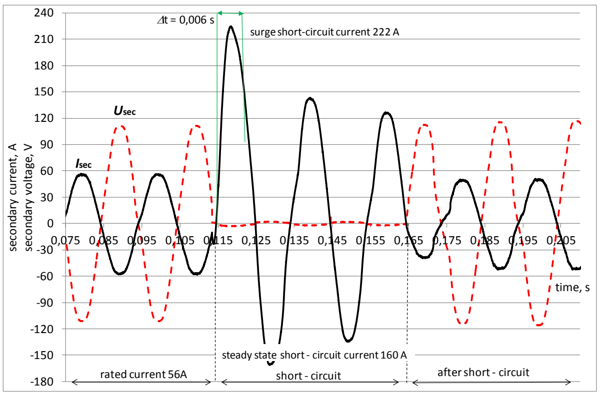

Fig. 3. Waveforms of secondary voltage and current- δ = 0.01 m

The short-circuit duration was 0.05 s. The time Δ*t*, after that the surge current was limited to the value of steady-state short-circuit current, was about 0,006 s for both value of δ. That means that when the short-circuit current crosses the value of the critical current, short -circuit impedance Z_f increases from values in the superconducting state (I) to the values in the resistive state (II), respectively from 0.28 Ω (I) to 1.91 Ω (II) for a transformer with an air gap.

Since the HTS transformer limits the fault current as a result of an increase of the HTS windings resistance, the short–circuit reactance of the transformer can be small. However, it is impossible to completely eliminate the short circuit reactance because there will always be an air-gap between the windings, so there will be a leakage inductance. Still, the contribution of short-circuit reactance to the limitation of the fault current, especially of its first peak, is significant because the steepness of the fault current ramp in the first quarter of its period is much greater than that resulting from the sinusoidal wave of the rated current. Fault current limitation (increasing of short - circuit reactance) occurs even before the fault current reaches the critical current of HTS winding, thus the limitation is more effective

Conclusion

Using the new 2G HTS tapes with proper values of resistivity in the resistive state at a temperature of 77 K, it is possible to build short-circuit resistance HTS transformers with small value of short-circuit voltage $u_{\%}$ since the increase of short-circuit impedance in the resistive state is sufficient to limit the fault current.

After the transition of the superconducting windings to the resistive state, the occurrence of the windings resistance causes a significant increase in the impedance of the transformer compared to its impedance in the superconducting state. The SCS4050 2G tape is suitable for this task as shown the results of the experimental examination of the transformer model

REFERENCES

[1] Janowski T., Głowacki B., Wojtasiewicz G., Kozak S., Kozak J., Kondratowicz-Kucewicz B., Majka M., Woźniak M., Fault Current Limitation in Power Network by the Superconducting Transformers Made of 2G HTS, *IEEE Trans. on Appl. Supercond.*, Vol. 21, No 3, 2011, 1413-1416

[2] Hayakawa N., Kojima H., Hanai M., Okubo H., Progress in Development of Superconducting Fault Current Limiting Transformer, *IEEE Trans. on Appl. Supercond.*, Vol. 21, Vo. 3, 2011, 1397-1399

[3] Kojima H., Kotari M., Kito T., Hayakawa N., Hanai M., Okubo H., Current Limiting and Recovery Characteristics of 2 MVA Class Superconducting Fault Current Limiting Transformer (SFCLT), *IEEE Trans. Appl. Supercond.*, Vol. 21, Vo. 3, 1401-1404, 2011

[4] Shirai Y., Nii T., Oda S., Shiotsu M., Current Limiting Characteristics of Transformer Type HTS Superconducting Fault Current Limiter with Rewound Structure, *Journal of Physics Conference Series*, Vol. 234, Article No. 032053, 2010

[5] Wojtasiewicz G., Janowski T., Kozak S., Kozak J., Majka M., Kondratowicz-Kucewicz B., Tests and Performance Analysis of 2G HTS Transformer, *IEEE Trans. on Appl. Supercond.*, Vol. 23, Vo 3, Article No: 5500505, 2013

[6] Lim S. H., Ko S., Han T. H., Analysis on current limiting characteristics of a transformer type SFCL with two triggering current levels", *Physica C- Supercond. and its Applications*, Vol. 484, 253-257, 2013

Authors: *dr inż. Grzegorz Wojtasiewicz, prof. dr hab. inż. Tadeusz Janowski, prof. dr hab. inż. Sławomir Kozak, dr inż. Janusz Kozak, dr inż. Michał Majka, mgr inż. Beata Kondratowicz-Kucewicz, Electrotechnical Institute in Warsaw, Laboratory of Superconducting Technologies in Lublin, Nadbystrzycka 36a, 20-618 Lublin, E-mail: g.wojtasiewicz@iel.waw.pl, t.janowski@pollub.pl, s.kozak@iel.waw.pl, j.kozak@iel.waw.pl, m.majka@iel.waw.pl, b.kondratowicz-kucewicz@iel.waw.pl*

8th International Conference
Electromagnetic Devices and Processes in Environment Protection ELMECO-8
joint with 11th Seminar Applications of Superconductors AoS-11
September 28 - October 1, 2014, Nałęczów, Poland

INFLUENCE OF SUPERCONDUCTING TRANSFORMER'S PARAMETERS ON TRANSIENT CURRENT LIMITING

Łukasz WOŹNIAK[1,2], Grzegorz WOJTASIEWICZ[3], Paweł SURDACKI[1], Grzegorz KOMARZYNIEC[1]

Politechnika Lubelska, Instytut Podstaw Elektrotechniki i Elektrotechnologii (1), ENEA Wytwarzanie S.A. (2),
Instytut Elektrotechniki w Warszawie (3)

Abstract. *In this paper, the analysis of the parameters of the superconducting transformer, which allows to limit transient currents, has been performed. The proper designing and carrying out the superconducting winding as well as selecting a proper superconducting 2G HTS tape allows to limit transient currents to the value of winding's rated current. The stage of computer modelling of the transformer transient behaviour will enable the optimization of the parameter and material design for superconducting transformer manufacture.*

Streszczenie. *W artykule dokonano analizy parametrów transformatora nadprzewodnikowego, które pozwalają ograniczać prądy w stanach przejściowych. Poprawne projektowanie i wykonanie uzwojeń nadprzewodnikowych wraz z doborem parametrów taśmy nadprzewodnikowej 2G pozwala na ograniczenie prądów w stanach przejściowych do wartości ich prądu znamionowego. Etap modelowania komputerowego uzwojeń pozwoli na optymalizacje doboru parametrów i materiałów do produkcji transformatorów nadprzewodnikowych.* ***(Wpływ parametrów transformatora nadprzewodnikowego na ograniczanie prądu w stanach przejściowych)****.*

Keywords: superconducting transformer, fault current limitation, superconductivity
Słowa kluczowe: transformator nadprzewodnikowy, ograniczanie prądów zwarcia, nadprzewodnictwo

Introduction

Currently using of the superconducting tapes HTS 2G in non-superconducting state have large resistance. Thanks to it, there is possibility to build superconducting transformers, which limit current in transitional states such as short circuit or plugging a transformer into power grid [8]. The resistance of winding is increasing after exceeding critical current density of a transformer to the value which allows to limit fault current [6].

To the main advantages of a transformer with superconducting winding belong:

- minor losses in windings,
- elimination of Joule's losses in the superconducting phase because of zero resistance,
- reducing the dimensions and mass of the transformer,
- lack of oil in cooling system of the transformer,
- resistance to short circuits. The fault current can not exceed the value of the critical current.

Parameters allowing to limit current in a short circuit phase

One of the main advantages of replacing conventional transformers by transformers with superconducting winding is their resistance to short circuits thanks to the restriction of fault current by superconducting winding. The value of limitation of fault current depends on the construction of superconducting winding and the parameters of a particular superconducting belt (tape) HTS 2G. The resistance to short circuit of the superconducting transformer is possible thanks to a minor value of the percentage voltage of short circuit. The electro-dynamic force at short circuits and the value of fault current depend on the basic transformer parameter, in other words on the voltage of u_z, given in per cents. In table 1 there was shown the percentage voltage of short circuit $u_z\%$ in conventional transformers and in superconducting transformers. The height of windings and the width of slits between windings is the same in both transformers [6].

Table 1. The percentage voltage of short circuit in conventional and superconducting transformers depending on the unit power [1,2,3]

Transformer	The percentage voltage of short circuit - $u_z\%$	
	Conventional	Superconducting
Low power	<6	< 2 – 5
High power	10-15	< 6 – 10

In transformers with superconducting windings the percentage voltage of short circuit is much smaller than in transformers with conventional windings. The higher the unit power is , the difference between the voltage is increasing.

The voltage of fault current in conventional transformers and superconducting transformers is proportional to the surface area of a trapezium (fig.1)

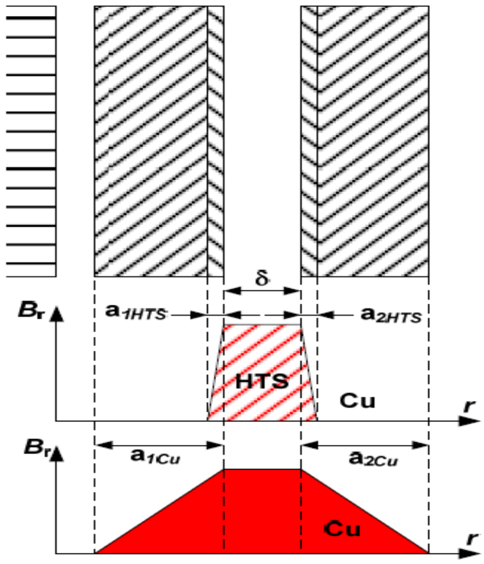

Fig. 1. The impact of the thickness of the transformer winding on the value of the short circuit voltage

Where:

$\boldsymbol{a_{1HTS}}$ – the thickness of the first winding of a superconducting transformer

$\boldsymbol{a_{2HTS}}$ – the thickness of the second winding of a superconducting transformer

$\boldsymbol{a_{1Cu}}$ – the thickness of the first winding of a conventional transformer

$\boldsymbol{a_{2Cu}}$ – the thickness of the second winding of a conventional transformer

$\boldsymbol{\delta}$ – the width of a slit between windings

The thickness of windings in superconducting transformers is much smaller than the thickness of windings made of copper, by the same size of air slit δ, that is why the surface area of a trapezium is also smaller. The smaller surface area of trapezium means the smaller percentage voltage of short circuit. In designing a superconducting transformer we can assume omitting the thickness of windings of superconducting transformers since they are very thin ($a_{Cu}>>a_{HTS}$) (Fig. 1). The percentage voltage of short circuit in superconducting transformers will depend only on the width of an air slit δ [7].

The selection of the proper percentage voltage of short circuit in conventional transformers depends on the acceptable value of fault current. In powerful transformers the value of fault current is supposed to be the smallest in order to limit dynamic effects of short circuit. Presently used method to limit fault current, which is also associated with dynamic force, is increasing the percentage voltage of short circuit in transformers. Next, the voltage increase of short circuit is made by the width increase of an air slit δ between windings [6].

In superconducting transformers, overcoming the critical current as a result of short circuit is that a superconductor comes into a resistant state which causes appearing the effect of self-limiting of fault current. The transition of the superconductor into a resistant state and the time of this transition depends on the characteristic of a current-voltage superconductor. In figure 2 there is presented the effect of fault current self-limitation in the winding of a superconducting transformer [4].

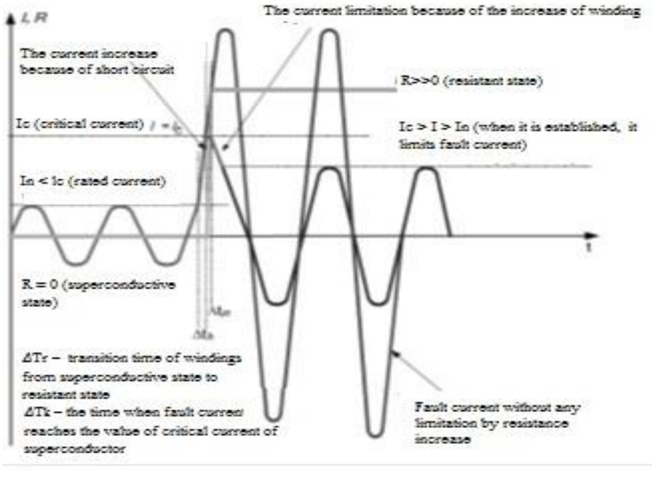

Fig. 2. The effect of self-limiting of fault current in the winding of a superconducting transformer

The superconducting winding in a superconductive state has zero resistance R . In the superconductive state, rated current I_n of a superconductor is smaller than critical current I_c ($I_n<I_c$). . During short circuit , rated current I_n of winding begins rising and at the time t_1 reaches the value of critical current I_c ($I_n=I_c$). After overcoming the value of critical current , superconducting winding turns into a transitional state, which lasts by the time t_2. At this time superconducting winding turns from the superconductive state into the resistant state. The resistance of winding reaches the value R>>0 and fault current is restricted to the value $I_c > I > I_n$. The duration of the time of a transitional state Δt in operation of superconducting winding is much shorter than ¼ of the duration of the time of fault current and it does not exceed 1 ms [5].

Conclusion

Fault current in superconducting transformers depends on the sort of a superconducting belt, the length and the thickness of winding, the width of a slit, the critical current of a superconductor and the percentage voltage of short circuit. Therefore the proper selection of these parameters will allow to create an optimal superconducting transformer at this stage of designing, thanks to which there will be possibility to limit current in transitional states (short circuit of transformer, plugging transformer into power grid). In order to achieve this aim we need to create a program which will reflect a real characteristic and verify calculations during a designing phase.

References

[1] Kalsi S.S, Application of high temperature superconductors to electrical power equipment Copyright © 2011 by John Willey & Sons, Inc.

[2] Jezierski E. Transformatory: Podstawy teoretyczne, WNT 1965.

[3] Donnier-Valentin G., Tixador P., Vinot P., Consideration about HTS superconducting transformers, IEEE Trans. on Applied Superconductivity, vol. 11, No.1, March 2001, pp. 1498-1501.

[4] Rose-Innes A.C., Rhoderick E.H., Nadprzewodnictwo, PWN, Warszawa 2009.

[5] Janowski T., Stryczewska H.D., Kozak S., Malinowski H., Wojtasiewicz G., Surdacki P., Kondratowicz-Kucewicz B., Kozak J., Nadprzewodnikowe ograniczniki prądu, Wydawnictwo Drukarnia LIBER, Lublin 2002

[6] Janowski T., Wojtasiewicz G., Transformatory nadprzewodnikowe odporne na zwarcia i ograniczające prądy zwarcia, Przegląd Elektrotechniczny, vol. 88, no. 9 B, 269-272. 2012

[7] Janowski T., Wojtasiewicz G., Transformatory nadprzewodnikowe ograniczające prądy zwarcia w sieciach elektroenergetycznych, Materiały konferencyjne, VIII Konferencja Naukowo-Techniczna: Transformatory energetyczne i specjalne; Kazimierz Dolny 13-15.X.2010, str.179-194, ISBN: 978-83-62742-00-4

[8] Komarzyniec G., Janowski T., Majka M., Kozak J., Kozak S., Kondratowicz – Kucewicz B., Prąd włączania transformatora nadprzewodnikowego, Przegląd Elektrotechniczny, ISSN 0033-2097, R. 89 NR 9/2013

***Authors**:*

mgr inż Łukasz Woźniak

e-mail: wozniak.lukasz1988@gmail.com. PhD student at Lublin University of Technology, Faculty of Electrical Eng. and Computer Science

Dr hab. inż. Paweł Surdacki, prof. PL

e-mail: p.surdacki@pollub.pl. Lublin University of Technology, Institute of Electrical Engineering and Electrotechnologies

Dr inż. Grzegorz Wojtasiewicz

e-mail: g.wojtasiewicz@iel.waw.pl. Electrotechnical Institute in Warsaw ul. Pożaryskiego 28, 04-703 Warszawa

Dr inż. Grzegorz Komarzyniec

e-mail: g.komarzyniec@pollub.pl. Lublin University of Technology, Institute of Electrical Engineering and Electrotechnologies

8th International Conference
Electromagnetic Devices and Processes in Environment Protection ELMECO-8
joint with 11th Seminar Applications of Superconductors AoS-11
September 28 - October 1, 2014, Nałęczów, Poland

BACKPACK-TYPE OZONE-MIST STERILIZATION SYSTEM DEVELOPED FOR NON-CHEMICAL AGRICULTURE PROCESSES

Yoshitaka YAMASHITA[1], Toshifumi YAMASHITA[1], Yukio HASHIMOTO[1], Kenji EBIHARA[2], Fumiaki MITSUGI[3], Tomoaki IKEGAMI[3], Henryka D. STRYCZEWSKA[4], Joanna PAWLAT[4], Shinriki TEII[5], Ta-LUN SUNG[5]

Sanwa hi-tech Co.Ltd (1), Environment and Energy Laboratory (2),Kumamoto University (3),
Lublin University of Technology (4), Lunghwa University of Science and Technology (5)

***Abstract**. Chemical reaction of ozone gas with air and water generates highly reactive radicals. These radical species show strong sterilization effect on harmful insects living on plants and nematodes in soil. We have proposed portable ozone sterilization system which is expected to be used at small scale agriculture farms generating water-mist and an ozone-mist spray with 4 nozzles. The sterilization experiments have been performed mostly at eko-farms in China, Taiwan and Japan.*

***Streszczenie.** Ozon reagujący z wodą powoduje powstanie rodników hydroksylowych o silnych właściwościach utleniających, które mogą być wykorzystane do usuwania naziemnych szkodników roślinnych oraz nicieni bytujących w glebie. Przedstawione będą wyniki testów przeprowadzonych w gospodarstwach eko-rolniczych w Chinach, Japonii i na Tajwanie przy użyciu przenośnego sterylizatora do zastosowań agrarnych produkującego wodę ozonowaną i mgłę ozonową.*

Keywords: ozone-mist , ozone sterilization, dielectric barrier discharge, harmful insect ,nematode, non-chemical agriculture.
Słowa kluczowe: mgła ozonowa, sterylizacja ozonowa, wyładowanie barierowe, szkodniki roślin, nicienie, eko-rolnictwo.

Introduction

We have required environmentally friendly sterilization method for agricultural production which is not polluted by agricultural chemicals. We have developed portable backpack-type ozone-mist sterilization system for small scale agriculture at remote rural areas [1-3]. The ozone-mist matter is generated injecting high dense ozone gas into sterilization space surrounded with water-mist. The sterilization characteristics was studied for harmful insects such as aphids and worm at various treatment conditions.

Most nematodes in soil are beneficial ,feeding on bacteria, fungi, or other microscopic organisms and are used as biological control organisms to help manage important insects. On the other hand, plant –parasitic nematodes feed on live plants and are detrimental to agricultural farms.

We have applied our ozone sterilization system to kill the nematodes in agricultural soil. High dense ozone gas was exposed to the soil. The effect of ozone treatment on free-living nematodes in soil is studied.

Experimental

Ozone-mist sterilization system developed consists of an ozone generator, a water-mist supply system, an AC-DC inverter connected to Li-ion battery, a lightweight oxygen vessel (FRP) with a pressure regulator, a water tank and a movable spray rod with ozone-mist nozzle as shown in Fig.1 [1-3]. Surface dielectric barrier discharge is used to generate high dense ozone. The AC electric power for the high frequency generator (15kHz, Vp-p=8kV) was supplied from the AC-DC inverter with Li-ion battery.

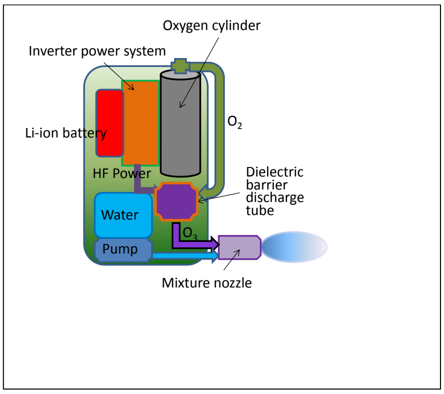

Fig.1 Structure of ozone-mist sterilization system

Ozone-mist is generated to introduce ozone gas into the water mist area formed by pumping water into four nozzles.

In this experiment, the target samples such as aphids were captured on the mesh sheet placed at the bottom of a test PET cup (top diameter 90mm, bottom diameter 60mm).

In the cultivation of crops, soil deseases is infected with nomatodes in the soil. The nomotodes that live in the soil were separated by using the Bellmann method. A microscope was used to count the number of nematodes contained in a water drop of the separated water.

Results and discussion

Fig.2 shows a typical picture of red aphid sterilization experiment under a treatment condition of ozone concentration 70 g/m^3 with 1 liter/min, mist-water 300ml/min, treatment time 30sec. In this case the sterilization rate was about 98%.

Fig.2 Red aphids after ozone-mis treatment.

Fig.3 shows sterilization rate as a function of treatment time. This result shows that sterilization rate rapidly lowers with decrease of treatment time. In the practical sterilization at farms, the treatment time on the targets object lower than about 10 sec is usually required keeping sterilization rate over 90%. We have to improve the spray system to give higher sterilization rate for many kinds of insects.

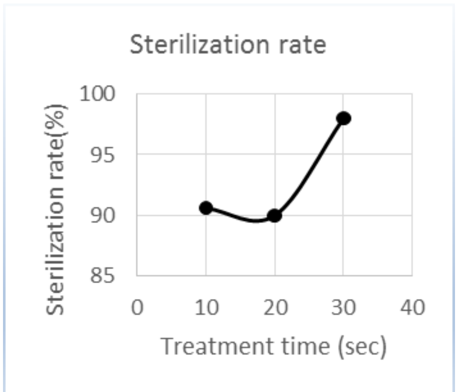

Fig.3 Sterilization rate of red aphids as a function of

Fig.4 is a typical microscopic image of a nematode in agricultural soil (30g) before ozone treatment for the soil. The length of the aphid is about 0.8mm.

Fig.4 A nematode sepatated from soil

Fig.5 shows sterilization effect on nematodes treated by ozone and agricultural chemical (Fenitrothion). Although average number (denoted by non) of nematodes in non-treated soil is 5, few numbers were detected in the cases of ozone(70g/m^3, 20min) and chemical sterilizations. The developed sterilization is considered to be a promising method to promote non-chemical sterilization in agriculture.

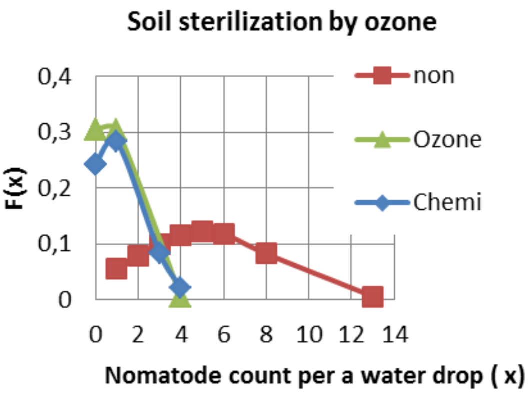

Fig.5 Normal distribution function F(x) of nomotode number (x) in ozone and agricultural chemical treatemnts for soil.

non: non-treat soil before treatment, Ozone: ozone(70g/m^3) treatment

Conclusion

A portable ozone sterilization system was developed to control the pests in agriculture. The system was applied to studying the effect on aphids living on plants and nematodes dwelling in soil. The experiments show that the survival rate for the aphids is about 10% for treatment time of 10—20 sec. Most of nematodes in soil were killed by the 20min treatment of 70g/m^3 ozone gas and the agricultural chemical treatment.
The non-chemical ozone sterilization method developed here will be a promising technology in agriculture.

We would like to express sincere thanks to Professors Emeritus Chikahisa Honda and Masahisa Otsubo for their kind support and encouragement to promote this R&D project.

REFERENCES

[1] Ebihara K.,Stryczewska H.D., Ikegami T., Mitsugi F., Pawlat J., Electrical Review, R.87 NR7/2011, pp.148-152, 2011.

[2] Ebihara K.,Stryczewska H.D., Mitsugi F., Ikegami T., Sakai T., Pawlat J., Teii S., Electrical Review, R.88 NR6/2012, pp.92-94, 2012.

[3] Ebihara K., Mitsugi F., Ikegami T., Nakamura N., Hashimoto Y., Yamashita Y., Baba S., Stryczewska H.D., Pawlat J., Teii S., Sung T.L., The European Physical Journal Applied Physics, Vol61,24318,pp.1-5,201

***Authors**: Yoshitaka Yamashita,Sanwa hi-tech Co.Ltd., Yoshitomi 205-4,Sisui-machi, Kikuchi City, Kumamoto 861-1201 Japan*
e-mail: yoshitaka_y@sanwa-hitech.com,
Kenji EBIHARA, Environment and Energy Laboratory, Ohtemon 1-4-15-404, Chuouku, Fukuoka City, Fukuoka 810-0074 Japan.
e-mail: kankyo@mild.ocn.ne.jp
The correspondence address is: *Prof. Kenji EBIHARA, Environment and Energy Laboratory, Ohtemon 1-4-15-404, Chuouku, Fukuoka City, Fukuoka 810-0074 Japan.*
e-mail: kankyo@mild.ocn.ne.jp

8th International Conference
Electromagnetic Devices and Processes in Environment Protection ELMECO-8
joint with 11th Seminar Applications of Superconductors AoS-11
September 28 - October 1, 2014, Nałęczów, Poland

WPŁYW ZMIAN WTRĄCENIOWYCH W FERROMAGNETYKU NA PĘTLĘ HISTEREZY RÓŻNICOWEJ DLA RÓŻNYCH CZĘSTOTLIWOŚCI STRUMIENIA MAGNETYCZNEGO

Effect of insertion changes in a ferromagnet at the differential hysteresis loop for various frequencies of magnetic flux

Andrzej WAC-WŁODARCZYK, Piotr ZIŃ, Tomasz GIŻEWSKI

Lublin University of Technology

Streszczenie. *Wykorzystując współczesne techniki pomiarowe pojawiają się nowe możliwości znalezienia dodatkowych funkcjonalności dla klasycznych układów elektrotechniki. W artykule przedstawiono próbę wykorzystania mostka pomiarowego zmiennoprądowego Maxwell'a w układzie porównawczym ze wzorcem. Układ ten wykazuje zdolności do identyfikacji, a w następnych krokach klasyfikacji zmian wtrąceniowych w ferromagnetykach.*

Abstract*. Using modern measurement techniques, there are new opportunities to find additional functionalities for the classical electrical engineering systems. The article presents an attempt to use the AC Maxwell bridge circuit in the comparative system with the pattern. This system demonstrates the ability to identify, and in the next steps, the classification of insertion changes in ferromagnet.*

Słowa kluczowe: histereza różnicowa, mostek pomiarowy Maxwell'a, identyfikacja
Keywords: identification, differential hysteresis, Maxwell bridge

Wstęp

Zmiany pętli histerezy ferromagnetyka mogą wskazywać na fluktuację parametrów fizycznych materiału. Dlatego, ważne jest by móc zmierzyć te zmiany oraz w następnych krokach sklasyfikować badany ferromagnetyk. Warto zauważyć że pole pętli histerezy obrazuje straty związane, między innymi, z przemagnesowywaniem ferromagnetyka.

Do pomiarów zastosowano model defektoskopu indukcyjnego, wykonanego w IPEiE Politechniki Lubelskiej [2][3].

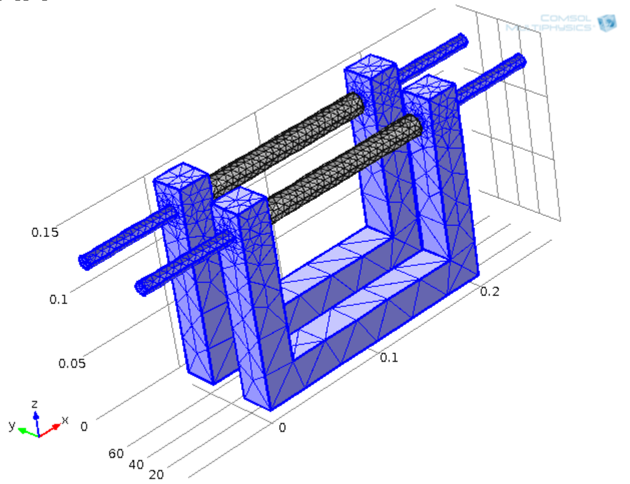

Rys.1. Uproszczony schemat magnetowodów stanowiska pomiarowego.

Urządzenie to pracuje w układzie mostka pomiarowego zmiennoprądowego, w którym istnieją dwa magnetowody z cewkami (Rys.1.) oraz zestaw cewek będących opcjonalnymi elementami urządzenia badawczego.

Układ pomiarowy

W przeprowadzonych badaniach zastosowano klasyczny układ mostka Maxwell'a z indukcyjnościami nieliniowymi w ramionach pierwszym oraz trzecim [4]. Zastosowane elementy indukcyjne stanowią jednakowe cewki z rdzeniami ferromagnetycznymi, wzorcowym oraz badanym. Defekt materiałowy badanego rdzenia, powoduje zmiany jego strumienia magnetycznego, co prowadzi do pojawienia się zmiany napięcia nierównowagi U_w

$$U_w = \frac{d(\Psi_1 - \Psi_3)}{dt} \quad (1)$$

gdzie: U_w – napięcie nierównowagi mostka, Ψ_1 *oraz* Ψ_3 – strumienie magnetyczny skojarzone z cewką ramienia pierwszego oraz trzeciego mostka pomiarowego [1].

Pomiary

Przykład pętli histerezy różnicowej dla częstotliwości 80Hz pokazany jest na rys.2. Dla częstotliwości poniżej 200 Hz pętla ta ma kształt liter S [5].

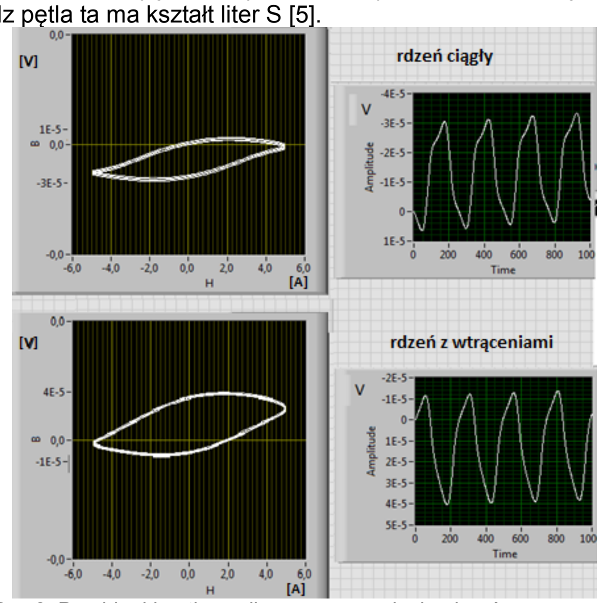

Rys.2. Przebiegi i pętla scałkowanego napięcia niezrównoważenia mostka dla rdzenia ciągłego i z wtrąceniami

Pętlę histerezy różnicowej można uzyskać podając napięcie powstałe w wyniku przepływu prądu magnesującego na okładziny odchylania poziomego oraz scałkowane napięcie nierównowagi mostka na okładziny odchylania pionowego oscyloskopu. Jak widać na rys.2. pod wpływem zmian wtrąceniowych rdzenia, przykładowo nacięcie na obwodzie, pętla histerezy zmienia kształt, oraz rozmiary. Rozmiary pętli wyraża amplituda międzyszczytowa scałkowanego napięcia nierównowagi mostka.

Napięcie skuteczne niezrównoważenia

Na rys.3. przedstawione zostały pomiary zmiany napięcia skutecznego na głównej przekątnej mostka dla różnych częstotliwości przy zmianach wtrąceniowych w rdzeniu. Kwadraty oznaczają punkty pomiarowe dla rdzenia z nacięciem, romby pomiary rdzenia ciągłego. Różnicę bezwzględną ilustrują trójkątne punkty pomiarowe.

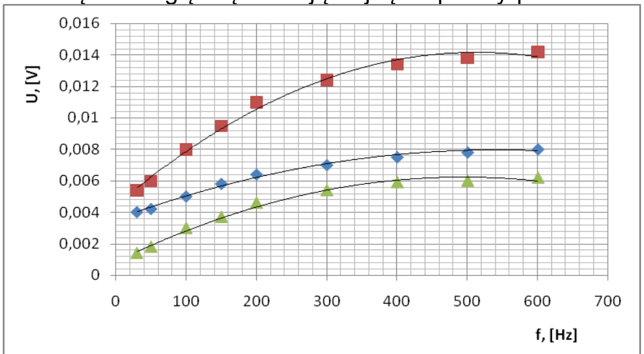

Rys.3. Napięcie niezrównoważenia mostka dla różnych częstotliwości.

Wartość różnicy względnej napięcia skutecznego niezrównoważenia dla rdzenia z i bez nacięcia pokazana jest na rys.4. Różnica względna jest liczona względem wskazań z rdzeniem ciągłym.

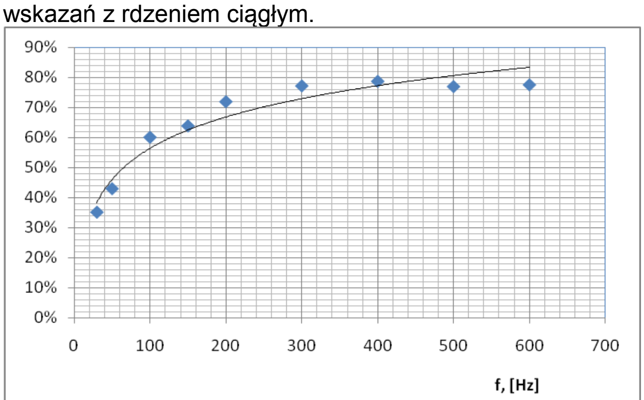

Rys.4. Różnica względna napięcie niezrównoważenia mostka dla różnych częstotliwości.

Amplituda międzyszczytowa scałkowanego napięcia niezrównoważenia

Wartość amplitudy międzyszczytowej scałkowanego napięcia niezrównoważenia można zobaczyć na rys.2, jako wysokość pętli histerezy różnicowej lub odległość w pionie między szczytami w przebiegu napięcia. Pomiary zostały zebrane i pokazane na rysunkach 5 oraz 6. Zmiany scałkowanego napięcia na głównej przekątnej mostka dla różnych częstotliwości przy rdzeniu ciągłym ilustrują punkty pomiarowe w kształcie rombu, rdzeń z nacięciem to punkty-kwadraty. Różnicę bezwzględną wskazują trójkątne punkty pomiarowe. Na rys.6. przedstawiono wykres różnicy względnej względem pomiaru z rdzenia bez nacięcia. Widać z niego że wartości te po dużym rozrzucie przy częstotliwościach poniżej 200Hz stabilizują się na poziomie 80% wzrostu amplitudy.

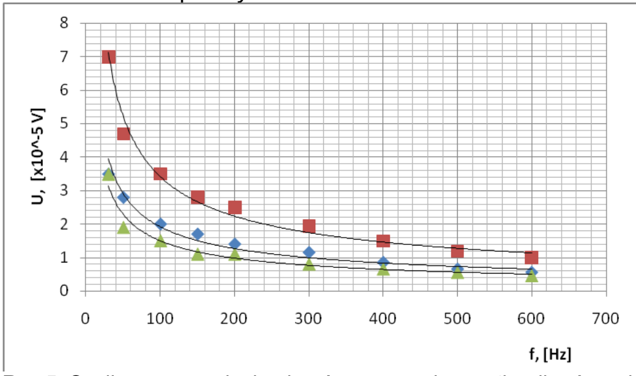

Rys.5. Scałkowane napięcie niezrównoważenia mostka dla różnych częstotliwości

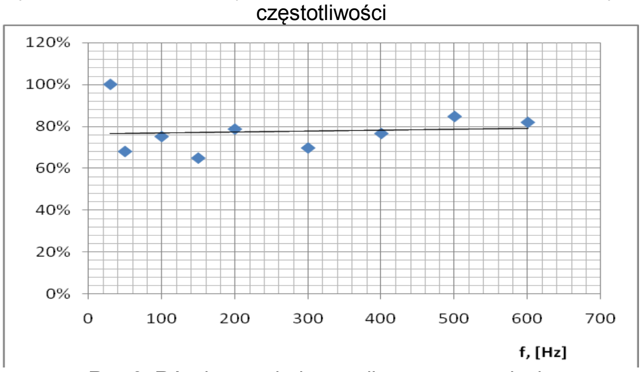

Rys.6. Różnica względna scałkowanego napięcia niezrównoważenia mostka dla różnych częstotliwości.

Wnioski

- Zmiany napięcia skutecznego niezrównoważenia pod wpływem zmian wtrąceniowych w rdzeniu są znacząco wyższe powyżej 100 Hz.
- Nacięcie na rdzeniu ma wpływ na wielkość pętli histerezy różnicowej, przy wzroście częstotliwości ten wpływ stabilizuje się na około 80% powiększeniu pętli.
- Ze wzrostem częstotliwości pętla histerezy różnicowej zmienia kształt z litery S na zbliżony do elipsy.

LITERATURA

[1] Wac-Włodarczyk A., Goleman R., Czerwiński D., Giżewski T.: *Symulacja pracy mostkowego układu porównawczego materiałów ferromagnetycznych,* Przegląd Elektrotechniczny 12/2000, s.141-144.

[2] Wac-Włodarczyk A., Goleman R., Giżewski T., *Eksperymentalna identyfikacja różnicowej powierzchni Preisacha w układzie mostka zmiennoprądowego,* Przegląd Elektrotechniczny 12/2010, s.160-163.

[3] Wac-Włodarczyk A., Goleman R., Giżewski T., *Zastosowanie algorytmu sztucznych sieci neuronowych w identyfikacji uszkodzeń materiałów ferromagnetycznych,* Dozór Techniczny, nr 2/2008, s.41-45.

[4] Ziń P., *Zastosowanie mostka sprzężonego indukcyjnie w badaniach nieniszczących ferromagnetyków*, Warsztaty doktoranckie OWD Wisła 2013, s.258-261.

[5] Wac-Włodarczyk A., Ziń P., Giżewski T., *Pętla histerezy różnicowej w mostku Maxwell'a dla różnych częstotliwości strumienia magnetycznego*, XXIV Sympozjum Środowiskowe PTZE, Hucisko 2014, s.217-218.

***Autorzy**: prof. dr hab. inż. Andrzej Wac-Włodarczyk, Politechnika Lubelska, Instytut Podstaw Elektrotechniki i Elektrotechnologii, e-mail: a.wac-wlodarczyk@pollub.pl; mgr inż. Piotr Ziń, Politechnika Lubelska, Instytut Podstaw Elektrotechniki i Elektrotechnologii, e-mail: p.zin@pollub.pl; dr inż. Tomasz Giżewski, Politechnika Lubelska, Instytut Podstaw Elektrotechniki i Elektrotechnologii, e-mail: t.gizewski@pollub.pl;*

8th International Conference
Electromagnetic Devices and Processes in Environment Protection **ELMECO-8**
joint with 11th Seminar Applications of Superconductors **AoS-11**
September 28 - October 1, 2014, Nałęczów, Poland

THE INTERACTION OF THE PLASMA REACTOR SYSTEM FOR POWER SYSTEM

Paweł A. MAZUREK

Lublin University of Technology

Abstract. *The quality of work the installation and the electrical equipment (especially industrial) interacts strongly on the quality of electricity. The paper will present the results of preliminary studies and analyzes carried out in the power supply circuit of the plasma reactor. The analysis applies to low-frequency disturbances.*

Streszczenie. *W artykule zostaną zaprezentowane wyniki wstępnych badań i analiz przeprowadzonych w torze zasilania reaktora plazmowego typu Glid-Arc, w zakresie zaburzeń częstotliwości przemysłowej.*

Keywords: quality of energy, electromagnetic compatibility, Glid-Arc plasma reactor.
Słowa kluczowe: jakość energii, kompatybilność elektromagnetyczna, reaktor Glid-Arc

Introduction

Considering the problems of electromagnetic compatibility, we need to analyze their impact on the energy system. Every electrical appliance or installation is located in a certain electromagnetic environment, so there are still some impact.

Quality in relation to electricity can be assessed based on its indicators. The parameters defining the electricity quality include: voltage, distortion sine wave voltage, voltage fluctuations, frequency variations, voltage dips, surges, voltage imbalance.

Plasma reactor

For technical or scientific generates a low-temperature plasma in devices called plasma reactors. One of the types of plasma reactors with an expansion arch is reactor Glidarc. Its main feature is the possibility of generation of non-thermal plasma in a polluted gas directly at atmospheric pressure and under conditions in which the exhaust gases are emitted into the atmosphere.

The reactor consists of three working electrodes and the plug placed in the discharge chamber. The gas flows through the chamber and is subjected to a plasma treatment. Due to the research nature of the reactor operation, the working fluid was a mixture of air fed to the discharge space. The working electrode are arranged at 120 degrees radially from the axis of the discharge chamber. Width of the gap between their measured from the axis of the discharge chamber electrode is approx. 2.5 mm in the discharge ignition zone.

Measurements of power quality parameters are normally executed by a special device - power quality analyzers. Meters measure the voltages and currents, and are capable of calculating and displaying multiple standard parameters. Measurements are made in accordance with the guidelines contained in the standards of PN-EN 61000-4-30, PN-EN 61000-4-15, PN-EN 61000-4-7. The basis for assessing the conditions of supply requirements are included in the polish Regulation of the Minister of Economy of 4 May 2007 on the detailed conditions for the operation of the power system and the guidelines of PN-EN 50160.

Tested installation

Evaluation of the quality of reactor system associated with the recommendations of compatibility requires a lot of testing in the laboratory. In order to comply with the requirements of the EMC Directive, the installation of the reactor must be in accordance with the requirements specified in harmonized standards.

Fig.1. Measurement position – plasma reactor Glid-Arc

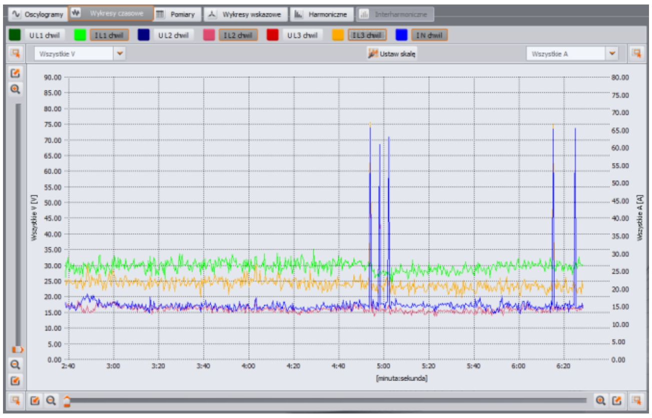

Fig.2. Levels of currents and voltages in the circuit of the reactor

Fig.3. The harmonics current on the power reactor

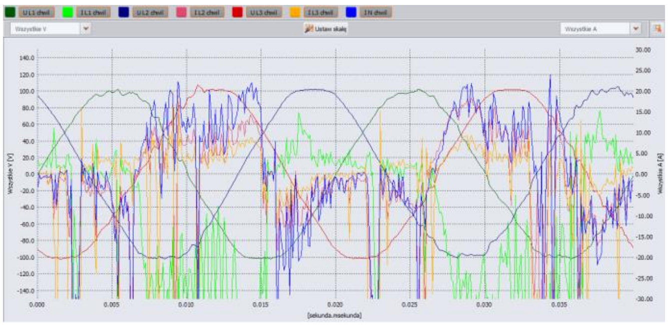

Fig.4. Oscillograms of voltage and current in the power circuit

Measurements were made in the installation of Glid-Arc plasma reactor. There located in the building Asppect in the Laboratory of Electromagnetic Compatibility. The study done by use of analyzer "Sonel PQT700", clamps "C5" and the software "Sonel Analysis".

Measured current and voltage of the primary power supply and made waveforms during operation of the plasma reactor with gliding arc discharge.

On the first picture presented investigated the position. The next graphs, are the screenshots of the software that was used to analyze the quality of electricity in the circuit of the reactor.

Arcing is highly nonlinear and asymmetric load associated with the dynamically changing phenomena of temporary and short-circuit. This translates into a well on the random nature of electromagnetic disturbances.

In few minutes operation of the reactor detected significant harmonics of both even and odd. This confirms the highly deformed nature of the course of the current. This phenomenon is observed in all phases.

The reactor is the source of disturbances acting through the power path to the local energy system. This situation forces the growth of interest in problems of the harmonious operation of the reactor in an environment other equipment and power systems.

Obtained from the study disturbance size will be the basis for solutions that improve the quality of power supply circuit of the plasma reactor. Will also help ensure compliance with the standards of the level of electromagnetic compatibility.

Conclusion

The study is a preliminary identification of threats that may enter the plasma reactor system to the local power system. The resulting studies show strongly non-linear and unbalanced nature of the reactor. Observed crossing the harmonic content in all phases of the power supply. Also identified problems associated with high electromagnetic interference, which increase the uncertainty of measurement of the analyzer.

Further research is planned to track the quality of energy supply and the development of a new measurement method takes into account the increase compatibility with the installation of the measuring circuit of the reactor.

REFERENCES

[1] Dyrektywa unijna EMC, 2004/108/EC

[2] Janowski T., H. D. Stryczewska, A. Wac-Włodarczyk, Technologie nadprzewodnikowe i plazmowe w energetyce, Lubelskie Towarzystwo Naukowe, ISBN: 978-83-61391-76-9, Lublin 2009.

[3] Mazurek P. A., Rozkład emisji pola elektrycznego i magnetycznego wokół reaktora plazmowego typu GLIDARC, *Przegląd Elektrotechniczny*, ISSN 0033-2097, R. 86 NR 12/2010, str. 95-98.

[4] Mazurek P.A., Selected methods to improve the electromagnetic compatibility of the plasma reactor, *Electrical Review*, ISSN 0033-2097, R. 88 NR 7a/2012, p. 158-160

[5] Stryczewska H. D.: Technologie plazmowe w energetyce i inżynierii środowiska. Wydawnictwo Politechniki Lubelskiej, Lublin 2009

***Author**: dr inż. Paweł A. Mazurek, Politechnika Lubelska, Instytut Podstaw Elektrotechniki i Elektrotechnologii, ul. Nadbystrzycka 38a, 20-416 Lublin, e-mail: p.mazurek@pollub.pl.*

8th International Conference
Electromagnetic Devices and Processes in Environment Protection ELMECO-8
joint with 11th Seminar Applications of Superconductors AoS-11
September 28 - October 1, 2014, Nałęczów, Poland

ADVANCED TECHNOLOGICAL PLASMAS

Justyna JAROSZYŃSKA-WOLIŃSKA[1], P. Anthony F. HERBERT[2], Anna TATARCZAK[1]

Department of Civil Engineering, Lublin University of Technology (1), Plasma Ireland, Cork, Ireland (2)

***Abstract**. This research investigates the deposition of functional coatings by cool, atmospheric pressure plasma. Dry plasma deposition of functional coatings has many advantages. The objective is to find a generic plasma process that delivers Soft Plasma Polymerization (SPP) for depositing coatings comprising large bio-molecules. Key SPP criteria are excellent cross-linking/polymerization to deliver coating durability with minimal damage to precursor molecules delivering the full functionality of the original monomer. In this work, two very simple models were used to estimate specific plasma energies, found to be the key parameter in the achievement of SPP.*

***Streszczenie.** Obecne badania mają ma na celu użytkowy rozwój techniki (SPP) do otrzymywania nowych powierzchni materiałów. Zasadniczo dotyczą zoptymalizowania parametrów procesu tej technologii do rozwoju wysokiej wartości bio-funkcjonalnych powłok z prekursorów o dużej masie cząsteczkowej. W tej pracy oparto się na dwóch prostych modelach w celu oszacowania gęstości energii.

Keywords: soft plasma polymerization (SPP), plasma deposition, functional coatings
Słowa kluczowe: SPP soft plazma, wiązanie/ polimeryzacja

Introduction

Plasma is widely used across industry in the processing of semiconductor and microelectronics, paper/packaging, plastics (adhesion), metals, etc. Non-thermal equilibrium plasmas where the free electrons are hot (~10,000 K) but the ion and neutral populations are close to room temperature combine a cool system (electron mass negligible) rich in active species generated by fast electrons including ions, excited states, photons, radicals and molecular fragments. Two non-thermal plasma pressure regimes are used by industry. Low pressure plasmas easily maintain a controlled gas atmosphere and, thus, controlled plasma chemistry to run repeatable processes. They also easily generate cool, large volume plasmas for materials processing. Cool atmospheric pressure plasmas (APP) are harder to generate and control as the higher the pressure, the more the plasma tends to reduce in volume and thermalise towards the temperatures of typical thermal equilibrium plasmas ~1000K. However non-thermal APP is attractive to industry due to reduced equipment cost and the ability to handle demanding substrates and use coating precursors that cannot survive vacuum offering potential for innovation.

Plasma polymerisation using low pressure plasma technology to produce polymeric coatings – plasma enhanced chemical vapour deposition (PECVD) - bombards gas/vapour phase precursors with aggressive plasma species producing fragmentation and re-arrangement of precursor monomers and a variety of random fragments which deposit on a substrate. The resulting thin film layer contains many of the atoms present in the starting monomer but the coating shows little resemblance to the original precursor molecule and deposited films show little or no repeating structure and no definable molecular weight distribution. Coating functionality is limited to simple materials such as SiO_x, SiN or TiO_2 and complex chemistry cannot be deposited using such systems.

The APP technique used in this work is simple, low cost and, critically, can put down coatings that are both polymerised (i.e. cross-linked) to give durability and contain large, high molecular weight molecules that have not been damaged or denatured by the process. The process of putting down large, undamaged molecules in a cross-linked coating is called soft plasma polymerisation (SPP).

The work determined that a ‘pin corona’ type plasma can achieve SPP [1]. Figure 1 shows the plasma emitted as a jet or spray discharge from a sharp point when a high voltage is applied to the pin:

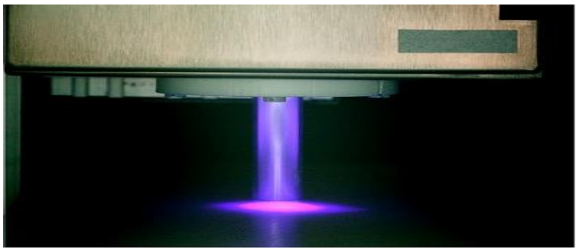

Figure 1: Generation of pin corona plasma

This type of plasma has been found to have a very low energy density, just enough to cross-link gas or vapour monomer precursor molecules injected into it but not high enough to damage them. The potential importance of the technique is that it could extend dry, rapid and low cost industrial plasma coating technology by providing a new capability to deposit high molecular weight polymerised coatings of largely undamaged molecules which retain the large majority of the monomer functionality. Plasma has many advantages for industry over wet and/or heat based processing but has been prevented from reaching its full potential because of the problem of molecular damage. The technique shows potential to remove that roadblock.

Experimental

Coating analysis using solvent wash and high resolution XPS was applied to pin corona deposited coatings on silicon wafers generated from Heptadecafluorodecyl acrylate (HDFDA) monomer injected into the plasma in vapour state. Excellent cross-linking via the polymerisable vinyl group was demonstrated by the coating surviving repeated solvent wash. XPS showed survival of the functional long perfluoro chain. Curve fitting of high resolution C1s XPS spectra as shown in Figure 2 showed two peaks at 292.4 and 294.6 eV being the CF_2 and CF_3 species. The peaks are well resolved and ratio of CF_2 to CF_3 is 5.8:1. This is lower than the 7:1 of the starting monomer and indicates some monomer degradation has occurred. But peak ratios suggest that > 80% retention of the perfluoro- chain has been achieved.

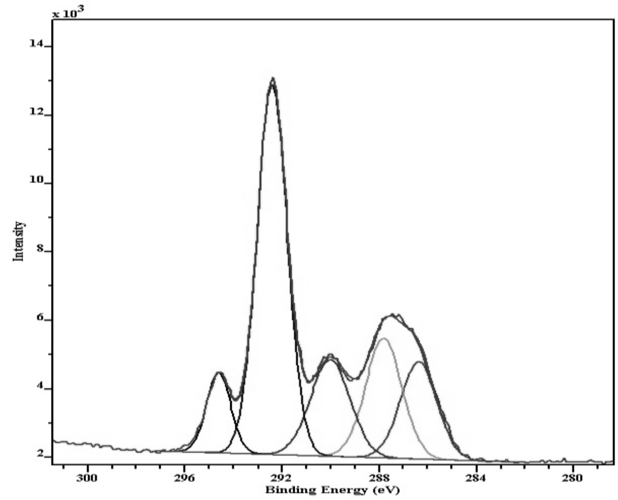

Figure 2: Curve fitting of the C1s XPS spectrum of HDFDA deposited on Si wafer for 30 seconds

Modelling

Empirical work [2, 4] of Warburg (1909) and Becker (1920) connected key plasma discharge parameters with the efficiency of chemical reactions in the discharge. Becker showed that the governing reaction parameter, R, is proportional to the power input per flow of gas, i.e. to the specific energy in J/cm^3. Studies by Rutscher and Wagner (1993) and Hegemann (2007) showed that in non-isothermal plasma chemistry (including plasma polymerization) the specific energy [J/cm^3] is indeed the decisive parameter. Direct measurements of plasma voltage and current were carried out on the pin corona plasma as shown in Figure 3:

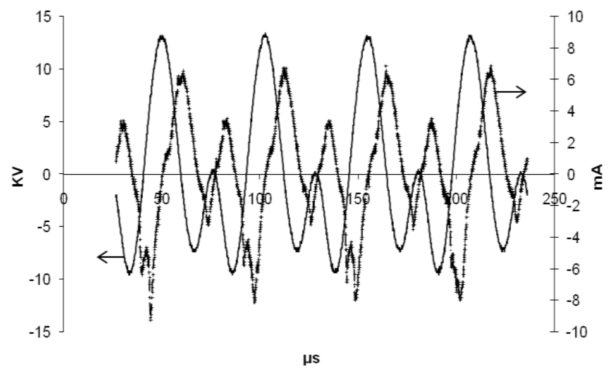

Figure 3: Voltage vs. Time (light trace) and Current vs. Time (dark trace) Corona Discharge characteristics

The data was used to calculate the effective power density with two models:

Model 1

- All discharge energy is coupled uniformly into the gas volume enclosed by tube.
- The discharge energy is partitioned evenly over all elementary entities (atoms/molecules).
- The gas mix of helium plus HDFDA precursor is modeled as an Ideal Gas at SLC (Standard Laboratory Conditions)

Model 2

- The helium is only an inert background gas and the plasma directly or indirectly, e.g. via helium metastables, eventually imparts all energy to the HDFDA.
- Such energy is partitioned evenly over all HDFDA molecules.
- The HDFDA gas is, again, modeled as an Ideal Gas at SLC.

Application of the models gave the following results:

Model 1: Specific energy = 0.029 J/cm^3 or 0.72 kJ/mol or 0.02 eV/entity

Model 2: Specific energy = 54 J/cm^3 or 1327 kJ/mol or 35 eV/entity

We can compare these figures against real molecular bond dissociation energy values: C-C 348 kJ/mol, C-O 360 kJ/mol, C-H 413 kJ/mol, C-F 488 kJ/mol, O=O 498 kJ/mol and the pi-bond of the C=C bond approximately 264 kJ/mol. It is clear that both models are wrong and represent extremes. However, Model 2 is closer to reality, particularly when the energy lost to tube surfaces, helium atoms, etc. are considered.

Conclusion

Soft Plasma Polymerisation from a gas state precursor at atmospheric pressure was seen to deliver coatings largely replicating the chemistry of the monomer precursor.

The process uses cool, atmospheric pressure, highly non-isothermal equilibrium corona discharge.

Retention of chemical functionality is likely to be due to low energy density [J/cm^3] coupled into the plasma.

It appears that this corona plasma type is inherently predisposed to deliver low specific energy into the reaction zone and, hence, to SPP, even using gas precursors.

The Corona plasma energy density appears to be high enough to break C=C bonds to enable cross-linking but no higher energy bonds thus allowing minimal molecular damage and de-naturing and retention of functionality.

Acknowledgments

We acknowledge support from Polish Ministry of Science and Higher Education under the statutory research number S/14/2014

REFERENCES

[1] Patent Cooperation Treaty Application No.PCT/EP2010/001703
[2] Suhr, H. Plasma Chemistry and Plasma Processing, 3 (1983), No. 1, 1
[3] Forch, R.; Zhang, Z.; Knoll, W.,Plasma Process. Polym., (2005) 2, 351
[4] Yoshimura, K.; Hozumi, K. J. Photopolym. Sci. Technol., , 9, (1996) No 2, 225

***Authors**: dr hab.prof. PL. J. Jaroszyńska-Wolińska, Politechnika Lubelska, Katedra Budownictwa Ogólnego, ul.Nadbystrzycka 40, 20-618 Lublin, e-mail: j.wolinska@gmail.com; Dr. P.A.F. Herbert, Ph.D., M.Eng.Sc., Plasma Ireland, 22 Summerhill North, Cork, Ireland e-mail: therbert@irishprecisionoptics.com; mgr A.Tatarczak Politechnika Lubelska, Katedra Budownictwa Ogólnego, ul. Nadbystrzycka 40, 20-618 Lublin, e-mail: anna.tatarczak@tatacommunications.com*